Theoretical Modeling of Compact Astrophysical Objects in Relativistic Gravity

A THESIS

submitted by

LIPI BASKEY

in partial fulfillment for the award of the degree

of

DOCTOR OF PHILOSOPHY (SCIENCE)

under the joint supervision of

Prof. Farook Rahaman and Dr. Shyam Das

DEPARTMENT OF MATHEMATICS, FACULTY OF SCIENCE

JADAVPUR UNIVERSITY

KOLKATA

2023

Dedicated to

my family

"No research without action, no action without research"

- Kurt Lewin

যাদবপুর বিশ্ববিদ্যালয়

FACULTY OF SCIENCE
DEPARTMENT OF MATHEMATICS

JADAVPUR UNIVERSITY
Kolkata-700 032, India
Telephone : 91 (33) 2414 6717

CERTIFICATE FROM THE SUPERVISORS

This is to certify that the thesis entitled "**Theoretical Modeling of Compact Astrophysical Objects in Relativistic Gravity**", submitted by **Lipi Baskey**, who got her name registered on **07.10.2020** for the award of **Ph.D. (Science)** degree of Jadavpur University, is absolutely based upon her own work under the supervision of **Prof. Farook Rahaman** and **Dr. Shyam Das** and that neither this thesis nor any part of it has been submitted for either any degree/ diploma or any other academic award anywhere before.

Shyam Das 4/9/23

(Signature of the Supervisor and date official seal)

Associate Professor in Physics
Malda College,
Malda

Farook Rahaman 4/9/23

(Signature of the Supervisor and date with with official seal)

DR. FAROOK RAHAMAN
Professor
Department of Mathematics
JADAVPUR UNIVERSITY
Kolkata - 700032, W.B., INDIA

Declaration

I, **Lipi Baskey**, hereby declare that the thesis entitled "**Theoretical Modeling of Compact Astrophysical Objects in Relativistic Gravity**" being submitted to **Jadavpur University, Kolkata, West Bengal, India** in partial fulfillment of the requirement for the award of degree of **Doctor of Philosophy (Science)** through the **Department of Mathematics** has not been submitted earlier to any other Institute or University for the award of any degree or diploma.

This work does not contain any texts, images and/or tables copied and pasted from the Internet without being specifically acknowledged, and the source being detailed in the thesis and in the Bibliography sections.

Lipi Baskey 4/9/23

LIPI BASKEY

Acknowledgment

Writing acknowledgment is equally tough as writing the thesis itself. There are so many people who have helped me in so many ways, who were always there when I needed them the most.

First and foremost I would like to thank my supervisor, Prof. Farook Rahaman for giving me the opportunity to conduct research under his guidance and for providing invaluable support during the course of my journey. His scholarly suggestions, indefatigable spirit, immense inquisitiveness, and affectionate behaviour have been a great source of inspiration for me. I am extremely grateful for all the knowledge that I have learned from him and I could not have imagined another supervisor and mentor like him. I would like to express my heartfelt gratitude to my co-supervisor, Dr. Shyam Das for his continuous support, patience, motivation, enthusiasm, and immense knowledge which has helped me during my research. Without his genuine and continuous guidance, this thesis would not have been a reality. It was my privilege and honour to work and as well as study under the guidance of my supervisors.

My sincere thanks go to Prof. Gopal Chandra Shit, Dr. Ranjan Sharma, Prof. Saibal Ray, Dr. Koushik Chakraborty and Dr. Kshetrimeyam Newton Singh for encouraging me

and offering me insightful comments, and stimulating discussions.

I am thankful to all my 'FR Sir Fan Club' friends especially Somi Akter, Bidisha Samanta, Monimala Mondal, Dr. Sayeed Ul Islam, Dr. Monsur Rahaman, Anikul Islam, Anupama Roy Chowdhury for all the discussions, academic support and friendship.

I have saved the best for the last. Finally I would like to thank my Ma, Jaba Laxmi Baskey and Baba, Sunil Baran Baskey, for showering me with all the love and support throughout my entire life. I would like to thank my sisters, Shilpi and Shaily for all the banters which turned out to be an excellent stress buster. I am extremely obligated to my Dadu, late Rupchand Hembram for all the knowledge, support and motivation that has inspired me to carry out research. A ton of thanks to my best friend Bhaskar for all the patience, love and support. My heartfelt thanks to my mother-in-law, Sovabati Tudu and brother from another mother, Swaraj, for all the support and motivation. Furthermore, I place my sense of gratitude to one and all who have helped me, directly or indirectly, throughout the process.

Place: Kolkata
Date: 4/9/23

Lipi Baskey

LIPI BASKEY

List of Publications in Journals

- Shyam Das, Farook Rahaman, Lipi Baskey, *A new class of compact stellar model compatible with observational data*, The European Physical Journal C **79** (2019) 853

- Shyam Das, Ranjan Sharma, Koushik Chakraborty, Lipi Baskey, *Anisotropic compact stellar model of embedding class-I satisfying Karmarkar's condition in Vaidya and Tikekar spheroidal geometry*, General Relativity and Gravitation **52** (2020) 101

- Shyam Das, Ksh Newton Singh, Lipi Baskey, Farook Rahaman, Anil Aria, *Modeling of compact stars: an anisotropic approach*, General Relativity and Gravitation **53** (2021) 25

- Lipi Baskey, Shyam Das, Farook Rahaman, *An analytical anisotropic compact stellar model of embedding class I*, Modern Physics Letters A **36(05)** (2021) 2150028

- Shyam Das, Koushik Chakraborty, Lipi Baskey, Saibal Ray, *A study on the effect of anisotropy under Finch-Skea geometry*, The Chinese Journal of Physics **82** (2023) 362

- Lipi Baskey, Saibal Ray, Shyam Das, Shreya Majumder, Ananya Das, *Anisotropic Compact Stellar Solution in General Relativity*, The European Physical Journal C **83** (2023) 307

- Lipi Baskey, Shyam Das, Ranjan Sharma, Farook Rahaman, *Impact of spacetime curvature on the physical behaviour of Vaidya and Tikekar (VT) type anisotropic compact objects*, submitted to New Astronomy

Conferences Attended

- Lipi Baskey, Farook Rahaman, *A simple anisotropic compact star model with Chaplygin Equation of State*, Webinar on Recent Advances in Applied Mathematics:Theory & Computation, University of Calcutta (2021)

- Lipi Baskey *Vaidya-Tikekar type stars in $f(R,T)$ gravity assuming Class I condition*, National Level seminar on Recent Development in Mathematics & its Application, K.K. Das College, Garia, Kolkata (2023)

Abstract

In the framework of the General Theory of Relativity, gravity is described in terms of space-time geometry and thus proper theoretical description of astrophysical systems under strong gravity is one of the key areas of recent research. Compact stellar objects which are the end stage of stellar evolution, act as *'natural laboratories'* and they provide extremely high gravity for testing the theory of general relativity. To study the physical properties of these objects several approaches have been adopted and these approaches are found to be compatible with physical observational data. Seeking exact solutions to Einstein field equations and developing physically viable models corresponding to compact stellar objects by incorporating pressure anisotropy, charge, electromagnetic field, etc., is the motivation for the present work. For the study of compact stars, one requires the equation of state (EoS) (relation between pressure and density) to explore the properties of a compact star by using the Tolman-Oppenheimer-Volkov (TOV) equation. At extreme conditions, in the absence of any information about particle interaction, one can adopt alternative approaches like physically reasonable geometry or the fall-off behaviour of density or pressure of the matter source.

The thesis focuses on developing analytical models of compact stellar objects in a spherically symmetric system by generating new classes of solutions assuming specific choices of anisotropy or geometrically inspired form of metric potential or employing additional con-

ditions on the metric potentials viz. Karmarkar condition. The mass-radius relationship, the stability of the obtained solution and the overall physical behaviour of such classes of solutions that describe compact stars have also been studied to test their acceptability as viable models.

The work is completely theoretical in nature but recently observed experimental data has been taken into account for validating the developed configurations.

Thesis Outline

The objective of the present work is to construct stable configurations which can describe static, spherically symmetric compact stellar objects. This thesis delves on finding exact solutions to the Einstein field equations and thus obtain some metric potentials assuming certain criteria that can be formulated to describe stable compact stellar configurations. The thesis has been organized in the following way:

- **Chapter 1:** A brief introduction to compact stars and the outline of the process to obtain stellar model is discussed in Chapter. 1. Some of the remarkable works on this particular arena have also been brought up to highlight the known available data for conducting this work.

- **Chapter 2:** Chapter. 2 focuses on finding a new class of closed-form solutions of the Einstein field equations for spherically symmetric, static, anisotropic matter distribution assuming a physically reasonable metric potential and a specific choice of the anisotropy. This class of solutions has been used to develop viable models for observed pulsars. A particular pulsar, $4\mathrm{U}1608-52$ having current estimated mass $(1.58^{+0.30}_{-0.29}\ M_{\odot})$ and radius $(9.8 \pm 1.8\ km)$ has been employed for testing the physical

acceptability of the developed model graphically. The stability of the model has also been discussed. Additionally, analyzing the mass-radius relationship for this model, the maximum mass is found to be $\approx 3.024 M_{\odot}$ corresponding to the radius $10.31\ km$.

- **Chapter 3:** Chapter. 3 presents a class of singularity free interior solutions assuming a physically reasonable metric potential and a specific choice of the anisotropy. The obtained solutions pass all the stability criteria for a compact stellar structure. This model assumes a maximum mass of $3.011\ M_{\odot}$ corresponding to the radius of $10.47\ km$. Moreover, comparing the results with a slow rotating configuration, the moment of inertia and the time period have also been argued.

- **Chapter 4:** Chapter. 4 investigates the solution of stellar structure assuming the Finch-Skea metric potential and thus establishes a configuration which is seen to fulfill all the criteria for a anisotropic compact star. The presented class of exact solutions to the field equations is observed after considering the corresponding two cases: (i) the positive value of the anisotropic parameter, and (ii) the absence of any anisotropy. Along with the stability criteria, the density variation parameter, ratio of the density at the surface to that at the center, is also observed for the model.

- **Chapter 5:** The well known metric, Vaidya-Tikekar ansatz has been considered to study the anisotropic model of a compact star in Chapter. 5. Additionally the polytropic-type equation of state $p_r = k\rho^{1+\frac{1}{n}} - \beta$ has been assumed to develop the model. The model has been studied mathematically as well as graphically for the polytropic index $n = 1$. However, for $n = 2$, this model fails to represent any viable relativistic compact stellar configuration. Chapter. 5 emphasizes on the impact of the spheroidal curvature parameter K on the stellar structure in view of the relevant physical parameters and on the mass radius relationship. It is found that with

the decrease of the curvature parameter, the basic physical properties of the structure increase.

- **Chapter 6:** Chapter. 6 examines the stellar model using embedding class I Karmarkar's condition. This chapter investigates two models corresponding to spherically symmetric, static, anisotropic stellar candidates. Assuming special form of Buchdahl ansatz and plugging in the class I condition, the stellar configuration for the Model I has been obtained. This model is found to fulfill the physical properties and the stability criteria. The model exhibits the linear equation of state and the maximum mass possessed by the model is found to be $\approx 4.6\ M_{\odot}$.

  Model II represents a class of solutions for a spherically symmetric, anisotropic matter distribution in Vaidya and Tikekar spheroidal geometry. Co-dependency of the metric potential comes from the Karmarkar's condition. The obtained solution has been checked for its stability and acceptability. The dependence of the curvature parameter K of the model, which characterizes a departure from homogeneous spherical distribution, is also investigated.

- **Chapter 7:** Chapter. 7 discusses the concluding remarks on the entire thesis. Additionally the future prospects based on the present work have also been addressed.

It is to be noted that each chapter is self-consistent. Therefore, the end of each chapter consists of corresponding conclusion remarks, discussions and perspectives.

Farook Rahaman 4.9.23

DR. FAROOK RAHAMAN
Professor
Department of Mathematics
JADAVPUR UNIVERSITY
Kolkata - [illegible] INDIA

Shyam Dey 4/9/23

Associate Professor in Physics
Malda College,
Malda

Lipi Baskey 4/9/23

Contents

List of Figures

List of Tables

Chapter 1

Introduction

1.1 From birth to death: a journey of stars

In the dense molecular clouds of gas located in the arm of galaxies, there lies the birthplace of the stars. Like the beautiful chain of life: these '*dusty*' molecular clouds are formed in the cool surfaces of 'super-giants', massive stars in the late stage of stellar evolution. Since the cloud interior is guarded against ultraviolet starlight due to the dust, the core interior of the molecular cloud eventually becomes cooler. Inside these dense clouds, massive turbulence are formed which makes these dense structures to collapse under their gravitational forces. These happen as the gas and the dust within the clouds give rise to knots with sufficient mass. These dense regions in the clouds collapse to form *"protostars"*, the hot core of collapsing clouds eventually forming a star. The source of energy for its *"life"* is gravitational energy which is converted to heat by compression. In the state of quasi-hydrostatic equilibrium, the temperature and the thermal pressure gradient approximately balance the gravity. Once the *"protostars"* are contracted enough, due to the energy loss by the radiation at its surface, the core temperature rises to a point of ignition so that it can

burn hydrogen to helium. Afterward, fusion takes the place of being the dominant source of energy, and the gravity of the whole *'structure'* is then balanced by the thermal and the radiation pressure till the timescale becomes approximately to the inverse square of the stellar masses. These *"protostars"* then convert to the *"main sequence"* stars. About 90 percent of the stars in the universe, including the Sun, are main sequence stars.

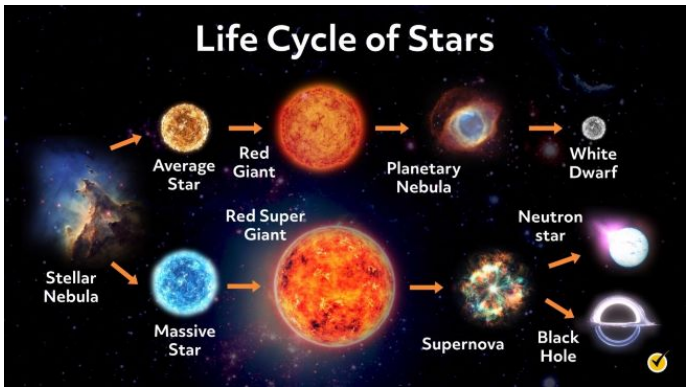

Figure 1.1: A schematic representation of the life cycle of stars: from nebula to compact star. Fig Courtesy: Mometrix

When the nuclear fuel runs out, these luminous stars *"die"* thus forming Compact stars, term that broadly describe white dwarfs, neutron stars, black holes etc. Fundamentally compact stellar objects are different from the normal stars in two ways: first of all, since there is no remaining nuclear fuel left to burn, they cannot generate thermal pressure to support themselves against the gravitational collapse. Instead, white dwarfs are supported by the pressure of degenerate electrons while neutron stars are supported largely by the pressure of degenerate neutrons. Furthermore, Black holes are completely collapsed stars and these structures are so dense that they could not find any means to hold back the inward pull of gravity and therefore collapsed to singularities. Secondly compared to any normal stars with similar masses, compact stellar objects have exceedingly small radii and hence,

much stronger gravitational fields on the surface (Shapiro and Teukolsky, 1983). Masses of the progenitor stars define the nature of these end products of stellar evolution. Studies suggest that the white dwarfs are originated from light stars with masses $\leq 4M_{\odot}$ while the neutron stars and the black holes originate from more massive stars.

1.2 Revisiting compact stars

1.2.1 White and Black Dwarfs

For any stars with masses upto few solar masses, contraction begins when hydrogen is depleted in the core, triggering next layer of helium to burn. With the increase of the temperature the envelope begins to expand while the core continues to contract and heat up, hence forming the red giant. For most of the red giants the envelope becomes unstable, resulting in the spectacular event of the planetary nebula - expanding and ejecting glowing shell of ionized gas (Glendenning, 1997).

Depending on the layer of the red giants up to which the impact of the reactions have reached, the remaining stellar core is left mostly with helium, carbon and, or oxygen. Since the instability of the structure removed the compressing weight of the bulk of the star, the combustion temperature fails to maintain its configuration with its sufficient mass and thus get contracted forming a white dwarf. White dwarf appears white, hence the name, because of its extremely high surface temperature of about 8000 K. But among all compact objects, white dwarfs are pretty big in their structures with the radius of few thousand kilometers and density of the order of 10^6 of that of the Earth (the density of the Earth is $5.513\ gm/cc$ and that of the Sun is $1.408\ gm/cc$). Interestingly white dwarfs radiate their

residue from the hot surface, making the surface cooler and eventually crystallizing and then disappearing as black dwarfs. Mass of the largest known white dwarf is $1.52M_{\odot}$(WD $1143 + 321$) and that of the smallest one being $0.33M_{\odot}$ (WD $0349 + 27$), although on an average, masses of white dwarfs are sharply peaked around $0.6M_{\odot}$. Nearest known white dwarf *Sirius B* possesses the mass of $1.053 \pm 0.028M_{\odot}$.

Figure 1.2: Planetary Nebula NGC2440 sheathing one of the hottest known white dwarfs. Fig Courtesy: H. Bond (STScI), R. Ciardullo (PSU), WFPC2, HST, NASA.

1.2.2 Neutron Star

Since the stellar evolution of the progenitor stars of higher mass is much more motivated by the gravity than that of the lower mass progenitor stars so the thermonuclear process is much more intense for the former case making the star even more hotter until it expands into a super red giant of radius $> 10^8$ km. Since the burning happens up to the iron core and thus gravity crushes the core making the degenerate non relativistic electrons relativistic and support the structure against the gravitational collapse.

Extremely hot core now approaching towards its collapse under the consequence of its neutronization. Now the region above the core is no longer supported by the core and a decompression wave travels outward in the diffused state of red giants at the speed of the light. These give rise to free fall of the material which meets the stalled shock-front only to create an accretion shock. The enormous density core along with this accretion shock create a bubble like region. These complex processes of neutrino heating allow small fraction of such immense gravitational binding energy to provide the kinetic energy to form something exceptionally beautiful - the supernova explosion which ejects almost all the bubble structure leaving out only the collapsed hot core or the *'protoneutron'* star. Cooling from a temperature of tens of MeV to an MeV, the collapsed core reaches a final equilibrium (Burrows and Lattimer, 1986), which creates an amalgamation of neutrons, protons, quark, hyperons and leprons. This structure is known as neutron star, a structure of the radius of merely ten kilometers and density of 10^{14} times that of the Earth.

Observation of supernova started way early in the year 1054 AD and the appearance of the Crab Nebula supernova was mentioned in Sung-shih [Annals of Sung dynasty] (Astronomical Treatise, Chapter 56). Yang Wei-te, Director of the astronomical bureau in the Sung empire, wrote, "I humbly observe that a guest star has appeared. Above the star in question there is a faint glow, yellow in colour". Theoretically the notion of the neutron star was first conceived by Walter Baade and Fritz Zwicky at Caltech in December 1933, shortly after the discovery of the neutrons by Chadwick. Interestingly, Lev Landau introduced the concept of the neutron star even before its discovery. While discussing the discovery of the neutrons, Landau suggested that these *'unheimliche Sterne'*, weird stars, would be invisible and unknown unless they collide with visible stars when they would originate explosions, which might be supernovae (Yakovlev et al., 2013). These extremely dense core objects act

as the natural laboratories to study the nature and the structure of these stars as such high densities can not be produced in any terrestrial laboratories.

Theoretically the structure of compact stellar objects are first thoughtfully considered by three pioneers, Oppenheimer and Volkoff (Oppenheimer and Volkoff, 1939) and Tolman (Tolman, 1939) where they first derived the mathematical equation of the relativistic structure of compact stellar objects and found a stable configuration of radius 10 km and mass $0.75\ M_{\odot}$ approximately. A new era of observational astronomy emerge with the discovery of pulsar by Anthony Hewish and his doctoral student Jocelyn Bell at the Mullard Radio Astronomy Observatory in 1967. Fascinatingly, Hewish had designed a large phased array radio telescope and auxiliary equipment with a short time response and an extended observing routine primarily for observing interplanetary scintillation. His then student, Bell noticed a "bit of scruff" on her data for three months that was later identified as persistent periodic source, rapidly rotating neutron star. Thus the discovery of PSR B$1919 + 21$ with the pulse period of 1.337 seconds. Bell had detected a very small source of the pulsating radio signal outside the solar system and this trailblazer work got published in Nature (Hewish et al., 1968).

The Crab and Vela pulsars were discovered afterward although the observation of the Crab pulsar were dated back to 1054. Soon the large surveys of 1970s gave us 250 more pulsars. As of today more than 2000 pulsars have been discovered. Pulsars are of two types depending on its 'blinking': the slow pulsars rotate on the order of once per second while the millisecond pulsars rotate hundreds of times per second. Till now the fastest known pulsar PSR J$17448 - 2446$ad, discovered on 2004, have observed to rotate 716 times per second.

The pulsars are observed under a variety of circumstances such as they can be observed as the isolated stars, sometimes they are found in a binary orbit, in a X-ray binary system and perhaps in any γ-ray busters and soft gamma ray repeater (Rothchild et al., 1994). The advancement of X-ray, gamma-ray and radio telescopes have helped to accelerate the observational study of compact stars, the recent addition being India's first dedicated multi wavelength space telescope, Astrosat. Now to dig deeper into the behaviour of these dense compact stellar objects, it is quite reasonable to investigate all the astrophysical laws within the framework of the General Theory of Relativity.

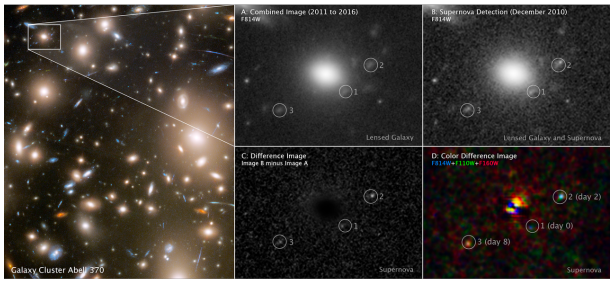

Figure 1.3: NASA's Hubble Space Telescope captures the three moments of supernova explosion from a far-off galaxy cluster Abell 370. Credits: SCIENCE: NASA, ESA, STScI, Wenlei Chen (UMN), Patrick Kelly (UMN), Hubble Frontier Fields.

1.2.3 Black Holes

The protoneutron star obtained from supernova explosion, continues to cool down for millions of years. The slow diffusion of photons to the surface and their radiation into the space manifest the process of cooling down of a 'star'. During this process of cooling down, neutron star exhausts the nuclear fuel in its core and eventually collapses under its own gravity.

This happens when the mass of the star exceeds the limiting mass (maximum mass required for a relativistic structure to remain stable against its gravity). Thus the progenitor star immediately collapse to a black hole in a supernova explosion and its mass being about that of the star before the supernova. Black holes of approximate mass of $8\ M_{\odot}$ to $50\ M_{\odot}$ are created in this process. This happens when the mass becomes larger than the maximum mass supported against the collapse by the pressure of degenerate neutrons and their interactive behaviour. Masses of black holes vary as after the black hole is born, it continues to enlarge as it engrosses mass from its surroundings. Another type of collapsed star can

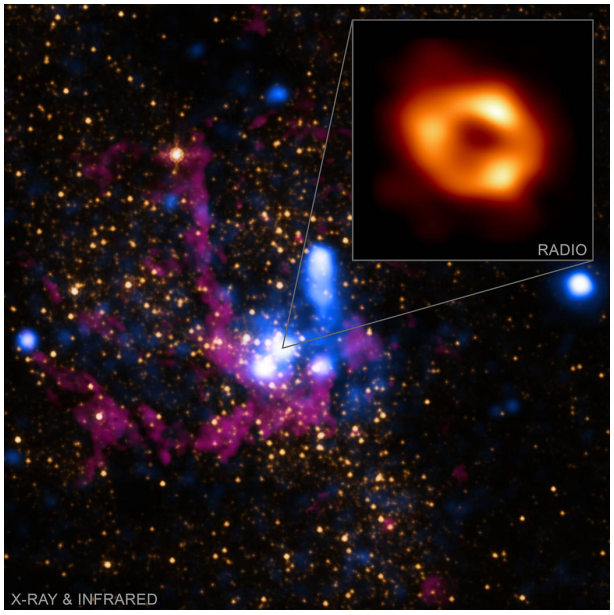

Figure 1.4: X-ray data from Chandra X-ray Observatory (blue) depicting hot gas that was blown away from massive stars near the black hole. Two images of infrared light at different wavelengths from NASA's Hubble Space Telescope show stars (orange) and cool gas (purple). These images are seven light years across at the distance of Sagittarius A* (supermassive black hole in the center of the Milky Way galaxy and 27000 light years from Earth). A pull-out shows the new Event Horizon Telescope image, which is only about 1.8×10^{-5} light years across (0:000018 light years, or about 10 light minutes).(Credit: X-ray: NASA/CXC/SAO; IR: NASA/HST/STScI. Inset: Radio (EHT Collaboration)).

be found where the collapse is delayed after the formation of a protoneutron star and its

ejection in a supernova. This retarded collapse occurs due to the process of hyperonization where the pressures obtained from neutrons and protons are reduced due to the conversion to hyperons (Glendenning, 1982, 1985). Hyperonization occurs to relieve the high pressure of the nucleons and achieve a lower energy of dense neutron star matter (Glendenning, 1995). This type of collapse may occur when the mass of the protoneutron star is close to that of the limiting mass even if the supernova ejects most of the progenitor star.

This process forms black hole of around $\sim 1.5\ M_{\odot}$. Similar masses of black holes can also be formed in the slow process of accretion-induced collapse of the neutron stars in the binary system where the higher dense star accrete matter from the less dense companion star surplussing its Eddington limit and eventually collapsing to a black hole. Eddington limit defines the maximum luminosity a body can achieve to balance the gravity acting onto itself with the outwards radiation. Extremely dense black holes are usually the final point in the evolution of a star. However there are another type of black holes that are giant whirlpools of active galactic nuclei and can be formed due to the condensation of the dense star clusters (Ipser, 1969).

These objects are so dense that even the light cannot escape from their gravity and hence observational studies on these objects require detecting their impact on surrounding matters. These type of astrophysical objects with strong gravitational fields were first considered by John Michell and Pierre-Simon Laplace in the 18th century (Montgomery et al., 2009). However for the sake of the present work the discussions on the black holes are kept short.

1.3 Brief discussions on the Theory of General Relativity

The theory of gravitation, discovered by Albert Einstein in the year 1915, describes the change of geometry of spacetime with respect to the matter and the energy. The *'story'* of the theory of relativity traces back to over two thousand years. The ancient Greek philosophy describes the space and the time to be absolute, that all velocities can be measured relative to an absolute rest frame. Galileo changed the concept which lead to the Newtonian mechanics and that suggested that although time remains absolute, one should always consider the spatial measurements as measurements relative to some fixed frame (known as the coordinate system). Later mid and late nineteenth century saw the wave phenomena in Maxwell's Theory considering the light propagation. Until now the existence of a medium, *aether* (Greek for upper air) is assumed in which the light is moving. Also the presence of an *aether* implies that there exists a preferred motion of an observer, namely the one in which she stays at rest with the medium (Samuelsson, 2003). The famous experiment by Michelson and Marley in 1887 supports this fact. Even Lorentz also suggested in favour of the existence of the *aether* by introducing an ad hoc transformed time such that along the motion the *aether* would contract objects thus cancelling the effect of the variable speed of light. Later Einstein postulated that the speed of light is a universal constant, does not depend on the motion of the observer. This postulate gives rise to the Special Theory of Relativity from where Einstein derived the Lorentz transformations and introduced a unified theory of the electromagnetism and mechanics. Since Lorentz transformation also transforms time, so that means one cannot define time universally. Instead time cannot be separated from the space, thus introducing the space-time.

The limitation of the applicability of the Special Relativity for any accelerated system

leads to the General Theory of Relativity. By assuming Weak Equivalence Principle, Einstein suggests that if one considers any two system, one in a static uniform gravitational field and one in a uniform accelerated motion with respect to the first, the laws of physics are unable to distinguish them. Thus time will flow faster in the gravitational field and this phenomena is known as the gravitational redshift. Furthermore, Einstein wrote series of four papers in the relativistic theory of gravitation, fourth paper provides the formulation of the General Relativity (Mehra, 1998). Essentially Strong equivalence principle ("*The laws of physics are same in all inertial frames* ") forms the foundation for the general theory of relativity. A striking consequence of the equivalence principle is that the geometry of spacetime cannot be flat, that is general relativity is a theory of the curved spacetime.

Essentially Einstein's general relativity depicts gravity as the deformation of the spacetime and the paths followed by the particles under the gravity are called geodesics. The theory of General Relativity qualified all the Solar System tests (Everitt et al., 2011; Will, 2006) and to describe extremely dense compact stellar objects for which the gravity is so intense, the theory of General relativity is very crucial.

1.4 Exact solutions of the Einstein field equations

Einstein field equations, which relate the local spacetime curvature (expressed by the Einstein tensor) with the local energy, momentum and stress within that spacetime (expressed by the stress energy tensor) have been expressed in the tensor form as

$$G_{\mu\nu} = \frac{8\pi G}{c^4}\mathcal{T}_{\mu\nu}, \tag{1.1}$$

where

$$G_{\mu\nu} = \mathcal{R}_{\mu\nu} - \frac{1}{2} g_{\mu\nu} \mathcal{R}, \tag{1.2}$$

is the Einstein curvature tensor, $\mathcal{R}_{\mu\nu}$ is the Ricci curvature tensor, $\mathcal{R} = g^{\mu\nu}\mathcal{R}_{\mu\nu}$ is the Ricci scalar, $g_{\mu\nu}$ is the metric tensor and $\mathcal{T}_{\mu\nu}$ is the stress-energy tensor. Here the gravitational constant G in C.G.S. unit is given by $6.67 \times 10^8\ dyne\ cm^2 gm^{-2}$ and the speed of the light in vacuum c is $2.9979 \times 10^{10}\ cm/s$. The Einstein field equation comprises of a set of *ten* non-linear second order partial differential equations. Furthermore symmetric Einstein tensor has an identically vanishing covariant divergence known as Bianchi identity and it is given by $\nabla^{\mu} G_{\mu\nu} = 0$, which reduces the number of independent equations to *six*.

The 4-dimensional spacetime associated with the spatial or temporal interval is described by the metric $g_{\mu\nu}$ as

$$ds^2 = g_{\mu\nu} dx^{\mu} dx^{\nu}, \tag{1.3}$$

where $\mu, \nu = 0, 1, 2, 3$. The curvature of space-time can be described by the Riemann tensor as following,

$$\mathcal{R}^{\alpha}_{\beta\mu\nu} = \partial_{\mu}\Gamma^{\alpha}_{\beta\nu} - \partial_{\nu}\Gamma^{\alpha}_{\beta\mu} + \Gamma^{\alpha}_{\mu\lambda}\Gamma^{\lambda}_{\beta\nu} - \Gamma^{\alpha}_{\nu\sigma}\Gamma^{\sigma}_{\beta\mu},$$

where the Christoffel symbols, which represent gravitational forces, are defined by,

$$\Gamma^{\alpha}_{\mu\nu} = \frac{1}{2} g^{\alpha\beta}\Big(\partial_{\mu} g_{\nu\beta} + \partial_{\nu} g_{\beta\mu} - \partial_{\beta} g_{\mu\nu}\Big).$$

The Christoffel symbols describe how the metric potential varies throughout spacetime so that the objects can accelerate. The Ricci scalar and Ricci tensor are obtained from the

Riemannian tensor from contraction as,

$$\mathcal{R}_{\alpha\beta} = \mathcal{R}^{\lambda}_{\alpha\lambda\beta}, \quad \text{and} \quad \mathcal{R} = \mathcal{R}_{\alpha\beta} g^{\alpha\beta}.$$

Now one can choose the spatial coordinates as $x^0 = t,\ x^1 = r,\ x^2 = \theta,\ x^3 = \phi$ and obtain the line element in the most general form as,

$$ds^2 = -A(r)dt^2 + B(r)dr^2 + C(r)r^2(d\theta^2 + \sin^2\theta d\phi^2). \tag{1.4}$$

Without loss of the spherical symmetry, one can also write the line element in many ways. It is written by doing $C(r) \equiv 1$ and one can write,

$$ds^2 = -e^{2\nu(r)}dt^2 + e^{2\lambda(r)}dr^2 + r^2(d\theta^2 + \sin^2\theta d\phi^2), \tag{1.5}$$

$\nu(r)$ and $\lambda(r)$ being the functions of r only.

Now the stress-energy tensor $\mathcal{T}_{\mu\nu}$ for an anisotropic fluid matter distribution can be describe as

$$\mathcal{T}_{\mu\nu} = \begin{pmatrix} \rho & 0 & 0 & 0 \\ 0 & -p_r & 0 & 0 \\ 0 & 0 & -p_t & 0 \\ 0 & 0 & 0 & -p_t \end{pmatrix}, \tag{1.6}$$

where ρ represents the energy-density, p_r and p_t, respectively denote fluid pressures along the radial and transverse directions of the fluid. The fluid four-velocity $\mathbf{u}$ is comoving and is given by $u^a = A_0^{-1}(r)\delta^a_0$.

In the presence of the strong gravitational fields, exact models of compact stars which are described by the spherically symmetric gravitational fields in static manifolds, require

to obtain the solution for the Einstein (uncharged) and Einstein-Maxwell (charged) system of field equations. The concept of compact stellar models have skyrocketed since Karl Schwarzschild first obtained the solution for the Einstein's field equations assuming fixed fluid density in 1916. The first solution to the Einstein's field equation is obtained by Schwarzschild. This exterior solution (Schwarzschild, 1916b) describes the geometry of a gravitational field outside a static spherically symmetric stellar structure. This solution is decisive as it plays important role in examining classic relativity tests (d'Inverno, 1992; Wald, 1984). To describe the interior of a spherically symmetric static structure, the Schwarzschild interior solution (Schwarzschild, 1916a) was the first and is a good approximation for a dense star in which the pressure is not too large. The interior and exterior Schwarzschild solutions together provided the first complete relativistic descriptions of the matter distribution and the spacetime geometry for a static star (Takisa, 2013).

Additionally for the case of a spherically symmetric non-rotating, charged star, the static solution to Einstein-Maxwell field equations is given by Reissner-Nordström solution (Nordström, 1918; Reissner, 1916). This solution describing unique exterior metric reduces to Schwarzschild exterior solution in the limit of vanishing electromagnetic field. Several studies have been conducted for obtaining the exact solution for interior charged perfect fluid. Furthermore, for the case of uncharged rotating black hole, the exact solution is given by Kerr (Kerr, 1963) and it suggests that this metric be interpreted as that arising from a spinning particle. The extension for this solution is given by Kerr-Newman metric (Newman and Janis, 1965) where it describe a spherically symmetric charged rotating black hole.

This work however focuses only on the closed form exact solutions of Einstein field

equations describing spherically symmetric, static, uncharged structures. A noteworthy number of exact solutions that represent static, uncharged interior solutions, have been investigated over the years. Considering the dynamical stability of isotropic spheres as an eigenvalue problem, Chandrasekhar (Chandrasekhar, 1964a) used an analytical approach to compute the eigen frequencies of the radial oscillations for the isotropic spherical stars. The study of the stability of a star then converted to a Sturm-Liouville problem. In the presence of a gravitational field, Vaidya (Vaidya, 1951) discovered the first radiating solution to the Einstein field equations that describes the radial flow of coherent null radiation. Since then several studies have been conducted to obtain the exact solutions to the field equations. Generalizing the Schwarzschild interior solution, a new exact solution of Einstein's equations is derived by Kuchowicz (Kuchowicz, 1975) which describes relativistic spheres with a finite density increase toward the centre. Details of these solutions are given by Stephani et al (Stephani et al., 2003). Some of the exact solutions can be found in the work of Finch (Finch, 1987) and from an unpublished work by Finch-Skea (Hernàndez and Nùñez, 2004) among others. Interestingly not all exact solutions can be accepted to describe spherically symmetric static stable structures. Acceptability of these obtained exact solutions are then studied rigorously by several researchers. Delgaty and Lake (Delgaty and Lake, 1998) developed a list of 127 candidate solutions describing isolated, static spherically symmetric perfect fluid. One fascinating thing to note that out of these only 16 solutions are found to fulfill the descriptions of bounded stellar structures and even meager 9 have the monotonically decreasing sound speed against the radial coordinate. These solutions are constructed by considering isotropy of the pressure of the structures. Additional assumptions being (i) regularity at the origin (ii) positive definiteness of the central density and the central pressure (iii) vanishing nature of the pressure at the stellar boundary (iv) monotonically decreasing density and pressure towards the surface and (v) the subliminal sound speed.

It was initially believed that the pressure inside the stellar interior are isotropic and thus the investigations were limited to the locally isotropic systems. However there are mainly three major astrophysical problems that isotropy fails to justify - the properties of the superdense matter, the details of the gravitational collapse (Thorne, 1971) and the nature of the quasars (Zeldovich and Novikov, 1972). Maximum mass determined from the equation of state (relationship between pressure and density) described by isotropy suggests that it can escape gravitational collapse. To get rid of this problem, anisotropy in super dense objects are considered. Moreover, Maurya et. al (Maurya et al., 2018c) suggested that due to the highly relativistic interaction among the particles which becomes too random to maintain any uniform distribution inside the structure, chances of possessing anisotropy is much more usual than the isotropic pressure. This relativistic nature of the particles in compact star could be one of the possible reason for giving birth to significant anisotropy inside the star. The anisotropy implies unequal principal stresses where the radial pressure is taken different from the transverse component of the pressure. It is therefore understood that the anisotropic force inside the star makes compact stellar object more compact than the isotropic condition which eventually makes possible transition of a neutron star to strange star (Maurya et al., 2018c). Equality of the transverse components of pressure ensures the spherical symmetry of the model (Dev and Gleiser, 2002). Even it is observed that in extremely high density regime ($10^{15}\ gm/cc$) anisotropy may develop (Ruderman, 1972). Another plausible explanation for the occurrence of anisotropy is the solid core in these high density structures (Canuto and Chitre, 1973). Within the density range of $4 \times 10^{14} - 3 \times 10^{15}\ gm/cc$, a solid state may indeed occur for cold matter (Canuto, 1974). Kippenhahn and Weigert (Kippenhahn et al., 2012) have observed that the existence of a solid core or type 3A superfluid in the star might generate anisotropy. Various

reasons are being pointed out by the researchers as the origin of anisotropy inside compact stars. Anisotropy can develop in the core of compact stars due to exotic phase transition at extreme density (Sokolov, 1980). Jones (Jones, 1975) predicted the presence of type II superconductor inside compact stars leading to the anisotropy of stress tensor. Pion condensation (Sawyer, 1972) is also identified as the possible cause of anisotropy. Liebling and Palenzuela (Liebling and Palenzuela, 2012) have shown that a scalar field in a Boson star may give rise to anisotropy. However, for review of the local anisotropy, one can look into the study conducted by Herrera and Santos (Herrera and Santos, 1997).

Several literature can be found on obtaining stellar solution of the field equations considering the anisotropic pressure. Some of the literature being: considering one metric potential in the form of Duragapal and Fuloria (Durgapal and Fuloria, 1985) and another one in the form of Lake (Lake, 2003), Maurya et al. (Maurya et al., 2015c) have obtained an anisotropic analog of the Durgapal and Fuloria (Durgapal and Fuloria, 1985) perfect fluid solution. Using Buchdahl ansatz (Buchdahl, 1959) and Lake (Lake, 2003) ansatz, Maurya et al. (Maurya et al., 2017) have studied new anisotropic stellar models. In the framework of general relativity, a class of new relativistic solutions describing anisotropic matter distribution for compact stars have been studied establishing a relation between metric potentials using class I Karmakar's condition and thus generating a specific form of mass function by Maurya et al. (Maurya et al., 2018a). Assuming the density profile suggested by Mak and Harko (Mak and Harko, 2002), a singularity free solution of the Einstein's field equations for spherically symmetric, static and anisotropic compact stellar objects is studied by Deb. et al (Deb et al., 2017). A relativistic, anisotropic stellar model has been proposed for quintessence stars and a quintessence dark energy having a characteristic parameter $\omega_q \in (-1, -\frac{1}{3})$ by Kalam et al. (Kalam et al., 2014). Kalam et al. (Kalam et al.,

2013a) have developed a well behaved star model and showed that central density depends on the anisotropic factor. For recent investigations, there have been important efforts in describing the relativistic stellar structure. A new class of exact solutions of Einstein's field equations depicting anisotropic matter distribution on pseudo-spheroidal spacetime is studied by Ratanpal et al. (Ratanpal et al., 2016). A singularity free solution describing neutron stars with a core layer having quark matter satisfying the MIT-bag equation of state (EoS), meso layer with Bose-Einstein condensate (BEC) matter satisfying modified BEC EoS and an envelope having neutron fluid and Coulomb liquids satisfying quadratic EoS have been obtained by Bisht et al. (Bisht et al., 2021). Assuming conformal symmetry, which generates an integral relationship between the metric potentials, Takisa et al. (Takisa et al., 2017) have studied spherical, anisotropic stellar models. The algorithms for obtaining solutions of the Einstein field equations via single monotone functions in closed form had already been discovered by several authors (Herrera et al., 2008; Lake, 2003; Maurya et al., 2019a; Thirukkanesh et al., 2018).

Chapter 2

A new class of stellar model compatible with recent observational data

2.1 Introduction

The key to deeply understand the physical properties of any astrophysical compact objects, its general rules and dependencies, approximate relations etc., simple stellar models need to be observed (Kippenhahn et al., 2012). Although numerical programmes compute stellar models much more accurately but one cannot disregard the importance of theoretical observations. The ongoing advances in observational study of these ultra-dense configurations of theoretical astrophysics have unveiled the mask of several characteristics of the relativistic compact stellar structures (Errehymy et al., 2019). Under the chassis of general relativity, this examination of properties and exact constitution of compact stellar spheres is of utmost relevance. This chapter emphasize on obtaining exact solutions in closed form that describes static, spherically symmetric structure that assumes the anisotropic pressure.

Static stellar systems like white dwarfs, which are supported against their gravity by Fermi pressure of degenerate electrons, possess maximum mass of upto $1.4\ M_{\odot}$ with the radii upto 5000 km, mean densities of around $10^{7}\ gm\ cm^{-3}$ and surface potential $\frac{GM}{Rc^{2}} \approx 10^{-4}$ (Errehymy et al., 2019). On the other hand neutron stars are supported by the Fermi pressure of degenerate neutrons against their gravity. It was believed that they can support maximum mass of $1.4 - 3\ M_{\odot}$. Even there was a firm theoretical upper limit of $3.2\ M_{\odot}$ (Rhoades and Ruffini, 1974) for a neutron star. Mean densities of neutron stars revolve around few times of $10^{15}\ gm\ cm^{-3}$ and it is larger than normal nuclear density $\rho_{nuclear} = 2.8 \times 10^{14}\ gm\ cm^{-3}$ which corresponds to a number density of $n_0 = 0.16$ baryons fm^{-3} ($1\ fm = 10^{-13}\ cm$), central baryon number density might reach $n_c \approx 1\ fm^{-3}$ (EKSÌ, 2016). Considering fully relativistic anisotropic superdense neutron star models, Heinzmann and Hillebrandt (Heintzmann and Hillebrandt, 1975) have established that there is no limiting mass of a neutron star for arbitrarily large anisotropy. However, the maximum mass of the neutron star ranges upto $3 - 4\ M_{\odot}$. Also it was found that the stability of fully relativistic anisotropic neutron star are just like that are obtained in isotropic models (Hillebrandt and Steinmetz, 1976). Interestingly just more than two decades ago Durgapal and Fuloria (Durgapal and Fuloria, 1985) obtained an analytic relativistic model where they have showed that the model supports all the tests for neutron stars. For the sound speed ≤ 1, the maximum mass for their model supports $4.17 M_{\odot}$ with the surface and central redshifts of 0.63 and 1.60 respectively.

Several anisotropic models have been investigated by incorporating aniostropic pressure in the stress-energy tensor of the material composition. From known isotropic solution, heuristic procedure is developed to obtain interior solution of Einstein's solution (Cosenza et al., 1981). Taking into the consideration of the generalization of $P = \alpha\rho$ solutions,

where the pressure is anisotropic, various analytic solutions and effect of anisotropy on the solutions are studied (Bayin, 1982). Modifying four well known Tolman solutions (viz. III, IV, V and VI), another four solutions for anisotropic matter are worked out in the framework of general relativity (Krori et al., 1984). The link between the value of the potential at the surface and the highest occurring ratio of the pressure tensor to the local density are examined in anisotropic structure (Bondi, 1992). For the stability of the anisotropic structure, it is found (Chan et al., 1993) that small difference of tangential pressure from the radial one might in principle lead to drastic change of the stability of the system. This result have further been used to extend the Jeans instability criterion in Newtonian gravity to systems with anisotropic pressures (Herrera and Santos, 1995).

By introducing an algorithm, new exact solutions of an anisotropic fluid distribution considering uniform energy density have proposed by Maharaj and Maartens (Maharaj and Maartens, 1989). Utilizing the Maharaj and Maartens algorithm, Gokhroo and Mehra (Gokhroo and Mehra, 1994) and Chaisi and Maharaj (Chaisi and Maharaj, 2005, 2006) have developed and studied new anisotropic fluid models. Several studies on anisotropic compact star models (Mak and Harko, 2003) have been conducted in the recent times. Upper limits for the mass-radius ratio are derived for compact general relativistic objects in the presence of a cosmological constant (Mak et al., 2000) and in the presence of a charge distribution (Mak et al., 2001). Dev and Gleiser (Dev and Gleiser, 2002) presented several exact solutions for anisotropic stars of constant density. It is shown that pressure anisotropy can have significant effects on the structure and properties of stellar objects and the maximum value of $\frac{2M}{b}$ can approach to unity ($\frac{2m}{b} < \frac{8}{9}$ for isotropic objects) and the surface redshift can be arbitrarily large. Assuming fixed form of density and using the Newtonian equation of hydrostatic equilibrium for an isotropic fluid sphere. Lake (Lake, 2009) has generated

exact anisotropic solutions of Einstein's equations. Thomas and coworkers have proposed models of gravitationally bound systems in equilibrium with an anisotropic fluid distribution: a core-envelope model for superdense matter distribution with the feature — core consisting of isotropic fluid distribution and envelope with anisotropic fluid distribution — is studied on the background of pseudo-spheroidal spacetime (Thomas et al., 2005), a core-envelope model for superdense matter distribution with the feature- core consisting of anisotropic fluid distribution and envelope with isotropic fluid distribution is reported on the background of pseudospheroidal space-time (Tikekar and Thomas, 2005). The non-adiabatic gravitational collapse of a spherical distribution of matter accompanied by radial heat flux has been studied on the background of a pseudo-spheroidal space–time where the spherical distribution is divided into two regions: a core consisting of anisotropic pressure distribution and an envelope consisting of isotropic pressure distribution (Thomas and Ratanpal, 2007). Assuming a linear EoS, Sharma and Maharaj (Sharma and Maharaj, 2007) have provided an exact analytic solution for the anisotropic matter distributions. Thirukkanesh and Maharaj (Thirukkanesh and Maharaj, 2008) have also analyzed an anisotropic fluid distribution to obtain a new class of exact solutions. For example, using the Finch and Skea (Finch and Skea, 1989) ansatz for the metric potential g_{rr}, Sharma and Ratanpal (Sharma and Ratanpal, 2013) have reported a static, spherically symmetric anisotropic star model which admits a quadratic EoS. Pandya et al. (Pandya et al., 2015) have developed a new class of solutions of static spherically symmetric anisotropic system by generalizing the Finch and Skea ansatz. The model proposed by Sharma and Ratanpal (Sharma and Ratanpal, 2013) is a sub-class of the solutions provided by Pandya et al. (Pandya et al., 2015). Bhar et al. (Bhar et al., 2015) studied the static spherically symmetric relativistic anisotropic stellar structure considering the Tolman VII solution as one of the metric potentials. A new anisotropic model of a strange star admitting the Chaplygin

equation of state was proposed by Bhar (Bhar, 2015a). This chapter generates a new class of solution describing static, spherically symmetric structure assuming specific choice of anisotropy.

This Chapter is organized as follows: the solution for the exact field equations is obtained in Sec. 2.2, the mass-radius relationship for the model assuming a specific surface density is discussed in Sec. 2.3. Smooth matching of the structure at the boundary and thus obtaining the model constants are discussed in Sec. 2.4. Compatibility around the known pulsar $4\mathrm{U}1608-52$ is discussed in Sec. 2.6. The stability analysis of the obtained solution have been examined in Sec. 2.7. Finally Sec. 2.8 consists of the concluding remarks.

2.2 Formation of the model

The line element describing the interior space-time of a spherically symmetric star in Schwarzschild (t, r, θ, ϕ) coordinates is expressed as

$$ds^2 = -A_0^2(r)dt^2 + B_0^2(r)dr^2 + r^2(d\theta^2 + \sin^2\theta d\phi^2), \tag{2.1}$$

where, $A_0(r)$ and $B_0(r)$ are the gravitational potentials. For the anisotropic matter distribution of the stellar interior, the energy-momentum tensor can be described in the form

$$T_{\alpha\beta} = (\rho + p_t)u_\alpha u_\beta + p_t g_{\alpha\beta} + (p_r - p_t)\chi_\alpha\chi_\beta, \tag{2.2}$$

where ρ represents the energy-density, p_r and p_t, respectively denote fluid pressures along the radial and transverse directions, u^α is the 4-velocity of the fluid and χ^α is a unit space-like 4-vector along the radial direction so that $u^\alpha u_\alpha = 1$, $\chi_\alpha\chi_\beta = -1$ and $u^\alpha\chi_\beta = 0$.

Setting the geometrized units of $G = c = 1$, the Einstein field equations governing the evolution of the system now reduces to

$$8\pi\rho = \left[\frac{1}{r^2} - \frac{1}{r^2 B_0^2} + \frac{2B_0'}{rB_0^3}\right], \tag{2.3}$$

$$8\pi p_r = \left[-\frac{1}{r^2} + \frac{1}{B_0^2 r^2} + \frac{2A_0'}{rA_0B_0^2}\right], \tag{2.4}$$

$$8\pi p_t = \left[\frac{A_0''}{A_0B_0^2} + \frac{A_0'}{rA_0B_0^2} - \frac{B_0'}{rB_0^3} - \frac{A_0'B_0'}{A_0B_0^3}\right], \tag{2.5}$$

where 'prime' in Eqs. (2.3)-(2.5) denotes differentiation with respect to the radial co ordinate r. Thus the anisotropy in pressure which is essentially the difference of the pressures is now obtained in the form

$$\Delta(r) = 8\pi(p_t - p_r) = \left[\frac{A_0''}{A_0B_0^2} - \frac{A_0'}{rA_0B_0^2} - \frac{B_0'}{rB_0^3}\frac{A_0'B_0'}{A_0B_0^3} - \frac{1}{r^2B_0^2} + \frac{1}{r^2}\right]. \tag{2.6}$$

To develop a physically reasonable model of the stellar configuration, the metric potential g_{rr}, for the present work, is assumed to be in the form

$$B_0^2(r) = \frac{1}{\left(1 - \frac{r^2}{\mathscr{R}^2}\right)^4}, \tag{2.7}$$

where $\mathscr{R}$ is the curvature parameter describing the geometry of the configuration having a dimension of length $[L]$ and it will be determined from the matching conditions. This choice of metric potential assures that function $B_0(r)$ is finite, continuous and well defined within stellar interior range. Also $B_0(r) = 1$ for $r = 0$. With this choice of $B_0(r)$ Eq. (2.6) then reduces to

$$\Delta(r) = \frac{(3r^6 - 8r^4\mathscr{R}^2 + 6r^2\mathscr{R}^4)A_0(r)}{\mathscr{R}^8 A_0(r)} + \frac{(r^2 - \mathscr{R}^2)^3(3r^2 + \mathscr{R}^2)(r^2 - \mathscr{R}^2)A_0''(r)}{\mathscr{R}^8 A_0(r)}. \tag{2.8}$$

On rearranging Eq. (2.8) one can obtain

$$\frac{A_0''(r)}{A_0(r)}+\frac{(3r^2+\mathscr{R}^2)A_0'(r)}{r(r^2-\mathscr{R}^2)A_0(r)}+\frac{(3r^6-8r^4\mathscr{R}^2+6r^2\mathscr{R}^4)}{(r^2-\mathscr{R}^2)^4}=\frac{\Delta(r)\mathscr{R}^8}{(r^2-\mathscr{R}^2)^4}. \tag{2.9}$$

Now the above Eq. (2.9) can be solved for $A_0(r)$ if $\Delta(r)$ is specified in particular form. To make the equation easily integrable the anisotropic parameter is assumed in the form of

$$\Delta(r)=\frac{(3r^6-8r^4\mathscr{R}^2+6r^2\mathscr{R}^4)}{\mathscr{R}^8}. \tag{2.10}$$

The above choice for anisotropy is physically reasonable, as at the center ($r=0$) anisotropy is vanishes as expected. It is to be marked that for the present work the anisotropy is considered in the form

$$\Delta(r)=X_2r^2+X_4r^4+X_6r^6,$$

i.e. upto order 6 of Taylor Series for Δ in terms of r. This choice of anisotropy is physically reasonable and also ensures that isotropic pressures can be regained by taking the values of the radial co-efficient as 0. Similar form of linear anisotropy, ($\Delta=\sum_i X_ir^i$) can also be found in several literature. Maharaj et. al (Maharaj et al., 2014) and Sunzu et. al (Sunzu et al., 2014a) discussed their model using the anisotropy in the form $\Delta=\sum_{i=0}^{3}X_ir^i$. Anisotropy in the form $\Delta=\sum_{i=1}^{3}X_ir^i$ can be found in the work of Sunzu et. al (Sunzu et al., 2014b). $\Delta=\sum_{i=1}^{5}X_ir^i$ have been discussed by Sunzu et. al (Sunzu et al., 2019) and anisotropy in the form of $\Delta=X_3r^3+X_4r^4$ is also fashioned in the work of Sunzu and Mahali (Sunzu and Mahali, 2018).

Thus the system of equations given by Eqs. (2.3) - (2.5), which is the system of four equations in six variables (ρ, p_r, p_t, $\Delta(r)$, $A_0(r)$, $B_0(r)$), reduces to a consistent system of

equations. Combining the choice of anisotropy onto the Eq. (2.9) provides the solution in a closed form as substituting Eq. (2.10) in Eq. (2.9) gives

$$A_0''(r) + \frac{(3r^2 + \mathscr{R}^2)}{r\,(r^2 - \mathscr{R}^2)} A_0'(r) = 0. \tag{2.11}$$

The simple solution of the Eq. (2.11) thus obtained in the form

$$A_0(r) = \frac{\mathcal{C}_1}{2\,(\mathscr{R}^2 - r^2)} + \mathcal{C}_2, \tag{2.12}$$

where $\mathcal{C}_1$ and $\mathcal{C}_2$ are integration constants.

Hence the values of metric potentials are obtained and with these choices the matter density, radial pressure, transverse pressure are obtained as

$$8\pi\rho = \frac{(-9r^6 + 28r^4\mathscr{R}^2 - 30r^2\mathscr{R}^4 + 12\mathscr{R}^6)}{\mathscr{R}^8}, \tag{2.13}$$

$$8\pi p_r = \frac{\mathcal{C}_1\,(-3r^6 + 8r^4\mathscr{R}^2 - 6r^2\mathscr{R}^4) - \mathcal{C}_2\,(r^8 - 5r^6\mathscr{R}^2 + 10r^4\mathscr{R}^4 - 10r^2\mathscr{R}^6 + 4\mathscr{R}^8)}{\mathscr{R}^8\,[\mathcal{C}_1 + 2\mathcal{C}_2\,(\mathscr{R}^2 - r^2)]}, \tag{2.14}$$

$$8\pi p_t = \frac{-8\mathcal{C}_2\,(r^2 - \mathscr{R}^2)^4}{\mathscr{R}^8\,[\mathcal{C}_1 + 2\mathcal{C}_2\,(\mathscr{R}^2 - r^2)]}. \tag{2.15}$$

2.3 Mass-radius relationship for the model

The mass contained within a sphere of the radius r is defined as

$$m(r) = \frac{1}{2}\int_0^r \omega^2\rho(\omega)d\omega. \tag{2.16}$$

For the present model the mass function takes the form of

$$m(r) = \frac{(-r^9 + 4r^7\mathscr{R}^2 - 6r^5\mathscr{R}^4 + 4r^3\mathscr{R}^6)}{2\mathscr{R}^8}. \tag{2.17}$$

Assuming the surface density as $8 \times 10^{14}\ gm/cm^3$ the mass-radius relation for the model is obtained. It can be seen from Fig. 2.1 that the model assumes the maximum mass of $3.024M_\odot$ corresponding to the radius 10.31 km. Upper bound to the maximum mass for

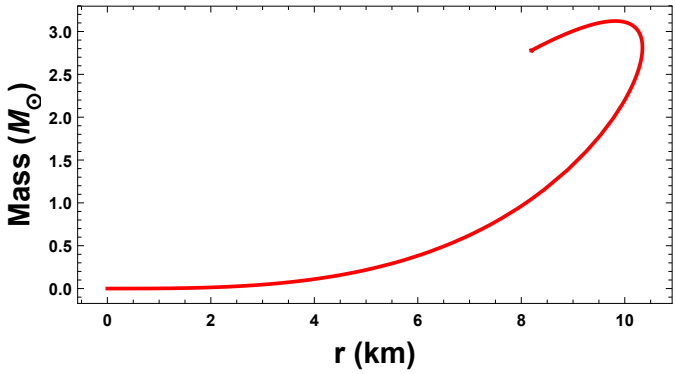

Figure 2.1: Mass-radius relation for the present model. Maximum acceptable mass for the model is $3.024M_\odot$ corresponding to the radius 10.31 km.

a neutron star, which is obtained by integrating Oppenheimer-Volkoff equation for density EoS is approximately $3.2M_\odot$ (Rhoades and Ruffini, 1974). For uniform density spheres where causality is not inherent, this limit in general relativity $\approx 5.2M_\odot$ (Shapiro and Teukolsky, 1983). The mass-radius relationship of neutron stars is of prime importance to understand the high-density low-temperature regime of the hadronic equation of state (EoS).

2.4 Exterior space-time and boundary conditions

The compact stellar object modeling requires the interior and exterior spacetime to be unified at the boundary of the star. These are known as the boundary conditions for the stellar configuration and it will be help to determine the values of $\mathscr{R}$, $\mathcal{C}_1$ and $\mathcal{C}_2$. These boundary conditions are as follows:

(i) The interior solution should smoothly match to the vacuum exterior spacetime for a non radiating Schwarzschild solution at the boundary. Now the exterior spacetime of a non radiating star can be described by Schwarzschild metric as

$$ds^2 = -\left(1-\frac{2M}{r}\right)dt^2 + \left(1-\frac{2M}{r}\right)^{-1}dr^2 + r^2(d\theta^2+\sin^2\theta d\phi^2), \qquad (2.18)$$

where $r > 2M$, M being the total mass of the stellar object. The interior spacetime metric (2.1) must be matched to the exterior Schwarzschild spacetime metric Eq. (2.18) at the boundary of the star $r = b$. Continuity of the metric across the boundary leads to

$$\begin{aligned} A_0^2(r)|_{r=b} &= \left(1-\frac{2M}{r}\right)\Big|_{r=b} \quad \text{and} \quad B_0^2(r)|_{r=b} = \left(1-\frac{2M}{r}\right)^{-1}\Big|_{r=b}, \\ \text{or,} \quad \frac{\mathcal{C}_1}{2\left(\mathscr{R}^2-b^2\right)}+\mathcal{C}_2 &= \sqrt{\left(1-\frac{2M}{b}\right)} \quad \text{and} \quad \frac{1}{\left(1-\frac{b^2}{\mathscr{R}^2}\right)^4} = \left(1-\frac{2M}{b}\right)^{-1}. \end{aligned} \qquad (2.19)$$

Here b is the boundary of the star.

(ii) Another boundary condition comes from the nature of the pressure at the boundary. The radial pressure of a stellar structure must vanish at its boundary (Misner and

Sharpe, 1964) i.e. $(p_r(r=b)=0)$. This boundary $r=b$ is known as the radius of the star. However transverse pressure does not necessarily vanish at the surface although both the radial and transverse pressure need to be equal at the center of the star. Hence the radius of the star can be obtained by utilizing the condition $p_r(r=b)=0$.

The above boundary conditions determine the model constants as

$$\mathscr{R} = \sqrt{\frac{b^2}{1-\left(1-\frac{2M}{b}\right)^{\frac{1}{4}}}}, \tag{2.20}$$

$$\mathcal{C}_1 = -\frac{\left[1+\left(1-\frac{2M}{b}\right)^{\frac{1}{4}}\right]\left[1+\left(1-\frac{2M}{b}\right)^{\frac{1}{2}}\right]b^2}{2\left[-1+\left(1-\frac{2M}{b}\right)^{\frac{1}{4}}\right]}, \tag{2.21}$$

$$\mathcal{C}_2 = -\frac{\left(1-\frac{2M}{b}\right)^{\frac{3}{4}}\left[3M+2\left(-1+\left(1-\frac{2M}{b}\right)^{\frac{3}{4}}\right)b\right]}{2\left[-1+\left(1-\frac{2M}{b}\right)^{\frac{1}{4}}\right](b-2M)}. \tag{2.22}$$

2.5 Physical analysis of the model

2.5.1 The regularity conditions

The gravitational potentials in this model satisfy, $A_0^2(0)=\left(\frac{\mathcal{C}_1}{2\mathscr{R}^2}+\mathcal{C}_2\right)^2=$ constant, $B_0^2(0)=1$, i.e., finite at the center $(r=0)$ of the stellar configuration. Also one can easily check that $(A_0^2(r))'_{r=0}=(B_0^2(r))'_{r=0}=0$. These imply that the metric is regular at the center and well behaved throughout the stellar interior.

The central density, central radial pressure and central tangential pressure in this case are given by,

$$\rho(0)=\frac{12}{\mathscr{R}^2},\quad p_r(0)=\frac{-8\mathcal{C}_2}{(\mathcal{C}_1+2\mathcal{C}_2\mathscr{R}^2)},\quad p_t(0)=\frac{-8\mathcal{C}_2}{(\mathcal{C}_1+2\mathcal{C}_2\mathscr{R}^2)}.$$

Note that the density is always positive as $\mathscr{R}$ is a positive quantity. The radial pressure and tangential pressure at the centre are equal which means pressure anisotropy vanishes at the center. The radial and tangential pressure at the center will be non-negative if one choose the model parameters satisfying the conditions $\mathcal{C}_2 < 0$ and $\mathcal{C}_1 > 2\mathcal{C}_2\mathscr{R}^2$ or $\mathcal{C}_2 > 0$ and, $\mathcal{C}_1 < 2\mathcal{C}_2\mathscr{R}^2$. Also according to Zeldovich's condition, $\frac{p_r}{\rho}$ must be ≤ 1 at the centre. Therefore, $\frac{-8\mathcal{C}_2\mathscr{R}^2}{12(\mathcal{C}_1+2\mathcal{C}_2\mathscr{R}^2)} \leq 1$.

Using above equation along with the central pressure leads to the inequality $|\frac{\mathcal{C}_1}{\mathcal{C}_2}| \geq \frac{5\mathscr{R}^2}{6}$.

2.5.2 Gradients of the matter variables

For the present model, the gradient of energy density, radial pressure and tangential pressure are respectively obtained as:

$$\frac{d\rho}{dr} = \frac{(-54r^5 + 112r^3\mathscr{R}^2 - 60r\mathscr{R}^4)}{\mathscr{R}^8}, \tag{2.23}$$

$$\begin{aligned}\frac{dp_r}{dr} &= \frac{2r}{\mathscr{R}^8\left[\mathcal{C}_1 + 2\mathcal{C}_2\left(\mathscr{R}^2 - r^2\right)\right]^2} \times \Big[\mathcal{C}_1^2\left(-9r^4 + 16r^2\mathscr{R}^2 - 6\mathscr{R}^4\right) \\ &+ 4\mathcal{C}_1\mathcal{C}_2(r^2 - \mathscr{R}^2)\left(r^4 - 2\mathscr{R}^4\right) + 4\mathcal{C}_2^2\left(r^2 - \mathscr{R}^2\right)^2\left(3r^4 - 8r^2\mathscr{R}^2 + 6\mathscr{R}^4\right)\Big],\end{aligned} \tag{2.24}$$

$$\frac{dp_t}{dr} = \frac{32\mathcal{C}_2 r(r^2 - \mathscr{R}^2)^3\left[-2\mathcal{C}_1 + 3\mathcal{C}_2\left(r^2 - \mathscr{R}^2\right)\right]}{\mathscr{R}^8\left[\mathcal{C}_1 + 2\mathcal{C}_2(\mathscr{R}^2 - r^2)\right]^2}. \tag{2.25}$$

The negative nature of the gradient of the density, radial pressure and tangential pressure inside the stellar body are shown graphically in the next section.

2.5.3 Herrera cracking method

The radial and transverse velocity of sound ($c = 1$) are obtained as

$$\begin{aligned} v_{sr}^2 = \frac{dp_r}{d\rho} &= \frac{1}{(27r^4 - 56r^2\mathscr{R}^2 + 30\mathscr{R}^4)\left[\mathcal{C}_1 + 2\mathcal{C}_2\left(\mathscr{R}^2 - r^2\right)\right]^2} \\ &\times \Big[\mathcal{C}_1^2\left(9r^4 - 16r^2\mathscr{R}^2 + 6\mathscr{R}^4\right) - 4\mathcal{C}_1\mathcal{C}_2(r-\mathscr{R})(r+\mathscr{R})\left(r^4 - 2\mathscr{R}^4\right) \\ &- 4\mathcal{C}_2^2\left(r^2 - \mathscr{R}^2\right)^2\left(3r^4 - 8r^2\mathscr{R}^2 + 6\mathscr{R}^4\right)\Big], \end{aligned} \tag{2.26}$$

$$v_{st}^2 = \frac{dp_t}{d\rho} = \frac{16\mathcal{C}_2(r^2 - \mathscr{R}^2)^3\left(2\mathcal{C}_1 - 3\mathcal{C}_2r^2 + 3\mathcal{C}_2\mathscr{R}^2\right)}{(27r^4 - 56r^2\mathscr{R}^2 + 30\mathscr{R}^4)\left[\mathcal{C}_1 + 2\mathcal{C}_2(\mathscr{R}^2 - r^2)\right]^2}. \tag{2.27}$$

In this model the speed of sound are smaller than 1 in the interior of the star, i.e., $0 \leq \frac{dp_r}{d\rho} \leq 1$, $0 \leq \frac{dp_t}{d\rho} \leq 1$ which has been shown graphically in the next section.

Based on the cracking method to study the stability of anisotropic stars proposed by Herrera (Herrera, 1992), Abreu et al. (Abreu et al., 2007) proved that the region of an anisotropic fluid sphere is stable where $-1 \leq v_{st}^2 - v_{sr}^2 \leq 0$ is potentially stable. The model is shown to be stable considering this condition.

2.5.4 Energy conditions

The energy-momentum tensor is made up of contributions of several different matter fields, thus the occurrence of singularities obtained from right hand side of Einstein field equations are hard to predict. Hence certain inequalities are tested for the energy-momentum tensor. These inequalities are sufficient to prove the existence of singularities independent of the exact form of the given energy-momentum tensor and these are known as energy conditions.

- *Weak Energy Condition (WEC):* WEC stipulates that for every timelike vector field

$\vec{X}$, the matter density observed by any corresponding observer is always non-negative.

$$\rho = \mathcal{T}_a b X^a X^b \geq 0.$$

Essentially this condition states that the energy density is non-negative to any observer.

$$WEC : \rho(r) \geq 0. \tag{2.28}$$

- *Null energy Condition (NEC):* For every future pointing null vector field $\vec{k}$, the matter energy momentum tensor obeys

$$\mathcal{T}_{\mu\nu} k^\mu k^\nu > 0.$$

This NEC is an important assumption of the Penrose singularity theorem. The theorem states that if NEC holds and if Cauchi hyperspace is non-compact, one there is a trapped surface in space then there will be singularity in future (Rubakov, 2014). A closed surface on which outward pointing light rays are converging (moving inwards), such surfaces are called trapped surface.

For spherically symmetric case for a sphere of having area of $4\pi R^2$, the sphere is a trapped surface if R decreases along any future null direction (i.e. all light rays from the sphere move towards the centre).

$$NEC|_r : \rho(r) + p_r(r) \geq 0; NEC|_t : \rho(r) + p_t(r) \geq 0; \tag{2.29}$$

where $NEC|_r$ and $NEC|_t$ are NECs along the radial and transverse directions respectively.

- *Dominant Energy Condition (DEC):* For every time-like vector $\vec{W}$, $\mathcal{T}^{ab}W_aW_b \geq 0$ and $\mathcal{T}^{ab}W_a$ is a non space-like vector (Hawking and Ellis, 1973). To any observer the local energy density appears non negative and local energy flow vector is non space-like. Equivalently this condition can be state that in any orthonormal basis the energy dominates the other components of $\mathcal{T}_{ab}$, or $\mathcal{T}^{00} \geq |\mathcal{T}^{ab}|$ for each a, b. That is mass energy can never be observed flowing faster than light. DEC suggests that matter density should always be greater than the pressure. Mathematically

$$DEC|_r : \rho(r) - |p_r(r)| \geq 0; DEC|_t : \rho(r) - |p_t(r)| \geq 0. \tag{2.30}$$

- *Strong Energy Condition (SEC):* A physically reasonably energy condition but still stricter restriction than WEC is another energy condition known as strong energy condition (SEC). SEC states that for every time-like vector field $\vec{X}$, the trace of tidal tensor is always non negative as measured by an observer.

$$\left(\mathcal{T}_{ab} - \frac{1}{2}\mathcal{T}g_{ab}\right) X^a X^b \geq 0.$$

SEC implies that for a perfect fluid not only the expression $\rho(r) - p(r)$ need to be ≥ 0, but also $\rho(r) - 3p(r) \geq 0$ must hold. For an anisotropic fluid SEC is given as

$$SEC : \rho(r) + p_r(r) + 2p_t(r) \geq 0. \tag{2.31}$$

SEC implies the NEC but SEC does not imply the WEC (Hawking and Ellis, 1973; Poisson, 2004).

2.6 Compatibility with observational data

2.6.1 Discussions around $4\mathrm{U}1608-52$

The physical acceptability of this model has been examined by plugging the masses and radii of observed pulsars as input parameters. In order to validate our model, I have considered the pulsar $4U1608-52$ whose estimated mass and radius are $M = 1.58^{+0.30}_{-0.29}\ M_{\odot}$ and $b = 9.8 \pm 1.8\ km$, respectively (Özel et al., 2016). Using these values of mass and radius as an input parameter, the boundary conditions have been utilized to determine the constants as $\mathscr{R} = 25.3855$, $\mathcal{C}_1 = 1028.29$ and $\mathcal{C}_2 = -0.213415$. Making use of these values of constants and plugging the values of Gravitational constant G and speed of light in vacuum c in the expressions, various physical variables have been plotted graphically. Regular and well-behaved nature of all the relevant physically meaningful quantities imply that all the requirements of a realistic star are satisfied in this model. Fig. 2.2 depicts the regularity of the metric potentials considering the pulsar $4U1608-52$.

Fig. 2.3 shows the variation of gradients of matter variables which are negative through-

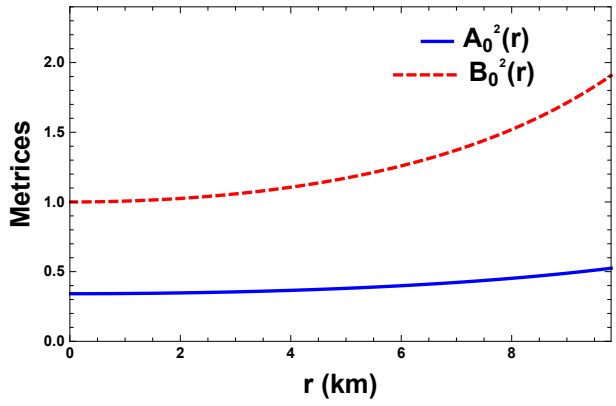

Figure 2.2: Variation of the metric potentials $A_0^2(r)$ (solid blue) and $B_0^2(r)$ (dashed red) against the radial coordinate r corresponding to the pulsar $4\mathrm{U}1820-30$.

out the stellar configuration ensures the decreasing nature of density, radial and transverse pressures. Fig. 2.4 shows that the density decrease from its maximum value at the cen-

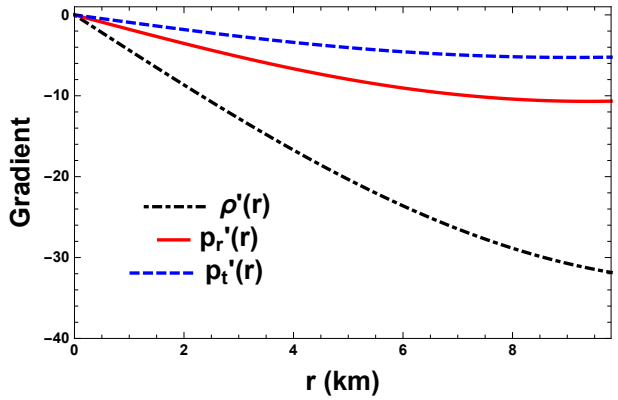

Figure 2.3: Variation of the gradient of pressures (gradient of the radial pressure (solid red), the transverse pressure (dashed blue)) and the density (dot dashed black) with respect to the radial coordinate r corresponding to the pulsar $4U1820-30$.

ter towards its boundary. Variation of radial and tangential pressures has been plotted in

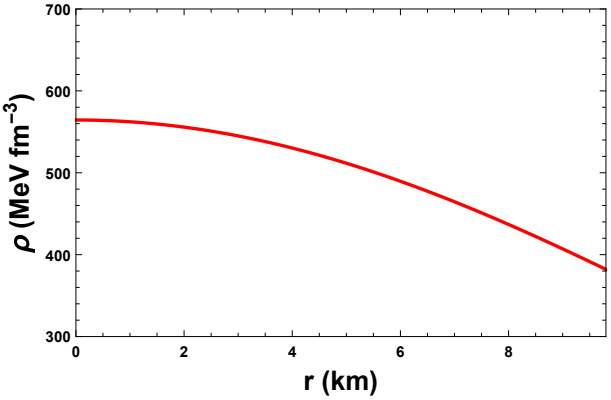

Figure 2.4: Monotonically decreasing nature of the density against the radial coordinate r corresponding to the pulsar $4\mathrm{U}1820-30$.

Fig. 2.5, which are also radially decreasing outwards from its maximum value at the center and in case of radial pressure it drops to zero at the boundary as it should be but the tangential pressure remains non zero at the boundary. Radial variation of anisotropy has been

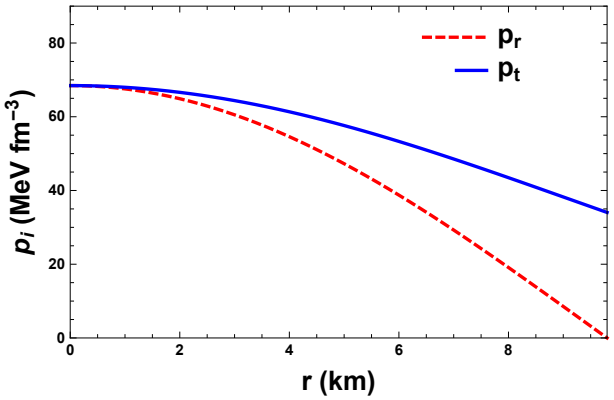

Figure 2.5: Nature of the radial (dashed red) and the transverse pressures (solid blue) against the radial coordinate r corresponding to the pulsar $4\mathrm{U}1820-30$. The radial pressure vanishes at the surface of the star.

shown in Fig. 2.6 which is zero as center as expected and is maximum at the surface. In

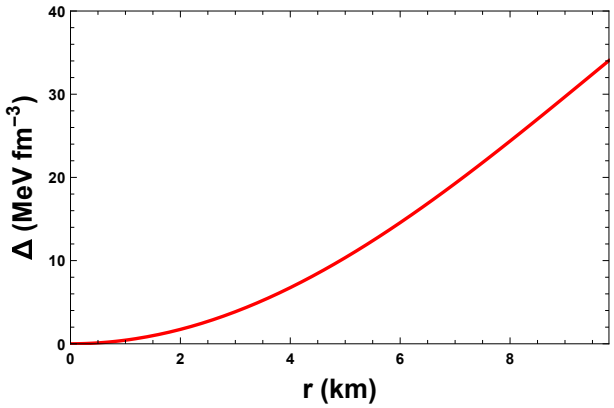

Figure 2.6: Monotonically increasing nature of the anisotropy Δ against the radial coordinate r corresponding to the pulsar $4\mathrm{U}1820-30$. The anisotropy in seen to vanish at the centre.

Fig. 2.7, the sound speed in radial and transverse directions have been plotted against the radial parameter which ensures the non-violations of causality condition in the interior of the star. The energy conditions are plotted in Fig. 2.8, which are positive throughout the stellar configuration as required for a physically meaningful stellar model. Fig. 2.9 have

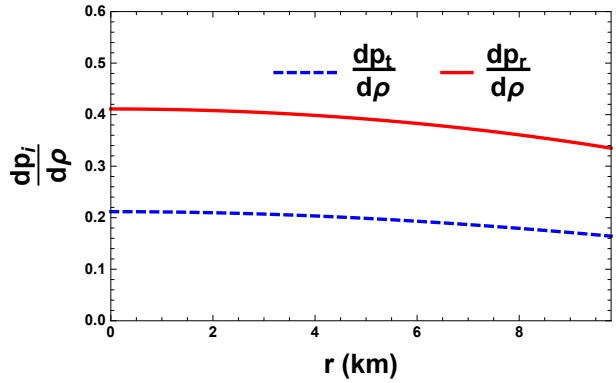

Figure 2.7: Variation of the radial (solid red) and transverse (dashed blue) velocity of sound against the radial coordinate r corresponding to the pulsar $4\mathrm{U}1820-30$. Both the sound speeds for the structure are within $(0,1)$.

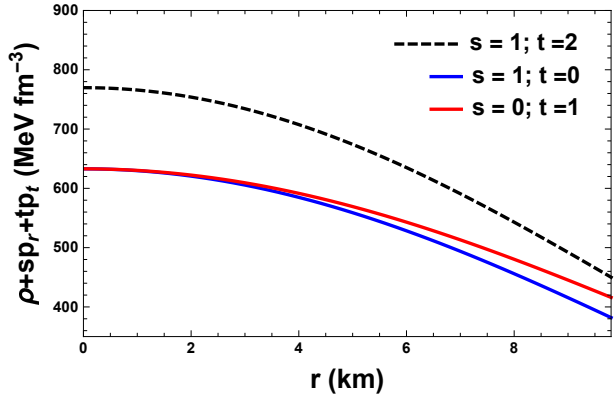

Figure 2.8: Different energy conditions, SEC (dashed black), NEC along the radial direction (solid blue) and NEC along transverse direction (solid red) are plotted against the radial coordinate r corresponding to the pulsar $4\mathrm{U}1820-30$.

depicted the smooth matching of the interior and exterior metrices at the boundary. The

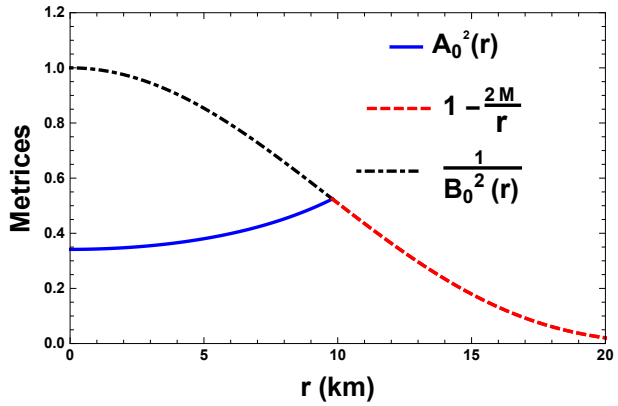

Figure 2.9: Smooth matching of $A_0^2(r)$ and $B_0^2(r)$ with the exterior Schwarzschild metrices at the boundary of the star.

relationship between the thermodynamic parameters energy density and pressure which reflects the nature of the equation of state (EoS) of the matter distribution of a given pulsar is plotted in Fig. 2.10 which shows an almost linear relationship. Considering the EoS for the

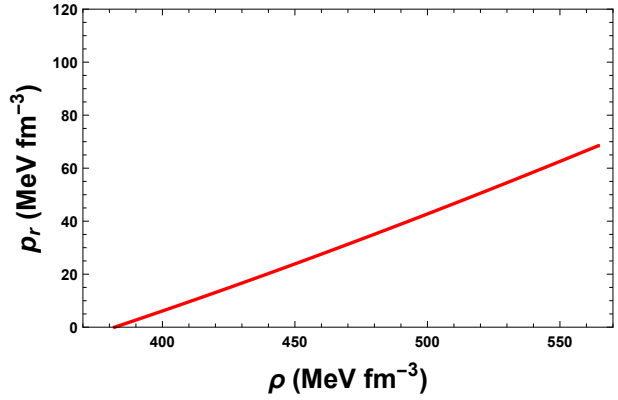

Figure 2.10: Nature of equation of state for the present model. It shows that the model assumes linear EoS.

radial pressure in Fig. 2.10, I have plotted the data for ρ and p_r across the range of the radius for the pulsar $4U1608-52$. It is estimated that best fitted relation between ρ and p_r is given

by the expression $0.382962\rho - 148.169$ which is illustrated in Fig. 2.11. The mass func-

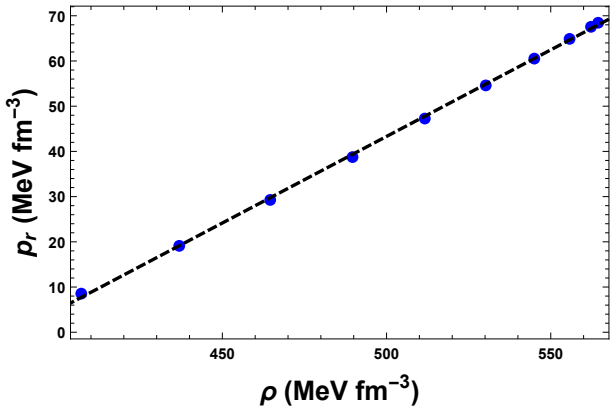

Figure 2.11: Best fit for the curve depicting the EoS for the present model.

tion is given in Eq. (2.17) is monotonically increasing the function of r and $m(0) = 0$ as depicted in Fig. 2.12. For the compactness of a model ($u(r) = \frac{m(r)}{r}$) limit condition need

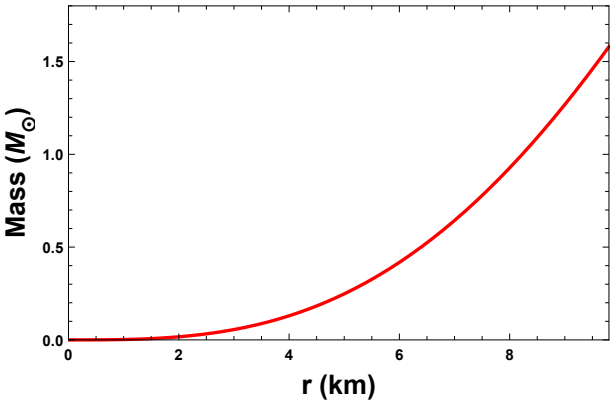

Figure 2.12: Variation of the mass function against the radial coordinate r corresponding to the pulsar $4\text{U}1820 - 30$.

to be satisfied as suggested by Buchdahl. Buchdahl limit suggests that the ratio of mass to the radius for any stable stellar structure should lie within the range $\frac{2M}{b} < \frac{8}{9}$ (Buchdahl, 1959). It can be easily checked that the present model possesses its compactness as

$\frac{m(b)}{b} = 0.4326 < \frac{4}{9} = 0.44$, i.e. Buchdahl conditions are being satisfied for this model. Moreover, the gravitational redshift is expressed by

$$z = \left(1 - \frac{2M}{r}\right)^{-\frac{1}{2}} - 1. \tag{2.32}$$

In Fig. 2.13, variation of the gravitational redshift is plotted. The surface redshift of this model is 1.7242. The upper limit of surface redshift is 2 (Buchdahl, 1966), although it was extended later as according to Bohmer and Harko, the surface red shift should always be ≤ 5 (Böhmer and Harko, 2006).

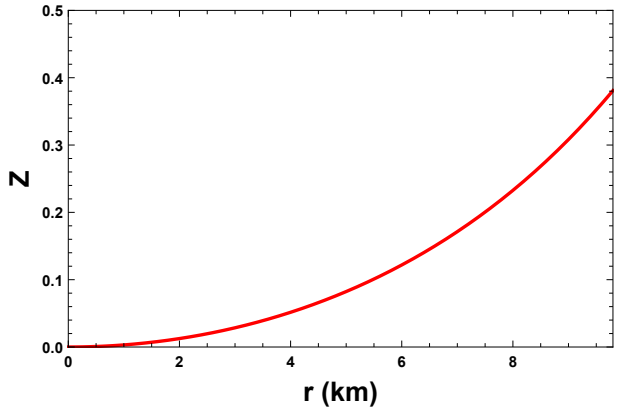

Figure 2.13: Variation of the gravitational redshift z against the radial coordinate r for the pulsar $4U1820 - 30$.

The equation of State (EoS) parameter as is shown in Fig. 2.14 and the EoS parameter lies between 0 and 1 indicating an non exotic configuration.

2.6.2 Discussions around other Pulsars

To show that this model has a wide range of applicability for highly compact stars, I have also analyzed the validity of my model by considering some well-known pulsars such as

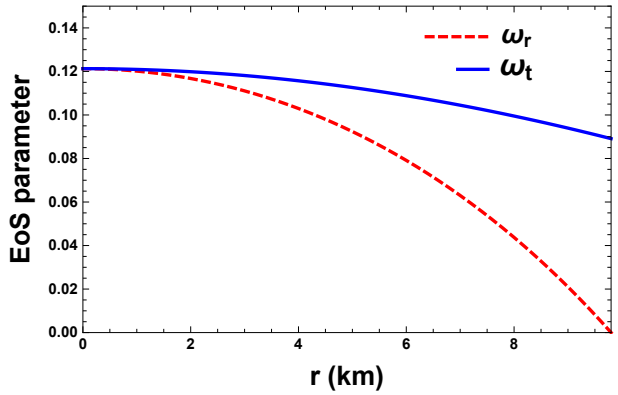

Figure 2.14: Variation of the EoS parameter in the radial (dashed red) and transverse directions (solid blue) against the radial coordinate r for the present model.

Pulsar	**Mass** ($M_\odot$)	**Radius (km)**	$\mathcal{C}_1$	$\mathcal{C}_2$	$\mathscr{R}$
RX J $1856-37$	0.9 ± 0.2	6^{-1}_{+2}	431.23	-0.1953	16.275
EXO $1785-248$	1.3 ± 0.2	8.849 ± 0.4	968.04	-0.1905	24.319
Her X-1	0.85 ± 0.15	8.1 ± 0.41	1298.06	-0.1289	27.235
PSR J $1614-2230$	1.97 ± 0.04	9.69 ± 0.2	672.61	-0.2887	21.422
Cen X-3	1.49 ± 0.08	9.178 ± 0.13	892.01	-0.2152	23.668

Table 2.1: Values of the model parameters for several different known compact stellar objects.

RX J $1856-37$(Mass= $0.9 \pm 0.2 M_\odot$, Radius= 6 km) (Pons et al., 2002), EXO $1785-248$ (Mass= $1.3 \pm 0.2 M_\odot$, Radius= 8.849 ± 0.4 km) (Özel et al., 2009), Her X-1(Mass= $0.85 \pm 0.15 M_\odot$, Radius= 8.1 ± 0.41 km) (Abubekerov et al., 2008), PSR J $1614-2230$ (Mass= $1.97 \pm 0.04 M_\odot$, Radius= 9.69 ± 0.2 km), Cen X-3 (Mass= $1.49 \pm 0.08 M_\odot$, Radius= 9.178 ± 0.13 km).

The estimated masses and radii of these pulsars have been used to determine the corresponding model parameters $\mathcal{C}_1$, $\mathcal{C}_2$ and $\mathscr{R}$ as given in Table (2.1). Making use of these values, in Table (2.2), I have calculated the values of the physically reasonable parameters

Pulsar	$\rho\|_0$	$\rho\|_b$	$\frac{dp_r}{d\rho}\|_0$	$\frac{dp_r}{d\rho}\|_b$	$\frac{dp_t}{d\rho}\|_0$	$\frac{dp_t}{d\rho}\|_b$	$TEC\|_0$	$TEC\|_b$	$z\|_b$
RXJ $1856-37$	1373	963	0.38	0.32	0.18	0.14	941	809	0.195
EXO $1785-248$	615	435	0.37	0.31	0.17	0.14	429	368	0.189
Her X-1	490	391	0.29	0.27	0.09	0.08	406	352	0.125
PSRJ$1614-2230$	793	459	0.60	0.42	0.40	0.26	279	339	0.298
Cen X-3	649	438	0.41	0.34	0.21	0.17	410	359	0.216

Table 2.2: Values of the physical quantities of different known compact stellar objects. Here the values of the physical quantities are considered at the centre and at the surface. Additionally, the values of the trace energy condition TEC = $\rho - p_r - 2p_t$ are calculated for several stars.

which are sufficient to justify the requirements of a physically realistic star. From Table 2.2 it is clear that central density is greater than the surface density, which is one of the important criterion for the stability of a compact stellar model. It can also be easily checked the same for radial and transverse pressure. Note that I have used $()|_0$ and $()|_b$ to denote the evaluated values of the physical parameters at the center and surface of the star, respectively. Here, radial velocity and transverse velocity of the sound for these pulsars are decreasing away from the centre, consequently satisfying the causality condition. Moreover the differences of transverse velocity and radial velocity of the sound for these pulsars are also lying between -1 and 0, thus satisfying Herrera Cracking Criterion. Energy Condition is positive throughout the stellar configuration and decreasing towards the boundary except for the pulsar PSR J 1614-2230. Since for the present model, ρ, p_r and p_t are all positive, so reasonably SEC $= \rho + p_r + 2p_t$ will be positive. Thus to observe the energy condition corresponding to the model, I have studied TEC $= \rho - p_r - 2p_t$ for various compact stars in Table. 2.2 Additionally, mass-radius and other parameters of some other stars are discussed in Table. 2.1. It can be seen from Table. 2.2 that this presented model satisfy Buchdahl condition as well as surface redshift condition for other pulsars as $z_b \leq 2$.

2.7 Stability analysis of the model

2.7.1 Stability under three different forces

A star remains in static equilibrium under the forces namely, gravitational force, hydrostatics force and anisotropic force. This condition is formulated mathematically as TOV equation by Tolman-Oppenheimer-Volkoff which is

$$-\frac{M_G}{r}(\rho+p_r)\frac{A_0(r)}{B_0(r)}-\frac{dp_r}{dr}+\frac{2}{r}(p_t-p_r)=0, \tag{2.33}$$

where $M_G(r)$ is the gravitational mass of the star within the radius r, can be derived from the Tolman-Whittaker formula and Einstein's field equations and it is defined by

$$M_G(r)=\frac{rB_0(r)A_0'(r)}{A_0^2(r)}. \tag{2.34}$$

Using the expression of $M_G(r)$ in Eq. (2.33) one can obtain

$$-\frac{A_0'(r)}{A_0(r)}(\rho+p_r)-\frac{dp_r}{dr}+\frac{2}{r}(p_t-p_r)=0. \tag{2.35}$$

The above equation is equivalent to the following

$$F_g+F_h+F_a=0, \tag{2.36}$$

where

$$F_g=-\frac{A_0'(r)}{A_0(r)}(\rho+p_r),\ F_h=-\frac{dp_r}{dr}\ F_a=\frac{2}{r}(p_t-p_r),$$

represent the gravitational, hydrostatics and anisotropic forces respectively. For the present model the expression for F_g, F_h and F_a can be written as,

$$F_g = -\frac{8\mathcal{C}_1 r(r^2-\mathscr{R}^2)^2\left(3\mathcal{C}_1-4\mathcal{C}_2r^2+4\mathcal{C}_2\mathscr{R}^2\right)}{\mathscr{R}^8\left(\mathcal{C}_1-2\mathcal{C}_2r^2+2\mathcal{C}_2\mathscr{R}^2\right)^2}, \tag{2.37}$$

$$F_h = -\frac{2r}{\mathscr{R}^8\left[\mathcal{C}_1+2\mathcal{C}_2(\mathscr{R}^2-r^2)\right]^2}\times\Big[-4\mathcal{C}_1\mathcal{C}_2(r^2-\mathscr{R}^2)(r^4-\mathscr{R}^4)+\mathcal{C}_1^2(9r^4 - 16r^2\mathscr{R}^2+6\mathscr{R}^4)-4\mathcal{C}_2(r^2-\mathscr{R}^2)^2\left(3r^4-8r^2\mathscr{R}^2+6\mathscr{R}^4\right)\Big], \tag{2.38}$$

$$F_a = \frac{2r}{R^8}\left(3r^4-8r^2\mathscr{R}^2+6\mathscr{R}^4\right) \tag{2.39}$$

The three different forces are plotted in Fig. 2.15. The figure shows that hydrostatics and anisotropic force are positive and is dominated by the gravitational force which is negative to keep the system in static equilibrium.

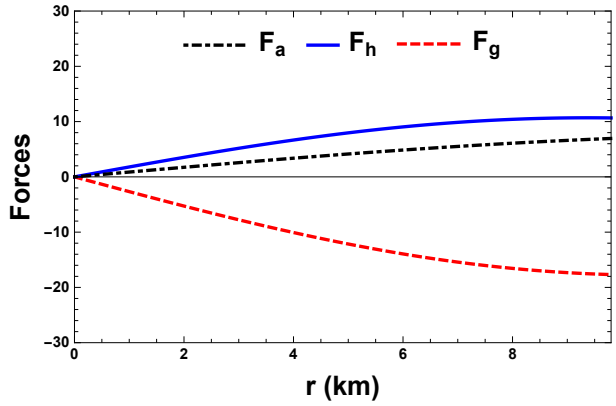

Figure 2.15: Variation of different types of forces, hydrostatics force (solid blue), anisotropic force (dot dashed black) and gravitational force (dashed red) against the radial coordinate r corresponding to the pulsar $4\mathrm{U}1820-30$.

2.7.2 Adiabatic index

The adiabatic index, which is defined as

$$\Gamma = \frac{\rho + p}{p}\frac{dp}{d\rho}, \tag{2.40}$$

is related to the stability of a relativistic anisotropic stellar configuration. A Newtonian isotropic sphere will be in stable equilibrium if the adiabatic index $\Gamma > \frac{4}{3}$ as per Heintzmann and Hillebrandth's concept (Heintzmann and Hillebrandt, 1975) and for $\Gamma = \frac{4}{3}$, isotropic sphere will be in neutral equilibrium. However, for a relativistic anisotropic fluid sphere the above condition for stability does not hold good. Thus the modifications based on some recent works of Chan et al. (Chan et al., 1993) have been implemented and one can demand the following condition for the stability of a relativistic anisotropic sphere, $\Gamma > \gamma$, where

$$\gamma = \frac{4}{3} - \left[\frac{4(p_r - p_t)}{3|p_r'|r}\right]_{max}, \tag{2.41}$$

and $\Gamma > \frac{4}{3}$. In Fig. 2.16, I have plotted Γ_r, Γ_t, γ respectively. clearly, it can be seen that values of Γ_r and Γ_t are greater than γ throughout the stellar interior and hence the stability condition is fulfilled.

Interestingly, it is to be noted that the adiabatic index γ is a local characteristic of a specific EoS and depends on the interior fluid density.

2.7.3 Causality condition

For a physically acceptable model of relativistic anisotropic star the radial and transverse velocity speed of sound must be smaller than $1(c = 1)$ in the interior of the star, i.e., $0 \leq \frac{dp_r}{d\rho} \leq 1$, $0 \leq \frac{dp_t}{d\rho} \leq 1$. This condition is known as causality condition and is veri-

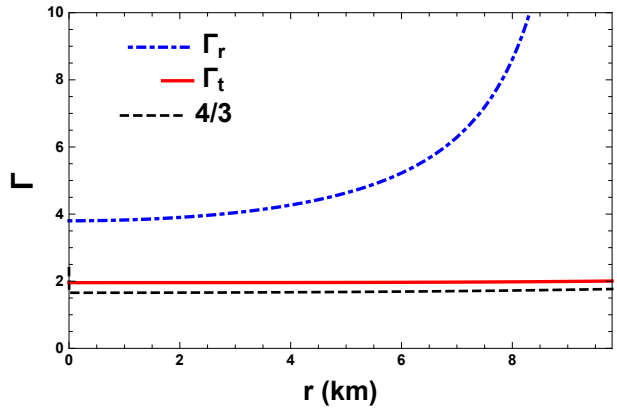

Figure 2.16: Variation of adiabatic indices along the radial (dot dashed blue) and transverse direction (solid red) against the radial coordinate r corresponding to the pulsar $4\mathrm{U}1820-30$. Here the adiabatic indices Γ are seen to be $> \frac{4}{3}$.

fied in Fig. 2.17. Moreover Abreu et al. (Abreu et al., 2007) proved that the region of an anisotropic fluid sphere where $-1 \leq v_{st}^2 - v_{sr}^2 \leq 0$ is potentially stable which is shown graphically in Fig. 2.18.

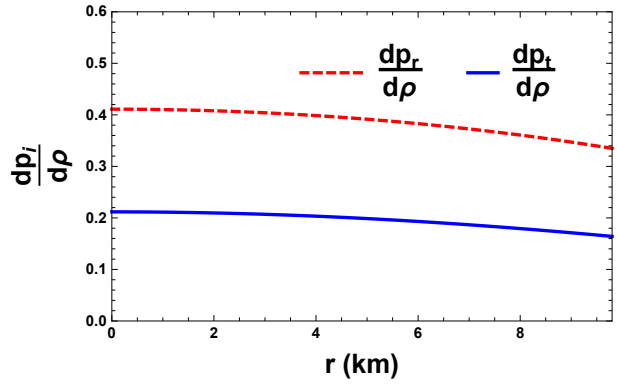

Figure 2.17: Variation of $\frac{dp_r}{d\rho}$ and $\frac{dp_t}{d\rho}$ against the radial coordinate r corresponding to the pulsar $4\mathrm{U}1820-30$.

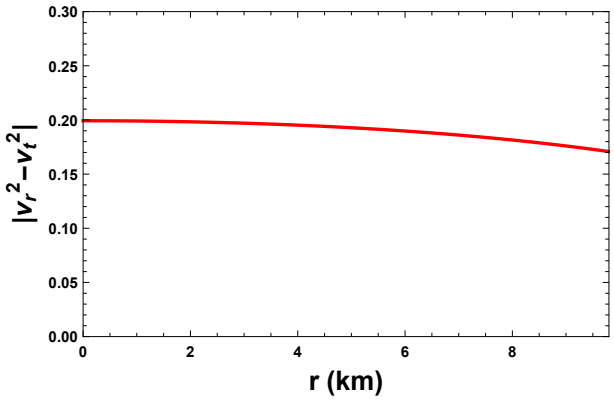

Figure 2.18: Variation of $|v_{st}^2 - v_{sr}^2|$ against the radial coordinate r corresponding to the pulsar $4U1820 - 30$.

2.8 Discussions and summary

In this chapter, a static spherically symmetric anisotropic fluid model has been developed by assuming a physically reasonable metric potential and a particular form of the anisotropy. The presented solution satisfies all the physical criterion of a physically well behaved compact stellar object. All the physical quantities are regular and well behaved throughout the stellar interior. Energy density, radial pressure and transverse pressure are decreasing functions towards the surface of the star. Here anisotropy is finite, continuous and monotonically increasing function of the radial co-ordinate 'r' away from the stellar centre i.e. anisotropic force is repulsive in nature. Similar profile for anisotropy can be found in the work of Sunzu et. al (Sunzu et al., 2014a).

The model is shown to remain stable in hydrostatic equilibrium against different forces. The developed model has been shown to fit a wide range of recently observed values of masses and radii of pulsars. The mass-radius relation is also explored here. It is also to be observed from Fig. 2.12, mass function is increasing function of 'r'. Here we have con-

sidered static and spherically symmetric spacetime and have incorporated linear equation of state. The maximum mass for the model is $3.021\ M_{\odot}$ and it is obtained for the radius $b = 10.31$ km (see Fig. 2.1), which is stable as the mass $\leq 5\ M_{\odot}$ (Rhoades and Ruffini, 1974).

The above model can be of significant study for the astrophysical objects with large masses. Other new results and hence models can be analyzed by using different metric potentials, different measure of anisotropy and another choice of equation of state.

Chapter 3

A study on anisotropic compact star modeling

3.1 Introduction

Observation of any stellar structure that follows anisotropic pressure is much more complicated than the isotropic ones. Obtaining exact solutions of the field equations that describe anisotropic stellar structure, which have started almost half a century ago, have escalated in the recent times. The assumption of static spherically symmetric structure for a star reduces the complexity of the field equations to a certain extent - second-order partial differential equations into ordinary second-order differential equations (Tello-Ortiz et al., 2020a). The remaining strongly coupled system of equations are then solved by implementing some assumptions on the model. Despite the isotropic pressure is more '*easier*' to solve, describing a relativistic compact stellar configuration requires considering the pressure anisotropy where both the pressures are unequal throughout the structure except at the centre (Mak and Harko, 2002, 2003). These anisotropic structures are studied by assuming some very

specific ansatz; either for some specific metric component, or for some specific relationship between the components of the stress-energy tensor (Boonserm et al., 2016).

Apart from using specific metric potentials, one can use specific form of equation of state (EoS), which directs the relation between the pressure and the density and enables to solve the field equation. The properties of elementary interactions of the nuclear matter within the extreme dense neutron star core navigate their behaviour within the system. But these properties are still not very clear to us. It is well known that the properties of the neutron stars depend extensively on the equation of state (EoS). However several studies have suggested that the properties of general-relativistic stellar configurations in equilibrium can be expressed in terms of functions that do not depend on the specific equation of state employed to describe matter at nuclear densities (Breu and Rezzolla, 2016). These *universal relations* between several dimensionless quantities can be applied in the case of weak dependence on their EoS and these relations hold for both static or stationary isolated stars, as well as for fully dynamical and merging binary systems. An approximation for the moment of inertia of a neutron star in terms of only its mass and radius have been presented through examining the behavior of the relativistic structural equations by Ravenhall and Pethick (Ravenhall and Pethick, 1994). This approximation is found to be accurate upto 10% for a variety of nuclear equations of states, for all except very low mass stars. They have displayed that moment of inertia can be approximated in terms of its mass M and radius R at the crust boundary for any neutron star model. In the case of EoSs without an extreme softening at super nuclear densities this relation of normalized moment of inertia $\frac{I}{MR^2}$ and the stellar compactness $\frac{M}{R}$, where I is the moment of inertia, was further fine tuned by Lattimer and Prakash (Lattimer and Prakash, 2001). Ravenhall and Pethick

suggested the following relation,

$$\frac{I}{MR^2} \approx \frac{0.21}{1-2u},$$

where u is the the compactness parameter $\frac{GM}{Rc^2}$. Later Lattimer and Prakash obtained that with the decrease of u, the quantity $\frac{I}{MR^2}$ rapidly decreases. Afterward Bejger and Haensel (Bejger and Haensel, 2002) introduced the empirical relation to obtain the moment of inertia based on numerical results obtained for thirty theoretical equations of state of dense matter. Later Lattimer and Schutz (Lattimer and Schutz, 2005) pointed out that using such an empirical relation it is possible to estimate the radius of a neutron star via the combined measurement of the mass and moment of inertia of a pulsar in a binary system. Present chapter focuses on the moment of the inertia for the obtained solution comparing the results with slow rotation approximation using Bejger-Haensel idea.

This Chapter is machinated as follows: assuming specific metric potential, solution to the EFEs in closed form is obtain in Sec. 3.2. The model parameters, obtained from smooth matching of the exterior spacetime with the interior one at the boundary are described in Sec. 3.3. Sec. 3.4 highlights the the physical requirements to be a stable structure. The physical and stability analysis for the obtained solution is depicted in Sec. 3.5. Comparative study of the model with some known stars and hence the concluding remarks are given in Sec. 3.6 and Sec. 3.7 respectively.

3.2 Closed form analytical solution

Recall that the line element describing the space-time of the interior of a spherically symmetric star with zero angular momentum in Schwarzschild coordinates $x^0 = t$, $x^1 = r$, $x^2 = \theta$, $x^3 = \phi$ can be written as

$$ds^2_- = -A_0^2(r)dt^2 + B_0^2(r)dr^2 + r^2(d\theta^2 + \sin^2\theta d\phi^2), \tag{3.1}$$

where $A_0(r)$ and $B_0(r)$ are called the gravitational potential and these metric functions will be determined by solving the field equations. Since the matter distribution of the stellar interior is anisotropic in nature, the energy-momentum tensor is described by that of a perfect fluid, in the form

$$T_{\alpha\beta} = (\rho + p_t)u_\alpha u_\beta - p_t g_{\alpha\beta} + (p_r - p_t)\chi_\alpha\chi_\beta, \tag{3.2}$$

where ρ represents the energy-density, p_r and p_t, respectively denote fluid pressures along the radial and transverse directions, u^α is the 4-velocity of the fluid and χ^α is a unit space-like 4-vector along the radial direction. Since the configuration of the system is considered to be in comoving coordinate system so one can have the following relations for the 4-vectors, $u^\alpha u_\alpha = 1$, $\chi^\alpha\chi_\alpha = -1$ and $u^\alpha\chi_\alpha = 0$. The Einstein field equations governing the evolution of the system are then obtained as (setting $G = c = 1$)

$$8\pi\rho = \left[\frac{1}{r^2} - \frac{1}{r^2B_0^2} + \frac{2B_0'}{rB_0^3}\right], \tag{3.3}$$

$$8\pi p_r = \left[-\frac{1}{r^2} + \frac{1}{B_0^2r^2} + \frac{2A_0'}{rA_0B_0^2}\right], \tag{3.4}$$

$$8\pi p_t = \left[\frac{A_0''}{A_0B_0^2} + \frac{A_0'}{rA_0B_0^2} - \frac{B_0'}{rB_0^3} - \frac{A_0'B_0'}{A_0B_0^3}\right], \tag{3.5}$$

where 'prime' in Eqs. (3.3)-(3.5) denotes differentiation with respect to radial co-ordinate r. Here the above system of equations is consists of three equations and five unknowns $(\rho,\ p_r,\ p_t,\ A_0,\ B_0)$ so that two of them can be chosen freely.

To develop a physically reasonable model of the stellar configuration, I chose viable metric potentials to solve the system of equations Eqs. (3.3)-(3.5). Now for selecting metric potentials, one needs to keep in mind the eligibility of a potential metric coefficient. Metric potentials to describe any viable model need to be finite at the center and monotonically increasing throughout the stellar interior as suggested in (Delgaty and Lake, 1998). Maurya et al. (Maurya et al., 2015a) have studied relativistic model for stable anisotropic super dense star considering the metric potential in the form $A_0(r) = D(1 - c_0 r^2)^n$, with $n = -1, -2, -3$ and where $c_0 > 0$ and D is an arbitrary positive constant. Earlier Maurya and Gupta (Maurya and Gupta, 2013) have investigated possible anisotropic solutions for Einstein field equations considering the metric potential $A_0^2(r) = D(1 - c_0 r^2)^{-n}$,for positive fractional values of n such that $N = \frac{1+n}{1-n}$ is positive integer and where c_0 is positive constant. Although the quest to form metric potential in this specific form was provided by Durgapal when he studied the metric potential $A_0^2(r)$ as it varies as $(1+x)^n$ for the integral values of n (Durgapal, 1982) and as it varies as $(1-x)^n$ for fractional values of n such that $N = \frac{1+n}{1-n}$ and where $x > 0$ (Durgapal et al., 1984). The present work can principally be treated as the special case of the work done by Maurya et al (Maurya et al., 2015a) where I have taken $D = 1$, $n = -3$ and $c_0 = \frac{1}{\mathscr{R}^2}$. This is the motivation to investigate the metric potential in this form considering it as a g_{rr} metric and it is given by,

$$B_0^2(r) = \left(1 - \frac{r^2}{\mathscr{R}^2}\right)^{-6}, \tag{3.6}$$

where $\mathscr{R}$ is the curvature parameter describing the geometry of the configuration having a dimension of length $[L]$, the value of which can be determined from the matching conditions. Clearly the metric is finite, continuous and well defined within the stellar structure. Here $B_0^2(r=0)=1$ depicts the finite nature and the non-singularity of the metric potential at the center of the stellar configuration. Also $(B_0^2(r))'_{r=0}=0$ represents the regularity of metric potentials at the center.

Making use of Eqs. (3.4) and (3.5), the anisotropic parameter of the stellar system is defined as (Herrera and Ponce de Leon, 1985)

$$\Delta(r)=8\pi(p_t-p_r)=\left[\frac{A_0''}{A_0B_0^2}-\frac{A_0'}{rA_0B_0^2}-\frac{B_0'}{rB_0^3}-\frac{A_0'B_0'}{A_0B_0^3}-\frac{1}{r^2B_0^2}+\frac{1}{r^2}\right]. \tag{3.7}$$

It is to be noted that anisotropy $\Delta(r)$ is assumed to vanish at the interior of a stellar configuration i.e. $p_r(r)=p_t(r)$. The anisotropic force which is defined as $2\Delta/r$ will be repulsive or attractive in nature depending upon whether $p_t>p_r$ or $p_t<p_r$. For the matter distribution I have considered, repulsive force $p_t>p_r$ supports the construction of compact stellar objects other than isotropic fluid spheres (Gokhroo and Mehra, 1994).

With this choice of $B_0(r)$ Eq. (3.7) then reduces to

$$\begin{aligned}\Delta(r) &= \frac{r^2\left(5r^8-24r^6\mathscr{R}^2+45r^4\mathscr{R}^4-40r^2\mathscr{R}^6+15\mathscr{R}^8\right)}{\mathscr{R}^{12}}+\frac{(r^2-\mathscr{R}^2)^5}{r\mathscr{R}^{12}A_0(r)}\\ &\times \left[(5r^2+\mathscr{R}^2)A_0'(r)+r(r^2-\mathscr{R}^2)A_0''(r)\right].\end{aligned} \tag{3.8}$$

On rearranging Eq. (3.8) one can get

$$\begin{aligned}&\frac{A_0''(r)}{A_0(r)}+\frac{(5r^2+\mathscr{R}^2)A_0'(r)}{r(r^2-\mathscr{R}^2)A_0(r)}+\frac{r^2(5r^8-24r^6\mathscr{R}^2+45r^4\mathscr{R}^4-40r^2\mathscr{R}^6+15\mathscr{R}^8)}{(r^2-\mathscr{R}^2)^6}\\ &=\frac{\Delta(r)\mathscr{R}^{12}}{(r^2-\mathscr{R}^2)^6}.\end{aligned} \tag{3.9}$$

Now the Eq. (3.9) can be solved for $A_0(r)$ if $\Delta(r)$ is specified in particular form. The anisotropy factor need to be taken in such a way that regularity at the center is satisfied and the factor becomes a monotonically increasing function of radial coordinate 'r' (Gokhroo and Mehra, 1994). The increasing trend of anisotropy generally yields well-behaved solution. I am considering anisotropy in polynomial form such that regularity and monotonically increasing condition are satisfied and at the same time Eq. (3.9) can be easily integrable.

Let us assume the anisotropic parameter in the form,

$$\Delta(r) = \frac{r^2(5r^8 - 24r^6\mathscr{R}^2 + 45r^4\mathscr{R}^4 - 40r^2\mathscr{R}^6 + 15\mathscr{R}^8)}{\mathscr{R}^{12}}. \tag{3.10}$$

The above choice for anisotropy is physically reasonable, as at the center ($r = 0$) anisotropy vanishes as expected. Also $\frac{d\Delta(r)}{dr}$ is positive throughout the stellar structure as r is positive, which makes $\Delta(r)$ a monotonically increasing function. Mathematically, writing Eq. (3.9) in the form,

$$A_0''(r) + \frac{5r^2 + \mathscr{R}^2}{r(r^2 - \mathscr{R}^2)}A_0'(r) + \left[\frac{r^2(5r^8 - 24r^6\mathscr{R}^2 + 45r^4\mathscr{R}^4 - 40r^2\mathscr{R}^6 + 15\mathscr{R}^8)}{(r^2 - \mathscr{R}^2)^6} - \frac{\Delta(r)\mathscr{R}^{12}}{(r^2 - \mathscr{R}^2)^6}\right]A_0(r) = 0, \tag{3.11}$$

$\Delta(r)$ are chosen in the form such that the coefficient of $A_0(r)$ vanishes. Essentially I have considered anisotropy in the polynomial form as

$$\Delta = X_1(r^2)^5 + X_2(r^2)^4 + X_3(r^2)^3 + X_4(r^2)^2 + X_5(r^2),$$

i.e. up to order 10 of Taylor Series for Δ in terms of r where $X_1 = \frac{5}{\mathscr{R}^{12}}$, $X_2 = -\frac{24}{\mathscr{R}^{10}}$,

$X_3 = \frac{45}{\mathscr{R}^8}$, $X_4 = -\frac{40}{\mathscr{R}^6}$ and $X_5 = \frac{15}{\mathscr{R}^4}$. This choice of anisotropy is physically reasonable as it ensures that the isotropic pressure can be regained by taking the values of co-efficient as 0. Earlier, similar polynomial form of anisotropy ($\Delta = \sum_i X_i r^i$) were used to study charged anisotropic system in several literature (Maharaj et al., 2014; Sunzu et al., 2014a,b, 2019). In their work, the isotropic pressure condition can be regained by setting arbitrary constants to zero.

Now this choice of anisotropy provides a solution to Eq. (3.9) in closed form. Substituting Eq. (3.10) in Eq. (3.9), one can obtain,

$$A_0''(r) + \frac{(5r^2 + \mathscr{R}^2)}{r(r^2 - \mathscr{R}^2)} A_0'(r) = 0. \tag{3.12}$$

A simple solution of the Eq. (3.12) thus obtained in the form

$$A_0(r) = -\frac{\mathscr{C}}{4(r^2 - \mathscr{R}^2)^2} + \mathscr{D}, \tag{3.13}$$

where $\mathscr{C}$ and $\mathscr{D}$ are integration constants and which will be obtained from the boundary conditions. With the choices of the metric potentials the expressions for the matter density, radial pressure, transverse pressure and the mass function are now obtained as

$$8\pi\rho = \frac{66r^8\mathscr{R}^2 - 13r^{10} - 135r^6\mathscr{R}^4 + 140r^4\mathscr{R}^6 - 75r^2\mathscr{R}^8 + 18\mathscr{R}^{10}}{\mathscr{R}^{12}}, \tag{3.14}$$

$$\begin{aligned} 8\pi p_r = {} & \frac{1}{\mathscr{R}^{12}\left[4\mathscr{D}(r^2 - \mathscr{R}^2)^2 - \mathscr{C}\right]} \Big[\mathscr{C}(7r^{10} - 34r^8\mathscr{R}^2 + 65r^6\mathscr{R}^4 - 60r^4\mathscr{R}^6 + 25r^2\mathscr{R}^8 \\ & - 2\mathscr{R}^{10}) + 4\mathscr{D}\left(r^{10} - 6r^8\mathscr{R}^2 + 15r^6\mathscr{R}^4 - 20r^4\mathscr{R}^6 + 15r^2\mathscr{R}^8 - 6\mathscr{R}^{10}\right)(r^2 \\ & - \mathscr{R}^2)^2\Big], \end{aligned} \tag{3.15}$$

$$8\pi p_t = \frac{2(r^2-\mathscr{R}^2)^5(\mathscr{C}+12\mathscr{D}(r^2-\mathscr{R}^2)^2)}{\mathscr{R}^{12}[4\mathscr{D}(r^2-\mathscr{R}^2)^2-\mathscr{C}]}, \tag{3.16}$$

$$m(r) = \frac{r^3(2\mathscr{R}^2-r^2)}{2\mathscr{R}^{12}}\Big[(r^4-r^2\mathscr{R}^2+\mathscr{R}^4)(r^4-3r^2\mathscr{R}^2+3\mathscr{R}^4)\Big], \tag{3.17}$$

where the mass contained within a radius r of the sphere is defined as

$$m(r) = 4\pi\int_0^r \omega^2\rho(\omega)d\omega. \tag{3.18}$$

3.3 Obtaining the model parameter

Using the boundary condition $p_r = 0$ at $r = b$, where b is the boundary of the star the system of equations in Sect. 3.2 is solved. Clearly mass at the boundary is constant and the interior metric can be joined smoothly with exterior Schwarzschild metric at the boundary provided the mass remains the same as above (Misner and Sharpe, 1964). The exterior space-time for a non radiating star can be described by Schwarzschild metric and it is given as

$$ds^2 = -\left(1-\frac{2\mathcal{M}}{r}\right)dt^2+\left(1-\frac{2\mathcal{M}}{r}\right)^{-1}dr^2+r^2(d\theta^2+\sin^2\theta d\phi^2), \tag{3.19}$$

where $r > 2\mathcal{M}$, $\mathcal{M}$ being the mass of the stellar. The interior space-time metric Eq. (3.1) must be matched to the exterior space-time Eq. (3.19) at the boundary of the star $r = b$. The continuity of the metric across the boundary leads to

$$A_0^2(b) = \left(1-\frac{2\mathcal{M}}{b}\right) \quad \text{and} \quad B_0^2(b) = \left(1-\frac{2\mathcal{M}}{b}\right)^{-1}. \tag{3.20}$$

Since radial pressure drops to zero at a finite value of r, known as the radius of the star, thus from the condition $p_r(r=b)=0$, one can easily find the radius of the star. Also from the above boundary conditions along with the condition $p_r(r=b)=0$ the constants are determined in terms of mass and radius of the star as

$$\begin{aligned}
\mathscr{R} &= \sqrt{\frac{b^2}{1-\left(1-\frac{2\mathcal{M}}{b}\right)^{\frac{1}{6}}}}, \\
\mathscr{C} &= \frac{\mathcal{M}b^3}{\left[-1+\left(1-\frac{2\mathcal{M}}{b}\right)^{\frac{1}{6}}\right]^3}, \\
\mathscr{D} &= \frac{\sqrt{1-\frac{2\mathcal{M}}{b}}\left[\mathcal{M}(8-7(1-\frac{2\mathcal{M}}{b})^{\frac{1}{6}})+4b(-1+(1-\frac{2\mathcal{M}}{b})^{\frac{1}{6}})\right]}{4(b-2\mathcal{M})\left[-1+(1-\frac{2\mathcal{M}}{b})^{\frac{1}{6}}\right]}.
\end{aligned} \tag{3.21}$$

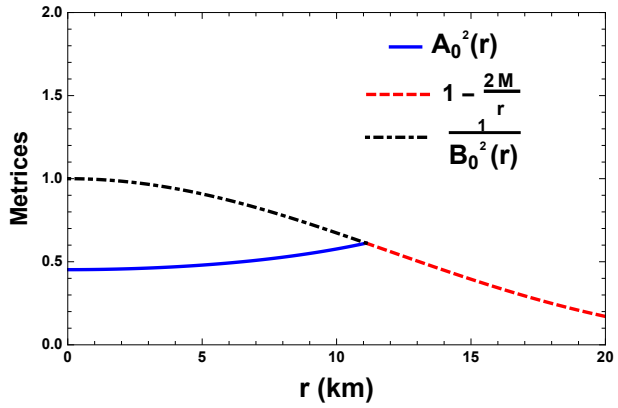

Figure 3.1: Smooth matching of the metric potentials $A_0^2(r)$ and $B_0^2(r)$ at the stellar boundary for the pulsar $4\mathrm{U}1820-30$.

3.4 Physical requirements for well-behaved solutions

For a physically viable stellar model, the non-singular interior solution for the anisotropic fluid sphere of Einstein gravitational field equations should satisfy the following conditions

throughout the stellar configuration:

(i) The gravitational potentials $A_0(r)$, $B_0(r)$ and the matter variables ρ, p_r, p_t should be well defined at the center and finite, regular as well as singularity free throughout the radius of the star.

(ii) The energy density ρ should be positive throughout the stellar interior i.e., $\rho \geq 0$. Its value at the center of the star should be positive, finite and it should be monotonically decreasing towards the boundary inside the stellar interior, mathematically $\frac{d\rho}{dr} \leq 0$ i.e. the energy density should be maximum at the center.

(iii) The radial pressure p_r and the tangential pressure p_t must be positive inside the fluid configuration i.e., $p_r \geq 0, \quad p_t \geq 0$. Additionally $p_r(0) = p_t(0)$ (Ivanov, 2002). All the matter variables are expected to have maximum value at the center of the stellar structure, $\rho'(0) = p_r'(0) = p_t'(0) = 0$ and the gradient of the pressure must be negative inside the stellar body, i.e., $\frac{dp_r}{dr} < 0, \quad \frac{dp_t}{dr} < 0$. At the stellar boundary $r = b$ the radial pressure p_r should vanish but the tangential pressure p_t may not be zero at the boundary. In fact tangential pressure should be greater than radial one except at the center.

At the center both the pressures are equal which means the anisotropy should vanishes at the center, $\Delta(r = 0) = 0$. Also anisotropic factor should be increasing towards the surface.

(iv) For an anisotropic fluid sphere fulfillment of energy conditions refer to the following inequalities in every point inside the fluid sphere is required:

Null Energy Condition (NEC) which includes $\rho + p_r \geq 0$, Strong Energy Condition (SEC) which includes $\rho + p_t \geq 0$; $\rho + p_r + 2p_t \geq 0$ (Hawking and Ellis, 1973),

Dominant Energy Conditions (DEC) which includes $\rho \geq p_r$ and $\rho \geq p_t$.

(v) Causality condition have to be satisfied to be a realistic model i.e. the speed of sound must be smaller than speed of light(assuming the speed of light c=1) in the interior of the star, i.e., $0 \leq \frac{dp_r}{d\rho} \leq 1$, $0 \leq \frac{dp_t}{d\rho} \leq 1$ (Herrera, 1992). The requirements can be compiled into a region as $-1 \leq v_t^2 - v_r^2 \leq 0$ (Abreu et al., 2007) where v_r, v_t are radial and transverse speed respectively.

(vi) The interior metric functions should match smoothly to the exterior Schwarzschild space-time metric at the boundary (Schwarzschild, 1916b). Moreover, these matching criteria generate the value of the model parameter for the metric potentials.

(vii) For a stable model, the adiabatic index i.e. ratio of two specific heats (Chan et al., 1993; Heintzmann and Hillebrandt, 1975; Herrera and Santos, 1997) should be greater than $\frac{4}{3}$.

(viii) The redshift parameter z should be positive, finite and monotonically decreasing outwards.

3.5 Analysis of the physical features of the model

3.5.1 Regularity of the metric

For the model in the present work the gravitational potentials satisfy, $A_0^2(0) = \left(\mathscr{D} - \frac{\mathscr{C}}{4\mathscr{R}^4}\right)^2 =$ constant, $B_0^2(0) = 1$, i.e. finite at the center ($r = 0$). Also, $(A_0^2(r))'_{r=0} = (B_0^2(r))'_{r=0} = 0$, indicate the regularity of the metric potentials at the center and well-behaved nature throughout the stellar interior. Fig. 3.1 depicts the regularity of the metric potentials considering the pulsar $4U1820-30$.

A physical acceptable model should comply with the regularity of matter variables along with that of the metric potentials both at the center and stellar interior. The density ρ, radial pressure p_r and the tangential pressure p_t should be positive inside the star and $\rho(0)$, $p_r(0)$ and $p_t(0)$ should be finite at the center. It is evident from the Figs. 3.3 and 3.4 that the model satisfy the regularity of matter variables. It shows that the density decrease from its maximum value at the center towards its boundary. The radial and tangential pressures are also radially decreasing outwards its boundary from its maximum value at the center. The radial pressure drops to zero at the boundary but the tangential pressure remains non zero at the boundary. The central density, central radial pressure and central tangential pressure in this case are given as

$$\rho(0) = \frac{18}{\mathscr{R}^2}, \quad p_r(0) = p_t(0) = \frac{2\mathscr{C} + 24\mathscr{D}\mathscr{R}^4}{\mathscr{R}^2(\mathscr{C} - 4\mathscr{D}\mathscr{R}^4)}.$$

Since $\mathscr{R}$ is a positive quantity so central density is always positive.

The key feature of the model is the similarity of $p_r(0)$ and $p_t(0)$ i.e. the absence of anisotropy at the center. However, the anisotropy is increasing within the configuration as shown in Fig. 3.5 indicating the direction of anisotropic force to be outward. Theoretically, it proves the existence of a repulsive force which interpolate more compact stellar objects using the anisotropic force rather than using the isotropic force. Using Zeldovich Condition for density and pressure of stable configuration one can have the bound on the model parameters as, $\frac{p_r}{\rho} \leq 1$ at the center i.e. $\frac{\mathscr{C}+12\mathscr{D}\mathscr{R}^4}{\mathscr{C}-4\mathscr{D}\mathscr{R}^4} \leq 9$ i.e. $\mathscr{D}\mathscr{R}^4 \leq \frac{\mathscr{C}}{6}$.

3.5.2 Gradients of the matter variables

Any model is considered to be viable model of anisotropic compact star if the energy density ρ and pressures (p_r, p_t) are maximum at the center and are decreasing monotonically to-

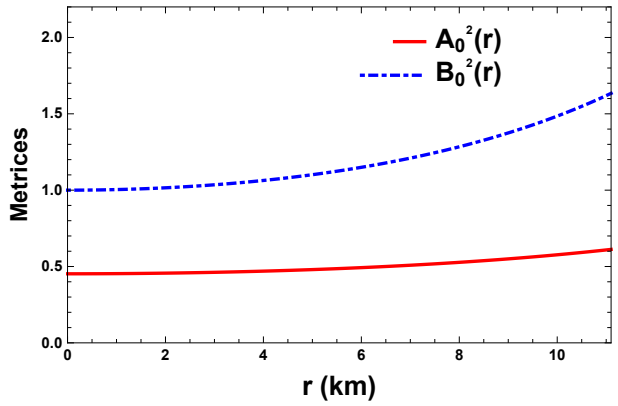

Figure 3.2: Variation of the metric potentials $A_0^2(r)$ (solid red) and $B_0^2(r)$ (dot dashed blue) against the radial coordinate r corresponding to the pulsar $4\mathrm{U}1820-30$.

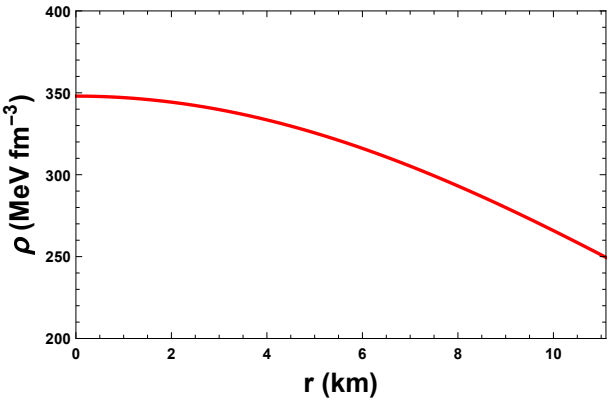

Figure 3.3: Density profile against the radial coordinate r corresponding to the pulsar $4\mathrm{U}1820-30$.

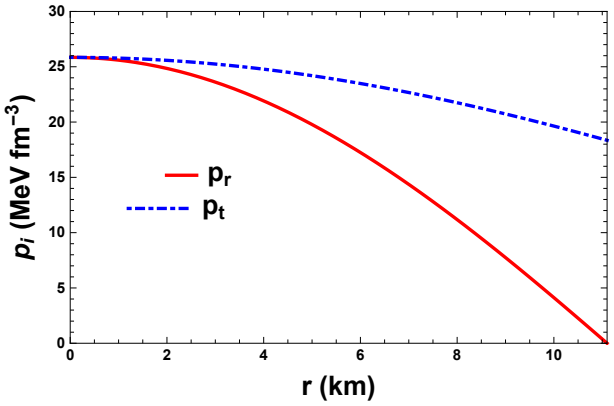

Figure 3.4: Variation of the radial pressure (solid red) and transverse pressure (dot) against the radial coordinate r corresponding to the pulsar $4\mathrm{U}1820-30$.

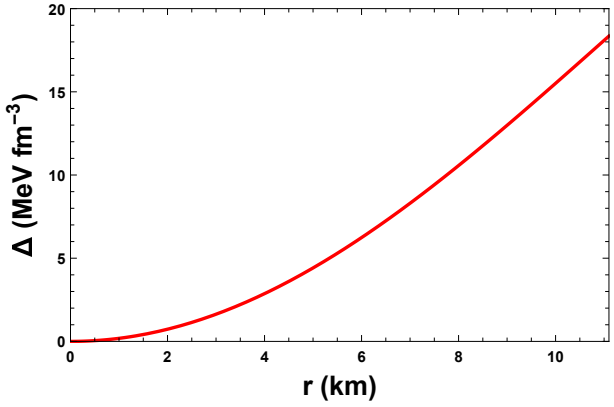

Figure 3.5: Variation of the anisotropy Δ with respect to the radial coordinate r corresponding to the pulsar $4U1820-30$.

wards the surface of the star i.e. $\left(\frac{d\rho}{dr}\right)_{r=0} = 0 = \left(\frac{dp}{dr}\right)_{r=0}$ and $\left(\frac{d^2\rho}{dr^2}\right)_{r=0} < 0$, $\left(\frac{d^2p}{dr^2}\right)_{r=0} < 0$ such that the gradients are negative within $0 < r < b$, b being radius of the star. Here the gradient of energy density, radial pressure and tangential pressure are respectively obtained as

$$8\pi\frac{d\rho}{dr} = \frac{-130r^9 + 528r^7\mathscr{R}^2 - 810r^5\mathscr{R}^4 + 560r^3\mathscr{R}^6 - 150\mathscr{R}^8}{\mathscr{R}^{12}}, \tag{3.22}$$

$$\begin{aligned} 8\pi\frac{dp_r}{dr} &= \frac{1}{\mathscr{R}^{12}\left[\mathscr{C} - 4\mathscr{D}(r^2-\mathscr{R}^2)^2\right]^2}\Big[2r\mathscr{C}^2(-35r^8 + 136r^6\mathscr{R}^2 - 195r^4\mathscr{R}^4 + 120r^2\mathscr{R}^6 \\ &- 25\mathscr{R}^8) + 16\mathscr{C}\mathscr{D}r(r^2-\mathscr{R}^2)^2(7r^8 - 24r^6\mathscr{R}^2 + 27r^4\mathscr{R}^4 - 8r^2\mathscr{R}^6 - 3\mathscr{R}^8) \\ &+ 32\mathscr{D}^2r(r^2-\mathscr{R}^2)^4(5r^8 - 24r^6\mathscr{R}^2 + 45r^4\mathscr{R}^4 - 40r^2\mathscr{R}^6 + 15\mathscr{R}^8)\Big], \end{aligned} \tag{3.23}$$

$$8\pi\frac{dp_t}{dr} = -\frac{4r(r^2-\mathscr{R}^2)^4\left[5\mathscr{C}^2 + 72\mathscr{C}\mathscr{D}(r^2-\mathscr{R}^2)^2 - 240\mathscr{D}^2(r^2-\mathscr{R}^2)^4\right]}{\mathscr{R}^{12}[\mathscr{C} - 4\mathscr{D}(r^2-\mathscr{R}^2)^2]^2}. \tag{3.24}$$

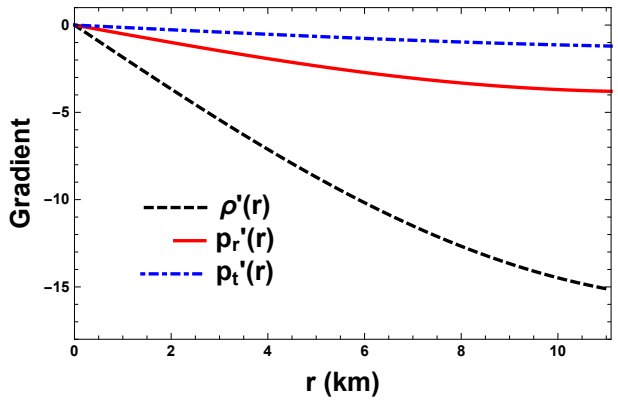

Figure 3.6: Variation of gradients of the pressures, (radial (solid red) and transverse pressure (dot dashed blue)) and the density (dashed black) against the radial coordinate r corresponding to the pulsar $4\mathrm{U}1820-30$.

The gradient of the density, radial pressure and tangential pressure are negative inside the stellar body as shown graphically in Fig. 3.6 which depicts the decreasing nature of

density, radial pressure and tangential pressure with the radial parameter.

3.5.3 Energy conditions

To be physically viable, a stellar composition must need to satisfy some energy conditions throughout the interior. Basically General Relativity framework allows to describe energy conditions as the local inequalities that process a relation between energy density ρ and pressures $(p_r,\ p_t)$ with some certain constraints.

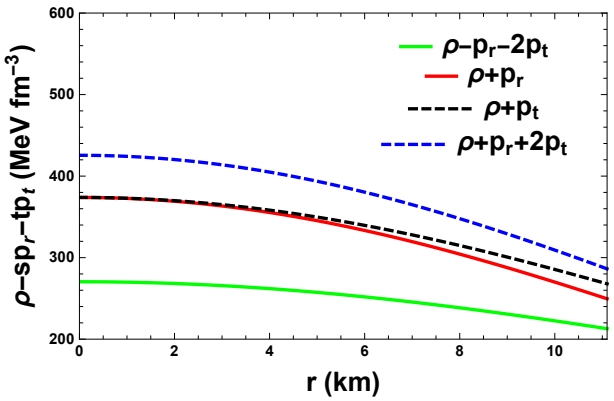

Figure 3.7: Different energy conditions, (SEC (dashed blue), NEC in the radial direction (solid red), NEC in the transverse direction (dashed black)) are plotted against the radial coordinate r corresponding to the pulsar $4U1820-30$. Additionally Trace Energy Condition (TEC): $\rho - p_r - 2p_t$ (solid green) is plotted against the radial coordinate r.

Though there are various ways to calculate energy conditions, our focus mainly revolves around NEC, WEC, SEC and DEC. These energy conditions are: Null Energy Condition (NEC), Weak Energy Condition (WEC), Strong Energy Condition (SEC) and Dominant

Energy Condition (DEC), defined as follows

$$\begin{aligned} NEC_r &: \rho(r)+p_r(r)\geq 0, \quad NEC_t : \rho(r)+p_t(r)\geq 0, \\ WEC_r &: \rho(r)\geq 0, \quad \rho(r)+p_r(r)\geq 0, \\ WEC_t &: \rho(r)\geq 0, \quad \rho(r)+p_t(r)\geq 0, \\ DEC_r &: \rho(r)-|p_r(r)|\geq 0, \quad DEC_t : \rho(r)-|p_t(r)|\geq 0, \\ SEC &: \rho(r)+p_r(r)+2p_t(r)\geq 0. \end{aligned} \tag{3.25}$$

All these energy conditions are satisfied simultaneously by the presented solutions as shown graphically in the Fig. 3.7.

3.5.4 Equation of state

Equation of state (EoS) of the matter distribution describes the relationship of energy density and pressure and is given as

$$\omega_r = \frac{p_r}{\rho}, \quad \omega_t = \frac{p_t}{\rho}. \tag{3.26}$$

For non-exotic configuration EoS parameter must be smaller than 1 i.e. $0 < \omega_r,\ \omega_t < 1$ as suggested by Rahaman et. al (Rahaman et al., 2010). In Fig. 3.8 radial and transverse variations of EoS parameters ω_r and ω_t have been plotted and it can be seen that throughout the interior of the star EoS parameters lie between 0 and 1. It is well known that different EoSs lead to different mass-radius relationships. For high density regime many researchers have suggested linear relationship between energy density and pressure to approximate EoS of the compact star (Dey et al., 1998; Frieman and Olinto, 1989; Gondek-Rosinska et al., 2000; Haensel and Zdunik, 1989; Harko and Cheng, 2002; Prakash et al., 1990). EoS of the

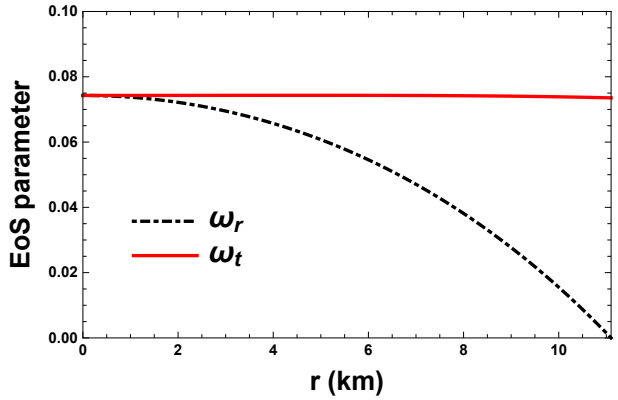

Figure 3.8: Variation of the EoS parameters ω_r and ω_t are plotted with respect to the radial coordinate r corresponding to the pulsar $4\mathrm{U}1820-30$.

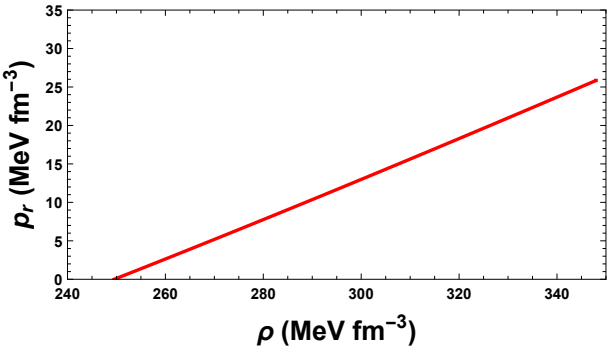

Figure 3.9: Nature of Equation of State (EoS) is plotted. It shows almost linear relationship between the pressure and the density.

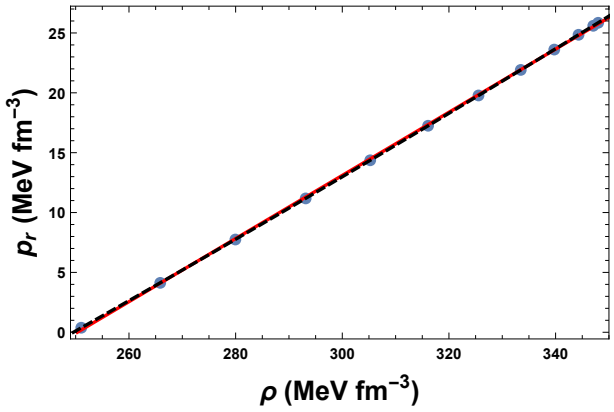

Figure 3.10: Best fit obtained for the EoS for the pulsar $4U1820-30$. Here the solid line (red) denotes linear fit and the dashed line (black) denotes quadratic fit.

matter distribution of a given pulsar is plotted in Fig. 3.9 which shows that the model allows both linear and quadratic relationship between density and pressure. Now one can estimate the best fitted relations between ρ and p_r which is illustrated in Fig. 3.10 as, linear fit is represented by the straight line $p_r = 0.263723\,\rho - 66.0145$ and quadratic fit is represented by $p_r = 0.0001086\,\rho^2 + 0.19782\,\rho - 56.1403$. One can argue that the model permits the quadratic fit slightly better than the linear fit and the MIT bag model is not permitted here. Obtained results are similar to the findings of Chanda et al. (Chanda et al., 2019). It is to be noted that in modeling the compact stellar object, without prescribing any EoS of the anisotropic matter distribution we are able to derive the dependence of radial pressure on the nuclear matter density of the matter distribution.

Mathematically the relation between the pressure and the density can be established for the prescribed model. Now, the expression of pressure and density from Eqs. (3.14) and

(3.15) can be written as,

$$\rho = \frac{1}{\mathscr{R}^2}\Big(18 - 75\epsilon^2y^2 + 140\epsilon^4y^4 - 135\epsilon^6y^6 + 66\epsilon^8y^8 - 13\epsilon^{10}y^{10}\Big), \tag{3.27}$$

$$\begin{aligned} p_r &= \frac{1}{\mathscr{R}^2\left[\mathscr{C} - 4\mathscr{D}\mathscr{R}^4(\epsilon^2y^2-1)^2\right]}\Big[C(2 - 25\epsilon^2y^2 + 60\epsilon^4y^4 - 65\epsilon^6y^6 + 34\epsilon^8y^8 \\ &- 7\epsilon^{10}y^{10}) - 4D\mathscr{R}^4(\epsilon^2y^2-2)(\epsilon^2y^2-1)^2(\epsilon^4y^4 - 3\epsilon^2y^2 + 3)(\epsilon^4y^4 - \epsilon^2y^2 + 1)\Big], \end{aligned} \tag{3.28}$$

where $\epsilon y = \frac{r}{\mathscr{R}}$ and ϵ arbitrarily small. Now near the center of the stellar structure where $r \to 0$, $\epsilon \to 0$. Thus the power series expansion for the density and pressure at the point $r = 0$ gives,

$$\begin{aligned} \rho &\approx \frac{18}{\mathscr{R}^2} + \mathcal{O}\left(\frac{1}{\epsilon^2}\right), \\ p_r &\approx \frac{2\mathscr{C} + 24\mathscr{D}\mathscr{R}^4}{\mathscr{R}^2(\mathscr{C} - 4\mathscr{D}\mathscr{R}^4)} + \mathcal{O}\left(\frac{1}{\epsilon^2}\right). \end{aligned} \tag{3.29}$$

Truncating the higher power of ϵ and eliminating $\mathscr{R}$ from above system of equations, the EoS at the center is obtained as, $p_r = \frac{\mathscr{C}\rho^3 + 3888\mathscr{D}\rho}{9(\mathscr{C}\rho^2 - 1296\mathscr{D})}$. Since $\mathscr{C} >> \mathscr{D}$ for the model, the EoS can be approximated as $p_r \approx \frac{\rho}{9}$.

Similarly, near the boundary for $r \to b$, b being the radius of the star, $\epsilon \to 1$, as R is the quantity $\approx b$. Thus we obtain the nature of the EoS as $p_r = -C\rho$, making it a linear relationship. For super dense stellar structure, C should be < 0, as C positive will represent the EoS of dark energy model.

Compact Star	Mass($M_\odot$)	Radius(km)	$\mathscr{R}$	$\mathscr{C} \times 10^6$	$\mathscr{D}$
PSR J 16142230	1.97 ± 0.04	10.977 ± 0.006	31.946	-2.335	-0.035
Vela X-1	1.77 ± 0.08	10.654 ± 0.14	32.695	-2.637	-0.008
GW170817-1	1.45 ± 0.09	11.9 ± 1.4	44.4879	-9.839	0.072
Cen X-3	1.49 ± 0.08	9.178 ± 0.13	28.6049	-1.5573	-0.0007
KS 1731-260	$1.61^{+0.35}_{-0.37}$	10.0 ± 2.2	31.34	-2.2501	0.0018
SAX J 1748.9-2021	$1.81^{+0.25}_{-0.37}$	11.7 ± 1.7	37.645	-4.7447	0.014
4U1608-52	$1.57^{+0.30}_{-0.29}$	9.8 ± 1.8	30.814	-2.1063	0.003

Table 3.1: Values of the different model parameters corresponding to the different known compact stars.

3.5.5 Matching boundary

The smooth matching of interior metric function with that of Schwarzschild exterior at the boundary of the stellar configuration is shown graphically in Fig. 3.1.

3.5.6 Stability analysis

3.5.6.1 Stability under three forces

A star remains in static equilibrium under three forces namely gravitational force, hydrostatics force and anisotropic force as suggested by Tolman-Oppenheimer-Volkoff as TOV equation. TOV equation (Oppenheimer and Volkoff, 1939; Tolman, 1939) defines the internal structure of a spherically symmetric compact stellar body and it is expressed in the presence of anisotropy as:

$$-\frac{M_G}{r}(\rho + p_r)\frac{A_0(r)}{B_0(r)} - \frac{dp_r}{dr} + \frac{2}{r}(p_t - p_r) = 0, \tag{3.30}$$

where $M_G(r)$ is the effective gravitational mass and it can be derived with the help of Tolman-Whittaker mass formula given as

$$M_G(r) = \frac{rB_0(r)A_0'(r)}{A_0(r)^2}. \tag{3.31}$$

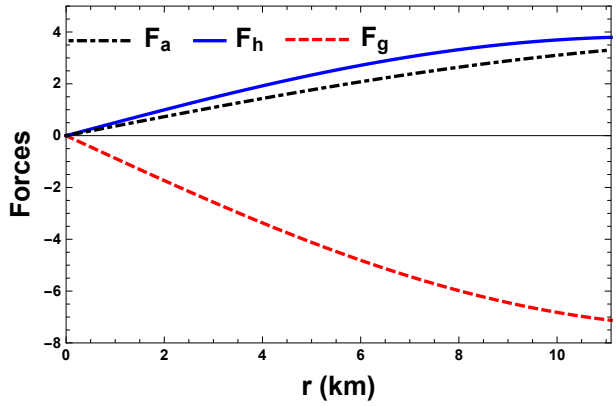

Figure 3.11: Static equilibrium of the model under three different forces namely, the hydrostatic force (solid blue), the anisotropic force (dashed black) and the gravitational force (dashed red).

Using the expression of $M_G(r)$ in Eq. (3.31) it is easy to obtain

$$-\frac{A_0'(r)}{A_0(r)}(\rho + p_r) - \frac{dp_r}{dr} + \frac{2}{r}(p_t - p_r) = 0, \tag{3.32}$$

which is equivalent to

$$F_g + F_h + F_a = 0, \tag{3.33}$$

where

$$F_g = -\frac{A_0'(r)}{A_0(r)}(\rho + p_r), \tag{3.34}$$

$$F_h = -\frac{dp_r}{dr}, \tag{3.35}$$

$$F_a = \frac{2}{r}(p_t - p_r), \tag{3.36}$$

represents gravitational force, hydrostatics force and anisotropic force respectively. Hence the expressions become

$$F_g = -\frac{16\mathscr{C}r(r^2-\mathscr{R}^2)^4\left[5\mathscr{C}-12\mathscr{D}(r^2-\mathscr{R}^2)^2\right]}{\mathscr{R}^{12}\left[\mathscr{C}-4\mathscr{D}(r^2-\mathscr{R}^2)^2\right]^2}, \tag{3.37}$$

$$\begin{aligned} F_h = {} & \frac{2r}{\mathscr{R}^{12}[\mathscr{C}-4\mathscr{D}(r^2-\mathscr{R}^2)^2]^2}\Big[\mathscr{C}^2(35r^8-136r^6\mathscr{R}^2+195r^4\mathscr{R}^4-120r^2\mathscr{R}^6+25\mathscr{R}^8) \\ & + 8\mathscr{C}\mathscr{D}(r^2-\mathscr{R}^2)^2(7r^8-24r^6\mathscr{R}^2+27r^4\mathscr{R}^4-8r^2\mathscr{R}^6-3\mathscr{R}^8)+16\mathscr{D}^2(r^2-\mathscr{R}^2)^4 \\ & (5r^8-24r^6\mathscr{R}^2+45r^4\mathscr{R}^4-40r^2\mathscr{R}^6+15\mathscr{R}^8)\Big], \end{aligned} \tag{3.38}$$

$$F_a = \frac{r}{\mathscr{R}^{12}}(5r^8-24r^6\mathscr{R}^2+45r^4\mathscr{R}^4-40r^2\mathscr{R}^6-15\mathscr{R}^8). \tag{3.39}$$

Clearly from Fig. 3.11 it can be concluded that gravitational force is negative, dominating in nature and is balanced by the combined effect of hydrostatic forces and anisotropic forces to keep the system in equilibrium.

3.5.6.2 Herrera Cracking Method

For self-gravitating compact stellar objects, the concept of cracking for anisotropic matter distribution are first studied by Herrera (Herrera, 1992). This condition is used to determine the stability of a configuration of anisotropic matter fluid. Herrera condition states that for a physically acceptable model both the sound speeds (radial and transverse) need to satisfy

causality conditions i.e. $0 \leq v_r^2 \leq 1$ and $0 \leq v_t^2 \leq 1$. The radial and transverse velocity of sound ($c = 1$) are given as

$$
\begin{aligned}
v_r^2 &= \frac{1}{[\mathscr{C} - 4\mathscr{D}(r^2 - \mathscr{R}^2)^2]^2(65r^8 - 264r^6\mathscr{R}^2 + 405r\mathscr{R}^4 - 280r^2\mathscr{R}^6 + 75\mathscr{R}^8)} \\
&\times \Big[\mathscr{C}^2(35r^8 - 136r^6\mathscr{R}^2 + 195r^4\mathscr{R}^4 - 120r^2\mathscr{R}^6 + 25\mathscr{R}^8) - 8\mathscr{C}\mathscr{D}(r^2 - \mathscr{R}^2)^2(7r^8 \\
&- 24r^6\mathscr{R}^2 + 27r^4\mathscr{R}^4 - 8r^2\mathscr{R}^6 - 3\mathscr{R}^8) - 16\mathscr{D}^2(r^2 - \mathscr{R}^2)^4(5r^8 - 24r^6\mathscr{R}^2 \\
&+ 45r^4\mathscr{R}^4 - 40r^2\mathscr{R}^6 + 15\mathscr{R}^8)\Big], \qquad (3.40) \\
v_t^2 &= \frac{2(r^2 - \mathscr{R}^2)^4[5\mathscr{C}^2 + 72\mathscr{C}\mathscr{D}(r^2 - \mathscr{R}^2)^2 - 240\mathscr{D}^2(r^2 - \mathscr{R}^2)^4]}{[\mathscr{C} - 4\mathscr{D}(r^2 - \mathscr{R}^2)^2]^2(65r^8 - 264r^6\mathscr{R}^2 + 405r\mathscr{R}^4 - 280r^2\mathscr{R}^6 + 75\mathscr{R}^8)}. \qquad (3.41)
\end{aligned}
$$

Fig. 3.12 supports the fulfillment of causality condition for the model. Later Abreu et al. (Abreu et al., 2007) reinstate Herrera's cracking concept to determine the range for a potentially stable (or unstable) anisotropic compact stellar object. As per their study a potentially stable model should follow the inequality $-1 \leq v_t^2 - v_r^2 \leq 0$ provided no sign change of $v_t^2 - v_r^2$ within the stellar radius.

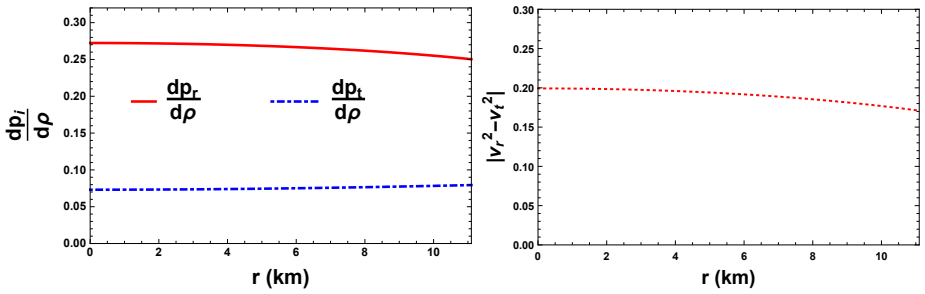

Figure 3.12: Variation of sound velocity (left) in the radial direction (solid red) and transverse direction (dot dashed blue) and variation of difference of the sound speeds (right) with respect to the radial coordinate r corresponding to the pulsar $4\mathrm{U}1820 - 30$.

This model fulfills $0 \leq v_r^2 \leq 1$ and $0 \leq v_t^2 \leq 1$ throughout the interior as shown in

Fig. 3.12 and the inequality $-1 \leq v_t^2 - v_r^2 \leq 0$ also holds for the present model as shown in Fig. 3.12.

3.5.6.3 Adiabatic index

For fixed energy density, the nature of EoS can be described by the adiabatic index. The stability of relativistic as well as non-relativistic compact star depends on the adiabatic index. For relativistic anisotropic structure, the adiabatic index Γ is described as the ratio of two specific heats and is defined as (Chan et al., 1993)

$$\Gamma = \frac{\rho + p}{p}\frac{dp}{d\rho}. \tag{3.42}$$

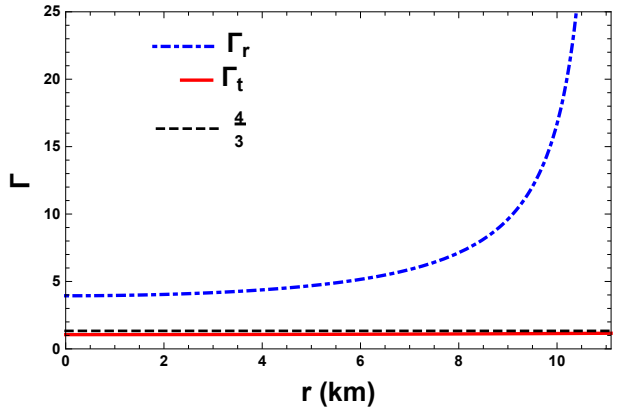

Figure 3.13: Variation of the adiabatic indices in the radial (dot dashed blue) and the transverse direction (solid red) with the radial coordinate r corresponding to the pulsar $4U1820-30$.

Bondi (Bondi, 1964) suggested for the Newtonian sphere the stability condition is $\Gamma > \frac{4}{3}$ and for neutral equilibrium the stability condition becomes $\Gamma = \frac{4}{3}$. Later, Heintzmann and Hillebrandth (Heintzmann and Hillebrandt, 1975) for an anisotropic sphere to be in equilibrium, the adiabatic index Γ must be $> \frac{4}{3}$. Fig. 3.13 shows that values of Γ are

greater than $\frac{4}{3}$ throughout the stellar configuration.

3.5.6.4 Mass-radius and compactness

To study the viability of any prescribed model, estimating mass-radius relation and thus finding maximum mass is of particular interest. It is possible to exhibit that the present model can illustrate a relativistic compact stellar object by choosing certain value of unknown parameters.

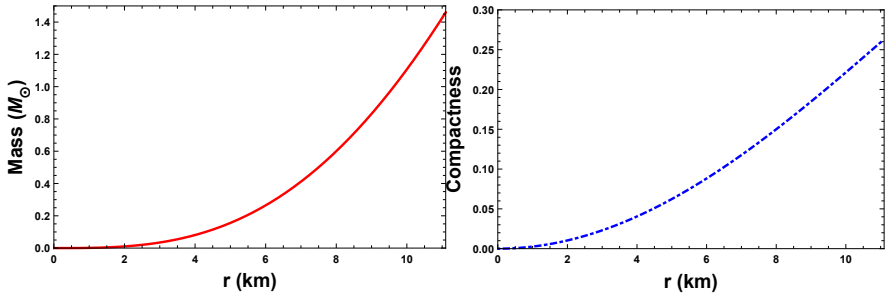

Figure 3.14: Increasing nature of the mass function (left) and the compactness factor (right) with the radial coordinate r corresponding to the pulsar $4\mathrm{U}1820-30$.

The mass function of the stellar structure is an increasing function of r as shown in Fig. 3.14 and the compactification factor (mass to radius ratio) are given as

$$u(r)=\frac{r^2(2\mathscr{R}^2-r^2)(r^4-r^2\mathscr{R}^2+\mathscr{R}^4)(r^4-3r^2\mathscr{R}^2+3\mathscr{R}^4)}{2\mathscr{R}^{12}}. \tag{3.43}$$

Specifying the surface density as considered by Sharma et al (Sharma et al., 2017) ($\rho(r=b)=7.5\times10^{14}$ gm cm^{-3}), the mass-radius ($M-b$) relationship for the present model is generated as shown in Fig. 3.15. The upper bound to the maximum mass allowed with this model is found to be $\approx 3.113\ M_\odot$ for the radius of value $10.49\ km$. It is well known that the limit on maximum mass for a neutron star is $\approx 3.2\ M_\odot$ (Rhoades

and Ruffini, 1974) and for uniform density spheres in general relativity this limit is $\approx$ 5.2 $M_{\odot}$ (Shapiro and Teukolsky, 1983).

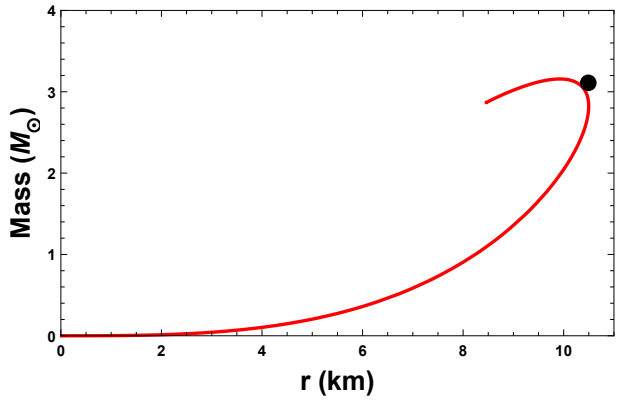

Figure 3.15: The mass-radius ($M - b$) plot for the model is plotted assuming the surface density $7.5 \times 10^{14} gm\ cm^{-3}$. The marked circle denotes the maximum mass as $3.113\ M_{\odot}$ for the radius $10.49\ km$.

For spherically symmetric fluid distribution the maximum limit for mass to radius ratio is given as $< \frac{4}{9}$ (Buchdahl, 1959) and it is satisfied by the model as depicted in Fig. 3.14.

3.5.6.5 Buchdahl Condition

For any given radius one can generate the total mass of an anisotropic star and vice-versa. For the stability of a compact stellar model, the mass-radius ratio or the compactness $[u(r) = m(r)/r]$ of the model should be < 0.44 (Buchdahl, 1959) as proposed by Buchdahl. Though Buchdahl have suggested the limit for a spherically symmetric isotropic fluid sphere, several studies have suggested that anistropic structure can remain stable if Buchdahl limit are satisfied for the model (Bhar, 2019; Gedela et al., 2019b; Singh et al., 2017). Additionally for more generalized expression for a mass-radius ratio can be known by Mak and Harko's work (Mak and Harko, 2003). Carvalho et al. (Carvalho et al., 2015) have studied the effect of mass-radius ratio on the EoS for compact stars.

Also, the gravitational redshift is given as

$$z = \left(1 - \frac{2M}{r}\right)^{-1/2} - 1. \tag{3.44}$$

From Eq. (3.44) it is evident that gravitational redshift increases with the increase of $\frac{M}{r}$.

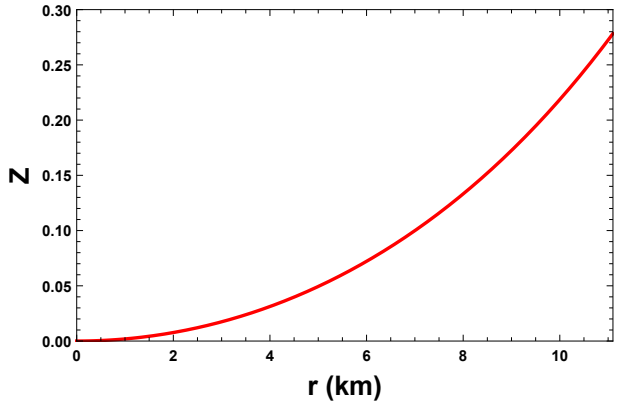

Figure 3.16: Variation of the gravitational redshift z with radial coordinate r corresponding to the pulsar $4\mathrm{U}1820-30$.

Since compactness of a star satisfies Buchdahl condition so there should exist an upper bound for gravitational surface redshifts, it cannot be arbitrarily large for any self-gravitating compact stellar object. The surface redshifts should obey the inequality $z < 2$ for a stable configuration (Buchdahl, 1966). In Fig. 3.16 the profile of the variation for the gravitational redshift is plotted.

3.5.6.6 Harrison-Zeldovich-Novikov Criterion

For a stable structure of an anisotropic compact star, the mass of a compact star should always increase with the increase of central density as suggested by Harrison-Zeldovich-Novikov criterion (Harrison et al., 1965; Zeldovich and Novikov, 1972). This stability condition states that $\frac{dM}{d\rho(0)} > 0$ leads to a stable configuration and $\frac{dM}{d\rho(0)} \leq 0$ for a unstable

one.

Here using the value of central density we can write the expressions for mass and gradient as

$$\begin{aligned} \rho(0) &= \frac{18}{\mathscr{R}^2}, \\ M(\rho(0)) &= \frac{b^3\rho(0)(36-b^2\rho(0))(\rho(0)^2b^4-18\rho(0)b^2+18^2)}{2\times 18^6} \\ &\times \left(b^4\rho(0)^2-54b^2\rho(0)+3\times 18^2\right), \qquad (3.45) \\ \frac{dM(\rho(0))}{d\rho(0)} &= \frac{b^3(18-b^2\rho(0))^5}{11337408}. \qquad (3.46) \end{aligned}$$

The Harrison-Zeldovich-Novikov criterion for the stability of our model is verified in Fig. 3.17. Both the mass function M and its gradient $\frac{dM}{d\rho(0)}$ as the functions of central density are positive throughout the structure to show a stable model.

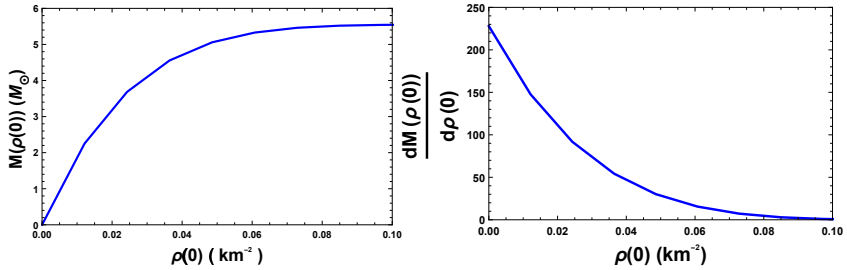

Figure 3.17: Mass is plotted as a function of the central density and it is seen to be increasing with the increase of central density corresponding to the pulsar $4U1820-30$ (left). Variation of $\frac{dM}{d\rho(0)}$ with the central density $\rho(0)$ corresponding to the pulsar $4U1820-30$ (right).

.

3.5.6.7 Radius-central density relationship

Any viable model is compact stellar model depending on the relationship between radius and the central density. The significance of radius-central density relation is that it allows

us to estimate the radius and hence the mass of an anisotropic compact stellar model for a given central density and vice-versa. For a specific choice of surface density we have plotted the radius vs central density in Fig. 3.18 and I have marked the point for which maximum mass is obtained. For radius $10.49\ km$ we have obtained central density as $1.738 \times 10^{18}\ kg\ m^{-3}$.

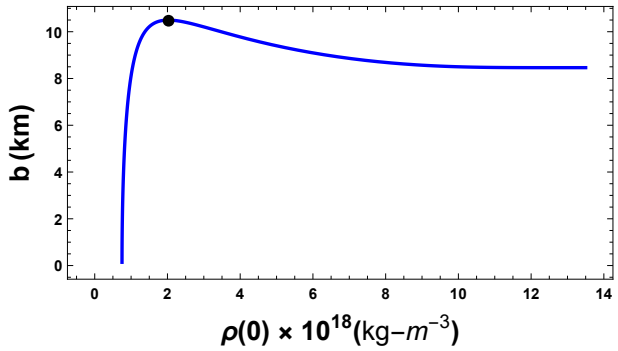

Figure 3.18: Variation of the radius of the model with the central density $\rho(0)$. The solid circle represents the central density corresponding to maximum mass for the model.

3.5.6.8 Moment of inertia and time period

The moment of inertia for a compact stellar object can be approximated using Bejger-Haensel (Bejger and Haensel, 2002) method which transforms a static system to a rotating system. The basic idea is to consider the effects of rotation as perturbation of a static spherically symmetric spacetime for a compact star. The approximation of the moment of inertia can be given as,

$$I = \frac{2}{5}(1+x)Mb^2, \tag{3.47}$$

where the parameter x can be defined as $x = (M/M\odot)(km/b)$. Variation of the moment of inertia with the mass is depicted in Fig. 3.19. From Fig. 3.19 it can be seen that maximum inertia obtained is $1247.1\ km^3$ for the mass $3.106\ M_\odot$. Now one can easily conclude

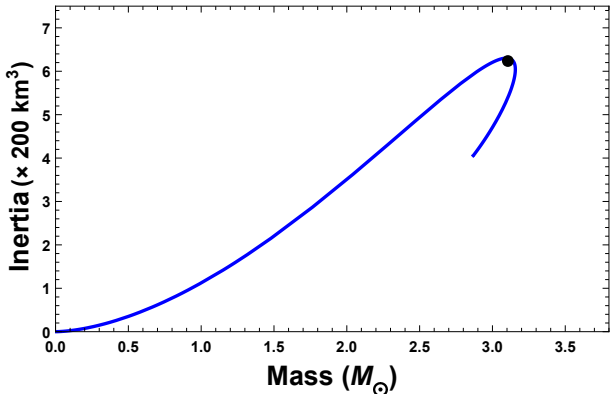

Figure 3.19: Variation of the moment of inertia with the mass of the model. The solid circle represents the moment of inertia corresponding to the maximum mass of the model.
.

that mass obtained for maximum inertia on Fig. 3.19 is slightly lower ($\approx 0.22\%$) than the maximum mass obtained from ($M - b$) curve in Fig. 3.15 suggesting that the EoS is free from any softening to an exotic state (Bejger et al., 2005).

For any rotating compact stellar objects minimum time period can be expressed by mass and radii of any non-rotating structures and it allows for clear understanding of the constraints resulting from the detection of a submillisecond pulsar in the mass-radius plane for non rotating structure (Haensel et al., 1995). The minimum time period of rotation can be approximated as,

$$\tau \approx 0.82 \left(\frac{M\odot}{M}\right)^{\frac{1}{2}} \left(\frac{b}{10\ km}\right)^{\frac{3}{2}}\ ms, \tag{3.48}$$

Fig. 3.20 depicts the profile of time period with the mass for the EoS. For this choice of EoS the minimum rotation frequency obtained, for maximum allowable mass, is $\approx 1.472\ ms$.

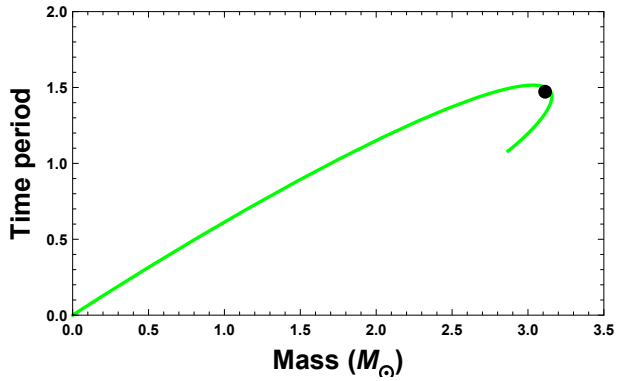

Figure 3.20: Variation of the time period with the mass. The solid circle represents the time period corresponding to the maximum allowable mass.

3.5.7 Generating Functions

The generating functions are used to present all feasible anisotropic solutions of the EFEs for the static spherically symmetric fluid matter as suggested by L. Herrera (Herrera et al., 2008). For the considered spacetime the generating function can be expressed as,

$$B_0(r) = \frac{1}{\sqrt{F - 2\int (\Pi(r) + \frac{1}{r^2} e^{\int \frac{N(r)}{D(r)} dr}) dr}}, \tag{3.49}$$

where,

$$\begin{aligned} N(r) &= Z(r)\Big\{r + 2r^2 + r^3 Z'(r) - r^5 Z''(r)\Big\} + r^4 Z''(r) + r^4(2r-1)Z'(r)^2 \\ &+ r^2(4r-3)Z'(r) - 2, \\ D(r) &= r^2(rZ'(r) - 1)\{1 + r^2 Z'(r)\}. \end{aligned}$$

Here F is a constant of integration and the corresponding generating functions are,

$$\begin{aligned} Z(r) &= \frac{1}{A_0}+\frac{1}{r}, \\ \Pi(r) &= 8\pi(p_r-p_t). \end{aligned} \tag{3.50}$$

Using the value of A_0 in Eq. (3.13) in Eq. (3.50), the generating functions to represent all the feasible solutions for our model becomes,

$$\begin{aligned} Z(r) &= \frac{1}{r}+\frac{4(r^2-R^2)^2}{4D(r^2-R^2)^2-C}, \\ \Pi(r) &= -8\pi\Delta(r), \end{aligned} \tag{3.51}$$

where $\Delta(r)$ is given in the Eq. (3.10).

3.6 Comparative study of the model

To examine the applicability of this model I have considered various well known pulsars and I have chosen the data from LIGO/VIRGO collaboration as well as the independent measurements of mass and radius of millisecond pulsars such as PSR J 1614-2230 (Mass $= 1.97 \pm 0.04 M_\odot$ (Demorest et al., 2010), Radius $= 10.977 \pm 0.006$ km (Deb et al., 2016)), Vela X-1 (Mass $= 1.77 \pm 0.08 M_\odot$, Radius $= 10.654 \pm 0.14$ km (Deb et al., 2016)), GW170817-1 (Mass $= 1.45 \pm 0.09 M_\odot$, Radius $= 11.9 \pm 1.4$ km (Abbott et al., 2018)), Cen X-3 (Mass $= 1.49 \pm 0.08 M_\odot$, Radius $= 9.178 \pm 0.13$ km (Gangopadhyay et al., 2013)), KS $1731-260$ (Mass $= 1.61^{+0.35}_{-0.37} M_\odot$, Radius $= 10.0 \pm 2.2$ km (Özel et al., 2016)), SAX J 1748.9-2021 (Mass $= 1.81^{+0.25}_{-0.37} M_\odot$, Radius $= 11.7 \pm 1.7$ km (Özel et al., 2016)) and 4U1608-52 (Mass $= 1.57^{+0.30}_{-0.29} M_\odot$, Radius $= 9.8 \pm 1.8$ km (Özel et al., 2016)). All the

detailed study have been given in tabular form. Table. 3.1 describes the values of the model parameter and using these values the physical parameters are calculated and compiled in a tabular form in Table. 3.2. In Table. 3.2 $|_0$ and $|_b$ respectively denote the values of the physical parameters at the center ($r = 0$) and at the boundary ($r = b$) of a star. Here for all the stars, it can be observed that central density is higher than surface density and SEC also decreases as it proceeds towards the surface from the center from a star. Moreover, both the radial and transverse velocity of the sound decreases from the center towards the boundary of the star. The decreasing nature of the physical matter variables fashions a physically viable model of a compact star. Additionally, surface redshifts for all the stars are consistent with the strange stars having a density higher than neutron stars, mathematically $z_b \leq 0.9$ (Lindblom, 1984).

3.7 Discussions

In this paper, I have studied a model for a spherically symmetric anisotropic matter fluid sphere by assuming a specific metric potential $B_0^2(r)$. By taking a specific form of anisotropy we solve the system of equations and found both the metric potentials. Comparing the obtained solutions with exterior Schwarzschild, I have obtained the expressions for constants $\mathcal{R}, \mathscr{C}, \mathscr{D}$.

In particular, the constraints and all physical properties have been compared considering the pulsar $4U1820-30$, i.e. taking mass$= 1.46\pm0.21M_\odot$ and radius $= 11.1\pm1.8$ km (Özel et al., 2016). Thus having the values as follows: $\mathscr{R} = 39.5968$, $\mathscr{C} = -6.0692 \times 10^6$ and $\mathscr{D} = 0.0553119$. Numerical values of the constant parameter for the model are given in Table 3.1 and all the matter variables for different well known compact stars are given in Table 3.2. Also, the graphical representation for the fulfillment of the physical and stability

conditions are given, revealing this model to be a potentially viable model.

- The metric potentials and the matter variables $\rho,\ p_r,\ p_t$ are depicted graphically in Figs. 3.1-3.4. The decreasing nature of the matter variables forms a base for our model to be a stable configuration. Also, the anisotropy depicted as Fig. 3.5 shows repulsive force and it confirms the formation for anisotropic compact stellar structure. Moreover, the radial derivative of matter variables vanish at the center and is negative for the stellar interior.

- Various energy conditions are studied for the model graphically in Fig. 3.7 and each energy conditions are satisfied inside the stellar structure. Also the SEC have been studied for various known compact stars in tabular form in Table 3.2.

- Different forces are shown graphically in Fig. 3.11 and it can be seen that dominant gravitational force is balanced by the combining effect of hydrostatic and anisotropic forces.

- EoS parameters for both the radial and transverse pressures are described in Fig. 3.9 and for the model EoS parameter for transverse pressure is greater than that of radial one. Also, the relationship between density and pressure is depicted in Fig. 3.8, it shows both linear and quadratic relationship. However the quadratic fit is slightly better fitted than the linear one as shown in Fig. 3.10.

- The stability of our model is investigated using Herrera cracking concept and the fulfillment of our model is shown in Fig. 3.12. Also, the absolute value of the difference between radial and transverse sound speed is in the range $(0, 1)$ portraying the stability of the model.

- Considering a specific surface density ($7.5 \times 10^{14}\ gm\ cm^{-3}$) the mass-radius relationship have been discussed in Fig. 3.15 and the maximum mass are calculated to be $3.113\ M_{\odot}$ for the radius $10.49\ km$ which is within the observable range as predicted by Ruffini (Rhoades and Ruffini, 1974). Moreover using the idea of perturbation the mass-moment of inertia relationship have also been discussed in Fig. 3.19 and it can be concluded that maximum mass on the $(M - b)$ plot is approximately 0.22% greater than the mass obtained for the maximum inertia in the Fig. 3.19 suggesting the stiffness of the EoS.

- The mass function and the compactness are the increasing functions of r and they attain maximum value at the surface. Additionally, the gravitational redshift against the radius of the star is depicted in Fig. 3.16. It can be observed that gravitational redshift vanishes at the center attaining its maximum at the surface. Additionally the compactness for the prescribed model is 0.437 which is within the limit predicted by Buchdahl and the surface redshift for this model is 1.8334 which is below the suggested upper bound (< 2) for a stable model.

- The radius-central density relationship have been studied graphically in Fig. 3.18 to illustrate the nature of the radius of the model with the change of central density and hence have estimated the central density to be $1.738 \times 10^{18}\ kg\ m^{-3}$.

Thus it can be concluded that several physical features and stability criteria required for a physically viable anisotropic compact stellar configuration are satisfied by the model. Hence this model can be of astrophysical relevance for studying anisotropic compact stars.

Compact Star	$\rho\|_0$	$\rho\|_b$	$\frac{dp_r}{d\rho}\|_0$	$\frac{dp_r}{d\rho}\|_b$	$\frac{dp_t}{d\rho}\|_0$	$\frac{dp_t}{d\rho}\|_b$	$(\rho+p_r+2p_t)\|_0$	$(\rho+p_r+2p_t)\|_b$	$z\|_b$
PSR J 1614-2230	534.59	323.34	0.382	0.318	0.183	0.164	758.95	399.26	0.45
Vela X-1	510.39	324.99	0.3427	0.2957	0.143	0.1365	689.53	392.37	0.40
GW170817-1	275.67	203.73	0.2579	0.2401	0.058	0.0663	329.63	230.72	0.249
Cen X-3	66.80	430.56	0.333	0.289	0.133	0.1293	889.436	516.685	0.3853
KS 1731-260	555.50	360.45	0.3298	0.2879	0.131	0.12682	737.71	431.63	0.38
SAXJ 1748.9-2021	384.98	255.5	0.3153	0.2789	0.116	0.1155	501.26	302.98	0.356
4U1608-52	574.609	373.92	0.3279	0.2868	0.129	0.1253	761.133	447.208	0.376

Table 3.2: Values of the different physical parameters corresponding to the different known compact stars using the values from Table. 3.1.

Chapter 4

Finch-Skea geometry under the effect of anisotropy

4.1 Introduction

Thorough reviews on exact solutions for Einstein field equations were published from time to time (Stephani et al., 2003). One such new exact solution to the Einstein field equations is obtained by Finch and Skea (Finch and Skea, 1989) by correcting the solution given by Duorah and Ray (Duorah and Ray, 1987). This solution fulfills all the criteria to describe static static spherically symmetric perfect fluid solutions as reviewed by Delgaty and Lake (Delgaty and Lake, 1998). One astonishing feature of the solution is that their model described compact star in isotropic pressure only. Therefore, here motivation for the present work is to consider a model of anisotropic star that reduces to the Finch-Skea solution for zero anisotropy.

The Finch-Skea metric (Finch and Skea, 1989) is well behaved and also has been shown

to be consistent with the Walecka theory (Walecka, 1974) for cold condensed star. Additionally, this metric is found to be consistent to study neutron star, especially to investigate central densities of neutron star in relativistic mean-field theory (Walecka, 1975). Essentially this spacetime satisfies the characteristic of a perfect fluid matter which obeys barotropic equation of state (EoS). The underlying approach to solving Einstein's equations for spherical symmetry involved *ad hoc* assumptions for one of the gravitational potentials as the system of field equations is under-determined and possesses one degree of freedom. It is interesting to note that the Finch-Skea metric involves theorizing a form for the radial potential which allows for the complete integration of the field equations whereupon all the remaining geometric and dynamical quantities may be determined (Chilambwe and Hansraj, 2015). Kalam et al. (Kalam et al., 2013a,b) have invested their time to model strange quark stars using the Finch-Skea metric considering the MIT bag model (Kalam et al., 2013b) as well as two fluid model (Kalam et al., 2013a) and have proposed quintessence stars combining anisotropic pressure corresponding to normal matter (Kalam et al., 2014).

On the other hand, Maharaj et al. (Maharaj et al., 2017) have shown that the Finch-Skea geometry can be generalized to include charge and anisotropy. Considering a particular solution to the charged anisotropy of this model Matondo et al. (Matondo et al., 2017) have predicted the masses of the stellar objects for three different scenarios, viz, (i) charged anisotropic, (ii) charged isotropic, and (iii) uncharged isotropic distributions which were found to be compatible with several known compact stellar objects. Tikekar and Jotania (Tikekar and Jotania, 2007) applied the Finch-Skea metric (Finch and Skea, 1989), by assuming the 3-space of the interior spacetime of a strange star is that of a three-paraboloid immersed in a 4-dimensional Euclidean space, to acquire a two-parameter family of physically viable relativistic models of neutron stars and showed that it admitted possibilities

of describing strange stars as well as other highly compact stellar configurations of matter in equilibrium. The Finch-Skea ansatz (Finch and Skea, 1989) was also used Sharma and Ratanpal (Sharma and Ratanpal, 2013) to generate a class of solutions describing the interior of a static spherically symmetric anisotropic star. Later, Pandya et al. (Pandya et al., 2015) have generalized the model of Sharma and Ratanpal (Sharma and Ratanpal, 2013) by incorporating a dimensionless parameter $n(> 0)$ in the Finch-Skea ansatz (Finch and Skea, 1989) by assuming the system to be anisotropic. Charged Finch-Skea stars were described in terms of Bessel functions and modified Bessel functions, by Hansraj and Maharaj (Hansraj and Maharaj, 2006) and Maharaj et al. (Maharaj et al., 2017), where both the models are found to obey a barotropic EoS.

Bhar et al. (Bhar et al., 2014) have produced anisotropic stars in $(2 + 1)$ dimensions and a quark EoS by using the Finch-Skea metric (Finch and Skea, 1989). A class of interior solutions corresponding to the BTZ (Bañados et al., 1992) exterior solution has been investigated by Banerjee et al. (Banerjee et al., 2013) under the Finch-Skea metric which is relevant for the description of realistic stars in $(3 + 1)$ dimensions as a complementary approach to the study by García et al. (García and Campuzano, 2003).

For higher dimensions, several researchers Hansraj (2017); Hansraj et al. (2015); Molina et al. (2017) have studied the Finch-Skea metric as well as its generalizations. Another fascinating study by Hansraj et al. Hansraj et al. (2015) shows that the Finch-Skea spacetime also arises in the 5-dimensional Einstein-Gauss-Bonnet modified theory of gravity, suggesting that the Finch-Skea geometry may play an important role in more general Lovelock polynomials with a Lagrangian containing higher order terms (Maharaj et al., 2017).

It is worthy to note that anisotropy in pressure plays a significant role in the structure and properties of compact star. Karmarkar et al. (Karmarkar et al., 2007) indicated that numerical value of the compactness parameter $\frac{2M}{R}$, M and R being the mass and radius of the star, may approach unity for anisotropic stars. The upper limit of the surface redshift for anisotropic stars becomes 3.842 and 5.211 when the transverse components of the pressure satisfy the strong and the dominant energy condition respectively (Ivanov, 2002). Mak and Harko (Mak and Harko, 2004a,b) have showed that anisotropy must be maximum at the surface of the compact star and it should be zero at the center of the fluid sphere. There are good number of models on anisotropic compact star under General Relativity in literature (Kumar et al., 2019; Mak and Harko, 2004a; Maurya et al., 2018b, 2019a; Maurya and Govender, 2017; Maurya et al., 2017, 2019b; Sharma and Maharaj, 2007). Several researchers have studied anisotropy on alternative theories of gravitation considering various ansatzs such as Buchdahl (Maurya et al., 2020a), modified Durgapal–Fuloria potential (Maurya and Tello-Ortiz, 2020) to name a few. Moreover, self-gravitating, charged isotropic fluids can also be studied for super compact star modeling (Kumar et al., 2018). In the present chapter I have examined the nature of anisotropy in Finch-Skea metric to model a stable compact star.

The present chapter is organized as follows: Sec. 4.2 depicts a brief highlight to the Einstein field equation. Exact solution to the field equations in the presence and absence of anisotropy and finding the model constants after smooth matching of spacetime at the boundary is provided in Sec. 4.3 and Sec. 4.4 respectively. The physical analysis and the stability analysis for the obtained solution are discussed in Sec. 4.5 and Sec. 4.6 respectively. Sec. 4.7 provides an insight of the mass-radius relationship for the model. Finally, concluding remarks are given in Sec. 4.8.

4.2 Einstein's field equation and the interior solution for the model

Let us consider the model which represents a static spherically symmetric fluid configuration. The line element describing the interior space-time of a spherically symmetric star in Schwarzschild coordinates $x^0 = t$, $x^1 = r$, $x^2 = \theta$, $x^3 = \phi$ can be written as

$$ds^2_- = -A_0^2(r)dt^2 + B_0^2(r)dr^2 + r^2(d\theta^2 + \sin^2\theta d\phi^2), \tag{4.1}$$

where $A_0(r)$ and $B_0(r)$ are the gravitational potential yet to be established.

To study stellar structure and stellar evolution the basic supposition made by the researchers is to consider the interior of a star as a perfect fluid (Clayton, 1983; Kippenhahn et al., 2012). The pressure in the interior of a star is considered to be isotropic to model this perfect fluid (Dev and Gleiser, 2002). Several studies in recent times have shown that, at very high density, alteration in isotropic pressure plays a vital role in studying the features of a stellar interior (Canuto, 1974; Ruderman, 1972). Thus the energy momentum tensor is anisotropic, isotropy being the extra assumptions on the behaviors of the fields or of the fluid modeling the stellar interior (Dev and Gleiser, 2002).

The matter distribution of the stellar interior is thus described by an energy-momentum tensor of the form

$$T_{\alpha\beta} = (\rho + p_t)u_\alpha u_\beta + p_t g_{\alpha\beta} + (p_r - p_t)\chi_\alpha\chi_\beta, \tag{4.2}$$

where ρ represents the energy-density, p_r and p_t, respectively denote fluid pressures along the radial and transverse directions, u^α is the 4-velocity of the fluid and χ^α is a unit space-

like 4-vector along the radial direction so that $u^\alpha u_\alpha = 1$, $\chi_\alpha \chi_\beta = -1$ and $u^\alpha \chi_\beta = 0$.

The Einstein field equations governing the evolution of the system is then obtained as (we set $G = c = 1$)

$$8\pi\rho = \left[\frac{1}{r^2} - \frac{1}{r^2 B_0^2} + \frac{2B_0'}{rB_0^3}\right], \tag{4.3}$$

$$8\pi p_r = \left[-\frac{1}{r^2} + \frac{1}{B_0^2 r^2} + \frac{2A_0'}{rA_0B_0^2}\right], \tag{4.4}$$

$$8\pi p_t = \left[\frac{A_0''}{A_0B_0^2} + \frac{A_0'}{rA_0B_0^2} - \frac{B_0'}{rB_0^3} - \frac{A_0'B_0'}{A_0B_0^3}\right], \tag{4.5}$$

where in above set of Eqs. (4.3) – (4.5), a 'prime' denotes differentiation with respect to r.

From the expression of radial and transverse pressure, the anisotropic parameter of the stellar system can be defined as

$$\Delta(r) = 8\pi(p_t - p_r) = \left[\frac{A_0''}{A_0B_0^2} - \frac{A_0'}{rA_0B_0^2} - \frac{B_0'}{rB_0^3} + \frac{A_0'B_0'}{A_0B_0^3} - \frac{1}{r^2B_0^2} + \frac{1}{r^2}\right]. \tag{4.6}$$

Moreover, the mass contained within a radius r of the sphere is defined as

$$m(r) = \frac{1}{2}\int_0^r \omega^2\rho(\omega)d\omega. \tag{4.7}$$

At this stage, we have a system of equations consisting of three equations Eq. (4.3) – Eq. (4.5) with five unknowns ρ, p_r, p_t, $A_0(r)$ and $B_0(r)$. Thus to find the exact solutions of the field equations and hence to model a stellar interior, we need to specify two of them. To model a physically reasonable stellar configuration, I can choose the metric potential g_{rr} is of the form as considered by Finch-Skea (Finch and Skea, 1989) and it is given by

$$B_0^2(r) = \left(1 + \frac{r^2}{R^2}\right), \tag{4.8}$$

where R is the curvature parameter describing the geometry of the configuration having a dimension of length. This choice of metric potential assures that the function $B_0^2(r)$ is finite, continuous and well defined within stellar interior range. Also $B_0^2(r) = 1$ for $r = 0$ ensures that it is finite at the center. Again, the metric is regular at the center since $(B_0^2(r))'_{r=0} = 0$.

With this choice of $B_0(r)$, Eq. (4.6) then reduces to

$$\Delta(r) = \frac{r^3 A_0 + R^2 \left[r\left(r^2+R^2\right) A_0'' - \left(R^2+2r^2\right) A_0'\right]}{r\left(r^2+R^2\right) A_0}. \tag{4.9}$$

On rearranging Eq. (4.9), one can get

$$\frac{R^2 A_0''}{A_0} - \frac{R^2\left(R^2+2r^2\right)}{r\left(r^2+R^2\right)}\frac{A_0'}{A_0} + \frac{r^2}{r^2+R^2} = \Delta(r). \tag{4.10}$$

Now the above Eq. (4.10) can be solved for $A_0(r)$ if the anisotropic parameter, $\Delta(r)$ is specified in particular form. One can easily obtain solutions for the following two cases from Eq. (4.10): (i) $\Delta(r) = 0$ and (ii) $\Delta(r) \neq 0$. I have discussed both the cases in the next Section.

4.3 Exact solutions to the field equations

To obtain an exact solution for Eq. (4.10), the anisotropy needs to be considered in some specific form. Therefore the anisotropic factor can be written as

$$\Delta = \frac{\alpha r^2 (R^2 - r^2)}{(R^2 + r^2)^3}, \tag{4.11}$$

where α is the parameter determining the measure of the anisotropy. Now this choice of anisotropy is feasible for the consideration of the anisotropic factor as Δ is regular for the radial coordinate r and also $\Delta(r=0)=0$ is satisfied at the center. Utilizing this choice of anisotropy in Eq. (4.10), the master equation reads in the form

$$\frac{\left[rR^2(r^2+R^2)^3\right]A_0'' - R^2(2r^2+R^2)(r^2+R^2)^2A_0'}{r(r^2+R^2)^3A_0} + \frac{r^3\left[(r^2+R^2)^2+\alpha(r^2-R^2)\right]A_0}{r(r^2+R^2)^3A_0} = 0. \tag{4.12}$$

Now the present work intents to study the exact solutions of the field equations for different values of α. Here I have investigated the values of α for $-1,\ 0$ and 1. It is worth mentioning that similar investigation have been conducted by Sharma and Das (Sharma and Das, 2013) using the Finch-Skea metric. Their model represents an initially static star which is either anisotropic or isotropic in nature and which eventually describes a gravitationally collapsing system. However, in the present work I am attempting to depict a spherically symmetric stable configuration, for both anisotropic and isotropic nature of pressure.

Now using Frobenius Method (Teschl, 2012) one can solve Eq. (4.12) at $r = 0$. Considering the solution in the series form, it can be written as

$$A_0 = \sum_{n=1}^{\infty} c_n r^{s+n},\ c_0 \neq 0. \tag{4.13}$$

Computing the values of A_0' and A_0'' and substituting all the values on Eq. (4.12), one can obtain the following differential equation as

$$rR^2\left(r^6+3r^4R^2+3r^2R^2+R^6\right)\sum_{n=1}^{\infty}(s+n)(s+n-1)c_nr^{s+n-2}$$

$$
\begin{aligned}
&- \quad R^2(2r^6+5r^4R^2+4r^2R^4+R^6)\sum_{n=1}^{\infty}(s+n)c_n r^{s+n-1} \\
&+ \quad r^3(r^4+2r^2R^2+R^4+\alpha r^2-\alpha R^2)\sum_{n=1}^{\infty}c_n r^{s+n}=0. \qquad (4.14)
\end{aligned}
$$

Equating to zero the coefficient of the smallest power of r and hence solving, one can get the roots of the indicial equation as 0 and 2. Further solving for each coefficient of r the solution of Eq. (4.12) yields

$$A_0 = Mu(r) + Nv(r), \qquad (4.15)$$

where M and N are two arbitrary constants and

$$
\begin{aligned}
u(r) &= 1+\frac{7}{2R^2}r^2+\frac{6R^2+\alpha}{8R^6}r^4+..., \qquad (4.16)\\
v(r) &= r^2\left[1+\frac{1}{4R^2}r^2+\frac{\alpha-2R^2}{24R^6}+...\right].
\end{aligned}
$$

However due to complexity of the solution I have investigated the exact solution of the model by considering specific values of α which is described in the following subsections.

4.3.1 Exact solution in the presence of anisotropy

4.3.1.1 Case I: $\alpha = -1$

To obtain an exact solution to Eq. (4.10), let us assume the anisotropic parameter to be in the form

$$\Delta(r) = \frac{r^2\left(r^2-R^2\right)}{\left(r^2+R^2\right)^3}. \qquad (4.17)$$

The above choice for the anisotropy is physically reasonable, as at the center ($r = 0$),

anisotropy vanishes as expected. Fig. 4.1 depicts the nature of anisotropy which clearly supports the regularity at the center. However the negative nature for the anisotropy leads us to some consequences as discussed subsequently. Similar profile of the anisotropic pressure can be observed in the work of Thirukkanesh et al. (Thirukkanesh et al., 2020). As a limitation of our model, I have not discussed the isotropic pressure condition from the specified anisotropic form.

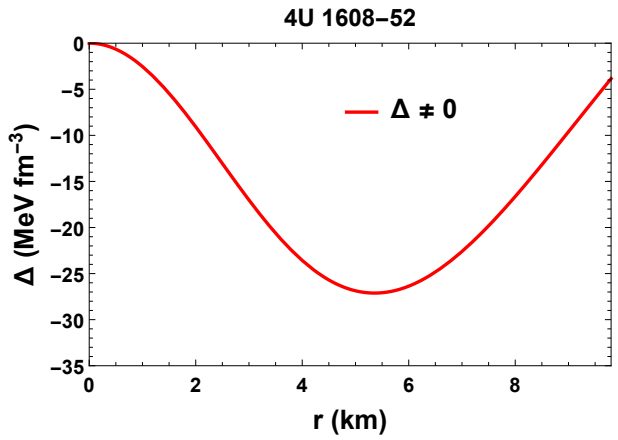

Figure 4.1: Behavior of the anisotropy within the configuration with respect to the radial coordinate r corresponding to the pulsar $4\mathrm{U}1608-52$.

Also, this choice provides a solution to Eq. (4.10) in closed form. Substituting Eq. (4.17) in Eq. (4.10) gives

$$\frac{R\left(r(r^2+R^2)^2A_0''-(r^2+R^2)(2r^2+R^2)A_0'+2r^3A_0\right)}{r(r^2+R^2)A_0}=0. \tag{4.18}$$

A simple solution to Eq. (4.18) can be obtained as follows:

$$A_0=\left(C\sqrt{r^2+R^2}+D\left(r^2+R^2\right)\right), \tag{4.19}$$

where C and D are integration constants which will be obtained from the boundary condi-

tions.

With these choices of the metric potentials the matter density, radial pressure, transverse pressure and mass are obtained as

$$8\pi\rho = \frac{r^2+3R^2}{\left(r^2+R^2\right)^2}, \tag{4.20}$$

$$8\pi p_r = \frac{C\left(R^2-r^2\right)-D\left(r^2-3R^2\right)\sqrt{r^2+R^2}}{\left(r^2+R^2\right)^2\left(C+D\sqrt{r^2+R^2}\right)}, \tag{4.21}$$

$$8\pi p_t = \frac{R^2\left[C\left(R^2-r^2\right)+D\sqrt{r^2+R^2}\left(r^2+3R^2\right)\right]}{\left(r^2+R^2\right)^3\left(C+D\sqrt{r^2+R^2}\right)}, \tag{4.22}$$

$$m(r) = \frac{r^3}{2\left(r^2+R^2\right)}. \tag{4.23}$$

Moreover, the gradients of the matter variables are obtained as

$$8\pi\frac{d\rho}{dr} = \frac{2r}{\left(r^2+R^2\right)^2}-\frac{4r\left(r^2+3R^2\right)}{\left(r^2+R^2\right)^3}, \tag{4.24}$$

$$\begin{aligned} 8\pi\frac{dp_r}{dr} &= \frac{2rC^2\left(r^2-3R^2\right)\sqrt{r^2+R^2}}{\left(r^2+R^2\right)^{7/2}\left(C+\ D\sqrt{r^2+R^2}\right)^2}+\frac{2rCD\left(2r^2-9R^2\right)\left(r^2+R^2\right)}{\left(r^2+R^2\right)^{7/2}\left(C+D\sqrt{r^2+R^2}\right)^2} \\ &+ \frac{2rD^2\left(r^2-7R^2\right)\left(r^2+R^2\right)^{3/2}}{\left(r^2+R^2\right)^{7/2}\left(C+D\sqrt{r^2+R^2}\right)^2}, \end{aligned} \tag{4.25}$$

$$8\pi\frac{dp_t}{dr} = \frac{R^2\left[C\left(R^2-r^2\right)+D\left(r^2+3R^2\right)\sqrt{r^2+R^2}\right]}{\left(r^2+R^2\right)^3\left(C+D\sqrt{r^2+R^2}\right)}. \tag{4.26}$$

4.3.1.2 Case II: $\alpha = 1$

The anisotropic factor now reduces to

$$\Delta = \frac{r^2(R^2-r^2)}{(R^2+r^2)^3}. \tag{4.27}$$

Using the value of Eq. (4.27), the master equation Eq. (4.10) reduces to the form

$$\frac{\left[r^2(r^2+R^2)A_0''-(2r^2+R^2)A_0'\right]R^2(r^2+R^2)}{r(r^2+R^2)A_0}+\frac{2r^4}{(r^2+R^2)}=0. \tag{4.28}$$

Since the solution generated from Eq. (4.28) are imaginary (See Appendix), so I am excluding this discussions from the present work.

It is to note that in the original Finch-Skea paper (Finch and Skea, 1989) the exact solution in the presence of isotropy is available, i.e. for $p = p_r = p_t$ as such the isotropic pressure condition has been adopted. The solution for Eq.(4.10) has the form,

$$A_0=\left(G-H\sqrt{1+\frac{r^2}{R^2}}\right)\cos\sqrt{1+\frac{r^2}{R^2}}+\left(G\sqrt{1+\frac{r^2}{R^2}}+H\right)\sin\sqrt{1+\frac{r^2}{R^2}}, \tag{4.29}$$

where the integration constants G and H will be obtained from the boundary conditions. Since further detailed calculation can be found in (Finch and Skea, 1989), so I am not repeating here the calculations based on the isotropic condition, however for the sake of comparison I have plotted graphs for both the cases which will help to observe the effect of anisotropy in the present model.

4.4 Exterior spacetime and boundary conditions

The exterior space-time, spacetime outside the spherically symmetric configuration, for a non-radiating star is empty and is described by the exterior Schwarzschild solution as

$$ds^2=-\left(1-\frac{2M}{r}\right)dt^2+\left(1-\frac{2M}{r}\right)^{-1}dr^2+r^2\left(d\theta^2+\sin^2\theta d\phi^2\right), \tag{4.30}$$

where $r > 2M$, M being the total mass of the stellar object. To study a compact stellar structure, the interior space-time metric (4.1) must be matched smoothly to the exterior Schwarzschild spacetime metric Eq. (4.30) at the boundary of the star $r = b$. This condition is known as the continuity of the first fundamental form or Darmois-Israel condition (Darmois, 1927; Israel, 1966) and the continuity of the metric functions across the boundary $r = b$ yields

$$A_0^2(b) = \left(1 - \frac{2M}{b}\right), \quad B_0^2(b) = \left(1 - \frac{2M}{b}\right)^{-1}. \tag{4.31}$$

The radial pressure drops to zero at a finite value of the radial parameter r, defined as the radius of the star. This is defined as the continuity of the second fundamental form and utilizing the condition $p_r(r = b) = 0$, the radius of the star can be obtained as follows

$$\left[-\frac{1}{b^2} + \frac{1}{B_0^2 b^2} + \frac{2A_0'}{bA_0B_0^2}\right] = 0. \tag{4.32}$$

Fulfillment of continuity for both the first and the second fundamental forms is known as the junction condition and it is utilized to determine the constants for isotropic as well as anisotropic cases. Thus the constants for the model are obtained in the forms:

$$R = \frac{b\sqrt{b-2M}}{\sqrt{2M}}, \tag{4.33}$$

$$C = \frac{M}{b^2}\left(3\sqrt{\frac{b-2M}{2M}} - \sqrt{\frac{2M}{b-2M}}\right), \tag{4.34}$$

$$D = \sqrt{\frac{2M^3}{b^7}}\left(\sqrt{\frac{2M}{b-2M}} - \sqrt{\frac{b-2M}{2M}}\right), \tag{4.35}$$

$$G = \frac{\sqrt{\frac{1}{\varphi}}\left(\sqrt{\varphi}\,\cos\left(\sqrt{\varphi}\right)+\sin\left(\sqrt{\varphi}\right)\right)}{2\sqrt{\varphi}\left(\cos\left(\varphi\right)+\sin\left(\varphi\right)\right)}, \tag{4.36}$$

$$H = \frac{\sqrt{\frac{1}{\varphi}}\left(\sqrt{\varphi}\,\sin\left(\sqrt{\varphi}\right)-\cos\left(\sqrt{\varphi}\right)\right)}{2\sqrt{\varphi}\left(\cos\left(\varphi\right)+\sin\left(\varphi\right)\right)}, \tag{4.37}$$

where $\frac{b}{b-2M} = \varphi$.

4.5 Physical analysis

To study the physical features of the prescribed model I have considered the values from the pulsar 4U $1608-52$ as mass $= 1.57^{+0.30}_{-0.29}\ M_{\odot}$ and radius $= 9.8 \pm 1.8$ km (Roupas and Nashed, 2020). The values of the model parameters thus obtained are $R = 10.3526$, $C = 0.0535902$, $D = -0.000185649$, $G = 0.328696$ and $H = 0.305526$. I have analyzed the profile of the model analytically as well as graphically by considering the aforementioned dataset. However, the values of the model parameters for some other known compact stellar objects are depicted in Table. 4.1.

4.5.1 Regularity condition

For any acceptable model, regularity of the solutions must be maintained. Analytically, the gravitational potentials should be free from any geometrical or physical singularity. Here, $A_0^2(0) = R^2(C+DR)^2$=constant (for anisotropic case), $A_0^2(0) = 0.5403(G-H)+0.84147(G+H)$= constant (for isotropic case) and $B_0^2(0) = 1$, i.e., finite at the center ($r = 0$) of the stellar configuration. Also one can easily check that $(A_0^2(r))'_{r=0} = (B_0^2(r))'_{r=0} = 0$. These imply that the metric is regular at the center and well behaved

throughout the stellar interior. Fig. 4.2 exhibits the profile of the metric potentials within the stellar structure for both the anisotropic and isotropic cases.

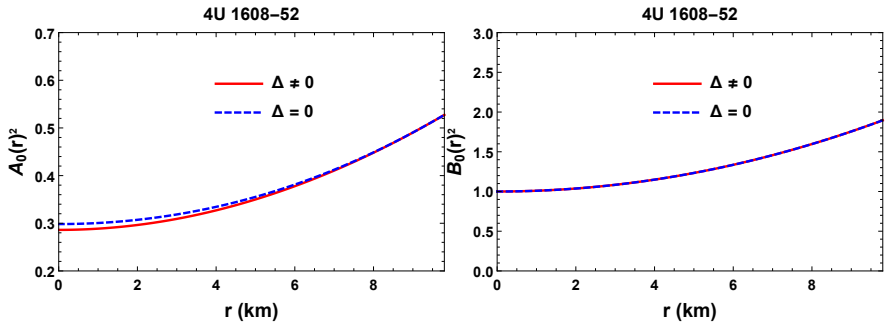

Figure 4.2: Variation of the metric potentials $A_0^2(r)$ (left) and $B_0^2(r)$ (right) with the radial coordinate r corresponding to the pulsar $4\mathrm{U}1608-52$. Here the solid lines (red) represent the anisotropic case and the dashed lines (blue) represent the isotropic case.

4.5.2 Zeldovich's condition

The central density, central radial pressure and central tangential pressure in this case are obtained as

$$8\pi\rho(0) = \frac{3}{R^2}, \tag{4.38}$$

$$8\pi p_r(0) = 8\pi p_t(0) = \frac{C+3DR}{R^2(C+DR)}, \tag{4.39}$$

for anisotropic case and

$$8\pi p_r(0) = 8\pi p_t(0) = \frac{(G+H)+1.5574(H-G)}{R^2\left[(G-H)+1.5574(G+H)\right]}, \tag{4.40}$$

for isotropic case.

Here R being the curvature parameter, it is always positive, thus making the central

density a positive quantity.

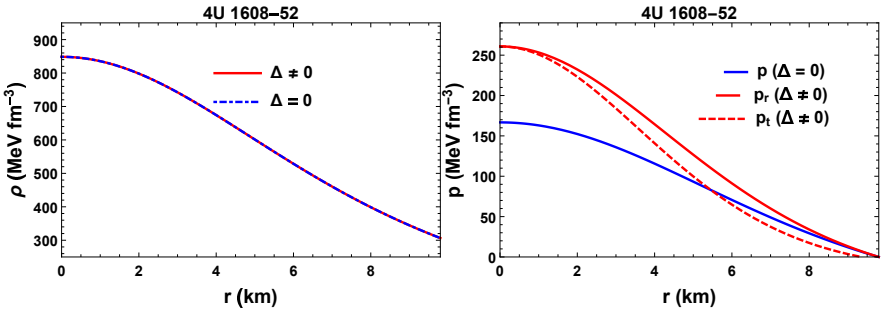

Figure 4.3: Variation of the matter variables, density (left) and pressure (right) in the radial (solid red), transverse direction (dashed red) for the anisotrpic case and pressure (solid blue) for the isotropic case, with the radial coordinate r corresponding to the pulsar $4\mathrm{U}1608-52$.

For isotropic nature, both the pressures should be always equal whereas for anisotropic profile, the equality of the central values of both the radial pressure and tangential pressure depicts the absence of anisotropy at the center. The radial and tangential pressures at the center will be non-negative provided the chosen model parameters are all positive. Also according to Zeldovich's condition (Zeldovich, 1962, 1972), p_r/ρ must be ≤ 1 at the center. Therefore

$$\frac{C+3DR}{3(C+DR)} \leq 1 \text{ and } \frac{(G+H)+1.5574(H-G)}{3\left[(G-H)+1.5574(G+H)\right]} \leq 1,$$

for anisotropic and isotropic cases respectively.

The density ρ, radial pressure p_r and transverse pressure p_t are positive inside the structure and monotonically decreasing outward. Fig. 4.3 supports the positive and monotonically decreasing behavior of the matter variables. However, since Fig. 4.3 depicts that the transverse force is always lower than the radial one throughout the structure implying the attractive nature of the anisotropic force. This type of force is known to make the model less stable than the repulsive force.

4.5.3 Density parameter

The density variation parameter λ is defined as the ratio of the density at the surface to that at the center. Now for the prescribed model, the density variation parameter can be expressed as

$$\lambda = \frac{\rho(b)}{\rho(0)} = \frac{R^2(b^2+3R^2)}{3(b^2+R^2)^2}.$$

Now for the fixed surface density of $2\times10^{14}\ gm/cc$, Parui and Sarma (Parui and Sarma, 1991) have deduced that minimum radius density (the ratio of the surface density to the radius of the star) is minimum for the $\lambda = 0.68$. Based on this study, later Parui (Parui, 1995) has generalized that for both the charged and uncharged neutron star of densities having 10^{15} and $10^{16}\ gm/cc$, λ_{max} becomes 0.68 in each cases. For our model, considering the fixed surface density $2\times10^{14}\ gm/cc$, the model parameter R supports the value 0.673623, the mass and radius become $0.6725\ M_{\odot}$ and 2.1743 km respectively for maximum limit of density variation parameter. However, the permissible value of λ for several different stars of different surface densities are presented in Table 4.2.

4.5.4 Energy density

The gradients of energy density, radial pressure and tangential pressures for anisotropic case are given in Eqs. (4.24)-(4.26). The gradient of the density, radial pressure and tangential pressure are negative inside the stellar body are shown graphically in Fig. 4.4.

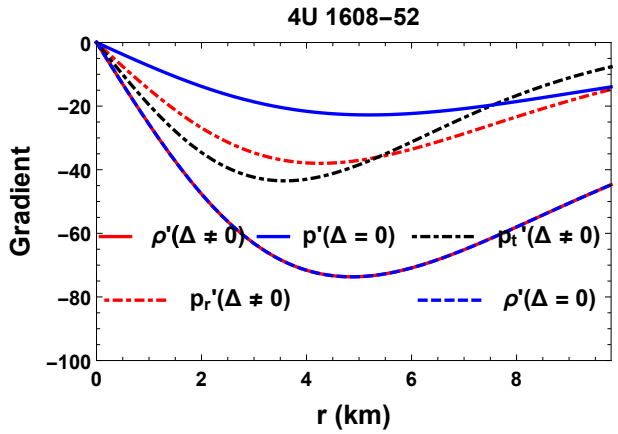

Figure 4.4: Variation of the gradients of the matter variables, the density for the anisotropic case (solid red), for the isotropic case (dashed blue), the radial pressure (dashed red), the transverse pressure (dot dashed black) for the anisotropic case and the pressure (solid blue) for the isotropic case with the radial coordinate r corresponding to the pulsar $4\mathrm{U}1608-52$.

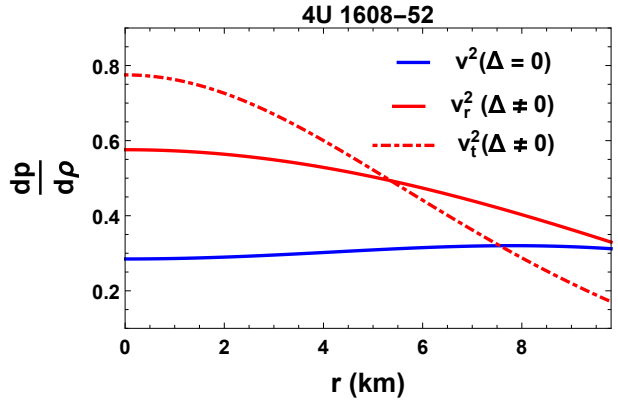

Figure 4.5: Variation of the sound speeds along the radial (solid red), transverse direction (dashed red) for the anisotropic case, sound speed (solid blue) for the isotropic case with the radial coordinate r corresponding to the pulsar $4\mathrm{U}1608-52$.

4.5.5 Herrera's Cracking Method

The radial and transverse velocity of sound ($c = 1$) are obtained as

$$\begin{aligned} v_r^2 &= \frac{-C^2(r^2-3R^2)}{(r^2+5R^2)(C+D\sqrt{r^2+R^2})^2} + \frac{D^2(r^4-6r^2R^2+7R^4)}{(r^2+5R^2)(C+D\sqrt{r^2+R^2})^2} \\ &+ \frac{CD(-2r^4+7r^2R^2+9R^4)}{\sqrt{r^2+R^2}(r^2+5R^2)(C+D\sqrt{r^2+R^2})^2}, \end{aligned} \tag{4.41}$$

$$\begin{aligned} v_t^2 &= \frac{-2R^2C^2(r^2-2R^2)}{(r^2+R^2)(r^2+5R^2)(C+D\sqrt{r^2+R^2})^2} \\ &+ \frac{2R^2D^2(r^4+5r^2R^2+4R^4)}{(r^2+R^2)(r^2+5R^2)(C+D\sqrt{r^2+R^2})^2} \\ &+ \frac{CDR^2(-r^4+10r^2R^2+11R^4)}{(r^2+R^2)^{\frac{3}{2}}(r^2+5R^2)(C+D\sqrt{r^2+R^2})^2}, \end{aligned} \tag{4.42}$$

$$\begin{aligned} v^2 &= \frac{(r^2+R^2)\,(G+H\tan\Gamma)}{\Gamma(r^2+5R^2)} \times \frac{(-H(r^2+R^2)+G\Gamma(r^2+2R^2))}{[R(G-H\Gamma)+(H+G\Gamma)\tan\Gamma]^2} \\ &+ \frac{(r^2+R^2)\,(G+H\tan\Gamma)}{\Gamma(r^2+5R^2)} \times \frac{(G(r^2+R^2)+H\Gamma(r^2+2R^2))\tan\Gamma}{[R(G-H\Gamma)+(H+G\Gamma)\tan\Gamma]^2}, \end{aligned} \tag{4.43}$$

where $\sqrt{1+\frac{r^2}{R^2}} = \Gamma$. v_r^2 and v_t^2 are $\frac{dp_r}{d\rho}$ and $\frac{dp_t}{d\rho}$ respectively, described for the case of anisotropy. For isotropic case, v^2 denotes $\frac{dp}{d\rho}$, p being the pressure for prescribed model.

In this model the speed of sound are smaller than 1 in the interior of the star, i.e., $0 \leq \frac{dp_r}{d\rho} \leq 1$, $0 \leq \frac{dp_t}{d\rho} \leq 1$ for anisotropic case and $0 \leq \frac{dp}{d\rho} \leq 1$ for isotropic case, which has been shown graphically in Fig. 4.5.

4.5.6 Energy Condition

The energy conditions play a crucial role to study the nature of the matter content in GR. The energy conditions are not physical constraints but are rather mathematically imposed boundary conditions on the matter variables. They restrict some contraction of the stress tensor at every spacetime point. The three main conditions studied here are: null energy

condition (NEC), weak energy condition (WEC) and strong energy condition (SEC). The expressions for the energy conditions are described as follows:

$$\begin{aligned} NEC_r &: \rho(r)+p_r(r)\geq 0, \quad NEC_t : \rho(r)+p_t(r)\geq 0, \\ WEC_r &: \rho(r)\geq 0, \quad \rho(r)+p_r(r)\geq 0, \\ WEC_t &: \rho(r)\geq 0, \quad \rho(r)+p_t(r)\geq 0, \\ SEC &: \rho(r)+p_r(r)+2p_t(r)\geq 0. \end{aligned}$$

However, for an isotropic fluid sphere, the equality of the radial and the transverse pressure implies the expressions for the energy conditions as $\rho + p_r \geq 0$ and $\rho + 3p_t \geq 0$, throughout the stellar interior. These quantities are shown to remain positive throughout the compact sphere graphically in Fig. 4.6. Although it is quite obvious that for non-negative

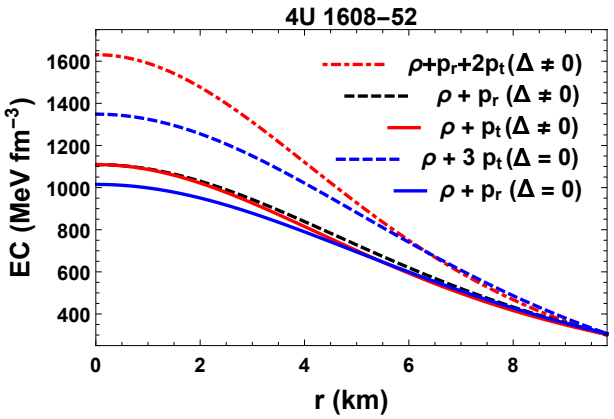

Figure 4.6: Variation of the various energy conditions, SEC for the anisotropic case (dashed red), for the isotropic case (dashed blue), NEC for the anisotropic case in the radial direction (dashed black), in the transverse direction (solid red), NEC for the isotropic case (solid blue) with the radial coordinate r corresponding to the pulsar $4\mathrm{U}1608-52$.

density and pressures, their sum should also be non-negative. However for understanding the nature of the energy conditions, I have studied Dominant Energy Conditions and Trace

energy Conditions. The expressions for these energy conditions are given as :

$$DEC_r \;:\; \rho(r) - p_r(r) \geq 0, \quad DEC_t : \rho(r) - p_t(r) \geq 0,$$
$$TEC \;:\; \rho(r) - p_r(r) - p_t(r) \geq 0.$$

These energy conditions are shown to be fulfilled in Fig. 4.7. Trace Energy Conditions were quite popular in the 50s and 60s to be a physically reasonable conditions, the discovery of the stiff equation of state for the neutron star matter have somehow faded the need for TEC (Barcelo and Visser, 2002).

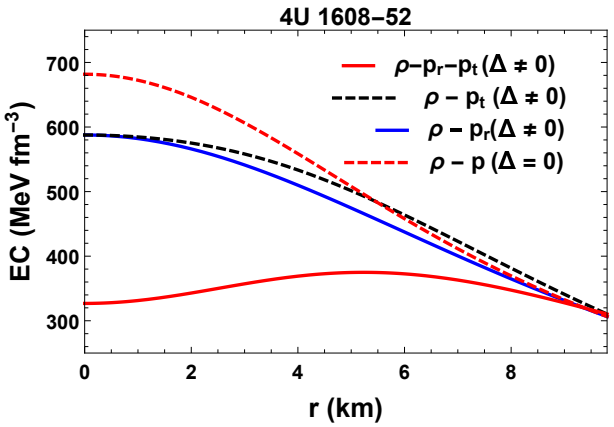

Figure 4.7: Variation of DEC in the radial direction (solid blue), transverse direction (dashed black) for the anisotropic case, DEC for the isotropic case (dashed red) and TEC (solid red) with the radial coordinate r corresponding to the pulsar $4\mathrm{U}1608-52$.

4.5.7 Metric function

The smooth matching of the interior metric function with that of the Schwarzschild exterior at the boundary is shown graphically in Fig. 4.8. However, the formulation of the model constants obtained from the smooth matching at the boundary have been described

in Sec. 4.4.

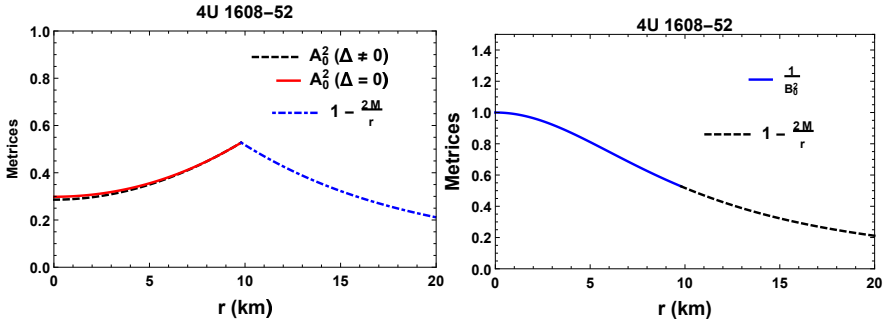

Figure 4.8: Smooth matching of the metric potentials with the Schwarzschild exterior solution at the boundary.

4.5.8 Equation of state parameter

To study cold high-density matter, compact stellar objects act as the natural laboratories and such behavior is governed by the relation between pressure and density, known as the Equation of State (EoS). We can study the mass and radius as well as other macroscopic properties such as moment of inertia and tidal deformability of a compact star.

The equation of state parameter is given by

$$\omega_r = \frac{p_r}{\rho}, \ \omega_t = \frac{p_t}{\rho}. \tag{4.44}$$

The variation of the pressure with the density is plotted in Fig. 4.9. It can be seen that the anisotropic pressure generates more stiff EoS than that of isotropic pressure. Since we know the stiffness of EoS can observed from the variation of the sound speed in stellar medium. To be non-exotic in nature the value of $\omega = p/\rho$ should lie within 0 and 1. The mathematical expressions for the EoS parameters can directly be obtained from the Eqs. (4.20)-(4.22). Graphically, our model is shown to satisfy the conditions $0 \leq \omega_r \leq 1$

Compact Star	R ($M\odot$)	C **(km)**	D	G	H
SAX J1748.9-2021	12.7697	0.045989	−0.000197	0.344066	0.302342
Cen X-3	9.5572	0.056641	−0.000163	0.322235	0.306764
Vela X-1	8.7142	0.06778	0.000409	0.255118	0.316001
PSR J0030 + 0451 $13.02^{+1.24}_{-1.06}$	18.7098	0.045295	−0.000407	0.457842	0.268874

Table 4.1: Values of the different model parameters corresponding to the different known compact stars (Miller et al., 2019; Roupas and Nashed, 2020)

and $0 \leq \omega_t \leq 1$ in Fig. 4.10.

Now stiffer EoS lead to larger tidal deformability with the anistropic pressure and the presence of anisotropy can reduce the value of the dimensionless tidal deformability by a significant amount for a given mass (Biswas and Bose, 2019). However, Biswas and Bose (Biswas and Bose, 2019) have exclusively studied the case for positive anisotropy.

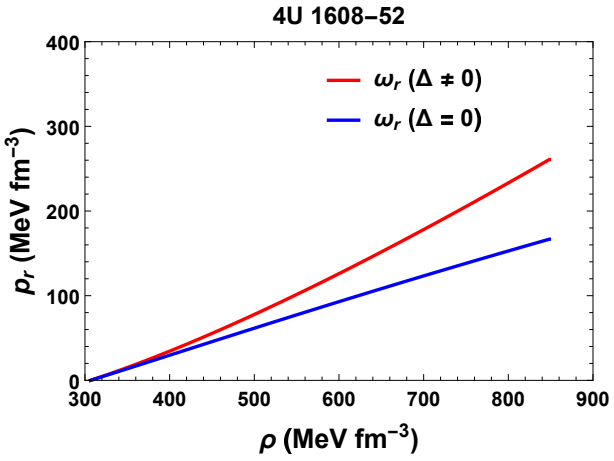

Figure 4.9: Variation of the radial pressure for the anisotropic case (solid red) and the isotropic case (solid blue) with respect to the density.

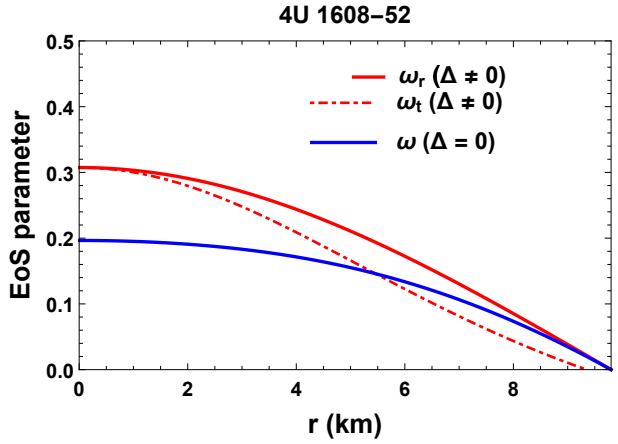

Figure 4.10: Variation of the EoS parameters inside the star for the anisotropic case in radial direction (solid red), transverse direction (dot dashed red) and for the isotropic case (solid blue) with the radial coordinate r corresponding to the pulsar $4\mathrm{U}1608-52$.

Matter variables	**SAX J**$1748.9-2021$	**Cen X-**3	Vela X-1	PSR J$0030+0451$
$\rho\|_0$	557.659	995.569	1197.49	259.772
$\rho\|_b$	210.926	352.714	345.562	136.949
λ	0.37823	0.35428	0.28857	0.52718
$v_r^2\|_0$	0.56381	0.58101	0.64117	0.48499
$v_r^2\|_b$	0.32863	0.33014	0.3392	0.3286
$v_t^2\|_0$	0.76306	0.78027	0.84043	0.68426
$v_t^2\|_b$	0.17529	0.16937	0.16679	0.22002
$v^2\|_0$	0.27526	0.28898	0.34177	0.23487
$v^2\|_b$	0.30125	0.31678	0.37189	0.23487
$(\rho+p_r+2p_t)\|_0$	1048.86	1931.26	2559.74	413.862
$(\rho+p_r+2p_t)\|_b$	202.906	345.893	363.771	123.771
$(\rho+3p)\|_0$	865.771	1598.53	2156.35	344.506
$(\rho+3p)\|_b$	210.925	352.714	345.562	136.949
$z\|_b$	0.35627	0.38586	0.48443	0.2183

Table 4.2: Numerical values of the matter variables for different compact stars. Here $|_0$ and $|_b$ denote the values of the matter variables at the center and the surface respectively.

Mass ($M\odot$)	Radius (km)	$\rho(0)$ (Walecka)	$\rho(0)$ (Model)	Error %
2.485	11.271	31.62	23.74	24.92
2.543	11.644	25.12	21.65	13.81
2.579	12.027	20.00	19.29	0.035
2.583	12.433	15.85	16.60	$-.047$
2.577	12.521	15.00	15.98	-0.065
2.530	12.798	12.59	13.847	-0.0998
2.387	13.081	10.00	11.046	-0.1046
2.268	13.167	8.913	9.65	-0.08268
2.119	13.188	7.943	8.399	-0.057
1.919	13.126	7.080	7.135	-0.00776
1.670	12.949	6.310	5.936	0.059
1.400	12.651	5.623	4.909	0.126
1.280	12.486	5.340	4.5079	0.1558
1.123	12.229	5.012	4.0276	0.196
0.594	11.033	3.981	2.514	0.368

Table 4.3: Comparison of the prescribed model with a neutron star model based on Walecka's relativistic mean field theory. Here densities are given in $10^{14}\ gm/cc$.

4.6 Stability analysis

4.6.1 Stability under different forces

Modeling of a compact star requires to examine the stability of the model. The important characteristic to study the stability of any model is to check the equilibrium condition of the model by using TOV equation. This stability equation given by Tolman (Tolman, 1939) and Oppenheimer and Volkoff (Oppenheimer and Volkoff, 1939) symbolizes the internal structure of a spherically static symmetric compact stellar object which is in equilibrium in the presence of anisotropy. The generalized TOV equation can be expressed as

$$-\frac{M_G}{r}[\rho(r)+p_r(r)]\frac{A_0(r)}{B_0(r)}-\frac{dp_r(r)}{dr}+\frac{2(p_t-p_r)}{r}=0, \tag{4.45}$$

where $M_G(r)$ is the gravitational mass within the compact stellar objects of radius r which can be derived using Tolman-Whittaker mass formula and it is defined by

$$M_G(r) = \frac{rB_0(r)A_0'(r)}{A_0^2(r)}. \tag{4.46}$$

Now, substituting the value of $M_G(r)$, Eq. (4.45) can also be written as

$$-\frac{A_0'(r)[\rho(r)+p_r(r)]}{A_0(r)} - \frac{dp_r(r)}{dr} + \frac{2(p_t-p_r)}{r} = 0. \tag{4.47}$$

Eq. (4.47) describe the equilibrium condition for the model under gravitational forces (F_g), hydrostatic forces (F_h) and anisotropic forces (F_a). The TOV equation can be expressed in a simple form as

$$F_g(r) + F_h(r) + F_a(r) = 0, \tag{4.48}$$

where

$$\begin{aligned} \text{Gravitational force} : F_g(r) &= -\frac{A_0'(r)[\rho(r)+p_r(r)]}{A_0(r)}, \\ \text{Hydrostatic force} : F_h(r) &= -\frac{dp_r(r)}{dr}, \\ \text{Anisotropic force} : F_a(r) &= \frac{2(p_t-p_r)}{r}. \end{aligned} \tag{4.49}$$

The expressions mentioned in Eq. (4.49) are examined graphically in the Fig. 4.11. It portrays the stability of the model under various forces. It can clearly be seen that, to keep the model stable in the equilibrium, hydrostatic force should be much larger such that it can counterbalance the combined forces of gravitational and anisotropic forces. However, in the presence of isotropy, the model should be in the stable equilibrium if the negative gravitational force equalize the positive hydrostatic force.

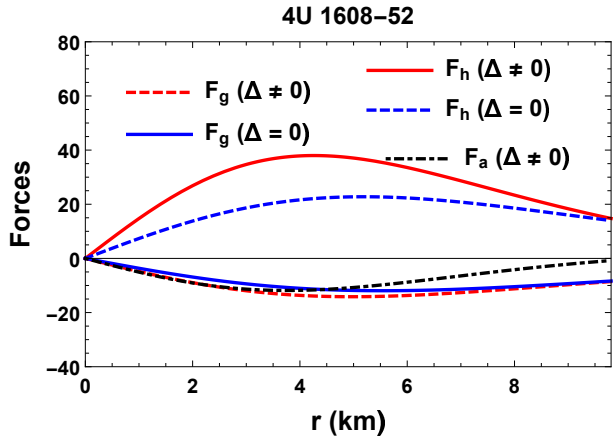

Figure 4.11: Variation of different forces for the anisotropic case (hydrostatic force (solid red), gravitational force (dashed red), anisotropic force (dot dashed black)) and the isotropic case (hydrostatic force (dashed blue), gravitational force (solid blue)) against the radial coordinate r corresponding to the pulsar $4\mathrm{U}1608-52$.

4.6.2 Stability under Causality Condition

To examine the stability of a physically acceptable model, the velocity of the sound must be less than the light's velocity (Abreu et al., 2007; Herrera, 1992). The sound velocity inside the compact star is expressed by

$$v_r(r) = \sqrt{\frac{dp_r(r)}{d\rho(r)}}, \quad v_t(r) = \sqrt{\frac{dp_t(r)}{d\rho(r)}}. \tag{4.50}$$

Since velocity of light $c = 1$, Thus the causality condition becomes $0 \leq v_r(r), v_t(r) < 1$. Fig. 4.5 shows the fulfillment of the causality condition for both anisotropic and isotropic case. The stability of any compact stellar object under the radial perturbation is investigated using Herrera's cracking concept (Herrera, 1992) and it is shown that to be a potentially stable model the absolute difference of sound speeds should be ≤ 1 (Andrèasson, 2009). Fig. 4.12 portrays the stability condition for the prescribed model with the anisotropic pressure. It is shown that the stability condition is satisfied by the model throughout the

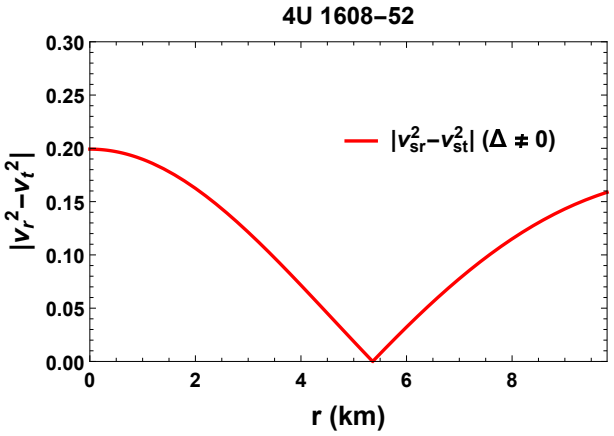

Figure 4.12: The absolute difference of the sound speeds is plotted against the radial coordinate r corresponding to the pulsar $4\mathrm{U}1608-52$.

structure with anisotropic pressure except at the point $r = 5.4$. However the difference of the sound speed soon starts to increase right after this point.

4.6.3 Stability under Adiabatic Index

The adiabatic index, the ratio of the specific heats at the constant pressure and volume, is the quantity which incorporates all the basic characteristics of the equation of state on the instability formula and consequently consists the bridge between the relativistic structure of a spherical static object and the equation of state of the interior fluid (Moustakidis, 2017). Essentially it is a function of the baryon density and consequently exhibits the radial dependence on the instability criterion (Tooper, 1965). Since the positive anisotropic factor may slow down the growth of instability which implies that the gravitational collapse occurs in the radial direction (Maurya and Tello-Ortiz, 2019). Therefore, it is enough to study about adiabatic index only in the radial direction which is given mathematically as

$$\Gamma_r(r) = \frac{\rho(r) + p_r(r)}{p_r(r)} \frac{dp_r(r)}{d\rho(r)}. \tag{4.51}$$

For Newtonian fluid, the collapsing condition results in $\Gamma < \frac{4}{3}$ (Bondi, 1999; Heintzmann

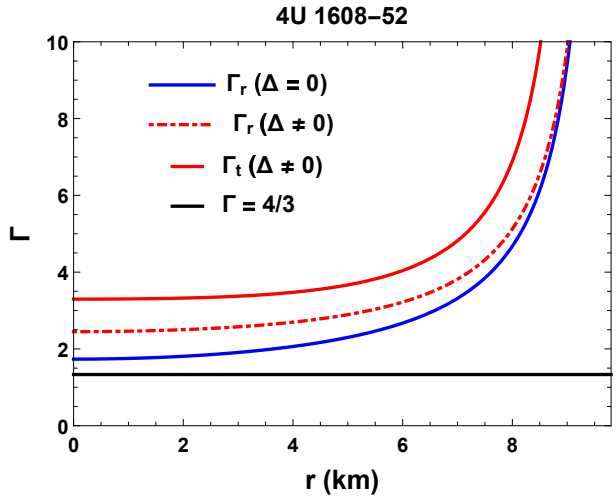

Figure 4.13: The adiabatic indices for the anisotropic case (in the radial (dashed red) and transverse direction (solid red)) and for the isotropic case (solid blue) are plotted against the radial coordinate r corresponding to the pulsar $4\mathrm{U}1608-52$.

and Hillebrandt, 1975). Now for relativistic fluid sphere some terms were added to the previous conditions which is perceived as the correction to the former (Chan et al., 1992, 1993) and it is expressed as

$$\Gamma < \frac{4}{3}\left[\frac{4}{3}\frac{(p_{t0}-p_{r0})}{r|p'_{r0}|}+\frac{8\pi}{3}\frac{\rho_0 p_{r0} r}{|p'_{r0}|}\right]_{max}, \tag{4.52}$$

where ρ_0, p_{r0} and p_{t0} are respectively initial density, radial and tangential pressures in unperturbed equilibrium. The second term in the right hand side of Eq.(4.52) corresponds to anisotropy and third term represents the relativistic corrections to the Newtonian perfect fluid. Remarkably this relativistic corrections could be the reason of instability inside the star (Chandrasekhar, 1964a) and the instability can be prevented by imposing strict condition on adiabatic condition, known as the critical value for adiabatic index. For stable stellar structure, the critical value depends on the amplitude of the Lagrangian displacement from

equilibrium and the compactness factor $u = \frac{M}{b}$. Thus taking a particular form of amplitude of the Lagrangian displacement the critical relativistic adiabatic index is given by

$$\Gamma_{crit} = \frac{4}{3} + \frac{19u}{21}. \tag{4.53}$$

Eventually the stability condition becomes $\Gamma \geq \Gamma_{crit}$. I have checked the stability criteria graphically in Fig. 4.13 and it can be seen that the model remains stable under both the anisotropic and isotropic pressures. In Fig. 4.14, adiabatic indices are found to be greater than the critical value of adiabatic index.

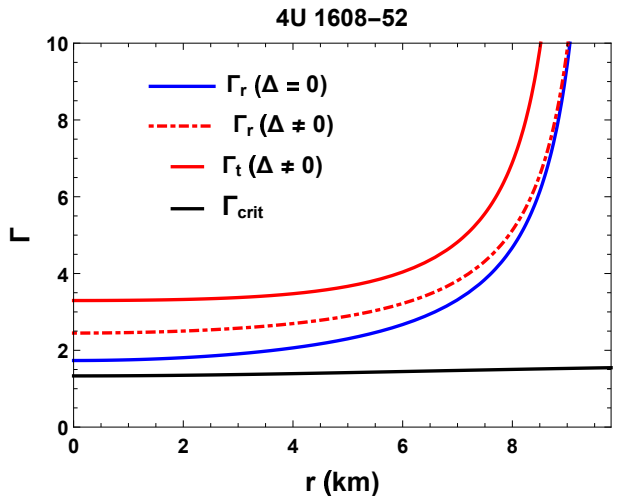

Figure 4.14: Variation of the adiabatic indices the anisotropic case (in the radial (dashed red) and transverse direction (solid red)) and for the isotropic case (solid blue) with respect to the radial coordinate r in presence of the critical value of the adiabatic index corresponding to the pulsar $4\mathrm{U}1608-52$.

4.6.4 Stability under the Harrison-Zeldovich-Novikov criterion

One of the most important step to test the stability of the anisotropic compact star model is to check the stability of the mass of the model under Harrison (Harrison et al., 1965)

and Zeldovich-Novikov (Zeldovich and Novikov, 1972) criterion. The general form is to test whether the mass is increasing with the increase of central density of a compact star model. Mathematically, $\frac{dM}{d\rho(0)}$ needs to be < 0 to be stable structure, otherwise declared the model to be unstable. For our model the mass can be written in the form central density as following:

$$M(\rho(0)) = \frac{b^3\rho(0)}{2(b^2\rho(0)+3)}, \tag{4.54}$$

$$\frac{dM}{d\rho(0)} = \frac{3b^3}{2(b^2\rho(0)+3)^2}. \tag{4.55}$$

The profile of the mass and the gradient of the mass in the form of the central density have been depicted in Figs. 4.15 and 4.16 respectively. It can clearly be seen that $\frac{dM}{d\rho}$ is positive throughout the stellar configuration making it stable.

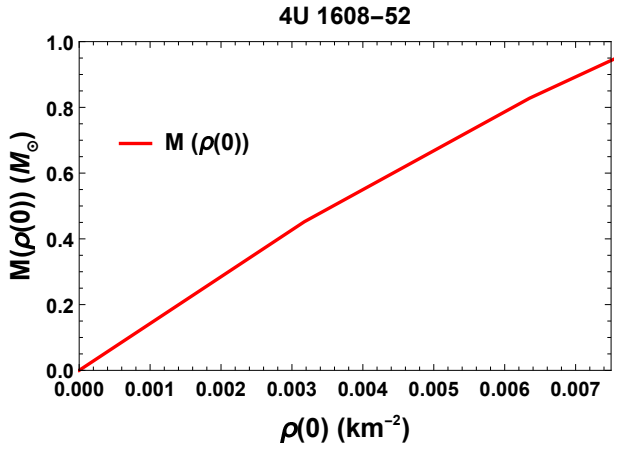

Figure 4.15: Variation of the mass with respect to the central density.

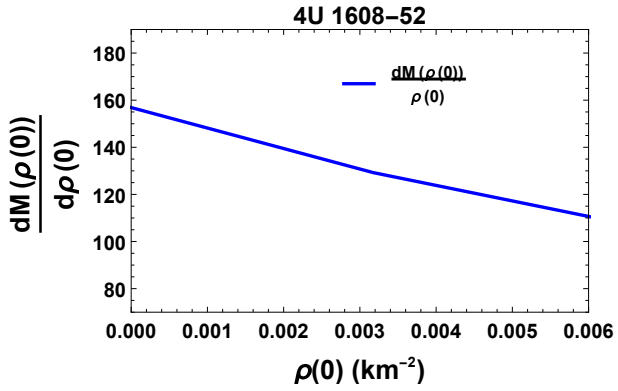

Figure 4.16: Variation of the gradient of the mass against the central density.

4.7 Mass-radius relationship and redshift

4.7.1 Mass function and mass-radius relationship

Recall that the mass function for the model is given in Eq (4.23). Since $\lim_{b\to 0} m(b) = 0$, so the mass function is regular at the center of the structure. Also Fig. 4.17 depicts the positive and monotonically increasing nature of the mass function with respect to the radial coordinate.

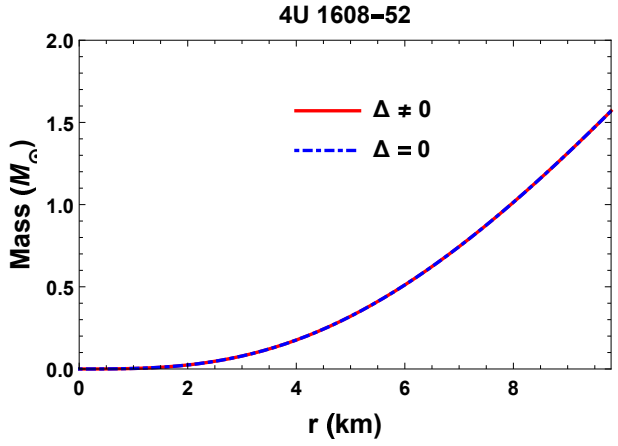

Figure 4.17: The profile of the mass function plotted against the radial coordinate r corresponding to the pulsar $4\mathrm{U}1608-52$.

The mass-radius relationship for the model is plotted in Fig. 4.18 and the maximum mass obtained is $1.731\ M_{\odot}$ corresponding to the radius $10.56\ km$ considering the fixed surface density $5.5 \times 10^{14}\ gm/cc$. Since we know from the works of Sharma et al. (Sharma et al., 2017) and Sunzu et al. (Sunzu et al., 2014a), the mass radius relationship is not affected by the pressure anisotropy. Hence the obtained mass-radius relation can be obtained both for anisotropy and isotropy cases. Also for spherically symmetric stable structure, Buchdahl limit (Buchdahl, 1959) needs to be satisfied, i.e. $\frac{2M}{b}$ must be less than $\frac{8}{9}$.

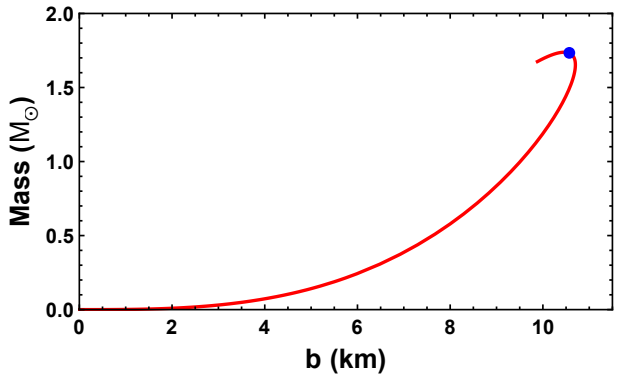

Figure 4.18: The mass-radius relationship for the prescribed compact stellar model. The solid circle represents the maximum mass attained by the model.

4.7.2 Mass-central density relationship

The stability of any model depends on the variation of mass with the central density and it is known as Harrison-Zeldovich-Novikov criterion (which is discussed in the previous sub-section). This criterion states that the model is stable in stellar system only if the mass of the model is increasing with the increase of central density. In Fig. 4.19 the increasing nature of mass with respect to central density is quite evident. Also it is to be noted that the central density does not vanish for the absence of mass. For the prescribed model, the maximum mass of the model corresponds to the central density $6.537 \times 10^{15}\ gm/cc$.

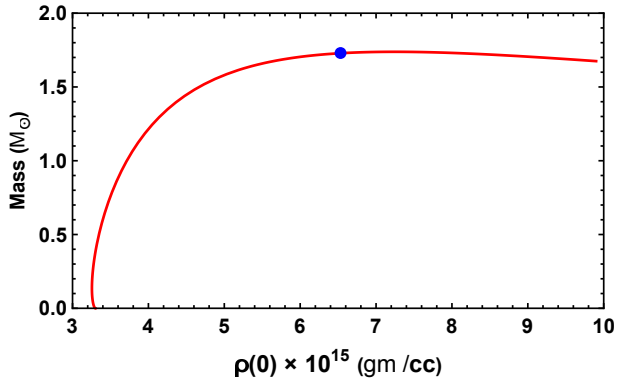

Figure 4.19: The mass-central density relationship for the prescribed compact star model. Here solid circle denotes the maximum mass for the model.

4.7.3 Radius-central density relationship

To examine any viable model it is important to investigate the central density against the radius along with the mass of the model.

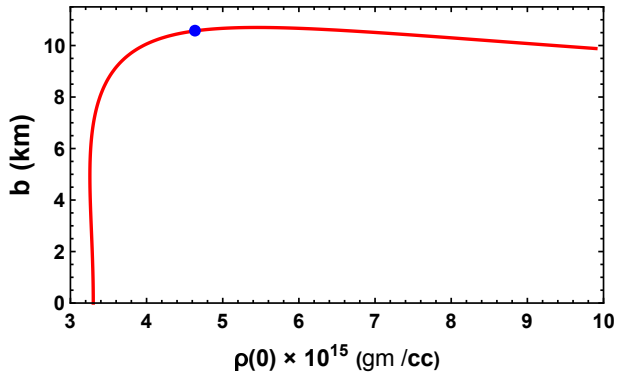

Figure 4.20: The radius-central density relationship for the prescribed compact stellar model. The solid circle represents the radius for which the maximum mass is attained.

The radius-central density relationship is plotted in Fig. 4.20. It can be observed that central density increases with the increase of radius of the model. Here the maximum central density corresponding to the radius $10.56\ km$ is obtained as $4.63 \times 10^{15}\ gm/cc$.

4.7.4 Gravitational redshift

The compactness of the model is defined by a dimensionless parameter $u(r) = \frac{m(r)}{r}$. According to Buchdahl limit (Buchdahl, 1959), the compactness of a model should be less than 0.444 to be a stable structure. For the present model one can have the compactness of the model as 0.2417 indicating the fulfillment of the Buchdahl condition.

The gravitational redshift of a spherically symmetric compact star object is defined by

$$z = \frac{1}{\sqrt{1-2u(r)}} - 1, \tag{4.56}$$

where $u(r) = m(r)/r$ is the compactness parameter for the model.

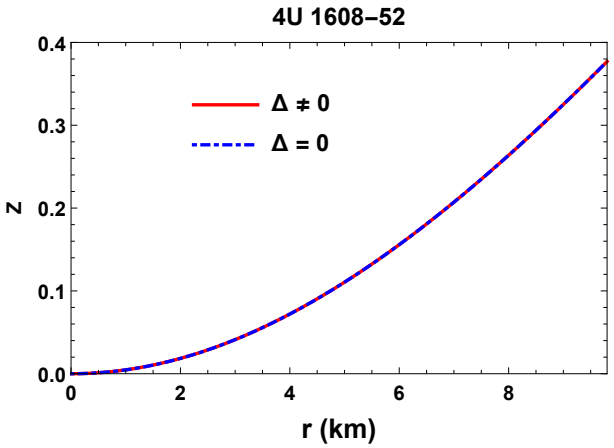

Figure 4.21: The gravitational redshift is plotted against the radial coordinate r corresponding to the pulsar $4\mathrm{U}1608-52$.

The gravitational redshift is plotted against the radial coordinate in Fig. 4.21.

4.8 Discussions and summary

In the present work I have analyzed the field equations adopting the Finch-Skea ansatz (Finch and Skea, 1989) and have obtained a solution that describes a compact star model with negative anisotropic pressure. Some salient features of the solution are described as follows:

(1) The profile for anisotropic pressure of the model have been studied in Fig. 4.1. Though the anisotropic parameter satisfies the regularity at the center ($r = 0$), it is shown to portray negative nature throughout the stellar structure, making the anisotropic force acting on the model to be attractive and which is proven to make the model less supportive against the gravitational collapse.

(2) All the matter variables for the compact stellar model satisfy the physical requirements to be a stable model. Energy density and the profile of pressures in the presence of anisotropy as well as isotropy are plotted in Fig. 4.3. In presence of anisotropy, transverse pressure is observed to be less than the radial one throughout the structure.

(3) Smooth matching of the interior solutions with the Schwarzschild exterior solutions at the boundary in Fig. 4.8 helps to generate the general form for the constants which further provides an outline of the compact stellar model.

(4) Variation of gradients of matter variables are shown to be negative throughout the star with zero gradients at the center.

(5) The causality condition is satisfied by the variation of the sound speed as shown in Fig. 4.5. Also the absolute difference of the sound speeds are plotted in Fig. 4.12, implying that the model does not satisfy the stability condition by Herrera Cracking concept.

(6) Fulfillment of various energy conditions by the model in presence of anisotropy and isotropy are shown in Fig. 4.6.

(7) The stability of the model under the effect of TOV equation is shown in Fig. 4.11. The model is shown to remain in static equilibrium if the hydrostatic force neutralize the combined effect of the anisotropic and gravitational forces.

(8) The monotonically increasing nature of the mass function and the gravitational redshifts are plotted in Figs. 4.17 and 4.21 respectively, which support the physical viability of the prescribed model.

(9) The maximum mass, obtained for the prescribed model, is $1.731\ M_{\odot}$ corresponding to the radius $10.56\ km$, which is stable as per Buchdahl limit. Also the radius-central density relationship depicted in Fig. 4.20 illustrate that the central density increases with the increase of radius of the model. The central density is obtained to be $4.63 \times 10^{15}\ gm/cc$ corresponding to the radius such that maximum mass is obtained in Fig. 4.18.

Furthermore, I have represented tables for a comparative study considering some well known stars. Table. 4.1 depicts the value of the model parameter while Table. 4.2 exhibits the values of the matter variables for both anisotropic and isotropic scenario. Obviously the obtained solution is reduced to the solution obtained by Finch-Skea (Finch and Skea, 1989) by assuming zero anisotropy.

Thus the model can be considered as a feasible candidate to describe spherically symmetric, static and anisotropic compact stellar structure.

Appendix

The solutions for Eq. (4.28) are obtained using technical computing system as

$$A_0(r) = 2^{\frac{-1}{4}}(-R)^{\frac{2n+3}{2}} s^{\frac{3}{2}} \left[M\mathcal{I}_n(s) - N(-1)^n \mathcal{K}_n(s)\right],$$

where $n = \frac{\sqrt{17}}{2}$, $s = \sqrt{\frac{-2(r^2+R^2)}{R^2}}$ and $\mathcal{I}$, $\mathcal{K}$ are the modified Bessel's functions of first and second order respectively.

Solving the equations in another approach namely, by transformation, one can obtain the following results.

If one uses Durgapal-Banerjii transformation (Durgapal and Bannerji, 1983), i.e., set $x = \frac{r^2}{R^2}$, $Z(x) = \frac{1}{B_0^2(r)}$ and $A^2y^2(x) = A_0^2(r)$, we get the the field equations along with the anisotropic factor to be transformed as

$$\begin{aligned}
8\pi\rho &= \frac{1-Z(x)}{xR^2} - \frac{2Z'}{R^2}, \\
8\pi p_r &= \frac{Z-1}{xR^2} + \frac{4Zy'}{R^2y}, \\
\Delta(x) &= \frac{x(1-x)}{R^2(1+x)^3}, \\
8\pi p_t &= 8\pi p_r + \Delta(x),
\end{aligned}$$

where (') denotes differentiation of the respective function with respect to x. Now combining all the above equations and using the transformation $Z(x) = \frac{1}{1+x}$, one can get a second order ODE as

$$4(1+x)^2y'' - 2(1+x)y' + (1+2x)y = 0. \tag{4.57}$$

Now we try to solve Eq. (4.57) using some known methods.

If again we use the transformations as $1 + x = V$ and $y = YV^{\frac{3}{4}}$ on Eq. (4.57), we get the new transformed ODE as

$$V^2\frac{d^2Y}{dV^2} + V\frac{dY}{dV} + \left(\frac{V}{2} - 1\right)Y = 0,$$

which cannot be simplified in Bessel's form of differential equations. Now as per series solutions, we cannot further use Frobenius Method to solve the above ODE as $\left(\frac{1}{V}\right)$ is not analytic at $V = 0$.

Chapter 5

Impact of spheroidal parameter for Vaidya-Tikekar type anisotropic compact star

5.1 Introduction

The singularity free interior solutions for compact stellar objects (white dwarf, neutron stars, black holes) have been the study of massive interest for theoretical physicists for over more than two decades now. Karl Scwarzschild was first to obtain two such solutions which describe the exterior (Schwarzschild, 1916b) of the space–time geometry of perfect fluid sphere in hydrostatic equilibrium and the second one, the interior Schwarzschild solution (Schwarzschild, 1916a) is related to the interior geometry of a fluid sphere having homogeneous distribution of energy density. The most ubiquitous way is to integrate the Tolman-Oppenheimer-Volkoff (TOV) equations using a certain form of equation of state (EoS). But observational data from compact stars indicates towards a discrepancy with

standard theoretical models. At nuclear and supranuclear densities, the interior properties of compacts stars depends heavily on the EoS. Theoretically this is achieved by estimating masses and radii of the stars. However, the profile of pulsar does not depend only on the stellar mass and radius, but also depends on several other features like moment of inertia, quadrupole moment and higher multi-pole moments etc. (Kumar et al., 2018). The motivation to undertake such a task was initiated by the discovery of the pulsar PSR J1614-2230 that produced hot spots on the surface of compact stars (Hessels et al., 2005) led to several interpretative problems such as neutron stars (NSs) and quark stars (QSs). Recent observation have also suggested that masses and radii of many compact stellar objects, namely, X-ray burster 4U 1820-30 (Bombacci, 1997), X-ray pulsar Her X-1 (Li et al., 1995), X-ray sources 4U 1728-34 (Li et al., 1999), PSR 0943+10 (Xu et al., 1999), RX J185635-3754 etc. are not compatible with the standard neutron star models. These compact stellar objects are observed to posses greater compactification factor (mass to radius ratio) having both larger mass and radius than the standard neutron stars. Unknown matter distribution at the highly dense core regions is still an unresolved issue in stellar modeling. Details of Neutron star masses- radii and their impact on the EoS can be found in (Li et al., 2019; Özel and Freire, 2016). Another approach to obtain exact solutions for Einstein field equations (EFE) is by considering certain metric ansatz. Vaidya and Tikekar (Vaidya and Tikekar, 1982) proposed an ansatz for the metric component g_{rr} which is characterised by two parameters, namely curvature parameter K and spheroidal geometry characterized by the parameter L. Sharma et al (Sharma et al., 2020) have studied the VT model in the linear regime. This chapter dives in the regime of polytropic EoS along with VT model. Thirukkanesh et al (Thirukkanesh et al., 2020) have investigates new set of spherically symmetric solutions for anisotropic compact star admitting similar type of polytropic EoS. In Astrophysics polytropic EoS have helped the studying of the dynamics and stability of galaxies (Wolan-

sky, 1999) to the description of the compact stellar object's inner structure (Chandrasekhar, 1964a; Kovetz, 1967; Tooper, 1965), passing through mechanisms involved in stellar evolution (Urango et al., 2022).

Numerous works have been done by including the pressure anisotropy in self gravitating system in the frame work of general relativity (Bhar et al., 2022; Das et al., 2022a,b; Maurya et al., 2019a, 2017; Paul et al., 2022) are to name a few.

Assuming the interior of a superdense stars to be filled with cold matter at a temperature of zero Kelvin along with a known form of equation of state, the relativistic models, in equilibrium, is obtained conventionally. Now, the Einsteins' field equations relate physical variables the energy density and fluid pressure of the matter with the interior geometry and the exterior of these stellar structure is assumed to be vacuum (Tikekar and Jotania, 2007). Since the Einstein field equations are highly non linear, the complex hydrodynamical system is analysed by adopting numerical procedures for obtaining their plausible solutions. Lattimer and Prakash (Lattimer and Prakash, 2001) have studied the structure of neutron stars by obtaining analytic solutions of field equation and carefully constrained the equation of state (Goswami et al., 2022). The main motivation for using VT ansatz is in the absence of reliable information about equation of state of matter content, the alternative approach of prescribing suitable geometry for their 3-spaces leads to physically viable models of superdense stars in equilibrium as suggested by Vaidya-Tikekar (Tikekar, 1990; Vaidya and Tikekar, 1982). Several remarkable works have been carried out using Vaidya Tikekar ansatz; under infinitesimal radial pulsation, the stability criterion was discussed by Knutsen (Knutsen, 1988). For different choice of spheroidal parameter, Maharaj and Leach (Maharaj and Leach, 1996) obtained a new set of solution of Tikekar superdense star, Mukherjee et al (Mukherjee et al., 1997) have obtained a new set of uncharged solution

using VT ansatz, later Gupta and Jasim (Gupta and Jasim, 2004) have obtained their work in terms of Gegenbauer functions, an alternate form of the general solution. VT model have also been extensively studied for charged compact stars; using Vaidya–Tikekar ansatz to generate exact solutions of the field equation in charge analog Gupta and Kumar (Gupta and Kumar, 2005) observed a particular form of electric field intensity, having positive gradient. Later this form of electric field intensity was used by Sharma et al. (Sharma et al., 2001). Additionally Komathiraj and Maharaj (Komathiraj and Maharaj, 2007) observed a similar result, explicitly observed a relationship directly relating the spheroidal parameter K to the electromagnetic field to show another kind of Vaidya–Tikekar type star. Bijalwan and Gupta (Bijalwan and Gupta, 2011, 2012) obtained a closed form for charged perfect fluid model of Vaidya–Tikekar type superdense stars with more generalized electric intensity. Chattopadhyay et al (Chattopadhyay et al., 2012) have observed that the size of a static compact charged star is more than that of a static compact star without charge, using VT metric with non-linear equation of state. Kumar et al. (Kumar et al., 2018) used the Vaidya-Tikekar metric potential to explore a class of charged compact stellar objects filled with self-gravitating, isotropic fluids. Bhar (Bhar, 2015b) observed physically acceptable solutions which admits conformal motions in the presence of a quintessence field which is characterized by a parameter ω_q where $\omega_q \in (-1, -\frac{1}{3})$. Hansraj (Hansraj, 2017) demonstrated that presecribing electric field intensity,the five-dimensional generalization of spheroidal spacetimes is applicable to dense objects in Einstein-Gauss Bonnet gravity. Sharma and researchers have studied a X-ray binary pulsar Her X-1 (Sharma and Mukherjee, 2001), low mass binary X-ray emitters SAX J$1808.4 - 3658$ (Sharma et al., 2002) using Vaidya Tikekar ansatz. Recently the pulsar PSR B$0943 + 10$ (Kumar and Bharti, 2022) have been studied as an isotropic VT-type compact star. Additionally, an alternative ansatz was proposed by Tikekar and Jotania (Tikekar and Jotania, 2005) where the physical

3-space of the star has the geometry of a 3 pseudo spheroid immersed in a four dimensional Euclidean space. Later, both these models were studied in a generalised way in higher dimensions (Chattopadhyay and Paul, 2010; Paul, 2004).

This Chapter has been organized as follows: the Einstein field equations to obtain the solution have been discussed in Sec. 5.2. Exact solutions of the field equations for the values of $n = 1$ and $n = 2$ are obtained in Sec. 5.3. Smooth matching of the exterior spacetime with the interior is depicted in Sec. 5.4. Sec. 5.5 portrays the bounds on the model parameters. The physical analysis and the stability analysis are given in Sec. 5.6 and Sec. 5.7 respectively. Impact of the curvature parameter on various properties of the model is discussed on Sec. 5.8. Finally Sec. 5.9 describes the concluding remarks.

5.2 The field equations

The interior of a spherically symmetric static star in Schwarzschild coordinates $(x^a) = (t,\ r,\ \theta,\ \phi)$ is assumed to be described by the line element

$$ds^2 = -e^{2\nu(r)}dt^2 + e^{2\lambda(r)}dr^2 + r^2(d\theta^2 + \sin^2\theta d\phi^2), \tag{5.1}$$

where ν and λ are functions of radial coordinate r only.

We assume that the stellar interior matter is anisotropic in character and the energy-momentum tensor has the specific form

$$T_{ij} = (\rho + p_t)u_i u_j + p_t g_{ij} + (p_r - p_t)\chi_i\chi_j, \tag{5.2}$$

where ρ represents the energy-density, p_r and p_t, respectively denote fluid pressures along

the radial and transverse directions, u^i is the 4-velocity of the fluid and χ^i is a unit space-like 4-vector along the radial direction so that $u^i u_i = -1$, $\chi^i \chi_j = 1$ and $u^i \chi_j = 0$. The Einstein field equations for the tensor given in Eq. (5.2) along with the spacetime given in Eq. (5.1) then reduces to

$$\rho = \frac{\left(1 - e^{-2\lambda}\right)}{r^2} + \frac{2\lambda' e^{-2\lambda}}{r}, \tag{5.3}$$

$$p_r = -\frac{1}{r^2}\left(1 - e^{-2\lambda}\right) + \frac{2\nu'}{r} e^{-2\lambda}, \tag{5.4}$$

$$p_t = e^{-2\lambda}\left(\nu'' + \nu'^2 + \frac{\nu'}{r} - \nu'\lambda' - \frac{\lambda'}{r}\right), \tag{5.5}$$

where primes denote differentiation with respect to r. In the field equations Eqs. (5.3)-(5.5), it is assumed that the coupling constant $\frac{8\pi G}{c^4}$ to be set equal to 1 and the speed of light scaled as $c = 1$. The system of equations Eqs. (5.3)-(5.5) governs the behaviour of the gravitational field for an anisotropic imperfect fluid distribution.

By definition the mass contained within a radius r of the sphere is defined as

$$m(r) = \frac{1}{2}\int_0^r \omega^2 \rho(\omega) d\omega. \tag{5.6}$$

At this stage, we have system of three equations given in Eqs. (5.3)-(5.5) with five unknowns ν, λ,ρ, p_r and p_t. So to obtain a solution that describes physically realistic relativistic star, i.e. to obtain the solution for this highly non-linear system of equations, I assume one metric potential to be described by Vaidya-Tikekar (VT) ansatz as

$$e^{2\lambda(r)} = \frac{1 - \frac{Kr^2}{L^2}}{1 - \frac{r^2}{L^2}}. \tag{5.7}$$

The VT metric has a definite geometric interpretation. In Schwarzschild coordinates, the

$t =$ constant hypersurface of the space-time metric has a spheroidal geometry characterized by the parameters L and K. Here L has a dimension of a length and K denotes departure from spherical geometry. This choice of metric potential is well motivated and well behaved for $r < L$ and $K < 1$. For $K = 1$, the $t =$ constant hypersurface represents flat 3 space–time.

The following transformation reduces the Einstein field equations in a different form as follows

$$x = \frac{r^2}{L^2}, \quad Z(x) = e^{-2\lambda(r)}, \quad y^2(x) = e^{2\nu(r)}. \tag{5.8}$$

Under the transformation Eq. (5.8), the system of equations Eqs. (5.3)-(5.5) become

$$\frac{1-Z}{x} - 2\dot{Z} = L^2\rho, \tag{5.9}$$

$$4Z\frac{\dot{y}}{y} + \frac{Z-1}{x} = L^2 p_r, \tag{5.10}$$

$$4xZ\frac{\ddot{y}}{y} + \left(4Z + 2x\dot{Z}\right)\frac{\dot{y}}{y} + \dot{Z} = L^2 p_t, \tag{5.11}$$

where dots denote differentiation with respect to the variable x. The mass function Eq. (5.6) consequently takes the form

$$m(x) = \frac{L^3}{4}\int_0^x \sqrt{w}\rho(w)dw. \tag{5.12}$$

For a physically realistic relativistic star the interior matter distribution should satisfy a barotropic equation of state of the form $p_r = p_r(\rho)$. For this particular problem I have assumed that the matter distribution to follow the polytropic-type equation of state, given

as

$$p_r = \alpha\rho^{1+\frac{1}{n}} - \beta, \tag{5.13}$$

where α and β are a real constants and n is the polytropic index. Then one can write the system of equations given in Eqs. (5.3) - (5.5) in the simpler form as

$$\begin{aligned}
L^2\rho &= \frac{1-Z}{x} - 2\dot{Z}, && (5.14)\\
p_r &= k\rho^{1+\frac{1}{n}}, && (5.15)\\
p_t &= p_r + \Delta, && (5.16)\\
L^2\Delta &= 4xZ\frac{\ddot{y}}{y} + \dot{Z}\left(1 + 2x\frac{\dot{y}}{y}\right) + \frac{1-Z}{x}, && (5.17)\\
\frac{\dot{y}}{y} &= \frac{k}{4L^{\frac{2}{n}}Z}\left[\frac{1-Z}{x} - 2\dot{Z}\right]^{1+\frac{1}{n}} + \frac{1-Z}{4xZ} - \frac{\beta L^2}{4Z}, && (5.18)
\end{aligned}$$

where the quantity $\Delta = p_t - p_r$ defines the measure of anisotropy in this model. This system of equations governs the behaviour of the gravitational field for an imperfect fluid source.

5.3 Exact solutions for the model

Under the transformation Eq. (5.8), the gravitational potential in Eq. (5.7) becomes

$$Z = \frac{1-x}{1-Kx}. \tag{5.19}$$

Substituting Eq. (5.19) into Eq. (5.18) one can obtain

$$\frac{\dot{y}}{y} = \frac{k}{4L^{2/n}}\frac{(1-K)^{1+1/n}}{(1-x)}\frac{(3-Kx)^{1+1/n}}{(1-Kx)^{1+2/n}} + \frac{(1-K)}{4(1-x)} - \frac{\beta L^2(1-Kx)}{4(1-x)}. \tag{5.20}$$

On principle, the equation Eq. (5.20) can be integrated if the values of n is specified. Here the following two cases of physical interest have been considered.

5.3.1 The case $n = 1$

When $n = 1$ the equation Eq. (5.20) becomes

$$\frac{\dot{y}}{y} = \frac{k}{4L^2}\frac{(1-K)^2}{(1-x)}\frac{(3-Kx)^2}{(1-Kx)^3} + \frac{(1-K)}{4(1-x)} - \frac{\beta L^2(1-Kx)}{4(1-x)}. \tag{5.21}$$

On integrating Eq. (5.21) one can obtain

$$\begin{aligned} y &= d_1\left(1-\frac{Kr^2}{L^2}\right)^{-\frac{\alpha(K-3)^2}{4(K-1)L^2}}\left(1-\frac{r^2}{L^2}\right)^{\frac{1}{4}\left\{\frac{\alpha(K-3)^2}{(K-1)L^2}-\beta(K-1)L^2+K-1\right\}} \\ &\times \exp\left[-\frac{\alpha\left\{(5-3K)L^2+2(K-2)Kr^2\right\}}{2\left(L^2-Kr^2\right)^2}-\frac{1}{4}\beta Kr^2\right], \end{aligned} \tag{5.22}$$

where d_1 is the constant of integration. Hence the system of equation describing the exact model is given as follows

$$e^{2\lambda(r)} = \frac{L^2-Kr^2}{L^2-r^2}, \tag{5.23}$$

$$\begin{aligned} e^{2\nu(r)} &= d_1\left(1-\frac{Kr^2}{L^2}\right)^{-\frac{\alpha(K-3)^2}{2(K-1)L^2}}\left(1-\frac{r^2}{L^2}\right)^{\frac{1}{2}\left\{\frac{\alpha(K-3)^2}{(K-1)L^2}-\beta(K-1)L^2+K-1\right\}} \\ &\times \exp\left[-\frac{\alpha\left\{(5-3K)L^2+2(K-2)Kr^2\right\}}{\left(L^2-Kr^2\right)^2}-\frac{1}{2}\beta Kr^2\right]. \end{aligned} \tag{5.24}$$

The matter variables, density and pressures can be written as

$$\rho = \frac{(K-1)\left(Kr^2-3L^2\right)}{\left(L^2-Kr^2\right)^2}, \tag{5.25}$$

$$p_r = \frac{\alpha(K-1)^2\left(Kr^2-3L^2\right)^2}{\left(L^2-Kr^2\right)^4}-\beta, \tag{5.26}$$

$$\begin{aligned} p_t &= \frac{1}{4(L-r)(L+r)\left(L^2-Kr^2\right)^7}\Bigg[L^{12}\Big\{28\beta^2K^2r^6+36\alpha(K-1)^2-2\beta K(55K \\ &+ 1)r^4-3(K-1)^2r^2(6\alpha\beta-1)\Big\}+4KL^{10}r^2\Big\{-14\beta^2K^2r^6-12\alpha(K-1)^2 \\ &+ \beta K(53K+3)r^4+(K-1)^2r^2(21\alpha\beta-4)\Big\}+L^8r^2\Big\{70\beta^2K^4r^8+(K-1)^2 \\ &\Big(35K^2r^4+81\alpha^2(K-1)^2-6\alpha K(K+17)r^2\Big)-2\beta K^2r^4\Big(79\alpha(K-1)^2 \\ &+ 5K(25K+3)r^2\Big)\Big\}+4KL^6r^4\Big\{-14\beta^2K^4r^8+(K-1)^2\Big(-10K^2r^4 \\ &- 27\alpha^2(K-1)^2+64\alpha Kr^2\Big)+2\beta K^2r^4\Big(19\alpha(K-1)^2+K(23K+5)r^2\Big)\Big\} \\ &+ K^2L^4r^6\Big\{28\beta^2K^4r^8+(K-1)^2\Big(25K^2r^4+54\alpha^2(K-1)^2+4\alpha K(8K-53)r^2\Big) \\ &- 2\beta K^2r^4\Big(39\alpha(K-1)^2+K(41K+15)r^2\Big)\Big\}+K^4r^{10}\Big\{\beta^2K^4r^8+(K-1)^2\Big(\alpha^2 \\ &+ K^2\left(\alpha+r^2\right)^2-2\alpha K\left(\alpha+3r^2\right)\Big)-2\beta K^2r^4\left(\alpha(K-1)^2+K(K+1)r^2\right)\Big\} \\ &+ 4K^3L^2r^8\Big\{-2\beta^2K^4r^8+(K-1)^2\left(-2K^2r^4-3\alpha^2(K-1)^2-4\alpha(K-4)Kr^2\right) \\ &+ \beta K^2r^4\left(5\alpha(K-1)^2+K(5K+3)r^2\right)\Big\}-8\beta KL^{14}r^2\left(\beta r^2-4\right)+\beta L^{16}\left(\beta r^2-4\right)\Bigg]. \end{aligned} \tag{5.27}$$

Also the anisotropic parameter becomes of the form,

$$\begin{aligned} \Delta &= \beta+\frac{L^{12}r^2\left[28\beta^2K^2r^4-2\beta\left\{9\alpha(K-1)^2+K(55K+1)r^2\right\}+3(K-1)^2\right]}{4(L-r)(L+r)\left(L^2-Kr^2\right)^7} \\ &+ \frac{4L^{10}r^2}{4(L-r)(L+r)\left(L^2-Kr^2\right)^7}\Big[9\alpha+K\Big\{-14\beta^2K^2r^6+3\alpha(K(7K-11)+1) \end{aligned}$$

$$
\begin{aligned}
&+ \quad \beta K(53K+3)r^4 + (K-1)^2 r^2(21\alpha\beta - 4)\Big\}\Big] + \frac{L^8 r^2}{4(L-r)(L+r)\left(L^2-Kr^2\right)^7} \\
&\quad \Big[70\beta^2 K^4 r^8 + (K-1)^2\Big\{35K^2 r^4 + 81\alpha^2(K-1)^2 - 2\alpha K(95K+117)r^2\Big\} \\
&- \quad 2\beta K^2 r^4\Big\{79\alpha(K-1)^2 + 5K(25K+3)r^2\Big\}\Big] + \frac{4KL^6 r^4}{4(L-r)(L+r)\left(L^2-Kr^2\right)^7} \\
&\quad \Big[-14\beta^2 K^4 r^8 + (K-1)^2\Big\{-10K^2 r^4 - 27\alpha^2(K-1)^2 + 10\alpha K(3K+11)r^2\Big\} \\
&+ \quad 2\beta K^2 r^4\Big\{19\alpha(K-1)^2 + K(23K+5)r^2\Big\}\Big] + \frac{K^2 L^4 r^6}{4(L-r)(L+r)\left(L^2-Kr^2\right)^7} \\
&\quad \Big[28\beta^2 K^4 r^8 + (K-1)^2\Big\{25K^2 r^4 + 54\alpha^2(K-1)^2 - 4\alpha K(K+83)r^2\Big\} \\
&- \quad 2\beta K^2 r^4\Big\{39\alpha(K-1)^2 + K(41K+15)r^2\Big\}\Big] + \frac{K^4 r^{10}}{4(L-r)(L+r)\left(L^2-Kr^2\right)^7} \\
&\quad \Big[\beta^2 K^4 r^8 + (K-1)^2\left\{\alpha^2 + K^2\left(\alpha+r^2\right)^2 - 2\alpha K\left(\alpha+5r^2\right)\right\} \\
&- \quad 2\beta K^2 r^4\left\{\alpha(K-1)^2 + K(K+1)r^2\right\}\Big] + \frac{4K^3 L^2 r^8}{4(L-r)(L+r)\left(L^2-Kr^2\right)^7} \\
&\quad \Big[-2\beta^2 K^4 r^8 + (K-1)^2\Big\{-2K^2 r^4 - 3\alpha^2(K-1)^2 + \alpha(25-3K)Kr^2\Big\} \\
&+ \quad \beta K^2 r^4\Big\{5\alpha(K-1)^2 + K(5K+3)r^2\Big\}\Big] \\
&- \quad \frac{8\beta K L^{14} r^2\left(\beta r^2 - 4\right) - \beta L^{16}\left(\beta r^2 - 4\right)}{4(L-r)(L+r)\left(L^2-Kr^2\right)^7}.
\end{aligned}
\tag{5.28}
$$

The solution Eqs. (5.23) - (5.28) is given in simple elementary function so it may be used to model an anisotropic star with quadratic equation of state. Moreover to investigate further, I have study the model for $n = 1$ both analytically and graphically on the next sections.

5.3.2 The case $n = 2$

Now let us discuss the solution of the model for $n = 2$. When $n = 2$ the equation Eq. (5.20) becomes

$$
\frac{\dot{y}}{y} = \frac{k}{4L}\frac{(1-K)^{3/2}}{(1-x)}\frac{(3-Kx)^{3/2}}{(1-Kx)^2} + \frac{(1-K)}{4(1-x)} - \frac{\beta L^2(1-Kx)}{4(1-x)}. \tag{5.29}
$$

On integrating Eq. (5.29) one can easily obtain the solution of the equation as:

$$\begin{aligned} y &= d_2 Exp\Bigg[\frac{-1}{4L}\Bigg(\beta K L^3(x-1)+2\alpha\sqrt{\frac{(K-1)(Kx-3)}{(Kx-1)^2}}-\frac{\sqrt{2}\alpha(3K-7)}{\sqrt{K-1}} \\ &\quad \tan^{-1}\left(\frac{\sqrt{\frac{(K-1)(Kx-3)}{(Kx-1)^2}}(Kx-1)}{\sqrt{2}\sqrt{K-1}}\right)+\frac{2\alpha(K-3)^2}{\sqrt{K^2-4K+3}} \\ &\quad \tanh^{-1}\left(\frac{\sqrt{\frac{(K-1)(Kx-3)}{(Kx-1)^2}}(Kx-1)}{\sqrt{K^2-4K+3}}\right)+(K-1)L\left(\beta L^2-1\right)\log(x-1)\Bigg)\Bigg], \end{aligned} \tag{5.30}$$

where d_2 is the constant of integration. Hence an exact model for the system of equations Eqs. (5.14) - (5.18) can be written as

$$e^{2\lambda} = \frac{L^2-Kr^2}{L^2-r^2}, \tag{5.31}$$

$$\begin{aligned} e^{2\nu} &= d_2\exp\Bigg[-\frac{1}{2L}\Bigg\{\frac{-2\alpha(K-3)^2\tanh^{-1}\left(\frac{\sqrt{(K-1)\left(\frac{Kr^2}{L^2}-3\right)}}{\sqrt{K^2-4K+3}}\right)}{\sqrt{K^2-4K+3}} \\ &\quad -\frac{2\alpha\sqrt{(K-1)\left(\frac{Kr^2}{L^2}-3\right)}}{\frac{Kr^2}{L^2}-1}+\frac{\sqrt{2}\alpha(3K-7)\tan^{-1}\left(\frac{\sqrt{(K-1)\left(\frac{Kr^2}{L^2}-3\right)}}{\sqrt{2}\sqrt{K-1}}\right)}{\sqrt{K-1}} \\ &\quad +(K-1)L\left(\beta L^2-1\right)\log\left(1-\frac{r^2}{L^2}\right)+\beta KLr^2\Bigg\}\Bigg]. \end{aligned} \tag{5.32}$$

Also the density takes similar form as of Eq. (5.25). However the pressures take the form as follows:

$$
\begin{aligned}
p_r &= \alpha\left(\frac{(K-1)\left(Kr^2-3L^2\right)}{\left(L^2-Kr^2\right)^2}\right)^{3/2}-\beta, && (5.33)\\
p_t &= p_r+\Delta, \ \text{where} && (5.34)\\
\Delta &= \beta+\frac{1}{4L(L-r)(L+r)\left(L^2-Kr^2\right)^5\sqrt{\frac{Kr^2}{L^2}-3}}\Bigg[2\alpha(K-1)^{3/2}K^4r^{10}\Big\{K(\beta r^2\\
&- 1)+2\Big\}-2\alpha(K-1)^{3/2}K^3L^2r^8\Big\{\left(K\left(9\beta r^2-8\right)+20\right\}\\
&+ 12\alpha(K-1)^{3/2}K^2L^4r^6\Big\{K(5\beta r^2-3)+9\Big\}\\
&+ K^3Lr^8\sqrt{\frac{Kr^2}{L^2}-3}\Big\{\beta^2K^3r^6-2\beta K^2(K+1)r^4+(K-1)^2(\alpha^2(K-1)\\
&+ Kr^2)\Big\}+L^7r^2\sqrt{\frac{Kr^2}{L^2}-3}\Big\{-20\beta^2K^3r^6+8\beta K^2(9K+1)r^4\\
&+ (K-1)^2(-27\alpha^2(K-1)-10Kr^2)\Big\}+3KL^5r^4\sqrt{\frac{Kr^2}{L^2}-3}\Big\{5\beta^2K^3r^6\\
&- 4\beta K^2(4K+1)r^4+(K-1)^2(9\alpha^2(K-1)+4Kr^2)\Big\}+K^2L^3r^6\sqrt{\frac{Kr^2}{L^2}-3}\\
&\Big\{-6\beta^2K^3r^6+8\beta K^2(2K+1)r^4-9\alpha^2(K-1)^3-6(K-1)^2Kr^2\Big\}\\
&- 18\alpha(K-1)^{3/2}L^{10}\left(\beta r^2-2\right)+6\alpha(K-1)^{3/2}KL^8r^2\left(11\beta r^2-7\right)\\
&- 4\alpha(K-1)^{3/2}KL^6r^4\Big\{K\left(23\beta r^2-7\right)+18\Big\})+\beta L^{13}\left(\beta r^2-4\right)\sqrt{\frac{Kr^2}{L^2}-3}\\
&- 6\beta KL^{11}r^2\left(\beta r^2-4\right)\sqrt{\frac{Kr^2}{L^2}-3}+L^9r^2\sqrt{\frac{Kr^2}{L^2}-3}\Big\{K(15\beta^2Kr^4\\
&- 2\beta(29K+1)r^2+3(K-2))+3\Big\}\Bigg]-\alpha\left(\frac{(K-1)\left(Kr^2-3L^2\right)}{\left(L^2-Kr^2\right)^2}\right)^{3/2}. && (5.35)
\end{aligned}
$$

5.4 Matching conditions

For a static star, at the boundary b, we need to match the interior solution with the Schwarzschild exterior metric given by

$$ds^2 = -\left(1-\frac{2M}{r}\right)dt^2 + \left(1-\frac{2M}{r}\right)^{-1}dr^2 - r^2(d\theta^2+\sin^2\theta\, d\phi^2), \tag{5.36}$$

where $M = m(b)$, the total mass of the star as seen by an external observer and $r > 2M$. Continuity of metric functions states that the metric potentials Eq. (5.23) and Eq. (5.24) must match smoothly with the exterior Schwarzschild solution Eq. (5.36) at the boundary $r = b$. The matching conditions of a static star at the boundary are given by

$$e^{\nu(r=b)} = \left(1-\frac{2M}{b}\right), \qquad e^{\lambda(r=b)} = \left(1-\frac{2M}{b}\right)^{-1}, \tag{5.37}$$

Additionally the continuity of the curvature states that at the finite value of the radial parameter r, radial pressure vanishes at the surface of the star known as the radius of the star $i.e.$,

$$p_r(r=b) = 0. \tag{5.38}$$

The above junction conditions determine the arbitrary constants, which yields

$$\begin{aligned} L &= \frac{b\sqrt{2MK-Kb+b}}{\sqrt{2M}} \\ d_1 &= \left(1-\frac{2M}{b}\right)\left(1-\frac{Kb^2}{L^2}\right)^{\frac{\alpha(K-3)^2}{2(K-1)L^2}}\left(1-\frac{b^2}{L^2}\right)^{-\frac{1}{2}\left(\frac{\alpha(K-3)^2}{(K-1)L^2}-\beta(K-1)L^2+K-1\right)} \\ &\quad \times \exp\left[\frac{\alpha\left\{(5-3K)L^2+2(K-2)Kb^2\right\}}{\left(L^2-Kb^2\right)^2}+\frac{1}{2}\beta Kb^2\right], \end{aligned} \tag{5.39}$$

For the case $n = 2$, the matching conditions are unable to produce any real value for the model constant d_2, for any value of $K < 1$. Thus I have discarded the case $n = 2$.

5.5 Bounds on the model parameters

For a physically acceptable stellar model, it is reasonable to assume that the following conditions should be satisfied (Delgaty and Lake, 1998) (i) $\rho > 0$, $p_r > 0$, $p_t > 0$; (ii) $\rho' < 0$, $p_r' < 0$, $p_t' < 0$; (iii) $0 \leq \frac{dp_r}{d\rho} \leq 1$; $0 \leq \frac{dp_t}{d\rho} \leq 1$ and (iv) $\rho + p_r + 2p_t > 0$. In addition, it is expected that the solution should be regular and well-behaved at all interior points of the stellar configuration. Based on the above requirements, there are certain bounds on the model parameters as discussed below:

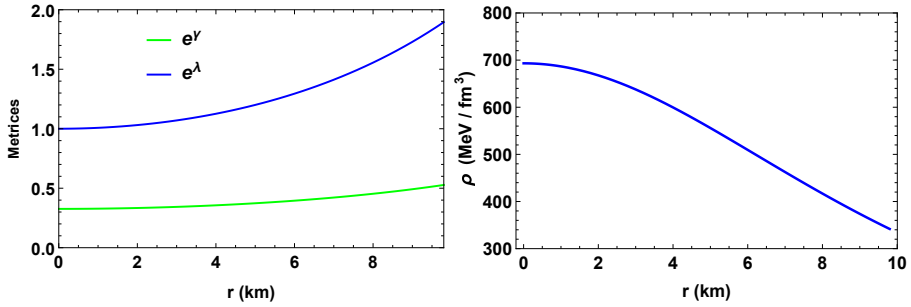

Figure 5.1: The metric potentials e^{ν} and e^{λ} are plotted against the radial coordinate r inside the stellar interior (left) and fall-off behaviour of energy density against the radial coordinate r (right) corresponding to the pulsar $4\mathrm{U}1608 - 52$.

5.5.1 Regularity conditions

1. The metric potentials $e^{\lambda(r)} > 0$, $e^{\nu(r)} > 0$ for $0 \leq r \leq b$.

   For appropriate choice of the model parameters, the above requirements are fulfilled in our model. The gravitational potentials in this model satisfy, $e^{\nu(0)} = d_1 e^{\frac{\alpha(3K-5)}{L^2}}$ =constant,

$e^{\lambda(0)} = 1$, i.e., finite at the centre ($r = 0$) of the stellar configuration. Also one can easily check that $(e^{\nu(r)})'_{r=0} = (e^{\lambda(r)})'_{r=0} = 0$. These imply that the metric is regular at the centre and well behaved throughout the stellar interior which will be analyzed graphically in the following section.

2. A physically relativistic star needs to following relations $\rho(r) \geq 0,\ p_r(r) \geq 0,\ p_t(r) \geq 0$ for $0 \leq r \leq b$. In our model, $\rho(r=0) = \frac{3(1-K)}{L^2} \geq 0$ is satisfied as $K < 1$. Thus, the density ρ is found to be regular and well behaved at the centre. Additionally, $p_r(r = 0) = (k\rho^2 - \beta)_{r=0}$ is ≥ 0 if $\frac{3(1-K)}{L^2} \geq \sqrt{\frac{\beta}{k}}$. The positivity of tangential pressure is ensured by the relation $\alpha > 0$. The nature profile of the metric potentials are discussed in the Fig. 5.1.

3. Continuity of the extrinsic curvature through the matching hyper-surface at the boundary of the stellar structure leads to the following constraint , $p_r(r = b) = 0$. This leads to the relation $\beta = \frac{\alpha(K-1)^2(Kb^2-3L^2)^2}{(L^2-Kb^2)^4}$. For specific choice of model parameter, the nature of radial and tangential pressures are discussed graphically in Fig. 5.1 and Fig. 5.2.

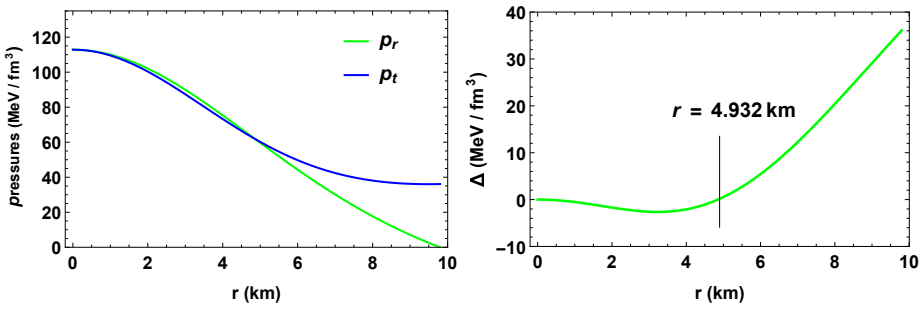

Figure 5.2: Fall-off behaviour of pressures, the radial (solid green) and the transverse pressure (solid blue)(left) and the variation of the anisotropy (right) against the radial coordinate r corresponding to the pulsar $4\mathrm{U}1608 - 52$.

4. For any stable realistic stellar model, the gradient of energy density and radial pressure should decrease monotonically from the centre to the surface boundary of the structure. A realistic stellar model should have the following properties: $\frac{d\rho}{dr} \leq 0$, $\frac{dp_r}{dr} \leq 0$, $\frac{dp_t}{dr} \leq 0$ for $0 \leq r \leq b$. With the choices of the model parameters within their proper bound it can be shown that both density and radial pressure decreases radially outward. The nature of gradient of density and pressures are discussed graphically in Fig. 5.6.

5. Anisotropy in the compact stellar model needs to be positive throughout the structure for the model to be stable as suggested by Gokhroo and Mehra (Gokhroo and Mehra, 1994). This specific model is shown to posses negative anisotropy upto 5 km but after that the anisotropy is shown to be increasing monotonically. The variation of anisotropy is seen in Fig. 5.2.

6. **Zeldovich Condition:** Any stable relativistic model needs to satisfy Zeldovich Condition given as $\frac{p_r}{\rho} \leq 1$ at the centre (Zeldovich and Novikov, 1972). Applying Zeldovich condition at the centre we get the relation as

$$-9\alpha \leq 3L^2 + \frac{\beta L^4}{1-K}. \tag{5.40}$$

5.5.2 Causality condition

We also know that for a physically acceptable model, the velocity of the sound (both radial and transverse) should be less than the speed of the light i.e., we should have $\frac{dp_r}{d\rho}, \frac{dp_t}{d\rho} < 1$ which is known as the causality condition. The causality condition is shown to satisfy in Fig. 5.3 and for our model The causality condition demands that $0 \leq \frac{dp_r}{d\rho} \leq 1$ and

$0 \leq \frac{dp_t}{d\rho} \leq 1$ at all interior points of the star. Thus we obtain the following:

$$
\begin{aligned}
\frac{dp_r}{d\rho} &= \frac{2\alpha(K-1)\left(Kr^2-3L^2\right)}{\left(L^2-Kr^2\right)^2}, \qquad (5.41)\\
\frac{dp_t}{d\rho} &= \frac{1}{4(K-1)K\left(L^2-r^2\right)^2\left(Kr^2-5L^2\right)\left(Kr^2-L^2\right)^5}\\
&\times \Bigg[L^{16}\Big\{\beta^2(-K)(44K+1)r^4+2\beta(K-1)\left(9\alpha(K-1)+14Kr^2\right)-3(K-1)^2\Big\}\\
&- \beta^2L^{20}+2L^{14}\Big\{(4\beta^2K^2(14K+1)r^6-\beta(K-1)Kr^2(30\alpha(K-1)\\
&+ (43K-1)r^2)+(K-1)^2\left(7Kr^2-6\alpha(17K+3)\right)\Big\}+K^5r^{12}\Big\{\beta^2\left(-K^4\right)r^8\\
&- 2\alpha\beta(K-1)^2K^2r^4+(K-1)^2(K^2r^4+3\alpha^2(K-1)^2+4\alpha(K-3)Kr^2)\Big\}\\
&+ 2K^4L^2r^{10}\Big\{(K-1)^2(-5K^2r^4-\alpha^2(K-1)^2(K+22)\\
&- \alpha K(K(K+16)-81)r^2)-\left(\alpha^2(K-1)^2(K+22)\right)-\beta(K-1)^2K^2r^4(Kr^2\\
&- 14\alpha)+\beta^2K^4(K+4)r^8\Big\}+KL^8r^4\Big\{(K-1)^2(-5(K-11)K^2r^4\\
&+ 27\alpha^2(K-1)^2(14K+17)-4\alpha K(K(32K+53)+25)r^2)+2\beta(K-1)K^2r^4\\
&\quad \left(2K(31K-10)r^2-\alpha(K-1)(33K+167)\right)-70\beta^2K^4(2K+1)r^8\Big\}\\
&+ 2KL^{10}r^2\Big\{(K-1)^2(-135\alpha^2(K-1)^2+K(10K-13)r^4+3\alpha(5(K-20)K\\
&- 17)r^2)-14\beta^2K^3(7K+2)r^8+\beta(K-1)Kr^4(5K(17K-3)r^2-2\alpha(K-1)\\
&\quad (6K+47))\Big\}+2K^2L^6r^6\Big\{(K-1)^2(-K^2(K+30)r^4-6\alpha^2(K-1)^2(14K+45)\\
&+ 2\alpha K(K(103-4K)+161)r^2)-4\beta^2K^4(8K+7)r^8+\beta(K-1)K^2r^4(K(29K\\
&- 15)r^2-2\alpha(K-1)(9K+74))\Big\}+L12\Big\{(K-1)^2(-81\alpha^2(K-1)^2\\
&+ 5K(1-5K)r^4+12\alpha K(25K+41)r^2)+2\beta(K-1)Kr^4\\
&\quad \left(3\alpha(K-1)(9K-7)+2K(38K-3)r^2\right)-14\beta^2K^3(13K+2)r^8\Big\}\\
&+ K^3L^4r^8\Big\{(K-1)^2(K^2(K+35)r^4+\alpha^2(K-1)^2(31K+234)
\end{aligned}
$$

$$+ \quad 4\alpha K(K(5K-7)-148)r^2) + 2\beta(K-1)K^2r^4(2K(4K-3)r^2$$
$$- \quad \alpha(K-1)(3K+67)) - \beta^2K^4(17K+28)r^8\Big\} + 2\beta L^{18}\left(K\left(5\beta r^2-2\right)+2\right)\Bigg]. \tag{5.42}$$

Moreover, combining both the equations at $r=0$, one can obtain the

$$\begin{aligned}
\frac{dp_r}{d\rho}|_{(r=0)} &= \frac{6\alpha(1-K)}{L^2}, \\
\frac{dp_t}{d\rho}|_{(r=0)} &= \frac{1}{20(K-1)KL^{16}} \\
&\times \Bigg[2\beta(2-2K)L^{18} + L^{16}\left(18\alpha\beta(K-1)^2 - 3(K-1)^2\right) - 12\alpha(K-1)^2 \\
&\quad (17K+3)L^{14} - 81\alpha^2(K-1)^4L^{12} - \beta^2L^{20}\Bigg].
\end{aligned}$$

Applying the causality condition on central sound speed in the radial direction, $\frac{dp_r}{d\rho}$ one can easily obtain the relation, $6\alpha \leq \frac{L^2}{1-K}$.

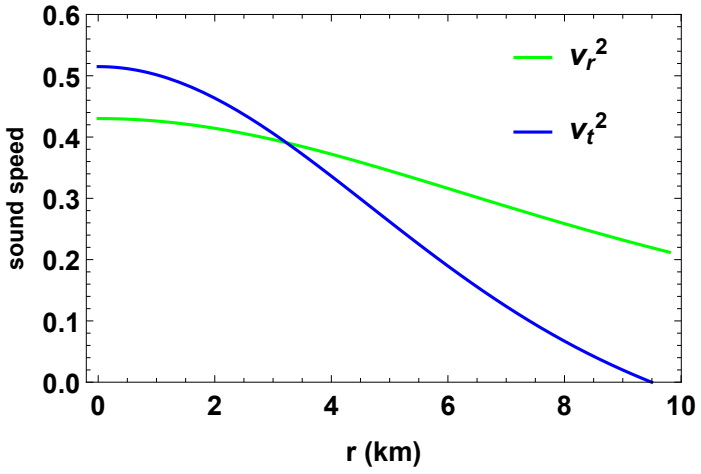

Figure 5.3: The radial (solid green) and transverse (solid blue) sound speeds against the radial coordinate r corresponding to the pulsar $4\mathrm{U}1608-52$.

5.5.3 Energy Conditions

For an anisotropic fluid sphere all the energy conditions, namely the Weak Energy Condition (WEC), the Null Energy Condition (NEC), the Strong Energy Condition (SEC) and the Dominant Energy Condition (DEC) should be satisfied i.e., the fluid should statisfy the following conditions:

(1) **NEC** : $\rho + p_r \geq 0,\ \rho + p_t \geq 0,$

(2) **WEC** : $p_r + \rho > 0,\ \rho > 0,$

(3) **SEC** : $\rho + p_r \geq 0,\ \rho + p_r + 2p_t \geq 0,$

(4) **DEC** : $\rho > |p_r|,\ \rho > |p_t|.$

Now, for positive density and pressures, it is quite obvious to satisfy the positivity of their sums. Thus to understand the true nature of the energy conditions of the model we study the DEC and the Trace Energy Condition (TEC). As suggested by Bondi (Bondi, 1999), a compact anisotropic spherical structure to be physically reliable, TEC needs to be positive. The TEC is expressed as: (5) **TEC**: $\rho - p_r - 2p_t \geq 0$. The behaviour of the Dominant and Trace Energy Conditions are discussed graphically in Fig. 5.4.

Using the SEC at the centre, we obtain

$$\rho + p_r + 2p_t(r = 0) \geq 0, \tag{5.43}$$

which yields the following inequality

$$\frac{K-1}{L^4}\left(9\alpha(K-1) - 3L^2 + 18\alpha(K-1)\right) \geq 3\beta. \tag{5.44}$$

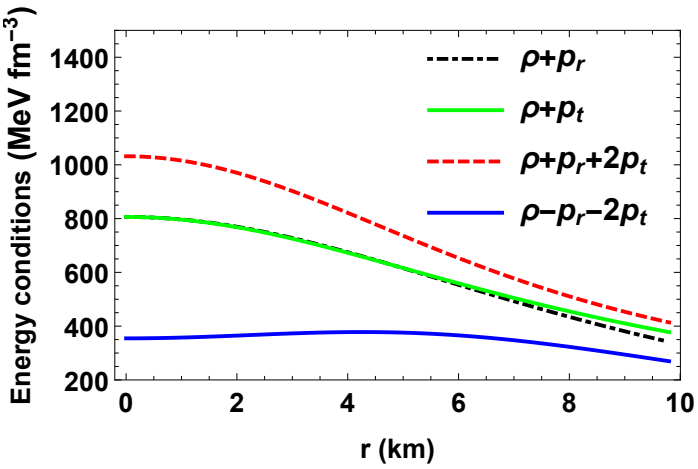

Figure 5.4: Verification of several energy conditions, SEC (solid red), NEC in the radial direction (dashed black), in the transverse direction (solid green), TEC (solid blue).

5.5.4 Adiabatic index

Stability of anisotropic compact star depends on the adiabatic index and it is described as the ratio of specific heat at constant pressure to the specific heat at constant volume. The adiabatic index determines the stability and the stiffness of the equation of state and is defined as

$$\Gamma = \frac{\rho(r) + p_r(r)}{p_r(r)} \frac{dp_r(r)}{d\rho(r)}, \tag{5.45}$$

is related to the stability of a relativistic anisotropic stellar configuration. Any stellar configuration will maintain its stability if adiabatic index $\Gamma_r > 4/3$ (Heintzmann and Hillebrandt, 1975). For our solution, the adiabatic index Γ takes the value more than $4/3$ throughout the interior of the compact star as evident in Fig. 5.5.

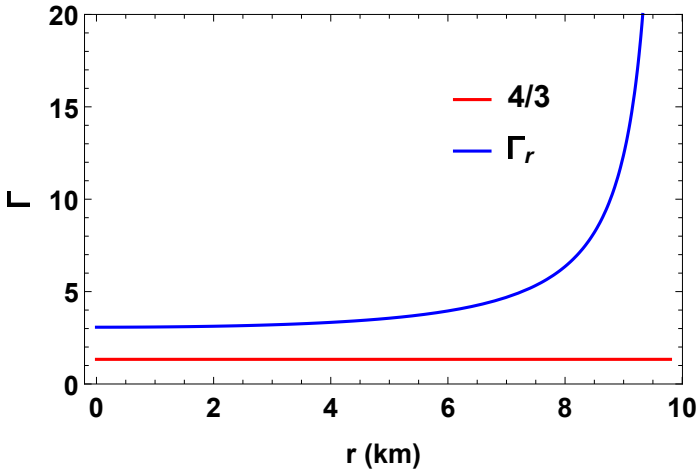

Figure 5.5: Variation of adiabatic index against the radial coordinate r corresponding to the pulsar $4\mathrm{U}1608-52$.

5.6 Physical analysis

Case -1 (n=1) is analyzed here in this section.

To study the physical features of the prescribed model we have considered the values from the pulsar $4\mathrm{U}\ 1608-52$, mass $= 1.97^{+0.30}_{-0.29} M_{\odot}$ and radius $= 9.8^{+1.8}_{-1.8}$ km, which leads to the value of the model parameters as $\beta = 0.0012$, $L = 22.9073$, $\alpha = 9.4407$, $d_1 = 0.419$.

5.7 Stability analysis

5.7.1 Stability under different forces

To represent any physically relativistic anisotropic structure, the model needs to be stable under different forces and this stability is checked using Tolman-Oppenheimer-Volkoff (TOV) equation. The TOV equation essentially represents the configuration of density and radial pressure for any anisotropic fluid sphere. To check the equilibrium of the model, we

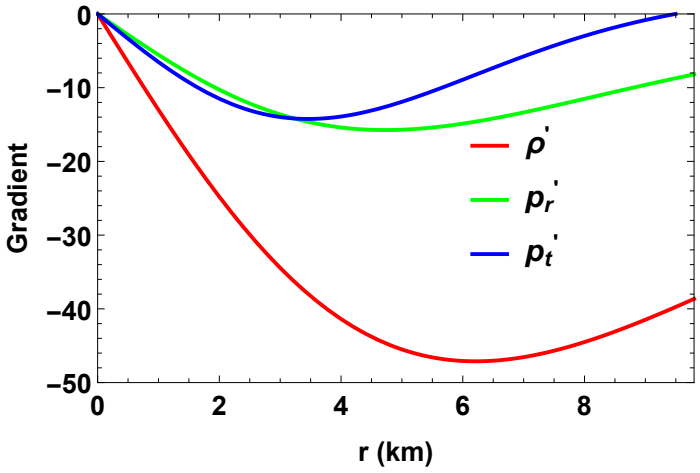

Figure 5.6: Variation of gradient of the density (solid red) and the pressures (in the radial (solid green) and the transverse (solid blue) directions) against the radial coordinate r corresponding to the pulsar $4\mathrm{U}1608-52$.

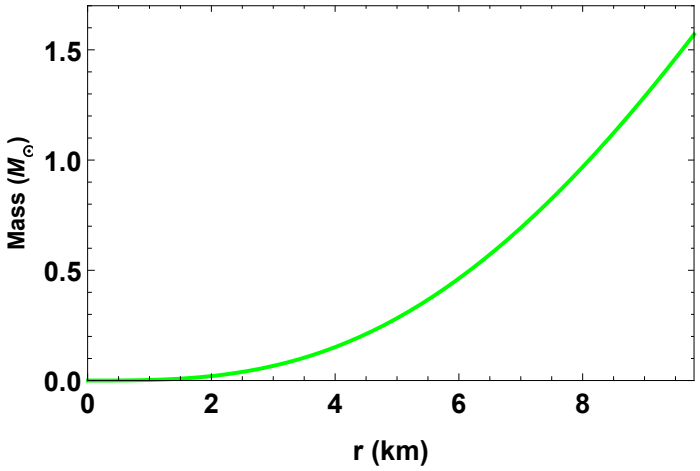

Figure 5.7: Variation of the mass function against the radial coordinate r corresponding to the pulsar $4\mathrm{U}1608-52$.

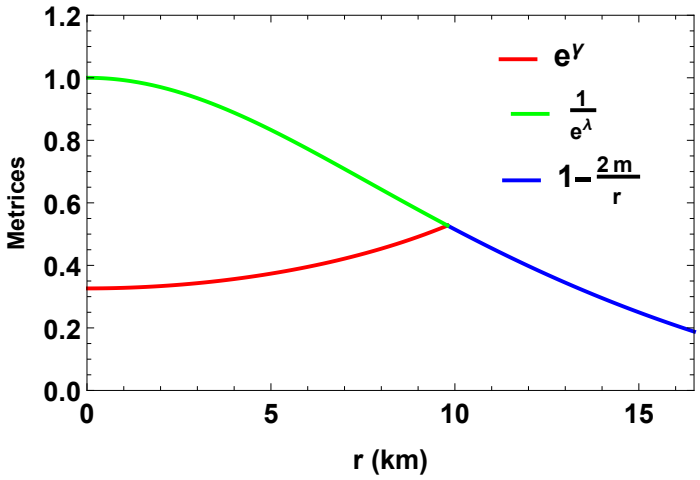

Figure 5.8: Smooth matching of the metric potentials at the stellar boundary.

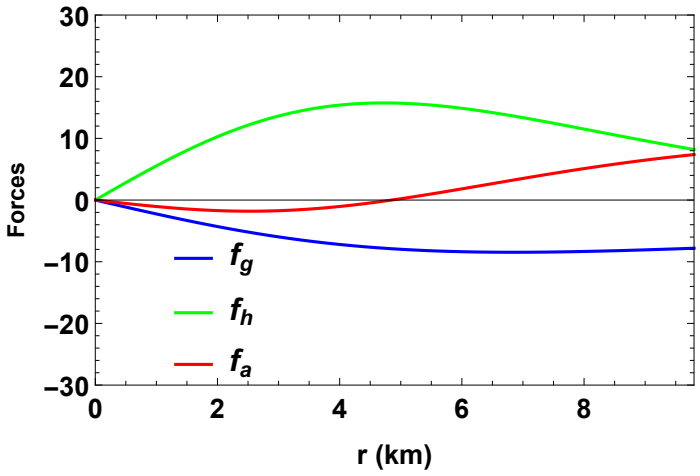

Figure 5.9: Variation of several forces, gravitational force (solid blue), hydrostatic force (solid green) and anisotropic force (solid red) within the star corresponding to the pulsar $4U1608-52$.

need to check the stability under three different forces, namely the anisotropic F_a, hydrostatic F_h and gravitational F_g forces. The general expression for TOV equation is expressed as:

$$\frac{M_g}{r^2}(\rho + p_r)e^{\left(\frac{\lambda-\nu}{2}\right)} - \frac{dp_r}{dr} + \frac{2}{r}(p_t - p_r) = 0, \tag{5.46}$$

where M_g is the gravitational mass within the compact stellar objects of radius r which can be derived using Tolman-Whittaker mass formula and it is defined by

$$M_g = \frac{1}{2}r^2 e^{\left(\frac{\nu-\lambda}{2}\right)}\frac{d\nu}{dr}. \tag{5.47}$$

Thus we get the expressions for several forces in the form:

$$\begin{aligned} F_g &= 1/2(\rho + p_r)\frac{d\nu}{dr}, \\ F_h &= -\frac{dp_r}{dr}, \\ F_a &= \frac{2}{r}(p_t - p_r). \end{aligned}$$

Fig. 5.9 shows the stability of the model as negative gravitational force is seen to be balanced by the combined force of hydrostatic and anisotropic forces.

5.7.2 Mass-radius relationship

The dynamic stability of any compact star model is checked by observing its mass-radius relationship. Even, any observed compact stellar objects can be identified as black holes if its maximum mass exceeds that of allowable limit for a stable compact stellar model (Hendi et al., 2017; Shapiro and Teukolsky, 1983). For the surface density $\rho(b) = 5.5 \times 10^{14}$ gm /cc, we have studied the mass radius relationship for the model in Fig. 5.10. It shows that

as the value of spheroidal parameter is decreased, the compactness of the star increases.

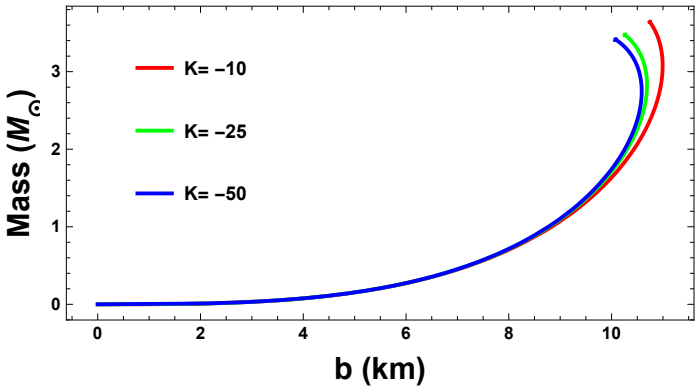

Figure 5.10: Mass-radius ($M - b$) relationship for the model corresponding to the surface density $\rho(b) = 5.5 \times 10^{14}$ gm /cc for different values of K.

5.7.3 Compactness and gravitational redshifts

The mass function of any stable compact stellar structure needs to be monotonically increasing inside the configuration. The regularity of the mass function is checked graphically in Fig. 5.7. Also the compactification factor of a compact star is defined by dimensionless term $m(r)/r$ and for stable configuration $2M(b)/b$ should be less than $8/9$ as suggested by Buchdahl (Buchdahl, 1959). Fig. 5.11 supports the fact that model satisfy the compactness factor.

Moreover, another important feature of the stellar structure is to study their gravitational redshifts. The gravitational redshifts for a spherically symmetric stellar structure are defined by ,

$$z(r) = \frac{1 - \sqrt{1 - 2u(r)}}{\sqrt{1 - 2u(r)}}. \tag{5.48}$$

The gravitational redshifts are supposed to attain maximum value at the centre and then decrease monotonically outwards. The variation of gravitational redshifts is depicted graph-

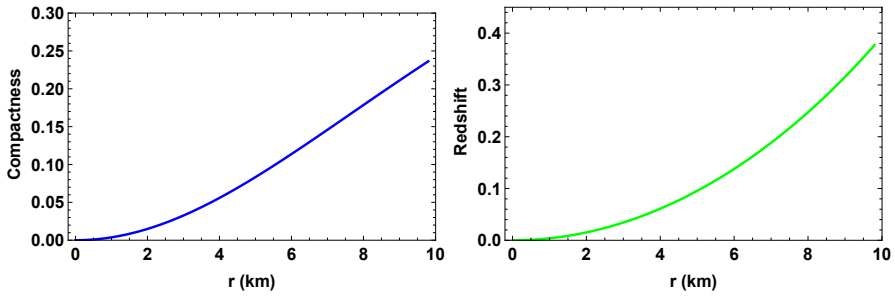

Figure 5.11: The compactness factor are plotted inside the stellar interior (left) and variation of the gravitational redshifts (right) against the radial coordinate r corresponding to the pulsar $4\mathrm{U}1608-52$.

ically in Fig. 5.11 which shows the increasing nature of gravitational redshifts with the radial coordinate. Studies by several authors have allowed us to specify an upper bound on the surface redshifts. In absence of cosmological constant, $z(r) \leq 2$ holds for an isotropic star as proposed by Barraco and Hamity (Barraco and Hamity, 2002). This specific model presented here satisfies the range $z(r) \leq 1$ as predicted by Hewish et. al (Hewish et al., 1968)

5.8 Impact of curvature parameter on the model

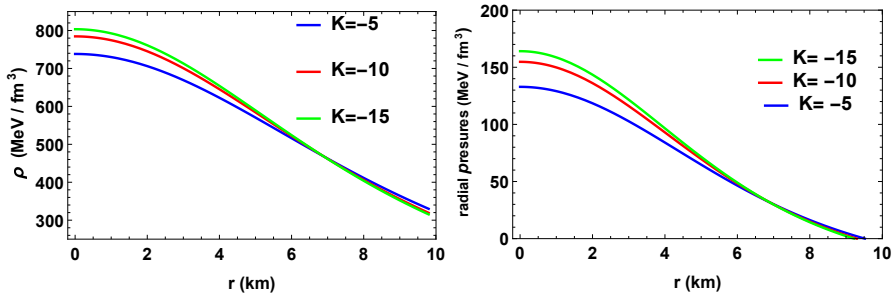

Figure 5.12: Variation of the density (left) and variation of the radial pressure (right) against the radial coordinate r for different values of K.

To study the suitability of the model to describe the interior of compact fluid spheres in equilibrium, we need to observe the curvature parameter. The law of variation of density of matter in the configuration is determined by the requirement to be the space time of a matter distribution in equilibrium be spheroidal (Sasidharan and Sabu, 2021).

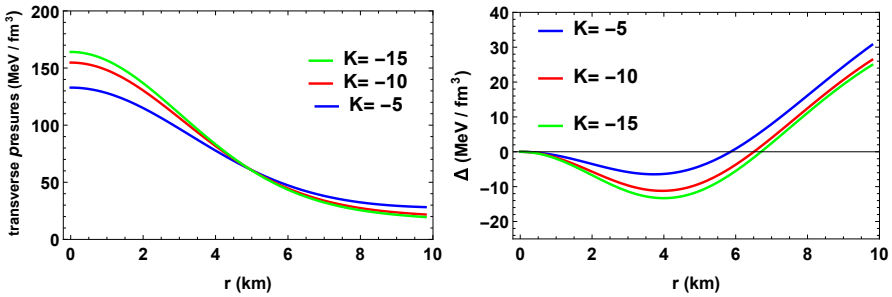

Figure 5.13: Variation of the transverse pressure (left) and variation of the anisotropy (right) against the radial coordinate r for different values of K.

Detailed study of the curvature for several cosmological models can be found in (Burghardt, 2016). In this work, the effect of K, on the model has been studied graphically. For fixed value of α and β, I have plotted the nature of primary matter variables . From Fig. 5.12, it can be seen that the decrease of the value of K leads to the increasing nature of the value density at the centre but the value at the surface seems to be decreasing. Same results can be observed for radial pressure (Fig. 5.12) and transverse pressure (Fig. 5.13) also. For anisotropy, higher the value of K, faster the anistropic pressure becomes positive.

Properties	**Vela X-**1	**Cen X-**3	**SAX J**$1748.9-2021$
$\rho\|_0$	663.697	860.38	489.211
$\rho\|_b$	285.729	379.448	226.298
$\frac{dp_r}{d\rho}\|_0$	0.4118	0.534	0.304
$\frac{dp_r}{d\rho}\|_b$	0.177	0.235	0.1404
$\frac{dp_t}{d\rho}\|_0$	0.523	0.699	0.368
$\frac{dp_t}{d\rho}\|_b$	0.0189	0.0237	0.0353
$(\rho+p_r+2p_t)\|_0$	563.249	666.915	415.186
$(\rho+p_r+2p_t)\|_b$	239.888	294.93	215.506

Table 5.1: Numerical values of the matter variables for different compact stars assuming $K=-5$. Here $|_0$ and $|_b$ denote the values of the matter variables at the center and surface respectively.

Properties	**Vela X-**1	**Cen X-**3	**SAX J**$1748.9-2021$
$\rho\|_0$	708.141	915.66	518.117
$\rho\|_b$	276.01	366.942	219.31
$\frac{dp_r}{d\rho}\|_0$	0.439	0.568	0.321
$\frac{dp_r}{d\rho}\|_b$	0.171	0.227	0.136
$\frac{dp_t}{d\rho}\|_0$	0.589	0.781	0.415
$\frac{dp_t}{d\rho}\|_b$	0.0415	0.0451	0.0513
$(\rho+p_r+2p_t)\|_0$	588.77	691.73	471.056
$(\rho+p_r+2p_t)\|_b$	238.978	296.701	213.505

Table 5.2: Numerical values of the matter variables for different stars assuming $K=-10$. Here $|_0$ and $|_b$ denote the values of the matter variables at the center and surface respectively.

Properties	**Vela X-**1	**Cen X-**3	**SAX J**1748.9 − 2021
$\rho\|_0$	726.381	938.276	529.85
$\rho\|_b$	272.366	362.253	216.69
$\frac{dp_r}{d\rho}\|_0$	0.450	0.582	0.3288
$\frac{dp_r}{d\rho}\|_b$	0.169	0.2248	0.13448
$\frac{dp_t}{d\rho}\|_0$	0.615	0.813	0.432
$\frac{dp_t}{d\rho}\|_b$	0.048	0.0508	0.056
$(\rho + p_r + 2p_t)\|_0$	598.89	701.334	478.97
$(\rho + p_r + 2p_t)\|_b$	238.391	296.948	212.63

Table 5.3: Numerical values of the matter variables for different stars assuming $K = -15$. Here $|_0$ and $|_b$ denote the values of the matter variables at the center and surface respectively.

5.9 Discussions

In this work I have studied Vaidya-Tikekar model to anisotropic compact spherical structure using polytropic equation of state. The model is seen to represent a stable compact stellar configuration. The model constants are obtained from the smooth matching of interior metric conditions with Schwarzschild exterior solution. Additionally, the model also fulfills the following conditions:

Regularity Conditions: The metric potentials are regular, well behaved throughout the structure. The energy density and pressures are finite and positive inside the star. The anisotropic parameter, however, is negative for upto 5 km then it is seen to increase monotonically throughout the star. The gradient of the density and pressures are negative inside the star making the structure stable for physically relativistic. Smooth matching of the stellar configuration with the Schwarzschild exterior spacetime leads the values of the model paramters. Graphically smooth matching of the exterior spacetime with the structure at the surface of the star in seen in Fig. 5.8.

Causality Conditions: The sound speed of the model is seen to satisfy the relations

$o \leq \frac{dp_r}{d\rho}, \frac{dp_t}{d\rho} \leq 1$.

Energy conditions: The model fulfills all the energy conditions inside the star. The positive profile of density and pressures ensures the fulfillment of the energy conditions. Graphically we have studied the trace of the energy condition $\rho - p_r - 2p_t \geq 0$, and it fulfills the TEC as seen in Fig. 5.4.

Adiabtic Index: I have observed the nature of adiabatic index for our model and it is found to be $> 4/3$ throughout the stellar structure.

TOV equation: Under the combined action of the gravitational, hydrostatic and anisotropic forces, this model remains in equilibrium as seen in Fig. 5.9.

Buchdahl limit: This model satisfies the Buchdahl limit, see Fig. 5.11. Also the gravitational redshifts $z(r)$ is depicted graphically in Fig. 5.11 which shows the increasing nature of gravitational redshifts with the radial coordinate.

Impact of curvature parameter: Moreover, I have studied the impact of K on our model. I have shown graphically that density and pressures are increasing with the decrease of K. Further we have checked this impact for other stars also and I have observed the similar result. The values of the matter variables are presented in a tabular form in Tables. 5.1, 5.2 and 5.3 for $K = -5, -10$ and -15 respectively.

Chapter 6

Study on anisotropic stellar model of embedding class-I satisfying Karmarkar's condition

6.1 The embedding problem

Riemannian geometry is the study of the geometric objects consisting of fields of the non-singular, symmetric, second order covariant tensors defined on differentials manifolds (Willmore, 1959). One of the rudimentary ideas of Riemann was to develop the notion of an n-dimensional "manifold" which will locally look like $\mathbb{R}^n$. Essentially, a manifold is a topological space covered by co-ordinate charts such that change of the co-ordinates between any two charts is also a smooth map (Meinrenken, 2002). Mathematically a differentiable manifold is associated with tangent space where at each point x, an inner product ψ_x varies differentiably with x. Recall that the inner product is given by a function ψ which maps a pair of contravariant vectors η, ζ to a real number such that

(i) ψ is bilinear

(ii) ψ is symmetric i.e. $\psi(\eta, \zeta) = \psi(\zeta, \eta)$ and

(iii) $\psi(\eta, x) = 0$ for all x imply $\psi = 0$.

Now the consideration of differential geometric surfaces naturally arise the question: is the surface isometric to a submanifold in an Euclidean space ? This problem is known as the Embedding problem.

This problem has been considered in various studies by several scholars. L. Schlaefli (Schlaefli, 1871) laid the foundation in 1871 when he conjectured that the spacetime can be embedded into higher dimensional pseudo-Euclidean space. He discussed the local form of this problem. He postulated that a neighbourhood in an n-manifold would generally require an $\frac{1}{2}n(n+1)$ dimensional embedding space. In 1901 Hilbert (Hilbert, 1901) showed that the hyperbolic plane which possess constant negative Gaussian curvature but is not "smooth' or "complete" surface in $\mathbb{E}^3$. Alternatively it can be state that a complete surface of constant negative curvature cannot be $\mathbf{C}^4$-isometrically embed in Euclidean-3 space. one specimen would would be n-torus which is not realizable in $2n$-dimensions. Janet (Janet, 1927) solved the local problems for two manifolds which later Cartan (Cartan, 1927) extended to n-manifolds forming the famously known Janet-Cartan theorem which states that *if* $(\mathbf{M}^n, g)$ *is a real-analytic Riemannian manifold and* $N = \frac{1}{2}n(n+1)$*, then every point of* $\mathbf{M}$ *has a neighbourhood which has a real-analytic isometric embedding into* $\mathbb{R}^n$. There exist real analytic Riemannian n-manifolds which do not possess smooth local isometric embedding in any Euclidean space of dimension strictly less than $\frac{1}{2}n(n+1)$. For example, an analytic Riemannian 3-manifolds can be locally and isometrically immersed into $\mathbb{E}^6$ (Ojha and Saxena, 2021). Similarly to embed any 4-dimensional space-time, both locally and isometrically, minimum 10-dimensions are needed. As an extension of local embedding,

now the question of globally embedding manifold transpire. In 1936 H. Whitney (Whitney, 1936, 1944a,b) proved that an n-manifold can always be embedded (without requiring isometry) in the Euclidean $2n$ space $\mathbb{E}^{2n}$ and can always be immersed as a closed set in $\mathbb{E}^{2n-1}$. this result was finally proved by Nash (Nash, 1954) in his groundbreaking work of forming *Nash Embedding Theorem* where he showed that any compact manifold with a metric of class C^k, $k \geq 3$ can be isometrically embedded in $\mathbb{R}^n$ where $N = \frac{1}{2}n(3n+11)$. Every non-compact Riemannian n-manifold can be isometrically embedded in any small portion of a Euclidean-N space where $N = \frac{1}{2}n(n+1)(3n+11)$. Subsequently, it was extended to manifold with an indefinite metric by Friedman (Friedman, 1965).

6.2 Embedding class one and Karmarkar's condition

A gravitational field is described by a Riemannian metric of four dimension in general relativity. Thus to describe a compact stellar model in relativistic field this gravitational field can be considered as a fields immersed in a flat space of higher dimensions. Embedding of n dimensional space V_n into a $n+p$ dimensional Euclidean space E_{n+p} is one of the fascinating way of studying stellar structure. Although the concept has been introduced much earlier but it has skyrocketed after the work on brane theory by Randall and Sundrum (Randall and Sundrum, 1999). An intriguing scheme to model stable configuration is to embed a 4-dimensional spacetime into higher dimensional space though another particular form of Buchdahl metric is also studied by Vaidya and Tikekar (Vaidya and Tikekar, 1982) and Tikekar (Tikekar, 1990) by embedding a 3-hyperspace into 4-dimensional space. Recently Buchdahl metric has been analyzed in spherically symmetric spacetime in terms of embedding by Singh et. al (Singh et al., 2017) and in terms of Vaidya-Tikekar and Finch-Skea model by Maurya et al (Maurya et al., 2019a). Condition for embedding a

4-dimensional spacetime metric into 5-dimensional Euclidean space was first derived by K. R. Karmarkar (Karmarkar, 1948), which is named after him as Karmarkar condition. In this condition, two metric potentials need to be dependent on each other. The simple expression between the metric potentials allows the researcher to choose general forms of metric potential having physical viability to generate acceptable compact stellar models. Any solution of EFEs satisfying Karmarkar condition is considered to be of Class I. Numerous researchers have devoted their time in the modeling of both charged and uncharged stars using Karmarkar condition. Some of the recent literature backing the modeling of anisotropic compact stars using embedding class I condition are authored by Pandya et al. (Pandya et al., 2020; Pandya and Thomas, 2019), Singh et al. (Singh et al., 2019, 2020a,b,c), Gedela et al. (Gedela et al., 2019a, 2020, 2019c) and many more (Fatema et al., 2019; Jasim et al., 2020; Maurya et al., 2020c; Prasad et al., 2019; Rahaman et al., 2020; Sarkar et al., 2019a,b; Shamir and Fayyaz, 2020; Tamta and Fuloria, 2020; Tello-Ortiz et al., 2019, 2020b). Recently, Govender et al (Govender et al., 2020) have studied the gravitational collapse of a spherically symmetric star by employing Karmarkar condition. It is worth mentioning that Schwarzschild exterior solution is of class II and the interior solution is of class I. The solution for the isotropic fluid sphere that satisfies Karmarkar condition is either Schwarzschild interior solution (Schwarzschild, 1916a,b) in which inner solution is conformally flat depicting limited configuration or Kohler-Chao (Kohler and Chao, 1965) solution for which inner solution is conformally non-flat depicting limitless configuration, yet is considered to obtain a new class of relativistic solutions.

The line element in 4D co-ordinate system $(t,\ r,\ \theta,\ \phi)$ to describe the interior of a static and spherically symmetric stellar configuration can be given as the following,

$$ds^2 = e^{\nu(r)}dt^2 - e^{\lambda(r)}dr^2 - r^2\left(d\theta^2 + \sin^2\theta d\phi^2\right), \tag{6.1}$$

where the metric potentials $e^{\nu(r)}$ and $e^{\lambda(r)}$ or more precisely $\nu(r)$ and $\lambda(r)$ are functions of the radial coordinate 'r' only.

Assuming $8\pi G = c = 1$ the Einstein field equations can be written as,

$$\mathcal{G}_{\mu\nu} = -\mathcal{T}_{\mu\nu} = \left(\mathcal{R}_{\mu\nu} - \frac{1}{2}\mathcal{R}\, g_{\mu\nu}\right), \tag{6.2}$$

where $\mathcal{G}_{\mu\nu},\ \mathcal{T}_{\mu\nu},\ \mathcal{R}_{\mu\nu},\ g_{\mu\nu}$ and $\mathcal{R}$ are Einstein tensor, the stress energy tensor, Ricci tensor, metric tensor and Ricci scalar respectively.

For an anisotropic matter distribution, the energy momentum tensor can be written as,

$$\mathcal{T}_{\mu\nu} = (\rho(r) + p_t(r))\, U_\mu U_\nu - p_t(r) g_{\mu\nu} + (p_r(r) - p_t(r))\, \chi_\mu \chi_\nu, \tag{6.3}$$

where $\rho(r)$ is the energy density, $p_r(r)$ and $p_t(r)$ represent pressures along the radial and the transverse directions of the fluid configuration respectively. U^μ is the 4-velocity and χ^μ is an unit 4-vector along the radial direction. The quantities obey the relations, $\chi_\mu \chi^\mu = 1$ and $\chi_\mu U^\mu = 0$.

The Einstein field equations given in Eq. (6.2) governing the evolution of the system read as the following form for the metric given in the Eq. (6.1) along with the energy tensor in Eq. (6.3),

$$\rho(r) = \frac{1 - e^{-\lambda}}{r^2} + \frac{e^{-\lambda}\lambda'}{r}, \tag{6.4}$$

$$p_r(r) = \frac{e^{-\lambda} - 1}{r^2} + \frac{e^{-\lambda}\nu'}{r}, \tag{6.5}$$

$$p_t(r) = \frac{e^{-\lambda}}{2}\left(\nu'' + \frac{\nu' - \lambda'}{r} + \frac{\nu'^2 - \nu'\lambda'}{2}\right), \tag{6.6}$$

where 'prime' in Eqs. (6.4)-(6.6) denotes differentiation with respect to radial co-ordinate r. Also, the anisotropic factor is defined as $\Delta(r) = (p_t(r) - p_r(r))$ and its expression for the stellar system is

$$\Delta(r) = \frac{e^{-\lambda}}{2}\left(\nu'' + \frac{\nu'^2}{2} - \frac{\nu'\lambda'}{2} - \frac{\nu' - \lambda'}{r}\right) + \frac{1 - e^{-\lambda}}{r^2}. \tag{6.7}$$

The general theory of relativity tells us that whenever an n dimensional spacetime is embedded in a Pseudo Euclidean spacetime of $n + p$ dimension then 'p' is called embedding class. A symmetric tensor $h_{\alpha\beta}$ of 4 dimensional Riemannian space can be embed into a 5 dimensional Pseudo Euclidean space if it is satisfies Gauss (Gauss, 1827) and Codazzi (Codazzi, 1868) condition and it can be written as,

$$\mathcal{R}_{\alpha\beta ij} = \epsilon\left(h_{\alpha i}h_{\beta j} - h_{\alpha j}h_{\beta i}\right), \tag{6.8}$$

$$h_{\alpha\beta;i} - h_{\alpha i;\beta} = 0, \tag{6.9}$$

where $\mathcal{R}_{\alpha\beta ij}$ denotes curvature tensor.

Here, the parameter ϵ is given as, $\epsilon = 1$, when normal to the manifold is spacelike and $\epsilon = -1$, when normal to the manifold is timelike and the symbol ';' represent covariant derivative. Earlier Kasner (Kasner, 1921) investigated in the year 1921 that a 4 dimensional spacetime of spherically symmetric object can always be embedded in 6 dimensional Pseudo Euclidean space and later Gupta and Goyel (1975) (Gupta and Goyel, 1975) have shown the same result with another coordinate transformation. In 1924, Eddington (Eddington Kasner, 1924) found that an n-dimensional spacetime can always be embedded in m-dimensional Pseudo Euclidean space with $m = \frac{1}{2}n(n+1)$ and to embed, the minimum extra dimension required is less than or equal to the number $(m - n)$ or same

as $\frac{1}{2}n(n-1)$. Therefore 4 dimensional spherically symmetric line element Eq. (6.1) is of embedding class II. From Eq. (6.1), the components of Riemann curvature tensor are expressed as,

$$\begin{aligned} R_{1414} &= -e^{\nu}\left(\frac{\nu''}{2}+\frac{\nu'^2}{4}-\frac{\lambda'\nu'}{4}\right), \quad R_{1212}=\frac{r\lambda'}{2}, \\ R_{2323} &= e^{-\lambda}r^2\sin^2\theta(e^{\lambda}-1), \quad R_{2424}=\frac{1}{2}\nu' r e^{\nu-\lambda}, \\ R_{3434} &= R_{2424}\sin^2\theta, \quad R_{1224}=0, \\ R_{1334} &= R_{1224}\sin^2\theta = 0. \end{aligned} \tag{6.10}$$

In 1948, K. R. Karmarkar derived a condition known as Karmarkar condition which allows us to embed any 4 dimensional spacetime into 5 dimension flat space. Now the non zero components of the tensor $h_{\alpha i}$ corresponding to Eq. (6.1) are h_{11}, h_{22}, h_{33}, h_{44} and $h_{14}(=h_{41})$ due to its symmetric nature and $h_{33}=h_{22}\sin^2\theta$.

Using these aforementioned components Eq. (6.10) reduced to

$$R_{1414}R_{2323} = R_{1212}R_{3434} + R_{1224}R_{1334}, \tag{6.11}$$

which is the expression for Karmarkar Condition. Later in 1981, Sharma and Pandey (Pandey and Sharma, 1981) clarified that condition (6.11) is only necessary condition for a class one spacetime to be 4 dimensional spacetime but it is not sufficient. In order to be a class one, a spacetime must satisfies Eq. (6.11) along with $R_{2323}\neq 0$.

On substituting all the values of Eq. (6.10) in Eq. (6.11), one can obtain the following differential equation,

$$\frac{2\nu''}{\nu'}+\nu' = \frac{\lambda' e^{\lambda}}{e^{\lambda}-1}, \tag{6.12}$$

with $e^{\lambda} \neq 1$. Solving Eq. (6.12) the relationship between λ and ν is obtained as,

$$e^{\nu(r)} = \left[C + D \int \sqrt{e^{\lambda(r)} - 1} dr\right]^2, \tag{6.13}$$

where C and D being non zero integrating constants. The distinctive feature of class I spacetime is condition given in Eq. (6.13) i.e. the co-dependency of the metric potentials which further provides scope to generate anisotropic model of embedding class I by specifically choosing one of the metric potentials.

According to Maurya et. al (Maurya et al., 2015b), anisotropic factor becomes,

$$\Delta(r) = \frac{\nu'(r)}{4e^{\lambda}} \left(\frac{\nu'(r)e^{\lambda}}{2rD^2} - 1\right) \left(\frac{2}{r} - \frac{\lambda'(r)}{e^{\lambda} - 1}\right). \tag{6.14}$$

Clearly, pressure anisotropy will vanish if either one of the term on RHS (right hand side) of Eq. (6.14) will become zero. Now if the term $\left(\frac{\nu'(r)e^{\lambda}}{2rD^2} - 1\right)$ vanishes then it leads to Kohler-Chao solution and if $\left(\frac{2}{r} - \frac{\lambda'(r)}{e^{\lambda}-1}\right)$ vanishes then it yields Schwarzschild interior solution.

6.3 Model I: anisotropic star with embedding class I

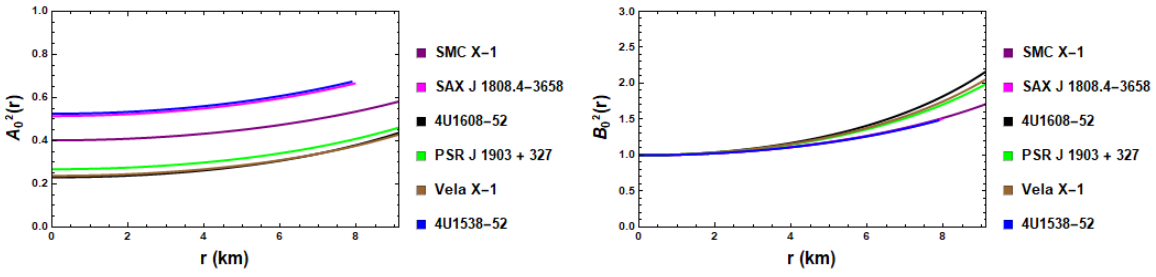

Figure 6.1: Behavior of metric potentials e^{ν} (left) and e^{λ} (right) with respect to the radial coordinate r for several compact stars corresponding to the numerical value of constants given in Table 6.1.

Maurya et al (Maurya et al., 2016) have investigated new solutions for EFEs using Karmarkar condition considering a specific form of metric potential viz. $e^{\lambda} = 1 + \frac{(a-b)r^2}{1+br^2}$, with $a \neq b$. In this paper, by utilizing the special case of this metric we have studied some new features of compact stars which was not discussed in their work. I have studied a solution of EFEs assuming a specific form of metric potential $e^{\lambda} = \frac{2(1+Ar^2)}{2-Ar^2}$, A being the constant parameter and r being the radial coordinate and hence delved into a relativistic model of an anisotropic compact star of embedding class I in static, symmetric and spherical geometry. The metric used for the present work can easily be obtained by substituting $a = A$ and $b = -\frac{A}{2}$ in the metric considered by (Maurya et al., 2016). Since Buchdahl metric (Buchdahl, 1959) is one such metric which satisfies all the criteria for physical acceptability of a stellar structure as listed by Delgaty and Lake (Delgaty and Lake, 1998), so I have considered ansatz which is a special form of Buchdahl metric. The model is shown to execute linear equation of state. The estimated mass and radius are revealed to be as similar as the observed data for the stars SMC X-1, SAX J $1808.4-3658$, 4U$1608-52$, PSR J $1903+327$, Vela X-1 and 4U$1538-52$. Additionally, we have also studied the mass-radius relationship and radius-central density relationship for the chosen metric. Comparing the obtained result for a slow rotating configuration, I have also studied the mass-moment of inertia relationship for our prescribed model.

The fundamental approach of theoretical modeling is to find the exact solutions of the system of equations represented by Eqs. (6.4)-(6.6) thus leading to determine the structure of spacetime for anisotropic fluid distribution. Clearly, if $p_r = p_t$ then the above system of equations lead to a perfect fluid like matter distribution. Now the EFEs are consist of three equations with five unknowns namely $\lambda(r)$, $\nu(r)$, $\rho(r)$, $p_r(r)$ and $p_t(r)$. However, Karmarkar condition furnish a relation between the two metric potentials $\lambda(r)$ and $\nu(r)$,

providing total four equations with five unknowns. To balance this system of equation we consider the metric potential which is a special form of Buchdahl ansatz (Buchdahl, 1959). Specifically this ansatz has been considered by Maurya et. al. (Maurya et al., 2017) and it is given as

$$e^{\lambda(r)} = \frac{2(1+Ar^2)}{2-Ar^2}, \tag{6.15}$$

where A is a non negative constant. It is also to be noted that as $A = 0$ makes the metric function flat as $e^{\lambda} = 1$, so clearly $A \neq 0$ making A strictly positive. Besides the regularity, known singularity and the fact that metric function is finite at the center of the star ($r = 0$) satisfies the basic physical requirement of a compact star thus making it a physically tenable model.

Plugging Eq. (6.15) onto Eq. (6.13) one can have,

$$e^{\nu(r)} = \left[C - \frac{D\sqrt{3(2-Ar^2)}}{\sqrt{A}}\right]^2. \tag{6.16}$$

Also the function e^{ν} needs to be finite and positive at the center. Observing Fig. 6.1 it can be concluded that e^{ν} is monotonically increasing with radial coordinate 'r' throughout the star, implying e^{ν} may produce a metric potential for a viable model as proposed by Lake (Lake, 2003). Eventually the expressions for energy density, radial pressure and transverse pressure are thus obtained as following,

$$\rho(r) = \frac{3A(3+Ar^2)}{2(1+Ar^2)^2}, \tag{6.17}$$

$$p_r(r) = \frac{A\left(3C\sqrt{\frac{A}{2-Ar^2}} - 5\sqrt{3}D\right)}{2(1+Ar^2)\left(\sqrt{3}D - C\sqrt{\frac{A}{2-Ar^2}}\right)}, \tag{6.18}$$

$$p_t(r) = \frac{A\left(3C\sqrt{\frac{A}{2-Ar^2}} - \sqrt{3}D(5+Ar^2)\right)}{2(1+Ar^2)^2\left(\sqrt{3}D - C\sqrt{\frac{A}{2-Ar^2}}\right)}. \tag{6.19}$$

The anisotropy becomes,

$$\Delta(r) = \frac{3Ar^3}{4(1+Ar^2)}. \tag{6.20}$$

Also the mass function and the compactness factor are given as,

$$m(r) = 4\pi\int_0^r \rho(\omega)\omega^2 d\omega = \frac{3Ar^3}{4(1+Ar^2)}, \tag{6.21}$$

$$u(r) = \frac{m(r)}{r} = \frac{3Ar^2}{4(1+Ar^2)}. \tag{6.22}$$

6.3.1 The boundary conditions

To analyze a compact stellar object in general theory of relativity it is important to model the spacetime insofar two distinct manifolds are unified at a common boundary. These junction conditions determine the constants for the anisotropic fluid configuration i.e. C, D and A in this case and these are given as,

(i) Continuity of the first fundamental form at the boundary i.e. the interior solution should be matched to the vacuum exterior Schwarzschild solution at the boundary $r = b$ of the star known as the radius of the star. Generally the process executed here is Darmois-Israel formalism based on Gauss-Codazzi decomposition of spacetime. It expresses the surface properties in terms of jump of extrinsic curvature across the boundary as the function of boundary's intrinsic coordinates (Mansouri and Khaorrami, 1966). Israel (Israel, 1966) formulated his work considering the idea that the 4 dimensional coordinates may be chosen independently on both side of the boundary. In his innovating work Darmois (Darmois, 1927) first calculated that the boundary of the structure is to be considered as the periphery

of two different manifolds glued together at this boundary.

(ii) Continuity of the second fundamental form at the boundary i.e. the radial pressure must vanish at the boundary. Mathematically $p_r(r=b)=0$ (Misner and Sharpe, 1964).

The exterior spacetime on Schwarzschild metric is expressed as,

$$ds^2=\left(1-\frac{2M}{r}\right)dt^2-\left(1-\frac{2M}{r}\right)^{-1}dr^2-r^2(d\theta^2+\sin^2\theta d\phi^2), \tag{6.23}$$

at $r>2M$, M being stellar mass. The advancement of metric function over the limiting surface i.e. at the boundary yields,

$$e^{\nu(b)}=\left(1-\frac{2M}{r}\right)\Bigg|_b, \qquad e^{-\lambda(b)}=\left(1-\frac{2M}{r}\right)\Bigg|_b. \tag{6.24}$$

Utilizing above equations with Eqs. (6.16) and (6.15) respectively we get,

$$\left(C-\frac{D\sqrt{3(2-Ab^2)}}{\sqrt{A}}\right)^2 = 1-\frac{2M}{b}, \tag{6.25}$$

$$\frac{2-Ab^2}{2(1+Ab^2)} = 1-\frac{2M}{b}. \tag{6.26}$$

Again the later condition $p_r(r=b)=0$ gives,

$$A\left(3C\sqrt{\frac{A}{2-Ab^2}}-5\sqrt{3}D\right)=0, \tag{6.27}$$

which prescribes a limitation on the model parameter A which can be further utilize to find the radius of the compact star model. Furthermore Eqs. (6.25)-(6.27) generate the

mathematical expressions of model parameter as,

$$\begin{aligned} A &= \frac{4M}{b^2(3b-4M)}, \\ C &= \frac{5}{2}\sqrt{1-\frac{2M}{b}}, \\ D &= \sqrt{\frac{M}{2b^3}}. \end{aligned} \tag{6.28}$$

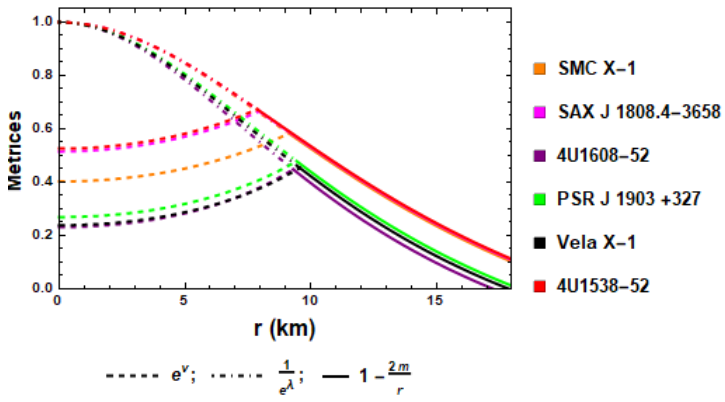

Figure 6.2: Junction conditions are satisfied at the stellar boundary for each of the compact stars.

In Fig. 6.2, I have illustrated the junction condition of the interior metric potentials with the exterior Schwarzschild metric at the boundary for each stars and it depicts the smooth matching of the boundary conditions.

6.3.2 Analysis of the features of the model

This section contains the inspection of various properties of the interior of the stellar structure. The significant features such as regularity, causality and stability criterion are discussed using numerical calculations and generating graphs. The spectrum of discussions revolve around the pulsars SMC X-1 (Mass = 1.29 $M\odot$, radius $=$ 9.13 km (Rahaman et al.,

Pulsar	Mass ($M_\odot$)	Radius (km)	A	C	D
SMC X-1	1.29	9.13	0.00461632	$\pm$1.90917	$\pm$0.0353565
SAX J $1808.4-3658$	0.9	7.951	0.00452972	$\pm$2.04034	$\pm$0.0363387
$4U1608-52$	1.74	9.3	0.00673108	$\pm$1.67344	$\pm$0.0399421
PSR J $1903+327$	1.667	9.438	0.00597525	$\pm$1.73016	$\pm$0.038241
Vela X-1	1.77	9.56	0.00626551	$\pm$1.68415	$\pm$0.0386528
$4U1538-52$	0.87	7.866	0.00449277	$\pm$2.05201	$\pm$0.0363086

Table 6.1: Values of the model parameters for different compact stellar objects.

2014)), SAX J $1808.4-3658$ (Mass $= 0.9\ M\odot$, radius $= 7.951$ km (Elebert et al, 2009)), $4U1608-52$ (Mass $= 1.74\ M\odot$, radius $= 9.3$ km (Güver et al., 2010)), PSR J$1903+327$ (Mass $= 1.667\ M\odot$, radius $= 9.438$ km (Freire et al, 2011)), Vela X-1 (Mass $= 1.77\ M\odot$, radius $= 9.56$ km (Rawl et al., 2011)) and $4U1538-52$ (Mass $= 0.87\ M\odot$, radius $= 7.866$ km (Rawl et al., 2011)) .

6.3.2.1 Regularity condition

To be a physically viable model of an anisotropic compact star, the model ought to satisfy some regularity conditions throughout the interior of the structure (Delgaty and Lake, 1998; Herrera and Santos, 1997; Leibovitz, 1969; Pant, 2011; Pant et al., 2010).

(i) The spacetime and hence the solutions need to be free from any singularity i.e. the energy density ρ and pressures $(p_r,\ p_t)$ should be finite and positive throughout the star. Also $e^{\lambda(r)}$ and $e^{\nu(r)}$ should be non zero and finite. Here $e^{\lambda(r)}\big|_{r=0} = 1$ and $e^{\nu(r)}\big|_{r=0} = C^2$ i.e. both are non zero and finite at the center. Also Fig. 6.1 shows that the metric potentials are positive throughout the stellar structure.

(ii) Energy density and pressures must be maximum at the center and monotonically decreasing towards the boundary of the star. Fig. 6.3 depicts that both the pressures are monotonically decreasing function of r with a maximum value at the center and radial pressure vanishes at the boundary for each of the stars. Moreover from Fig. 6.4, it can

be seen that energy density is monotonically decreasing in nature and the maximum value can be obtained at the center of the compact stellar model. Analytically, $\frac{d\rho}{dr}\big|_{r=0} = 0$ and $\frac{d^2\rho}{dr^2}\big|_{r=0} < 0$. Also Fig. 6.4 also represents the positive nature of anisotropy inside the stellar interior, which is an important feature for a stable compact stellar model as suggested by Gokhroo and Mehra (Gokhroo and Mehra, 1994).

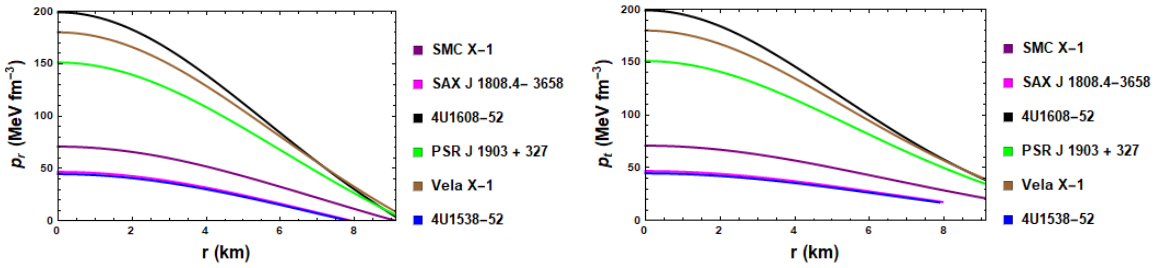

Figure 6.3: Variation of the radial (left) and the transverse (right) pressures against the radial coordinate r for different compact stars.

Central density, central radial and transverse pressures are given as,

$$\rho(0) = \frac{9A}{2}, \tag{6.29}$$

$$p_r(0) = p_t(0) = -\frac{A\left(5\sqrt{3}D - 3C\sqrt{\frac{A}{2}}\right)}{2\left(\sqrt{3}D - C\sqrt{\frac{A}{2}}\right)}. \tag{6.30}$$

Since A is positive so central density is always positive. Also, equality of both the pressures at the center indicates the absence of anisotropy at $r = 0$.

To configure a stable model it is require to satisfy Zeldovich's Condition for pressure and density which states that $\frac{p_r}{\rho}$ must be ≤ 1 at the center (Zeldovich and Novikov, 1972).

Therefore,

$$-\frac{5\sqrt{3}D-3C\sqrt{\frac{A}{2}}}{9\left(\sqrt{3}D-C\sqrt{\frac{A}{2}}\right)}\leq 1,$$
$$or,\ \frac{D}{C}\geq\frac{\sqrt{6A}}{7}. \tag{6.31}$$

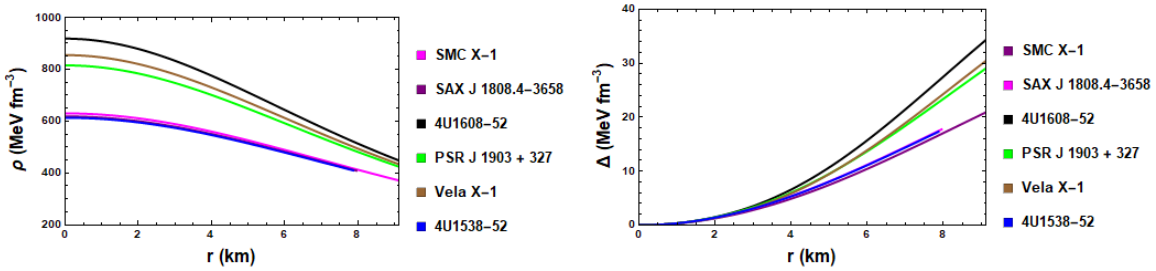

Figure 6.4: Behavior of the energy density (left) and anisotropy (right) with respect to the radial coordinate r for various compact stars.

Again the gradient of density and pressures can be expressed as,

$$\frac{d\rho}{dr} = -\frac{3A^2r(5+Ar^2)}{(1+Ar^2)^3}, \tag{6.32}$$

$$\frac{dp_r}{dr} = \frac{A^2\left(\sqrt{\frac{Ar^2}{2-Ar^2}}\left(6AC^2-3A^2C^2r+15D^2(2-Ar^2)\right)-\sqrt{3}ACDr(17+7Ar^2)\right)}{\sqrt{\frac{A}{2-Ar^2}}(2-Ar^2)^2(1+Ar^2)^2\left(\sqrt{3}D-C\sqrt{\frac{A}{2-Ar^2}}\right)^2}, \tag{6.33}$$

$$\frac{dp_t}{dr} = \frac{A^2\left(\sqrt{\frac{Ar^2}{2-Ar^2}}\left(12AC^2(2-Ar^2)+6D^2(2-Ar^2)(9+Ar^2)\right)\right)}{2\sqrt{\frac{A}{2-Ar^2}}(2-Ar^2)^2(1+Ar^2)^3\left(\sqrt{3}D-C\sqrt{\frac{A}{2-Ar^2}}\right)^2} + \frac{\sqrt{3}A^3CDr(A^2r^4+23Ar^2-62)}{2\sqrt{\frac{A}{2-Ar^2}}(2-Ar^2)^2(1+Ar^2)^3\left(\sqrt{3}D-C\sqrt{\frac{A}{2-Ar^2}}\right)^2}. \tag{6.34}$$

For a stable compact stellar model $\frac{dp_r}{dr}\big|_{r=0} = \frac{dp_t}{dr}\big|_{r=0} = 0$ and $\frac{d^2p_r}{dr^2}\big|_{r=0} < 0$ and

$\frac{d^2p_t}{dr}\big|_{r=0} < 0$ need to satisfy inside the star i.e. gradient of density and pressures are negative within $0 < r < b$. The negative nature of the gradient of density and pressures are shown graphically in Fig. 6.5.

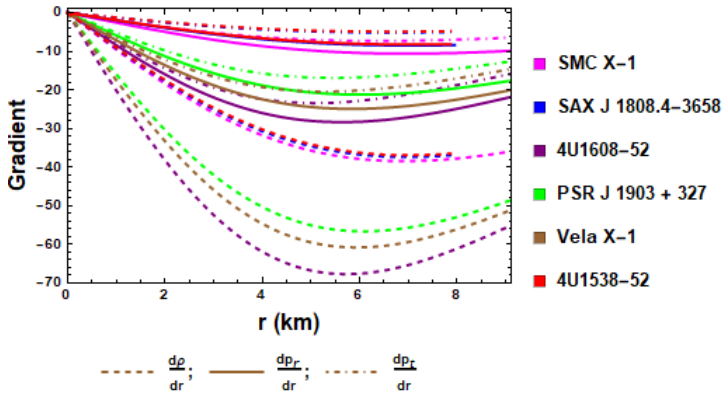

Figure 6.5: Variation of the energy density gradient and the pressures gradient against the radial coordinate r for different compact stars.

Also $p_r(0) = p_t(0) \geq 0$ gives the relation

$$\frac{\sqrt{3A}}{5\sqrt{2}} \leq \frac{D}{C} \leq \sqrt{\frac{A}{6}}. \tag{6.35}$$

Combining Eqs. (6.31) and (6.35) one can get the bounds on the model parameters as

$$\frac{\sqrt{6A}}{7} \leq \frac{D}{C} \leq \sqrt{\frac{A}{6}}. \tag{6.36}$$

6.3.2.2 Kretschmann scalar

In General Relativity, scalars are used to look for any singularity present in the metric. The simplest is the Ricci Scalar but since for vacuum solution, Ricci scalar is zero everywhere so to find any physical singularity present in the spacetime Kretschmann Scalar is used.

The approach is quite straightforward. For any line element,

$$ds^2 = e^{2\mu}dt^2 - e^{2\kappa}dr^2 - e^{2\zeta}(d\theta^2 + \sin^2\theta d\phi^2), \tag{6.37}$$

Kretschmann Scalar is calculated as,

$$K = 4K_1^2 + 8K_2^2 + 8K_3^2 + 4K_4^2, \tag{6.38}$$

where,

$$\begin{aligned}
K_1 &= e^{-(\mu+\kappa)}\frac{d}{dr}\left(\frac{d\mu}{dr}e^{\mu-\kappa}\right), \\
K_2 &= e^{-2\kappa}\frac{d\zeta}{dr}\frac{d\mu}{dr}, \\
K_3 &= e^{-(\kappa+\zeta)}\frac{d}{dr}\left(e^{\zeta-\kappa}\frac{d\zeta}{dr}\right), \\
K_4 &= -e^{-2\zeta} + e^{-2\kappa}\left(\frac{d\zeta}{dr}\right).
\end{aligned}$$

Computing all the components we have obtained Kretschmann Scalar for various compact stellar objects and it is shown graphically in Fig. 6.6. The divergence of Kretschmann Scalar at $r = 0$ depicts that there is no singularity at the center of the compact stellar model, although there is a singularity at $r = 1$.

6.3.2.3 The Tolman-Oppenheimer-Volkoff or TOV equation

To examine the stability of the model it is important to examine the equilibrium condition of the model using TOV equation. This stability equation given by Tolman (Tolman, 1939) and Oppenheimer and Volkoff (Oppenheimer and Volkoff, 1939) symbolizes the internal structure of a spherically symmetric static compact stellar object which is in equilibrium

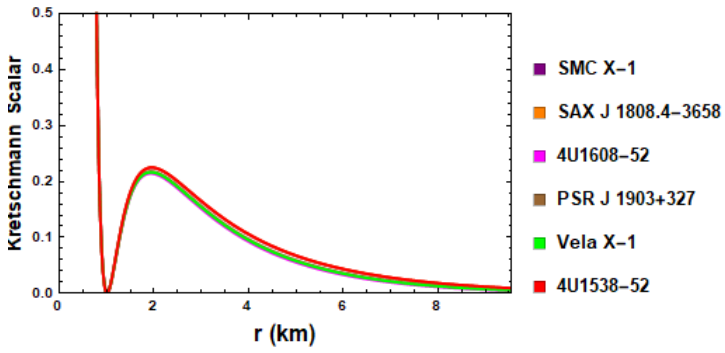

Figure 6.6: Profile of Kretschmann scalar against the radial coordinate r for different compact stars.

in presence of anisotropy. The generalized TOV equation can be expressed as (Ponce de León, 1993; Varela et al., 2010),

$$-\frac{1}{r}\left(\rho(r)+p_r(r)\right)\frac{d\nu}{dr}-\frac{dp_r(r)}{dr}+\frac{2(p_r-p_t)}{r}=0.$$

It can also be written as,

$$-\frac{M_g\left(\rho(r)+p_r(r)\right)}{r^2}e^{(\lambda-\nu)/2}-\frac{dp_r(r)}{dr}+\frac{2\Delta(r)}{r}=0, \tag{6.39}$$

where $M_g(r)$ is the effective gravitational mass inside a sphere of radius 'r' and it can be derived using Tolman-Whittaker mass formula is given by,

$$M_g(r)=\frac{1}{2}r^2e^{\frac{\nu-\lambda}{2}}\frac{d\nu}{dr}. \tag{6.40}$$

The TOV equation can be expressed in a simple form to describe the equilibrium condition by defining the forces as gravitational forces(F_g), hydrostatic forces(F_h) and

anisotropic forces(F_a). Thus,

$$F_g(r) + F_h(r) + F_a(r) = 0, \tag{6.41}$$

where,

$$\begin{aligned} \text{gravitational force, } F_g(r) &= -\frac{\nu'\left(\rho(r)+p_r(r)\right)}{2}, \\ \text{hydrostatic force, } F_h(r) &= -\frac{dp_r(r)}{dr}, \\ \text{anisotropic force, } F_a(r) &= \frac{2\Delta(r)}{r}. \end{aligned} \tag{6.42}$$

For the prescribed model the expressions for these forces become,

$$\begin{aligned} F_g(r) &= \frac{A^3Dr\left(3C\sqrt{\frac{A}{2-Ar^2}}-\sqrt{3}D(2-Ar^2)\right)}{\sqrt{\frac{A(2-Ar^2)}{3}}(1+Ar^2)^2\left(\sqrt{3}D-C\sqrt{\frac{A}{2-Ar^2}}\right)\left(AC-\sqrt{3}D\sqrt{A(2-Ar^2)}\right)}, \\ F_h(r) &= \frac{A^2r\left(\sqrt{3}ACD(17-7Ar^2)-3AC^2\sqrt{\frac{A}{2-Ar^2}}(2-Ar^2)-15D^2\sqrt{A}(2-Ar^2)^{\frac{3}{2}}\right)}{\sqrt{A}(2-Ar^2)^{\frac{3}{2}}(1+Ar^2)^2\left(\sqrt{3}D-C\sqrt{\frac{A}{2-Ar^2}}\right)^2}, \\ F_a(r) &= \frac{A^2r(4\sqrt{3}D-3C\sqrt{\frac{A}{2-Ar^2}})}{(1+Ar^2)^2(\sqrt{3}D-C\sqrt{\frac{A}{2-Ar^2}})}. \end{aligned} \tag{6.43}$$

Equations alluded in Eq. (6.43) are examined graphically in the Fig. 6.7. It can clearly be seen that negative gravitational force is balanced by the amalgamation of hydrostatic and anisotropic forces to keep the model in equilibrium.

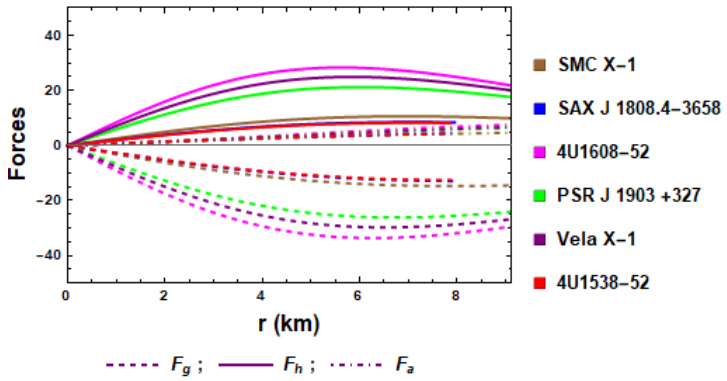

Figure 6.7: Variation of different forces against the radial coordinate r for different compact stars.

6.3.2.4 Energy condition

The acceptability of our model depends on fulfillment of some energy conditions namely, Null energy condition (NEC), Weak energy condition (WEC), Strong energy condition (SEC) and Dominant Energy Condition (DEC). All these energy conditions are some inequalities corresponding to stress-energy tensor and are defined as,

$$\begin{aligned} NEC_r &: \rho(r)+p_r(r)\geq 0, \quad NEC_t : \rho(r)+p_t(r)\geq 0. \\ WEC_r &: \rho(r)\geq 0, \ \ \rho(r)+p_r(r)\geq 0, \quad WEC_t : \rho(r)\geq 0, \ \ \rho(r)+p_t(r)\geq 0. \\ SEC &: \rho(r)+p_r(r)+2p_t(r)\geq 0. \\ DEC &: \rho(r)\geq p_r(r),\ p_t(r). \end{aligned} \tag{6.44}$$

Analytically NEC suggests that an eyewitness crossing a null bend will quantify the surrounding energy density to be non-negative. WEC implies that energy density estimated by an eyewitness traversing a time like bend is positive. SEC implies that the trace of tidal tensor estimated by the eyewitness is consistently positive (Maurya et al., 2020b). DEC

essentially indicates that to any observer the local energy density appears non-negative and local energy flow vector is non-spacelike (Hawking and Ellis, 1973).

I have discussed the energy conditions on our model graphically in Fig. 6.8, by plotting LHS (left hand side) of above inequalities.

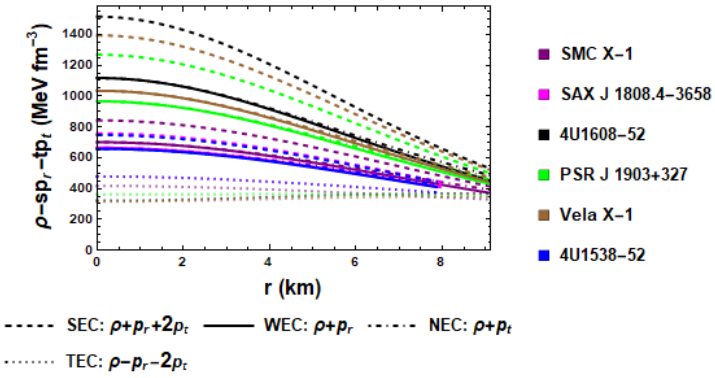

Figure 6.8: Behavior of different energy conditions against the radial coordinate r for different compact stars. The nature of Trace Energy Condition (TEC): $\rho - p_r - 2p_t$ is also plotted against the radial coordinate r for different compact stars.

Also for distinguishing configuration one can develop some limitation on our model parameter from inequalities in Eq. (6.44). Specifically I have obtained the following relations for the center ($r = 0$) of the stellar structure,

$$
\begin{aligned}
NEC_r &: \rho(0) + p_r(0) \geq 0, \quad NEC_t : \rho(0) + p_t(0) \geq 0. \\
WEC_r &: \rho(0) \geq 0, \;\; \rho(0) + p_r(0) \geq 0. \\
WEC_t &: \rho(0) \geq 0, \;\; \rho(0) + p_t(0) \geq 0. \\
SEC &: \rho(0) + p_r(0) + 2p_t(0) \geq 0. \\
DEC &: \rho(0) \geq p_r(0), \; p_t(0)
\end{aligned}
$$

$$\text{or} \quad \frac{9A}{2} \geq \frac{A\left(5\sqrt{3}D - C\sqrt{\frac{A}{2}}\right)}{2\left(\sqrt{3}D - C\sqrt{\frac{A}{2}}\right)}$$
$$\text{or} \quad \frac{D}{C} \geq \sqrt{\frac{2A}{3}}. \tag{6.45}$$

6.3.2.5 Causality condition

To study the stability of an anisotropic fluid stellar, L. Herrera (Herrera, 1992) proposed the *cracking method* or overturning method which states that the velocity of sound speeds (radial and transverse) should never exceed the speed of light inside the star i.e. $v^2 = \frac{dp}{d\rho} < 1$ should be maintained inside the stellar, taking the velocity of light $c = 1$. Also Le Chatelier's principle allows the matter of the star to satisfy $\frac{dp}{d\rho} \geq 0$ to be a stable configuration (Glendenning, 1997). The sound velocity inside the compact star is expressed by,

$$v_r(r) = \sqrt{\frac{dp_r(r)}{d\rho(r)}}, \quad v_t(r) = \sqrt{\frac{dp_t(r)}{d\rho(r)}}. \tag{6.46}$$

Combining the above conditions the causality condition becomes $0 \leq v_r(r),\ v_t(r) < 1$. Fig. 6.9 supports the fulfillment of causality condition of the prescribed model. Now using

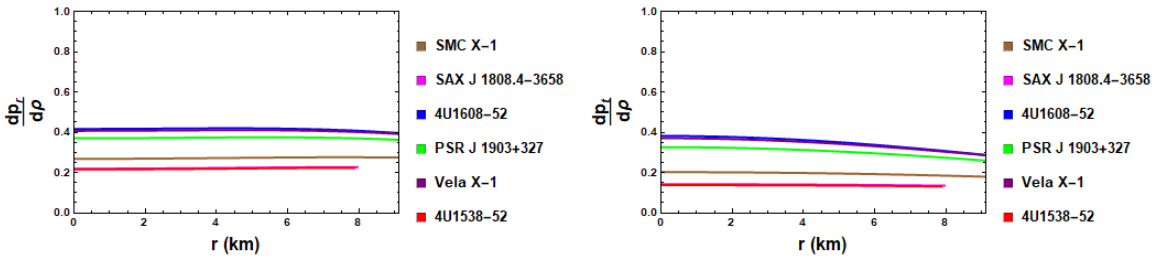

Figure 6.9: Variation of the radial (left) and the transverse (right) sound speeds against the radial coordinate r for different compact stars.

the concept of cracking, Abreu et al. (Abreu et al., 2007) provided the stability conditions with respect to the stability factor $(= \{v_t(r)\}^2 - \{v_r(r)\}^2)$ for anisotropic fluid model. The

conditions are **:** **(i)** The region is potentially stable if $-1 < \{v_t(r)\}^2 - \{v_r(r)\}^2 \leq 0$ and **(ii)** The region is potentially unstable if $0 < \{v_t(r)\}^2 - \{v_r(r)\}^2 < 1$.

The expressions for velocity of sound speeds are given below,

$$\begin{aligned} v_r^2 &= -\frac{\sqrt{\frac{A}{2-Ar^2}}(2-Ar^2)(1+Ar^2)(3AC^2+30D^2-15AD^2r^2)}{3\sqrt{\frac{A}{2-Ar^2}}(2-Ar^2)^2(5+Ar^2)\left(\sqrt{3}D-C\sqrt{\frac{A}{2-Ar^2}}\right)^2} \\ &+ \frac{\sqrt{3}ACD(1+Ar^2)(17-7Ar^2)}{3\sqrt{\frac{A}{2-Ar^2}}(2-Ar^2)^2(5+Ar^2)(\sqrt{3}D-C\sqrt{\frac{A}{2-Ar^2}})^2}, \end{aligned} \tag{6.47}$$

$$\begin{aligned} v_t^2 &= -\frac{\sqrt{\frac{A}{2-Ar^2}}\,(12AC^2(2-Ar^2)+6D^2(2-Ar^2)^2(9+Ar^2))}{6\sqrt{\frac{A}{2-Ar^2}}(2-Ar^2)^2(5+Ar^2)(\sqrt{3}D-C\sqrt{\frac{A}{2-Ar^2}})^2} \\ &- \frac{\sqrt{3}ACD(A^2r^4+23Ar^2-62)}{6\sqrt{\frac{A}{2-Ar^2}}(2-Ar^2)^2(5+Ar^2)(\sqrt{3}D-C\sqrt{\frac{A}{2-Ar^2}})^2}. \end{aligned} \tag{6.48}$$

Clearly the conditions $|{v_r}^2 - {v_t}^2| < 1$ and $-1 < \{v_t(r)\}^2 - \{v_r(r)\}^2 \leq 0$ are satisfied as depicted in Fig. 6.10.

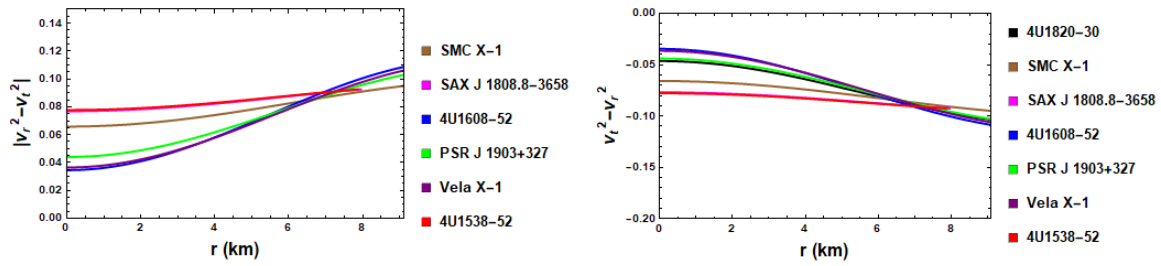

Figure 6.10: Variation of the absolute difference (left) and variation of the difference of the sound speeds (right) with the radial coordinate r for different compact stars.

6.3.2.6 Adiabatic Index

Stability of anisotropic compact star depends on the adiabatic index which is essentially the ratio of specific heat at constant pressure to the specific heat at constant volume. The adiabatic index determines the stability and the stiffness of the equation of state and it is defined as,

$$\Gamma(r) = \frac{\rho(r) + p(r)}{p(r)} \frac{dp(r)}{d\rho(r)}. \tag{6.49}$$

For the Newtonian limit, any stellar configuration will maintain its stability if adiabatic gravitational collapse $\Gamma(r) > 4/3$ (Heintzmann and Hillebrandt, 1975) and stellar structure will become catastrophic if $< 4/3$ (Bondi, 1964). Also, Chan et al. (Chan et al., 1993) have suggested that this condition changes depending on the nature of anisotropy for a relativistic fluid sphere. Additionally, Knutsen (Knutsen, 1988) showed that adiabatic index Γ is more than 1 if the ratio of density and pressure is monotonically decreasing outwards.

For the present solution, the value of adiabatic indices $\Gamma_r(r)$ and $\Gamma_t(r)$ are more than 4/3 throughout the outer region of a compact star, as evident from Fig. 6.11.

6.3.2.7 Harrison-Zeldovich-Novikov criterion

Since compact star models that are only in stable equilibrium, are of astrophysical interest so any acceptable model should satisfy the static stability criterion. The stability condition for a compact star with respect to 'r' requires the calculation of eigen-frequency of the fundamental mode (Haensel et al., 2007) of radial pulsation without any nodes as described by Chandrasekhar (Chandrasekhar, 1964b). The complexity of stability criterion was later simplified by Harrison-Zeldovich-Novikov (Harrison et al., 1965; Zeldovich and Novikov,

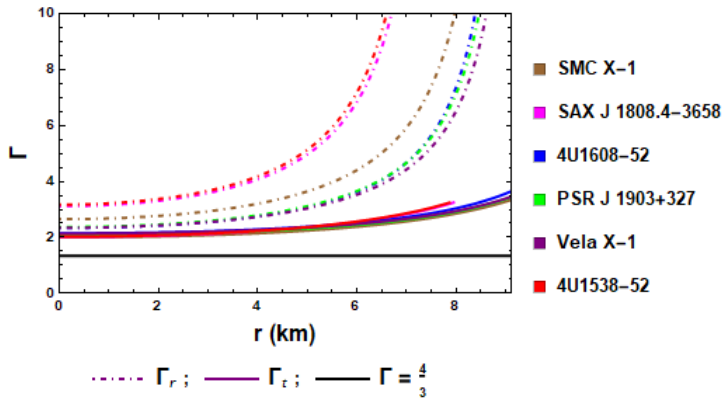

Figure 6.11: Variation of the adiabatic indices against the radial coordinate r for different compact stars.

1972). As per their suggestions, for stability of a compact stellar object the mass should also increase with the increase of the central density $\rho(0)$ i.e. $\frac{dM(\rho(0))}{d\rho(0)} > 0$ to be a stable structure. The Harrison-Zeldovich-Noikov criterion is a necessary condition, it is not an sufficient one. We write the mass function as function of central density as following,

$$\begin{aligned} M(\rho(0)) &= \frac{3b^3\rho(0)}{2\left(2\rho(0)b^2+9\right)}, \\ \frac{dM(\rho(0))}{d\rho(0)} &= \frac{27b^3}{2\left(2\rho(0)b^2+9\right)^2}. \end{aligned} \tag{6.50}$$

Clearly the fulfillment of Harrison-Zeldovich-Novikov conditions are shown graphically for several stars as shown in Fig. 6.12.

6.3.2.8 Buchdahl limit

The mass function of the proposed model is defined in Eq. (6.21) as $m(r) = \frac{3Ar^3}{4(1+Ar^2)}$ which is directly proportional to r i.e. $\lim_{r\to 0} m(r) = 0$ implying the regularity of the mass function at the center of the star. Fig. 6.13 graphically depicts the mass functions of

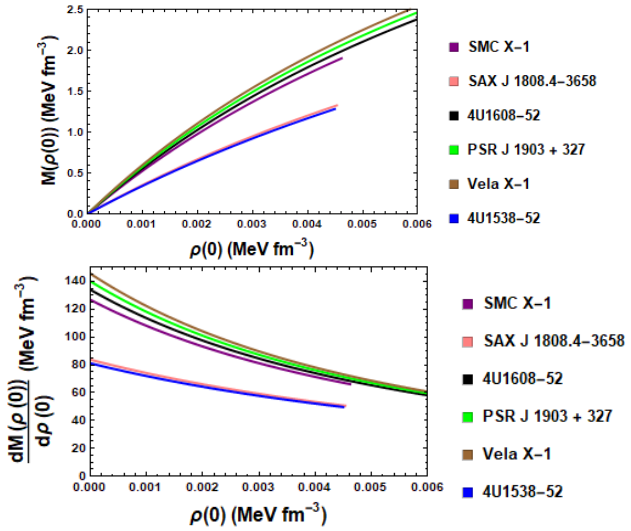

Figure 6.12: Variation of M and $\frac{dM}{d\rho(0)}$ with respect to the central density $\rho(0)$ for different compact stars.

various compact stellar objects.

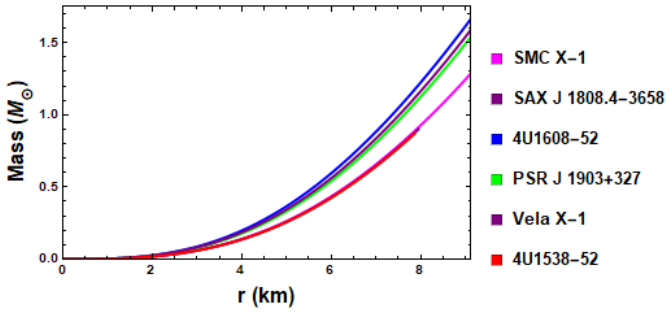

Figure 6.13: Variation of the mass function against the radial coordinate r for different compact stars. Here the mass function is shown to be monotonically increasing function of r.

For spherically symmetric configuration, the ratio of mass to the radius of a compact stellar object is supposed to fall within the limit $\frac{2M}{b} < \frac{8}{9}$ (considering $8\pi G = c = 1$) as suggested by Buchdahl (Buchdahl, 1959). This condition, named after Buchdahl, is clearly satisfied for our model as shown in Table 6.2.

6.3.2.9 Mass-radius relationship

For dynamical stability opposing gravitational collapse into a black hole, the maximum mass of any model needs to be considered to separate compact star and black holes. In fact, any observed compact stellar objects can be identified as black holes if the maximum mass of the compact stellar object exceeds the allowable maximum mass for a stable compact star model (Hendi et al., 2017; Shapiro and Teukolsky, 1983). To study the mass-radius relation and to calculate maximum mass we have plotted the $(M-b)$ graph in Fig. 6.14 considering the surface density $\rho(b) = 9.5 \times 10^{14}\ gm\ cm^{-3}$. I have considered surface density which is roughly similar to that chosen by some researchers (Sharma and Maharaj, 2007; Thirukkanesh and Maharaj, 2008) to study the mass-radius relationship of a compact stellar model.

Fig. 6.14 depicts the $(M-b)$ graph for the prescribed model. The maximum mass for the

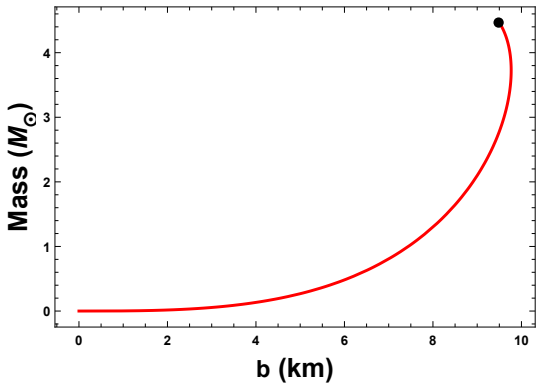

Figure 6.14: $(M-b)$ plot for the surface density $\rho(b) = 9.5 \times 10^{14}\ gm\ cm^{-3}$. The solid circle denotes the maximum allowable mass of the model.

model is calculated to be $4.632\ M_\odot$ with the radius 9.254 km. Though our model exceeds the Rhoades and Ruffini limit ($\approx 3.2\ M_\odot$) (Rhoades and Ruffini, 1974) of maximum mass for a neutron star, it remains within the prescribed range for the spheres in general rela-

tivity with uniform density ($5.2\ M_{\odot}$) as suggested by Shapiro and Teukolsky (Shapiro and Teukolsky, 1983).

I have also predicted masses and radii for several compact stars as given in Table 6.2. I have computed the masses and radii from EoSs considering EoS parameter $\omega = 0.003$ and it can clearly be seen that predicted masses and radii are almost similar to that of observed values.

Pulsar Name	Observed Mass ($M_{\odot}$)	Observed Radius (km)	Predicted Mass ($M_{\odot}$)	Predicted Radius (km)	Compactness Factor
SMC X-1	1.29	9.13	1.2513	8.9873	0.1392
SAX J $1808.4-3658$	0.9	7.951	0.8460	8.9168	0.0949
$4U1608-52$	1.74	9.3	1.7242	7.9172	0.2178
PSR J $1903+327$	1.667	9.438	1.6387	9.2310	0.1775
Vela X-1	1.77	9.56	1.7435	9.3755	0.1859
$4U1538-52$	0.87	7.866	0.8273	7.7138	0.1072

Table 6.2: Observed and predicted masses, radii and compactness factors for different compact stellar objects.

6.3.2.10 Compactness and gravitational redshifts

The dimensionless ratio $\frac{m(r)}{r}$ is known as the compactification factor $u(r)$ of a compact star. The expressions for compactness and gravitational redshifts are given as following,

$$\begin{aligned} u(r) &= \frac{m(r)}{r} = \frac{3Ar^2}{4(1+Ar^2)}, \\ z(r) &= \frac{1-(1-2u)^{\frac{1}{2}}}{(1-2u)^{\frac{1}{2}}} = \sqrt{\frac{2(1+Ar^2)}{2-Ar^2}} - 1. \end{aligned} \tag{6.51}$$

The compactness for our model is depicted in Fig. 6.15 which indicates the increasing nature of the compactification factor with respect to radial coordinate 'r'. From Table. 6.2 it can be seen that the model allows compactness within the range $(\frac{1}{4}, \frac{1}{2})$ as prescribed

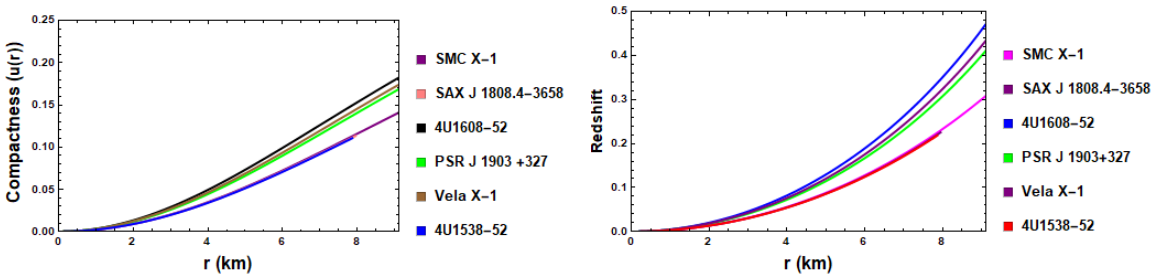

Figure 6.15: Variation of the compactness (left) and the gravitational redshift (right) with the radial coordinate r for different compact stars.

in (Jotania and Tikekar, 2006).

The gravitational redshifts $z(r)$ is depicted graphically in Fig. 6.15 which shows the increasing nature of gravitational redshifts with the radial coordinate. Studies by several authors have allowed us to specify an upper bound on the surface redshifts. In absence of cosmological constant, $z(r) \leq 2$ holds for an isotropic star as proposed by Barraco and Hamity (Barraco and Hamity, 2002). Whereas the presence of cosmological constant pushes the upper bound for an anisotropic star a bit higher, $z(r) \leq 5$ (Böhmer and Harko, 2006). Though the maximum acceptable limit for the surface redshift of a compact star is 5.211 (Ivanov, 2002), the model presented in this paper satisfies the range $z(r) \leq 1$ as predicted by Hewish et. al (Hewish et al., 1968) as can be seen in Table 6.3.

6.3.2.11 Equation of State

One of the significant features of a compact star is the description of its equation of state (EoS) i.e. the relation of the pressure with the energy density for barotropic EoS which then eventually designs the mass-radius relation. The form of the barotropic equation of state can be linear, quadratic, polytropic or some other dependence. Clearly different EoSs lead to different $(M-b)$ relations. Several authors have suggested that EoS can be estimated in the form of $p = p(\rho)$ i.e. pressure p can be written as the linear function of energy density

ρ in the presence of higher density to elucidate the structural properties of a compact stellar object (Dey et al., 1998; Frieman and Olinto, 1989; Haensel and Zdunik, 1989; Harko and Cheng, 2002; Maurya et al., 2019a; Prakash et al., 1990; Zdunik, 2000). I have obtained the exact similar observation as that of (Gondek-Rosinska et al., 2000; Maurya et al., 2019a,b).

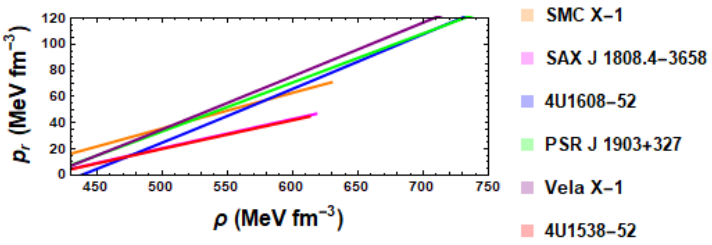

Figure 6.16: Variation of the radial pressure with the density for different compact star corresponding to the numerical value of constants given in Table 5.1.

For stable configuration the equation of state parameter defined as $\omega_r(r) = \frac{p_r}{\rho}$ and $\omega_t(r) = \frac{p_t}{\rho}$ should belong to $(0, 1)$ (Rahaman et al., 2010) otherwise known as exotic configuration. The radial EoS for various compact star are described graphically in Fig. 6.16, which shows linear relationship.

I also have calculated the best fit for each EoSs for each stars by using least squares method (Gondek-Rosinska et al., 2000; Zdunik, 2000). Fig. 6.17 describes graphically best fit for each EoSs. The approximation for the best fitted relation for each stars are given

as,

$$
\begin{aligned}
SMC\ X-1 \quad &: \quad p_r = 0.27393\,\rho - 101.376, \\
SAX\ J\ 1808.4-3658 \quad &: \quad p_r = 0.223828\,\rho - 91.344, \\
4U1608-52 \quad &: \quad p_r = 0.416461\,\rho - 183.463, \\
PSR\ J\ 1903+327 \quad &: \quad p_r = 0.37333\,\rho - 153.083, \\
Vela\ X-1 \quad &: \quad p_r = 0.408083\,\rho - 168.934, \\
4U1538-52 \quad &: \quad p_r = 0.220122\,\rho - 90.0515.
\end{aligned}
$$

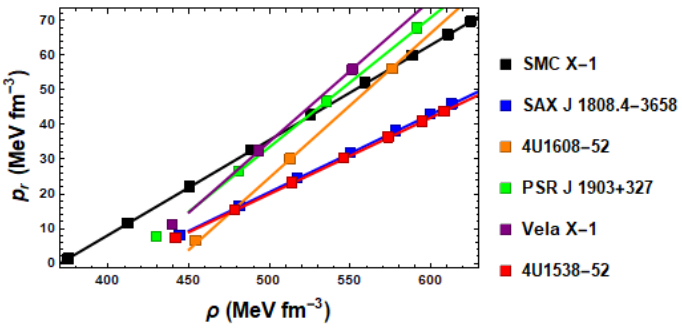

Figure 6.17: Best fit for EoSs for each of the compact stars.

6.3.2.12 Moment of inertia and time period

The study of moment of inertia plays a very important role in modeling of compact stellar objects as it allows us to test the stiffness of EoS. The empirical formula for the moment of inertia I transforms a static system to rotating system as suggested by Bejger-Haensel (Bejger and Haensel, 2002) and it is given by,

$$
I = \frac{2}{5}(1+x)Mb^2, \tag{6.52}
$$

where the parameter x is defined as $x = (M/M_{\odot})(km/b)$. Here the maximum mass of uniformly slow rotating configuration gives the approximate moment of inertia. The nature of moment of inertia I with respect to mass M is depicted in Fig. 6.18.

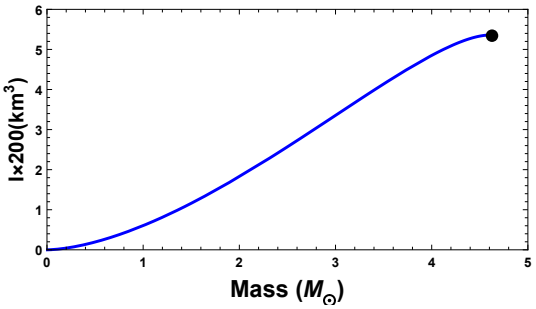

Figure 6.18: Variation of the moment of inertia with respect to the mass. The solid circle denotes the moment of inertia for the maximum mass for the model.

It can be seen that inertia I is an increasing as the increase of mass and it attains the maximum value for the mass $4.627\ M_{\odot}$ before declining rapidly. Considering the surface density $\rho(b) = 9.5 \times 10^{14}\ gm\ cm^{-3}$, I have calculated the I_{max} to be $1773.6\ km^3$. Comparing the masses of the model star on the Figs. 6.14 and 6.18, it can be seen that the mass corresponding to I_{max} is approximately lower by 0.11%.

This decline of mass indicate the softening of the EoSs without any strong high-density due to hyperonization or phase transition to an exotic state (Bejger et al., 2005).

For any non-rotating structure, minimum time-period can be estimated as below provided the EoS obey the sound speeds,

$$\tau \approx 0.82\sqrt{\left(\frac{M\odot}{M}\right)}\left(\frac{b}{10\ km}\right)^{\frac{3}{2}} ms. \tag{6.53}$$

Fig. 6.19 depicts the variation of time period with the mass of the model and the maximum time period is obtained to be $1.577\ ms$.

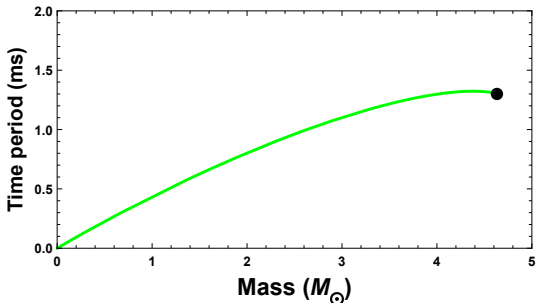

Figure 6.19: Variation of the time period of rotation with the mass. The solid circle denotes the time period corresponding to the maximum mass of the model.

6.3.2.13 Mass-central density relationship

It is evident that the models of cold static compact star represents one parameter family i.e. they can be labeled by using central density or by using central pressure (Haensel, 2008). Fig. 6.20 portrays the profile of mass against the central density and it can be observed that with the increase of the mass of the model, the central density also increases. Moreover, maximum mass is found to be $4.461\ M_\odot$ corresponding to the central density $32.11 \times 10^{18}\ kg/m^3$.

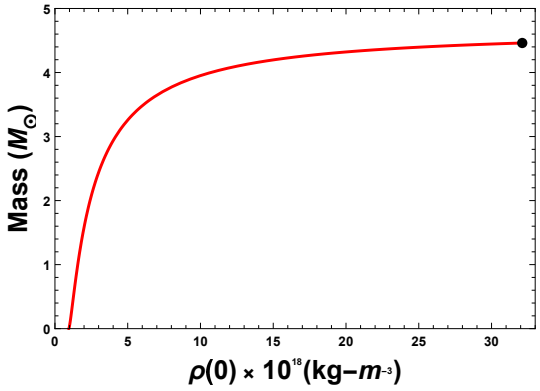

Figure 6.20: Variation of the central density with the mass.

6.3.2.14 Radius-central density relationship

The internal structure of any compact stellar model can be studied from its relationship of the radius with any of the matter variable. One such physical test is to study the variation of the central density with the radius of the model as this will allow us to comprehend the nature of the prescribed model. The radius - central density relationship will guide through the process of determining the mass of the compact stellar model and vice-versa. I have studied the nature of the central density with the radius graphically in Fig. 6.21. Here the radius increases with the increase of central density until it reaches the critical

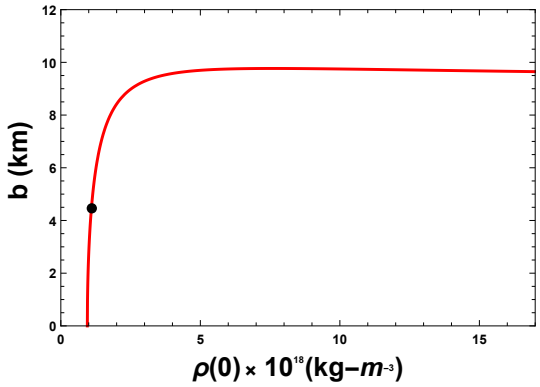

Figure 6.21: Variation of the central density with the radius. Solid circle denotes the the radius for which maximum mass of the model is obtained.

radius (maximum allowable radius) to remain almost unchanged with the increase of central density. However, the radius for which maximum mass is obtained in Fig. 6.14, corresponds to the central density $2.851 \times 10^{18}\ kg\ m^{-3}$. Additionally the maximum mass occurred in Fig. 6.20 corresponds to the central density $1.11 \times 10^{18}\ kg\ m^{-3}$.

6.3.2.15 Bounds on the model parameter

Bounds on the parameters A, C, D are described as,

Conditions	At center $(r=0)$	At surface $(r=b)$
$e^{\lambda}(r)>0$	satisfied	$-\frac{1}{b^2}<A<\frac{2}{b^2}$
$e^{\nu}(r)>0$	satisfied	satisfied
$\rho(r)>0$	$A>0$	$A>0$
$p_r(r)>0$	$\frac{6D^2}{C^2}<A<\frac{50D^2}{3C^2}$	$\frac{D}{C}=\frac{\sqrt{A}}{5\sqrt{3(2-Ab^2)}}$
$p_t(r)>0$	$\frac{6D^2}{C^2}<A<\frac{50D^2}{3C^2}$	$0<A<\frac{2}{b^2}$, $\frac{3A}{(2-Ab^2)(5+Ab^2)}<\frac{D^2}{C^2}<\frac{A}{3(2-Ab^2)}$
$\Delta(r)\geq 0$	0	$A>0$
$\frac{d\rho}{dr}\leq 0$	0	$A>0$
Zeldovich's Condition	$\frac{D}{C}\geq\frac{\sqrt{6A}}{7}$	-
$SEC(r)>0$	$\frac{A}{6}>\frac{D^2}{C^2}$	$\frac{C^2}{D^2}>\frac{3(2-Ab^2)}{A}$
Herrera Condition	$\frac{6D^2}{C^2}<A<\frac{32D^2}{3C^2}$	same

I also have calculated $\frac{dp_r}{dr}$, $\frac{dp_t}{dr}$, $\frac{dp_r}{d\rho}$, $\frac{dp_t}{d\rho}$ both at the center and at the surface and combining the above conditions one can get the following relations,

$$\begin{aligned} 0 \;<\; A \;&<\; \frac{32}{25b^2}, \\ \frac{25D^2}{6C^2} \;<\; A \;&<\; \frac{32D^2}{3C^2}. \end{aligned} \tag{6.54}$$

6.3.2.16 Herrera-Ospino-Di Prisco generating functions

Feasible anisotropic solution of EFEs can be obtained by using L. Herrera's (Herrera et al., 2008) algorithm. This formalism is essentially an extension of an algorithm proposed by Lake (Lake, 2003) and it introduces to all solutions with the help of generating functions. More specifically there are two generating functions as suggested by (Herrera et al., 2008)

to describe all the static spherically symmetric anisotropic fluid matter distribution and the algorithm can be expressed as,

$$e^{\lambda(r)}=\frac{Z^2(r)e^{\int\left(\frac{4}{r^2Z(r)}+2Z(r)\right)dr}}{r^2\left[F-2\int\frac{Z(r)(1+\Pi(r)r^2)e^{\int\left(\frac{4}{r^2Z(r)}+2Z(r)\right)dr}}{r^8}dr\right]}, \tag{6.55}$$

where F is an arbitrary integrating constant and the corresponding generating functions are as follows,

$$Z(r) = \frac{\nu'}{2}+\frac{1}{r}, \tag{6.56}$$

$$\Pi(r) = (p_r(r)-p_t(r))\,. \tag{6.57}$$

Here the generating function $Z(r)$ is related to the geometry of the spacetime and $\Pi(r)$ is related to the matter distribution as proposed by Rahaman et. al (Rahaman et al., 2019). Using Class-I embedding condition in Eq. (6.25), the generating functions given in Eqs. (6.56)-(6.57) take the form,

$$Z(r) = \frac{D\sqrt{e^{\lambda(r)}-1}}{C+D\int\sqrt{e^{\lambda(r)}-1}dr}+\frac{1}{r}, \tag{6.58}$$

$$\Pi(r) = (p_r(r)-p_t(r))\,. \tag{6.59}$$

Thus the generating functions to find all exact solutions for our model are given by,

$$Z(r) = \frac{\sqrt{3}AD\sqrt{\frac{Ar^2}{2-Ar^2}}}{AC-\sqrt{3}D\sqrt{\frac{A}{2-Ar^2}}(2-Ar^2)}+\frac{1}{r}, \tag{6.60}$$

$$\Pi(r) = -\Delta(r), \tag{6.61}$$

where $\Delta(r)$ is given in Eq. (6.20).

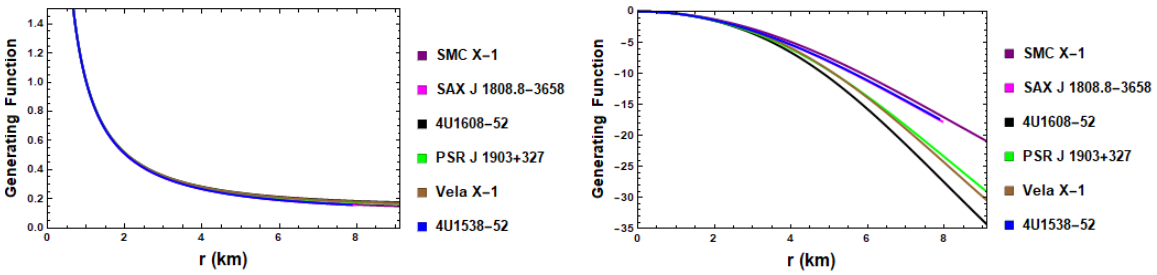

Figure 6.22: Behavior of the generating functions $Z(r)$ (left side) and $\Pi(r)$ (right side) with respect to the radial coordinate r for several compact stars.

Clearly it can be seen in Fig. 6.22, the generating function $Z(r)$ related to redshift function is always a positive and decreasing function of 'r' and the other generating function $\Pi(r)$ is always negative and decreasing in nature.

6.3.3 Discussions around various compact stellar objects

To understand our prescribed model I have calculated the parameters for the compact stars SMC X-1, SAX J $1808.4-3658$, 4U$1608-52$, PSR J $1903+327$, Vela X-1 and 4U$1538-52$ as given in Table 6.1. I have predicted the mass and radius of some compact stellar objects using a fixed EoS parameter in Table 6.2. Further, I have calculated matter variables such as density, radial and transverse sound speed and strong energy conditions for each of the compact stars both at the centers and at the surfaces. The calculated values so obtained are depicted in tabular form in Table 6.3. Here $|_0$ denotes the value of the matter variable at the center and $|_b$ denotes the same at the boundary of the stars. It can clearly be seen that the value of the matter variables at the surface is smaller than that of the central value, providing a more compact stellar structure. Additionally, the surface redshifts are also provided in Table 6.3 and surface redshifts for each compact stars are within the prescribed range.

Pulsar	$\rho\|_0$	$\rho\|_b$	$\frac{dp_r}{d\rho}\|_0$	$\frac{dp_r}{d\rho}\|_b$	$\frac{dp_t}{d\rho}\|_0$	$\frac{dp_t}{d\rho}\|_b$	$SEC\|_0$	$SEC\|_b$	$z\|_b$
SMC X-1	629.73	370.47	0.268	0.275	0.2025	0.1795	842.52	412.43	0.3095
SAXJ $1808.4-3658$	617.86	409.03	0.219	0.227	0.1425	0.1349	758.42	444.55	0.2253
$4U1608-52$	918.31	437.95	0.417	0.394	0.3821	0.2841	1515.54	508.86	0.4939
PSRJ $1903+327$	815.04	408.74	0.371	0.36	0.3264	0.2554	1268.52	470.10	0.445
Vela X-1	854.63	411.52	0.407	0.387	0.3707	0.2785	1394.45	477.24	0.4844
$4U1538-52$	612.82	409.97	0.216	0.224	0.138	0.1313	747.06	444.63	0.2183

Table 6.3: Values of the matter variables for different compact stellar objects. Here $|_0$ and $|_b$ denote the values of the matter variables at the center and surface respectively.

6.4 Model II: Vaidya-Tikekar model

In astrophysics, the problem of understanding the nature and composition of relativistic compact stars is an active field of research. In other words, the equation of state (EoS) of the constituent matter of an ultra-compact star is not well understood till date. The modeling of compact stars, therefore, remains as one of the challenging problems in astro-particle physics. In general, there are two different approaches for the modeling of relativistic ultra-compact stellar objects. If EoS is known, the Einstein field equations are solved numerically by integrating the TOV equations to analyze the behavior of physical quantities of the star. Alternatively, one assumes the geometry of the interior spacetime of the compact star. In this approach, for a suitable choice of the metric potentials, physical viability of the relevant physical quantities inside the star are analyzed (Dev and Gleiser, 2003; Esculpi et al., 2007; Maharaj and Govender, 2005; Vaidya and Tikekar, 1982). A somewhat similar approach is to suitably choose the energy density distribution inside the star and solve the relevant field equations (Dev and Gleiser, 2002; Misner and Zapolsky, 1964; Sharma and Maharaj, 2007). A combination of these two approaches can also be found in the literature as well (Rahaman et al., 2010; Varela et al., 2010).

In the present work, to close the system of field equations, I have assumed the VT ansatz

together with the Karmarkar's condition for a spherically symmetric anisotropic matter distribution. In the high density regime of compact stars, anisotropy is expected to develop as pointed out by many investigators in the past. Ruderman (Ruderman, 1972) theoretically predicted the existence of anisotropy inside compact stars. Sharma & Maharaj (Sharma and Maharaj, 2007) developed stellar models by assuming the pressure within a compact star could be anisotropic in nature. Herrera et al. (Herrera et al., 2004) have prescribed a general approach to solve the system of a spherically symmetric distribution of anisotropic fluid. In the recent past, several researchers (e.g., see (Maurya and Gupta, 2013; Maurya et al., 2015c; Maurya et al, 2019)) have developed relativistic model of compact stellar objects by introducing anisotropy.

In addition to anisotropic pressure, I have also assumed the Vaidya and Tikekar (VT) (Vaidya and Tikekar, 1982) ansatz to close our system of equations. The Vaidya and Tikekar ansatz has been utilized extensively in the past to develop realistic models of compact stars. In this approach, one assumes the metric function $g_{tt} = \frac{1-\frac{Kr^2}{L^2}}{1-\frac{r^2}{R^2}}$, which has a clear geometric interpretation. The considered metric function can be treated as the special case for the work done by Maurya et al (Maurya et al., 2016). In Schwarzschild coordinates, this provides a spheroidal geometry for the t = constant hyper-surface. The parameter K characterizes the departure from the spherical geometry and L is the curvature parameter.

Vaidya and Tikekar (VT) (Vaidya and Tikekar, 1982) have shown that for the modeling of realistic compact stars, the Einstein field equations can be solved by prescribing the geometric part (G_{ab}) of the Einstein field equations rather than specifying the matter part (T_{ab}) of the field equations. The VT prescription is outlined below.

Let us assume that the interior of a static spherically symmetric relativistic superdense star

is described by the line element

$$ds^2 = -e^{\nu(r)}dt^2 + e^{\lambda(r)}dr^2 + r^2(d\theta^2 + \sin^2\theta d\phi^2), \tag{6.62}$$

where $\nu(r)$ and $\lambda(r)$ are the gravitational potentials. The VT ansatz for the metric potential $e^{\lambda(r)}$ has the form,

$$e^{\lambda(r)} = \frac{1 - K(r^2/L^2)}{1 - (r^2/L^2)}. \tag{6.63}$$

Geometric interpretation for ansatz (6.63) is the following.

Let us consider a 4-dimensional Euclidean flat space as,

$$d\sigma^2 = dx^2 + dy^2 + dz^2 + dw^2. \tag{6.64}$$

A 3-spheroid immersed in the 4-dimensional Euclidean flat space has the form

$$\frac{x^2 + y^2 + z^2}{L^2} + \frac{w^2}{b^2} = 1. \tag{6.65}$$

Note that the sections w = constant of 3 spheroid will form concentric spheres whilst sections x =constant, y =constant or z =constant will generate confocal ellipsoid (Vaidya and Tikekar, 1982). Further, the parametrization

$$x = L\sin\delta\cos\theta\cos\phi,$$

$$y = L\sin\delta\sin\theta\sin\phi,$$

$$z = L\sin\delta\cos\theta,$$

$$w = b\cos\delta,$$

together with a transformation $r = L\sin\delta$ and substitution $1 - b^2/L^2 = K$ then allows us to write

$$d\sigma^2 = \frac{1 - K\frac{r^2}{L^2}}{1 - \frac{r^2}{L^2}}dr^2 + r^2(d\theta^2 + \sin^2\theta d\phi^2), \tag{6.66}$$

as the metric on the 3-spheroid. Therefore, in Schwarzschild coordinates, the $t =$ constant hypersurface of the space-time metric

$$ds^2 = -e^{\nu(r)}dt^2 + d\sigma^2 = -e^{\nu(r)}dt^2 + \frac{1 - K\frac{r^2}{L^2}}{1 - \frac{r^2}{L^2}}dr^2 + r^2(d\theta^2 + \sin^2\theta d\phi^2), \tag{6.67}$$

will have a spheroidal geometry characterized by the parameters L (which has dimension of a length) and K (which denotes departure from spherical geometry). The metric will be spherically symmetric and well behaved and also regular at the center for $r < L$ and $K < 1$. For $K = 1$, the spheroidal 3-space degenerates into flat 3-space. For $K = 0$, the spheroidal becomes spherical offering the Schwarzschild interior solution.

One can utilize the VT ansatz to generate a class of solutions for the metric potential $\nu(r)$ satisfying the Karmarkar's embedding class-I condition.

To develop a physically reasonable model of the stellar configuration, I have already considered the VT ansatz

$$e^{\lambda} = \frac{1 - \frac{Kr^2}{L^2}}{1 - \frac{r^2}{L^2}}, \tag{6.68}$$

Using (6.68) in (6.13), one can obtain

$$e^{\nu} = \left(C + D\sqrt{(K-1)(r^2 - L^2)}\right)^2. \tag{6.69}$$

Subsequently, the matter density, radial pressure, transverse pressure and the mass function

are obtained as

$$\rho = \frac{(K-1)(Kr^2-3L^2)}{(L^2-Kr^2)^2}, \tag{6.70}$$

$$p_r = \frac{(K-1)\left[D(K-3)\sqrt{r^2-L^2}+C\sqrt{K-1}\right]}{(L^2-Kr^2)\left[D(K-1)\sqrt{r^2-L^2}+C\sqrt{K-1}\right]}, \tag{6.71}$$

$$p_t = \frac{(K-1)\left[D(K-3)L^2\sqrt{r^2-L^2}+DKr^2\sqrt{r^2-L^2}+CL^2\sqrt{K-1}\right]}{(L^2-Kr^2)^2\left[D(K-1)\sqrt{r^2-L^2}+C\sqrt{K-1}\right]}, \tag{6.72}$$

$$\Delta = \frac{(K-1)Kr^2\left[D(K-2)\sqrt{r^2-L^2}+C\sqrt{K-1}\right]}{(L^2-Kr^2)^2\left[D(K-1)\sqrt{r^2-L^2}+C\sqrt{K-1}\right]}, \tag{6.73}$$

$$m(r) = \frac{(K-1)r^3}{2(L^2-Kr^2)}. \tag{6.74}$$

For a given K, the solution has 3 unknown constants namely, C, D and L which can be determined from the boundary conditions.

6.4.1 Exterior space-time and boundary conditions

The exterior spacetime of the static spherically star is described by the exterior Schwarzschild solution

$$ds^2 = \left(1-\frac{2M}{r}\right)dt^2 - \left(1-\frac{2M}{r}\right)^{-1}dr^2 - r^2\left(d\theta^2+\sin^2\theta d\phi^2\right). \tag{6.75}$$

The interior spacetime metric must be matched to the exterior Schwarzschild spacetime metric at the boundary of the star $r = b$. The continuity of the metric functions across the

boundary $r = b$ yields

$$\left(C + D\sqrt{(1-K)(L^2-b^2)}\right)^2 = \left(1 - \frac{2M}{b}\right), \tag{6.76}$$

$$\frac{1-\frac{Kb^2}{L^2}}{1-\frac{b^2}{L^2}} = \left(1-\frac{2M}{b}\right)^{-1}. \tag{6.77}$$

The radius is defined as the distance from the center where the radial pressure drops to zero i.e., $p_r(r = b) = 0$ which yields

$$C\sqrt{1-K} = D(3-K)\sqrt{L^2-b^2}. \tag{6.78}$$

The above boundary conditions help us to determine the constants as

$$L = \frac{b\sqrt{b+2KM-Kb}}{\sqrt{2M}}, \tag{6.79}$$

$$C = (b-2M)(3-K)\sqrt{\frac{b(1-K)}{8M(L^2-b^2)}}, \tag{6.80}$$

$$D = -\sqrt{\frac{M}{2b^3}}. \tag{6.81}$$

Thus for a specified value of K, the constants can be determined in terms of mass and radius of the star.

6.4.2 Physical analysis

The model has the following features:

1. The gravitational potentials in this model satisfy, $e^{\nu(0)} = (C + DL\sqrt{1-K})^2 =$ constant, $e^{\lambda(0)} = 1$, i.e., finite at the center ($r = 0$) of the stellar configuration. Moreover, $(e^{\nu(r)})'_{r=0} = (e^{\lambda(r)})'_{r=0} = 0$. These imply that the metric is regular at the center and well

behaved throughout the stellar interior as shown graphically in Fig. 6.23.

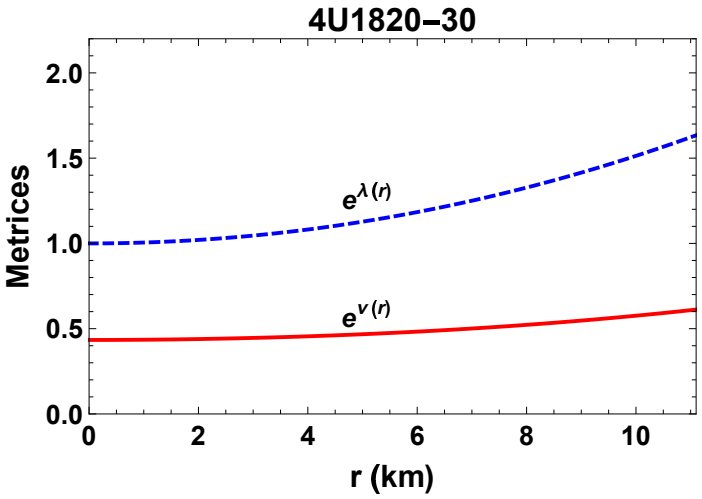

Figure 6.23: Metric potentials $e^{\lambda(r)}$ and $e^{\nu(r)}$ plotted against the radial coordinate r corresponding to the pulsar $4\mathrm{U}1820-30$.

2. The central density and central pressure are obtained as

$$\rho(0) = \frac{3(1-K)}{L^2}, \tag{6.82}$$

$$p_r(0) = p_t(0) = \frac{(1-K)\left[DL(3-K) - C\sqrt{1-K}\right]}{L^2\left[C\sqrt{1-K} - DL(1-K)\right]}. \tag{6.83}$$

Radial variation of density and two pressures and anisotropic parameter are shown in Figs. 6.24, 6.25 and 6.26, respectively.

3. The gradient of energy density, radial pressure and tangential pressure are respectively

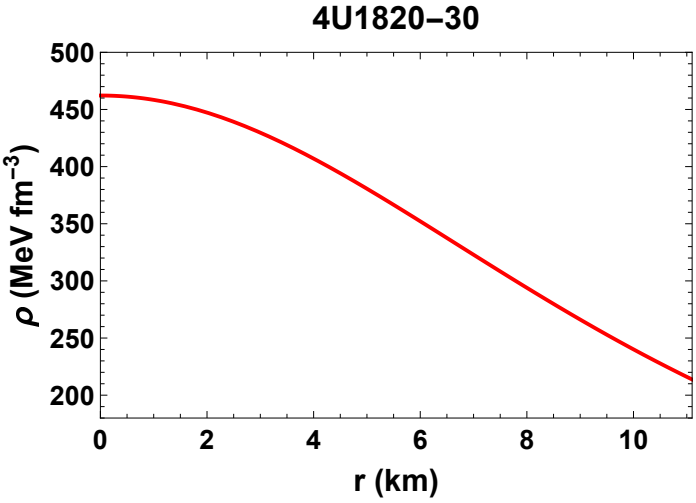

Figure 6.24: Variation of the energy density is plotted against the radial coordinate r corresponding to the pulsar $4\mathrm{U}1820-30$.

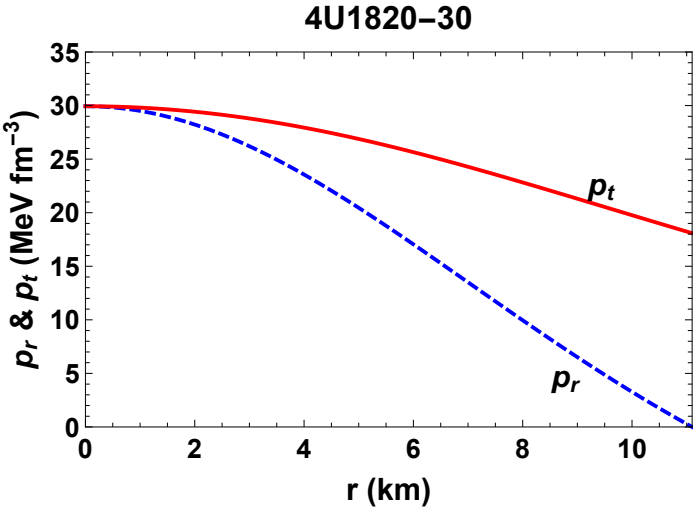

Figure 6.25: Variation of the radial pressure (dashed blue) and transverse pressure (solid red) are plotted against the radial coordinate r corresponding to the pulsar $4\mathrm{U}1820-30$.

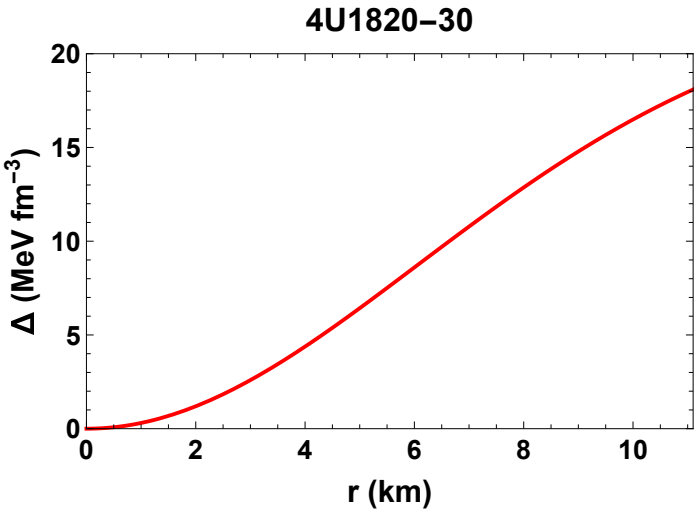

Figure 6.26: Anisotropic parameter Δ plotted against the radial coordinate r corresponding to the pulsar $4\mathrm{U}1820-30$.

obtained as

$$\frac{d\rho}{dr} = \frac{2Kr\left(1-K\right)\left(5L^2-Kr^2\right)}{\left(L^2-Kr^2\right)^3}, \tag{6.84}$$

$$\begin{aligned}\frac{dp_r}{dr} = & \frac{2r\left(1-K\right)^2}{\sqrt{\left(1-K\right)\left(L^2-r^2\right)}\left(L^2-Kr^2\right)^2\left[C\sqrt{1-K}-D\left(1-K\right)\sqrt{L^2-r^2}\right]^2} \\ & \Big[Kr^2\left(3-2K\right)-KD^2(3-K)\sqrt{1-K}(L^2-r^2)^{\frac{3}{2}} \\ & + CK\sqrt{(1-K)(r^2-L^2)}-CDL^2\left(1-4K+2K^2\right)\Big],\end{aligned} \tag{6.85}$$

$$\begin{aligned}\frac{dp_t}{dr} = & \frac{(1-K)^2}{\sqrt{(1-K)(L^2-r^2)}\left(L^2-Kr^2\right)^3\left[C\sqrt{1-K}-D(1-K)(L^2-r^2)\right]} \\ & \Big[4C^2KL^2r\sqrt{\left(1-K\right)\left(L^2-r^2\right)}+2D^2Kr\left(L^2-r^2\right)^{3/2}\sqrt{1-K} \\ & \left\{(2K-5)L^2+Kr^2\right\}+CDr\left\{KL^2r^2(6K-11)+K^2r^4\right\} \\ & - KD^2(3-K)\sqrt{1-K}\left(L^2-r^2\right)^{\frac{3}{2}}+CK\sqrt{(1-K)(r^2-L^2)} \\ & - CDL^2\left(1-4K+2K^2\right)\Big].\end{aligned} \tag{6.86}$$

The gradient of density, radial pressure and tangential pressure are negative inside the stellar body as shown graphically in Fig. 6.27 which ensures the decreasing nature of density, radial pressure and tangential pressure within the stellar interior.

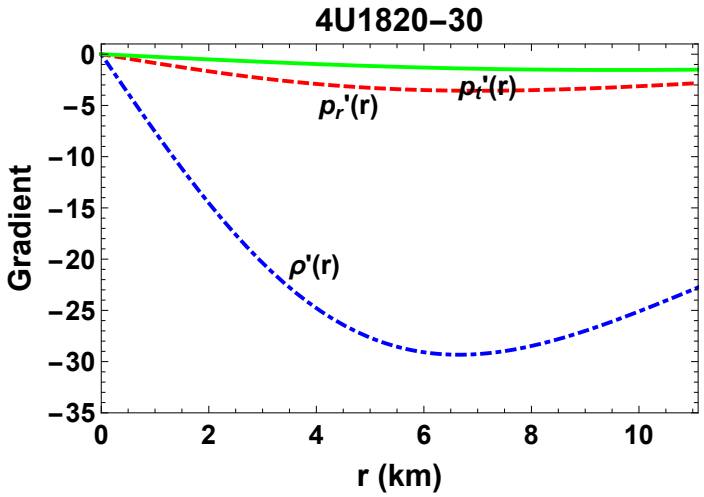

Figure 6.27: Variation of the density (dot dashed blue), radial pressure (dashed red) and transverse pressure (solid green) are plotted against the radial coordinate r corresponding to the pulsar $4\mathrm{U}1820-30$.

4. The radial and transverse velocity of sound are obtained as

$$
\begin{aligned}
v_r^2 &= \frac{dp_r}{d\rho} = \frac{\sqrt{(1-K)}\,(L^2-Kr^2)}{K\sqrt{L^2-r^2}(Kr^2-5L^2)\left\{C\sqrt{1-K}-D(1-K)\sqrt{L^2-r^2}\right\}^2} \\
&\quad \Big[KD^2(K-3)\sqrt{1-K}(L^2-r^2)^{3/2}-KC^2\sqrt{(1-K)(L^2-r^2)} \\
&\quad -CD(1-4K+2K^2)\left\{L^2+(3-2K)Kr^2\right\}\Big], \qquad (6.87) \\
v_t^2 &= \frac{dp_t}{d\rho} = -\frac{\sqrt{1-K}}{2K\sqrt{L^2-r^2}(Kr^2-5L^2)(D(K-1)+C\sqrt{1-K})^2} \\
&\quad \Big[4C^2KL^2\sqrt{(1-K)(L^2-r^2)}+2KD^2\sqrt{1-K}(L^2-r^2)^{3/2}\left\{(2K-5)L^2+Kr^2\right\} \\
&+ \quad CD\Big\{-2\left(1-7K+4K^2\right)L^4+K(6K-11)L^2r^2+K^2r^4\Big\}\Big]. \qquad (6.88)
\end{aligned}
$$

In this model, the sound speeds are found to be within the limit $[0,\ 1]$ within the stellar interior, i.e., $0 \leq \frac{dp_r}{d\rho} \leq 1$, $0 \leq \frac{dp_t}{d\rho} \leq 1$ which are shown graphically in Fig. 6.28.

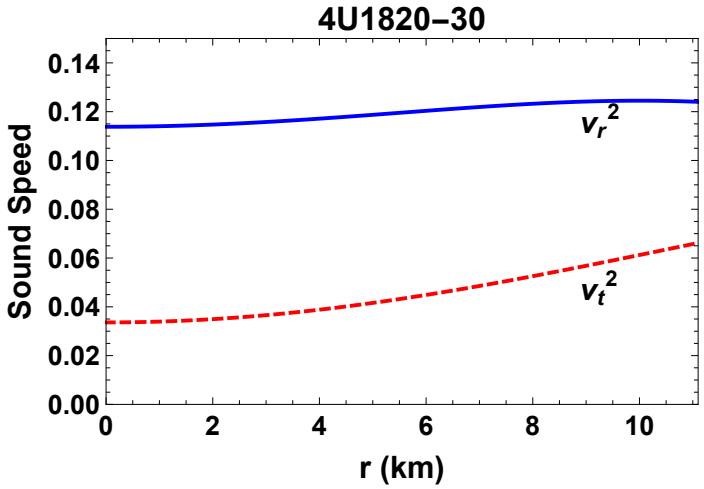

Figure 6.28: Variation of the radial (solid blue) and transverse (dashed red) sound speeds against the radial coordinate r corresponding to the pulsar $4\mathrm{U}1820-30$.

5. Energy conditions for an anisotropic fluid sphere imply the positive values of the terms $\rho+p_r \geq 0$, $\rho+p_t \geq 0$ and $\rho+p_r+2p_t \geq 0$, throughout the stellar interior. These quantities are shown to remain positive throughout the compact sphere graphically in Fig. 6.29 and hence the energy conditions are satisfied.

6. Smooth matching of the interior metric functions with that of the Schwarzschild exterior at the boundary are shown graphically in Figs. 6.30-6.31.

6.4.3 Observational compatibility

To examine the physical acceptability of the model, I have plugged in the observed values of mass and radius of known pulsars as input parameters. For graphical study , I have

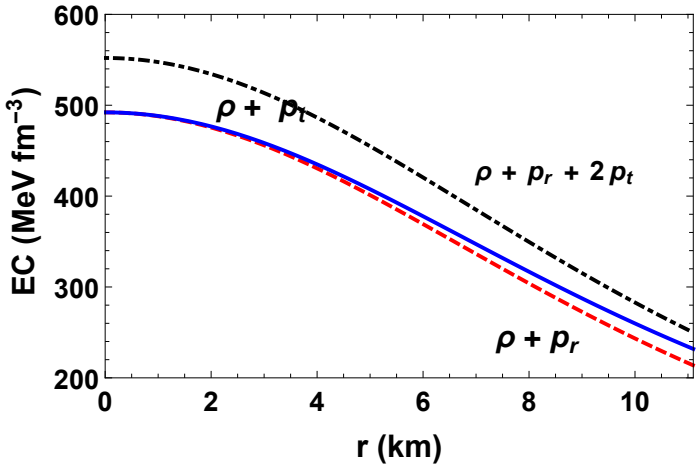

Figure 6.29: Fulfillment of various energy conditions, SEC (dot dashed black), NEC in radial direction (dashed red) and NEC in transverse direction (solid blue) within the stellar interior.

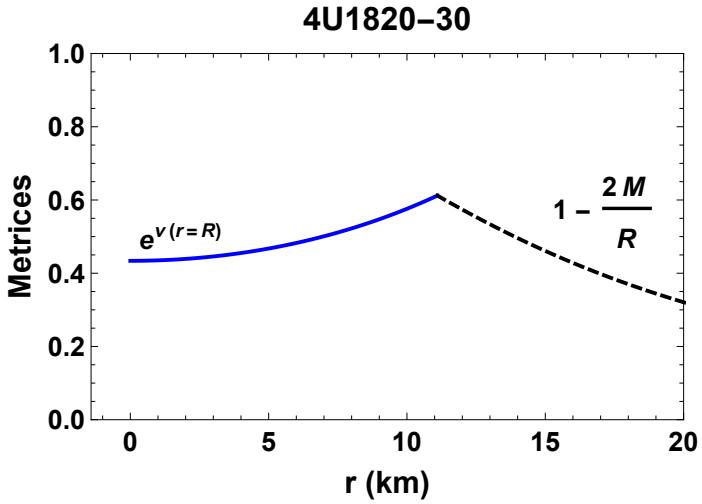

Figure 6.30: Matching of the metric $e^{\nu(r)}$ with the Schwarzschild exterior metric at the boundary.

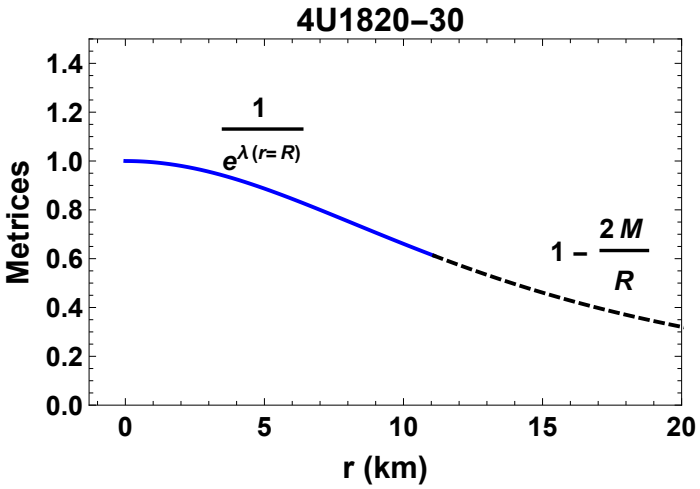

Figure 6.31: Matching of the metric $e^{\lambda(r)}$ with the Schwarzschild exterior metric at the boundary.

considered the pulsar $4\text{U}1820-30$ whose estimated mass and radius are $M = 1.46 \pm 0.21\ M_{\odot}$ and $b = 11.1 \pm 1.8$ km, respectively (Özel et al., 2016). Inserting these values in Eqs. (6.76)-(6.78), I have determined the constants. Using the values of the constants and also plugging in the values of G and c in appropriate places, I have shown the behavior of physically interesting quantities in Figs. 6.23-6.27. The plots clearly show the regular and well-behaved nature of all the physically meaningful quantities. The thermodynamic relationship between the energy density and radial pressure which reflects the nature of the equation of state (EoS) of the matter distribution of a given pulsar is plotted in Fig. 6.35 which shows an almost linear relationship. The mass function within the radius r is shown in Eq. (6.74) and the profile of mass function is shown graphically in Fig. 6.32. Note that the mass function is regular at the center. The surface redshift, defined as

$$z = \left(1 - \frac{2M}{b}\right)^{-\frac{1}{2}} - 1, \tag{6.89}$$

is plotted in Fig. 6.37.

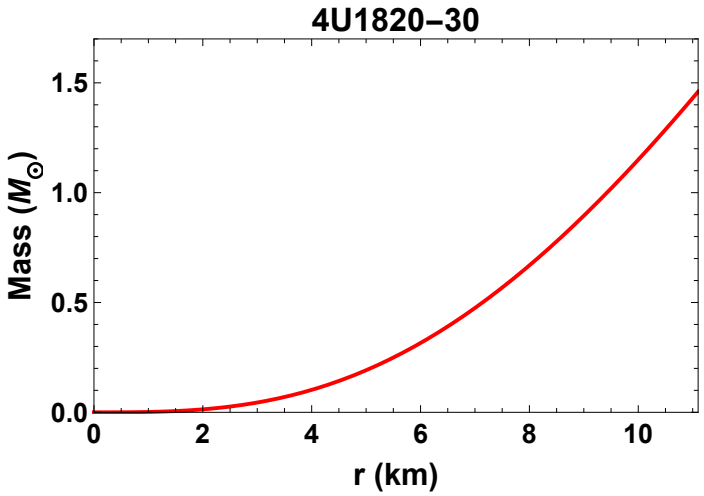

Figure 6.32: Variation of the mass function is plotted against the radial coordinate r corresponding to the pulsar $4\mathrm{U}1820-30$.

To show that this model can describe a wide range of compact stars, I have analyzed the applicability of our model by considering some well known pulsars such as RX J $1856-37$ (Pons et al., 2002), EXO $1785-248$ (Özel et al., 2009), Her X-1 (Abubekerov et al., 2008), PSR J $1614-2230$, Cen X-3 and $4\mathrm{U}\ 1608-52$. The estimated masses and radii of these pulsars are used to determine the corresponding model parameters as given in Table 6.4. In The values of the physically meaningful parameters are given in Table 6.5 which are sufficient to justify the applicability of the model. Note that I have used $()|_0$ and $()|_b$ to denote the evaluated values of the physical parameters at the center and surface of the star, respectively. I also have denoted the left hand side of the strong energy condition, $\rho + 2p_r + p_t$ by the notation SEC on the Table 6.5.

The model allows to examine the impact of departure from spherical geometry (K) of homogeneous distribution to an inhomogeneous distribution of matter on the mass radius relationship of a compact star. Fig. 6.33 portrays the impact of K by depicting the mass-

radius relationship for different values of the spheroidal parameter K for a given surface density. The plot indicates that the mass decreases as $|K|$ increases within a given radius. In other words, the compactness decreases with the departure from spherical geometry. Note that the Schwarzschild interior solution for a spherical distribution of constant density matter provides a star of compactness $M/b = 4/9$. However, a realistic star is expected to have a decreasing density profile. Our results show how the curvature parameter can be used to address the issue relating to the observed compactness of a wide range of stars. The $(M - b)$ relationship obtained for an assumed surface density $6 \times 10^{14}\ gm\ cm^{-3}$ for different values of K is shown in Fig. 6.33. The chosen surface density is roughly similar to that considered by Sharma et al (Sharma et al., 2017). It can be seen that maximum masses are $3.184\ M_{\odot}$ and $3.484\ M_{\odot}$ for the parameter $K = -100$ and $K = -10$ respectively.

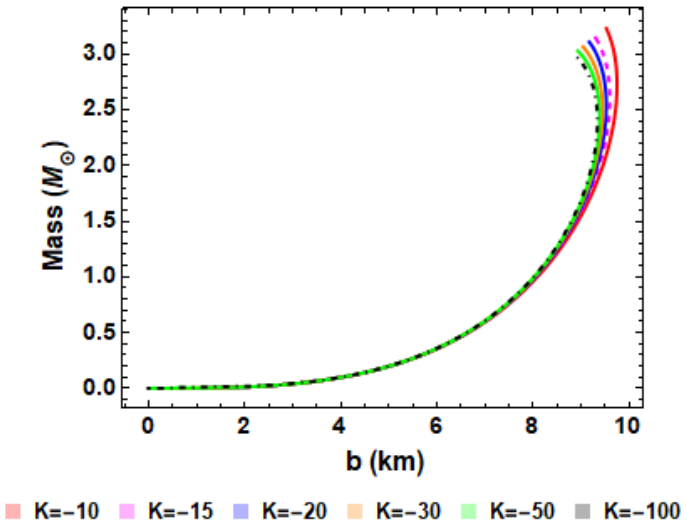

Figure 6.33: Mass-radius $(M - b)$ relationship for different K values. Assumed surface density $\rho_b = 6 \times 10^{14}$ gm cm^{-3}.

I have studied the variation of the radius with the central density graphically in Fig. 6.34.

It can easily be seen that the radius of the model increases gradually with the increase of the parameter K. Comparing Fig. 6.33 and 6.34 we can conclude that, for the minimum value of K (-100) the maximum mass is obtained for the radius $b = 9.652$ km corresponding to the central density $2.57 \times 10^{15}\ gm\ cm^{-3}$ and for the maximum value of the parameter $K = -10$, the radius for the maximum mass so obtained is $b = 10.26$ km corresponding to the central density $1.25 \times 10^{15}\ gm\ cm^{-3}$. So, with the increase of the parameter K the mass and the radius of the model also increases making the model less compact. Similar results can be found in the work of Deb et al (Deb et al., 2018).

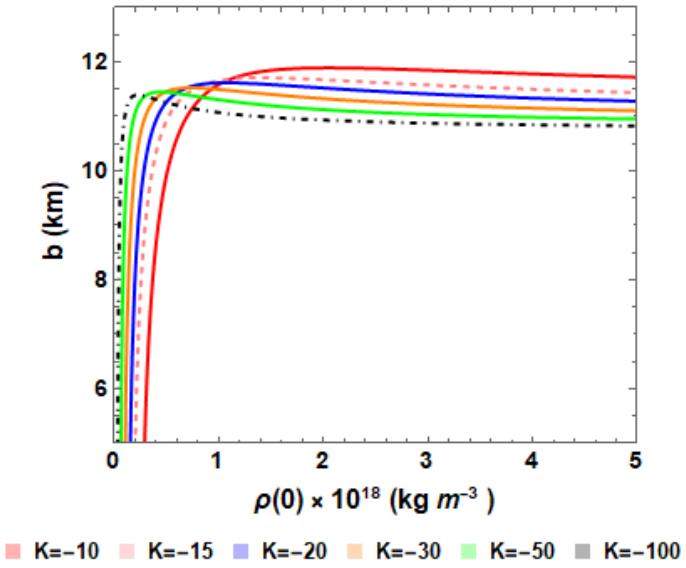

Figure 6.34: Relationship of the radius with the central density for different values of K.

The Equation of State (EoS) plays a crucial role in the modeling of a compact star which in our case may be inferred from the plot of density against pressure. Fig. 6.35 shows that the EoS corresponding to a particular set of values is linear. For the given set of values, we obtain a linear equation of the form $p_r = -25.5009 + 0.120308\ \rho$ for the best fitted curve of the EoS.

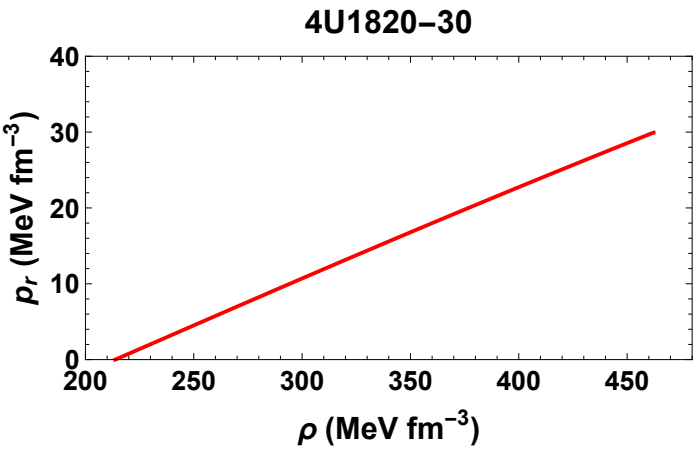

Figure 6.35: Variation of the density is plotted against the radial pressure.

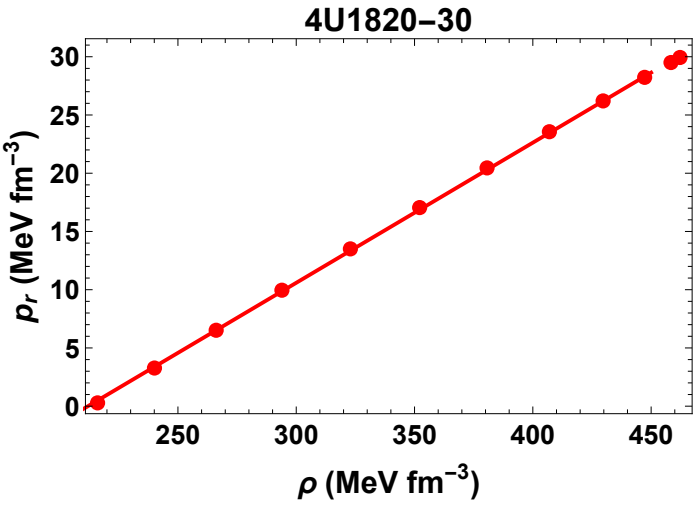

Figure 6.36: Best curve fit for the Eos given in Fig. 6.35. Here the estimate -67.711 happens to have a standard error of 0.715407 and estimate of coefficients of x, 0.182717 have a standard error of 0.000869986.

The regularity of EFEs motivate some certain bounds on the solutions and consequently on stellar configuration. One of such decisive upper bound for the static spherically symmetric compact star is Buchdahl, Bondi limit (Bondi, 1964; Buchdahl, 1959, 1966; Islam, 1969). Theoretically, it describes maximum amount of mass that can exist in a sphere before the sphere undergoes gravitational collapse to a black hole. Mathematically the limit states that for a physically viable compact star mass to radius ratio $(2M/R)$ must be less than $8/9$. Thus from the work of Buchdahl (Buchdahl, 1959) and Bondi (Bondi, 1964) it can be easily concluded that compactness factor $u(r) = \frac{m(r)}{r}$ must lie in the range $0 \leq u(r) < \frac{1}{2}$. For our model we have $u(r) = 0.486$ and it is less than 0.5. Hence Buchdahl condition is being satisfied by our model.

Also, the gravitational redshift of a compact star can be determined from the Eq. (6.89). The graphical representation of gravitational redshift of our model is shown in Fig. 6.37.

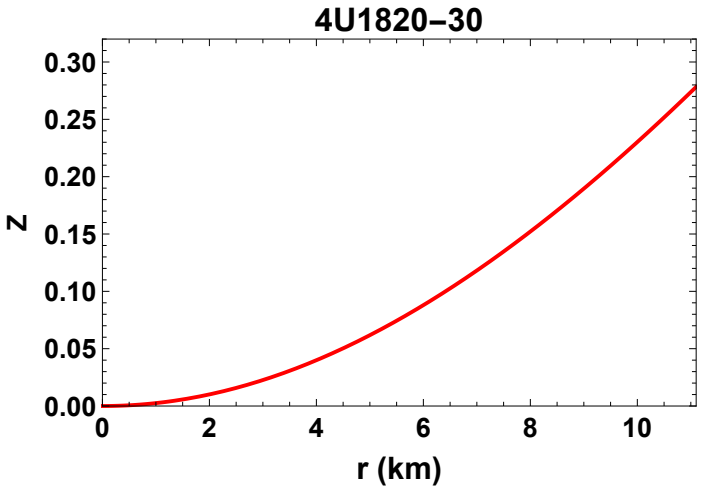

Figure 6.37: Variation of the gravitational redshift plotted against the radial coordinate r corresponding to the pulsar $4\text{U}1820-30$.

The value of maximum surface reshift obtained for our model is 0.765 which is less

Pulsar	Mass ($M_\odot$)	Radius (km)	C	D	L
RX J $1856-37$	0.9 ± 0.2	≈ 6	-19.7865	-0.0554339	48.4681
EXO $1785-248$	1.3 ± 0.2	8.849 ± 0.4	-19.9476	-0.0371973	72.7983
Her X-1	0.85 ± 0.15	8.1 ± 0.41	-22.0194	-0.034345	86.7668
PSR J $1614-2230$	1.97 ± 0.04	9.69 ± 0.2	-16.7655	-0.0399603	57.3568
Cen X-3	1.49 ± 0.08	9.178 ± 0.13	-19.1293	-0.0377009	68.9819
4U$1608-52$	1.74 ± 0.14	9.52 ± 0.15	-17.9892	-0.0385656	63.5691

Table 6.4: Values of the model parameters for different compact stars, taking K $= -50$.

than 2 as predicted by Barraco and Hamity (Barraco and Hamity, 2002).

6.4.4 Stability analysis of the model

6.4.4.1 Stability under three different forces

A star remains in static equilibrium under the forces namely, the gravitational force, hydrostatic force and anisotropic force. This condition can be formulated mathematically as

$$-\frac{M_G(r)(\rho+p_r)}{r}e^{\frac{\nu-\lambda}{2}}-\frac{dp_r}{dr}+\frac{2}{r}(p_t-p_r)=0, \tag{6.90}$$

where $M_G(r)$ is the gravitational mass of the star within the radius r, can be derived from the Tolman-Whittaker formula and the Einstein's field equations and is defined by

$$M_G(r)=\frac{1}{2}re^{\frac{\lambda-\nu}{2}\nu'}. \tag{6.91}$$

Using the expression of $M_G(r)$ in Eq. (6.90) one can obtain

$$-\frac{\nu'}{2}(\rho+p_r)-\frac{dp_r}{dr}+\frac{2}{r}(p_t-p_r)=0. \tag{6.92}$$

The above equation is equivalent to

$$F_g + F_h + F_a = 0, \tag{6.93}$$

where

$$F_g = -\frac{\nu'}{2}(\rho + p_r), \tag{6.94}$$

$$F_h = -\frac{dp_r}{dr}, \tag{6.95}$$

$$F_a = \frac{2}{r}(p_t - p_r). \tag{6.96}$$

Using the Eqs. (6.70)-(6.72), the expression for F_g, F_h and F_a can be written in terms of model parameters as,

$$F_g = \frac{2Dr^2(1-K)^2(DK(L^2-r^2)^{\frac{3}{2}} + CL^2\sqrt{1-K})}{(L^2-r^2)(L^2-Kr^2)^2(D(1-K)\sqrt{L^2-r^2} - C\sqrt{1-K})}, \tag{6.97}$$

$$F_h = \frac{2r(1-K)^2}{\sqrt{(1-K)(L^2-r^2)}(L^2-Kr^2)^2(C\sqrt{1-K} - D(1-K)\sqrt{L^2-r^2})^2}$$
$$(Kr^2(2K-3) + KD^2(3-K)\sqrt{1-K}(L^2-r^2)^{\frac{3}{2}}$$
$$- CK\sqrt{(1-K)(r^2-L^2)} + CDL^2(1-4K+2K^2)), \tag{6.98}$$

$$F_a = \frac{2(K-1)Kr[D(K-2)\sqrt{r^2-L^2} + C\sqrt{K-1}]}{(L^2-Kr^2)^2[D(K-1)\sqrt{r^2-L^2} + C\sqrt{K-1}]}, \tag{6.99}$$

which represent the gravitational, hydrostatics and anisotropic forces, respectively.

The three different forces are plotted in Fig. 6.38. The figure shows that hydrostatics and anisotropic force are positive and is dominated by the gravitational force, which is negative to keep the system in static equilibrium.

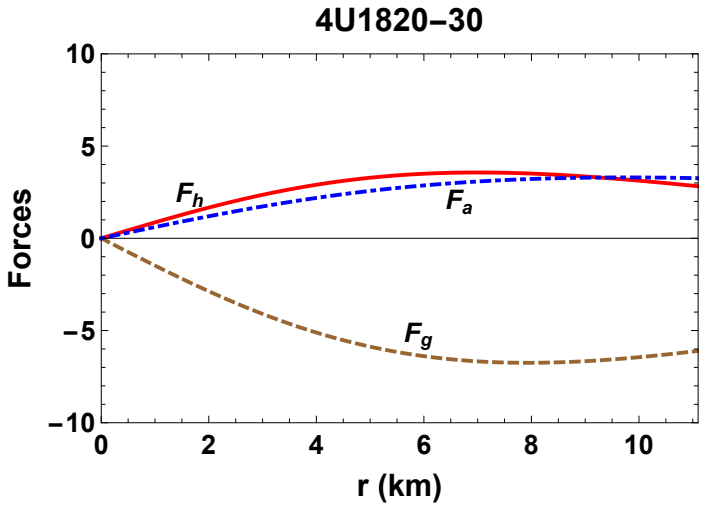

Figure 6.38: The variation of three different forces, hydrostatic force (solid red), gravitational force (dashed brown) and anisotropic force (dot dashed blue), acting on the system are plotted against the radial coordinate r corresponding to the pulsar $4\mathrm{U}1820-30$.

6.4.4.2 Adiabatic index

The adiabatic index which is defined as

$$\Gamma = \frac{\rho + p_r}{p_r}\frac{dp_r}{d\rho}, \tag{6.100}$$

is related to the stability of a relativistic anisotropic stellar configuration. Accordingly to Heinztmann and Hillebrandth Heintzmann and Hillebrandt (1975) an isotropic sphere will be in stable equilibrium if the adiabatic index $\Gamma > \frac{4}{3}$. From Fig. 6.39, it can be seen that Γ_r is greater than the value of $4/3$ throughout the stellar interior and hence the stability condition is fulfilled.

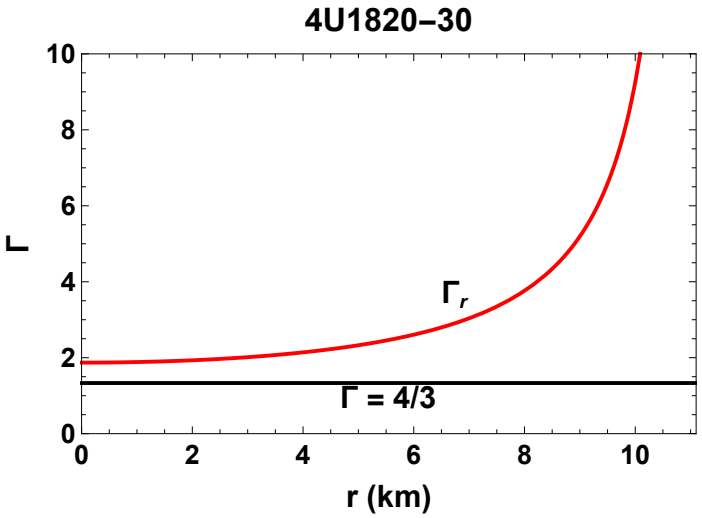

Figure 6.39: Variation of the relativistic adiabatic index is plotted against the radial coordinate r corresponding to the pulsar $4\mathrm{U}1820-30$.

6.4.4.3 Causality condition

For a physically acceptable model of relativistic anisotropic star the radial and transverse velocity speed of sound must be smaller than 1 ($c = 1$) in the interior of the star, i.e., $0 \leq \frac{dp_r}{d\rho} \leq 1, 0 \leq \frac{dp_t}{d\rho} \leq 1$. This condition is known as causality condition. Fig. 6.28 shows that both the radial and transverse speeds of sound for the model are less than 1. Based on Herrera's "cracking" concept (Herrera, 1992), Abreau et. al (Abreu et al., 2007) found that a compact stellar is potentially stable if $-1 \leq v_{st}^2 - v_{sr}^2 \leq 0$. Later Andréasson (Andrèasson, 2009) modified the result by concluding the range to be $0 < |v_{st}^2 - v_{sr}^2| < 1$ for a stable compact star. The plots in Fig. 6.40 show that the model satisfies the causality condition.

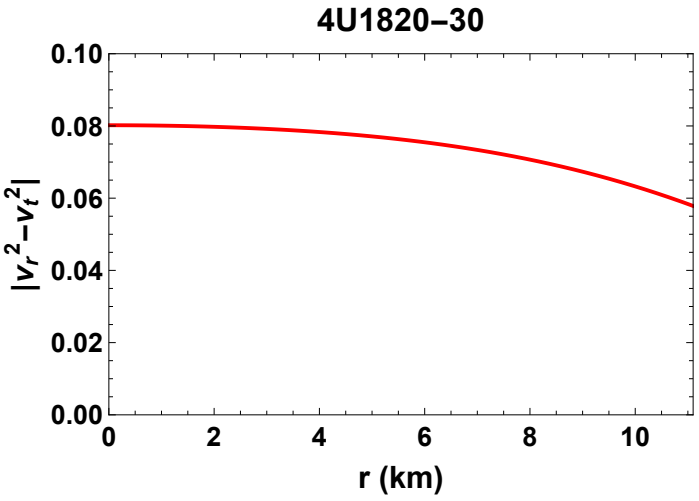

Figure 6.40: Variation of the absolute difference is plotted against the radial coordinate r corresponding to the pulsar $4\mathrm{U}1820-30$.

6.4.5 Generating functions

All the anisotropic solutions of the EFEs can be generated using L. Herrera's method of formulating generating functions Herrera et al. (2008) as given as:

$$e^{\lambda(r)}=\frac{Z^2(r)e^{\int\left[\frac{4}{r^2Z(r)}+2Z(r)\right]dr}}{r^6\left(F-2\int\frac{Z(r)(1+\Pi(r)r^2)e^{\int\left[\frac{4}{r^2Z(r)}+2Z(r)\right]dr}}{r^8}dr\right)}, \tag{6.101}$$

where F is the constant of integration. The generating functions are given as following

$$Z(r) = \frac{\nu'}{2}+\frac{1}{r}, \tag{6.102}$$

$$\Pi(r) = 8\pi\left(p_r-p_t\right). \tag{6.103}$$

The embedding class-I condition thus produces the generating functions as:

$$Z(r) = \frac{D\sqrt{e^{\lambda(r)}-1}}{C+D\int\sqrt{e^{\lambda(r)}-1}dr}+\frac{1}{r}, \tag{6.104}$$

$$\Pi(r) = -8\pi\Delta(r). \tag{6.105}$$

Incorporating the value of $e^{\lambda(r)}$ from Eq. (6.68) one can write the generating functions as:

$$Z(r) = \frac{Dr\sqrt{\frac{1-K}{L^2-r^2}}}{C+D\int r\sqrt{\frac{1-K}{L^2-r^2}}dr}+\frac{1}{r}, \tag{6.106}$$

$$\Pi(r) = -8\pi\Delta(r), \tag{6.107}$$

where $\Delta(r)$ is given in Eq. (6.73).

6.5 Discussions

In this work, I have presented a model for spherically symmetric anisotropic sphere considering a specific $e^{\lambda(r)}$. The model is assumed to satisfy Karmarkar condition and smooth matching of interior metric conditions with Schwarzschild exterior solution generate the constants of the model. To analyze our obtained solutions I have considered the physical parameters for some well-known compact stars SMC X-1, SAX J $1808.4-3658$, $4U1608-52$, PSR J $1903+327$, Vela X-1 and $4U1538-52$ to examine the acceptability of the model. Some of the key features of the obtained solutions are discussed briefly:

- Both the metric potentials are shown to be regular, well-defined and positive throughout the stellar interior. Moreover, both the metric potentials are described to be finite both at the center and at the boundary to provide an applicable compact stellar model,

Fig. 6.1 supports that.

- The energy density of a compact star is positive and monotonically decreasing in nature towards the surface with the maximum density at the center making the interior compact. The radial pressure and as well as transverse pressure are monotonically decreasing towards the surface. So all the potentials and parameters are well-valued as illustrated in Figs. 6.3 and 6.4. Moreover, the anisotropy is positive as depicted in Fig. 6.4 i.e. the anisotropic force is acting outwards and that leads to model a stable configuration.

- For singularity test, I have also computed Kretchsmann Scalar and found that the model has a singularity at $r = 1$ (see Fig. 6.6), though the model is free from any singularity at the center.

- All energy conditions are satisfied for this anisotropic physical matter distribution and evidently, one can see from Fig. 6.8 that our solutions satisfy all the energy conditions within the star. Additionally it can also be seen that inequality $\rho - p_r - 2p_t > 0$ is satisfied within the stellar interior.

- Under the combined action of gravitational, hydrostatic and anisotropic forces our model stays in equilibrium just like any anisotropic fluid configuration needs to be. The behaviour of the model in the effect of TOV equation is shown in Fig. 6.7.

- Stability of our model has been checked using Herrera (Herrera, 1992) condition. Also, the absolute value of the difference between radial and transverse sound speeds fulfil Herrera (Herrera, 1992) and Andréasson (Andrèasson, 2009) criteria making the model potentially stable.

- Compactness and gravitational redshifts are examined graphically for our model in Fig. 6.15. It is also examined numerically in Tables 6.2 and 6.3. Additionally, Fig. 6.15 depicts that maximum value is attained at the surface and redshifts vanishes at the centre and Table 6.3 shows that maximum value of surface redshifts are < 5.11 as suggested by Ivanov (Ivanov, 2002).

- I have plotted mass-radius plot in Fig. 6.14 and the maximum mass is obtained to be $4.632\ M_{\odot}$ for the radius 9.254 km. Also Fig. 6.18 depicts the mass-inertia plot where the maximum mass is approximately $0.11\ \%$ lower than that in Fig. 6.14, which expresses the stiffness of EoS.

- I have tested the stability of the model by studying mass-central density and radius-central density relationship of the model in the Figs. 6.20-6.21 respectively. The maximum radius of the model is obtained corresponding to the central density $32.11 \times 10^{18}\ kg/m^3$ in Fig. 6.20. Moreover, Fig. 6.21 suggests that the radius for which the maximum mass is obtained corresponds to the central density $2.851 \times 10^{18}\ kg/m^3$.

All the stability criterion both analytically and graphically are tested. Additionally, I have calculated mass and radius for some stars as given in Table. 6.2 taking a certain value of the EoS parameter and one can agree that the predicted radii are in good agreement with the observational data. The generating functions to find all possible exact solutions for our model are also generated. It is shown graphically that $Z(r)$ is always positive and decreasing in nature and $\Pi(r)$ is always negative and increasing in nature which is necessary to be a stable compact star. Thus it can be concluded that the model I satisfies all the properties to be anisotropic compact stellar configurations.

For the model II, using the VT metric ansatz as one of the metric potentials, a class

of interior solutions is obtained by utilizing Karmarkar's condition of embedding class-I. These regular and well-behaved solutions have been shown to be viable models of static, spherically symmetric anisotropic stellar matter distributions.

- The obtained solution is well behaved, singularity free and the regular throughout the stellar structure. The physical analysis of the obtained solution suggests the model satisfies all the properties for a feasible solution, namely, positive density, pressures at the centre, monotonically decreasing density and pressures towards the boundary, positive nature of anisotropy at the interior which vanishes at the centre,negative gradients of the density and pressures inside the structure.

- The model passes all the stability criteria for the anisotropic stellar structure. This model follows linear equation of state.

- I have analyzed the role of the curvature parameter, the deviation from sphericity of 3-surface geometry on the mass-radius relationship of the resultant configurations.. Assuming the surface density $6 \times 10^{14}\ gm\ cm^{-3}$, the mass-radius relationship corresponding to the obtained model is shown in Fig. 6.33. Here the maximum masses are $3.184\ M_{\odot}$ and $3.484\ M_{\odot}$ for the parameter $K = -100$ and $K = -10$ respectively.

  Observing the variation of the radius with the central density graphically in Fig. 6.34, one can see that the radius of the model increases gradually with the increase of the parameter K. Comparing Fig. 6.33 and 6.34 we can conclude that, for the minimum value of K (-100) the maximum mass is obtained for the radius $b = 9.652$ km corresponding to the central density $2.57 \times 10^{15}\ gm\ cm^{-3}$ and for the maximum value of the parameter $K = -10$, the radius for the maximum mass so obtained is $b = 10.26$ km corresponding to the central density $1.25 \times 10^{15}\ gm\ cm^{-3}$. So, with

the increase of the parameter K the mass and the radius of the model also increases making the model less compact.

Hence it can be conclude that the model can be consider as an acceptable model that describes spherically symmetric, static, anisotropic stellar structure.

Pulsar	$\rho\|_0$	$\rho\|_b$	$\frac{dp_r}{d\rho}\|_0$	$\frac{dp_r}{d\rho}\|_b$	$\frac{dp_t}{d\rho}\|_0$	$\frac{dp_t}{d\rho}\|_b$	$SEC\|_0$	$SEC\|_b$	$z\|_b$
RX J $1856-37$	1974.19	794.47	0.134	0.145	0.059	0.093	2477.71	955.49	0.339
EXO $1785-248$	875.1	360.73	0.129	0.141	0.055	0.088	1088.36	431.75	0.328
Her X-1	616.02	342.25	0.093	0.101	0.007	0.034	696.42	385.53	0.203
PSR J $1614-2230$	1409.71	353.15	0.258	0.249	0.220	0.209	2288.28	468.52	0.581
Cen X-3	974.07	355.17	0.151	0.162	0.082	0.114	1273.9	435.79	0.385
4U $1608-52$	1147.65	350.34	0.191	0.198	0.134	0.156	1634.94	445.3	0.473

Table 6.5: Values of the physical quantities for different known compact stars.

Chapter 7

Concluding remarks and future prospects

7.1 Conclusions

This thesis deals with obtaining singularity-free closed form interior solutions for the Einstein field equations that represent static, spherically symmetric, anisotropic stellar configurations. Considering the highly non-linearity of the field equations, some assumptions based on certain criteria are imposed to obtain the solutions. The goal of the thesis is to generate classes of closed form solutions to the Einstein's field equation that can be considered as viable models to describe spherically symmetric, static, anisotropic star and thus the chapters in this thesis have considered some assumptions which are discussed below briefly.

- Chapter. 2: Chapter 2 focuses on finding a new class of closed-form solutions of the Einstein field equation for a spherically symmetric anisotropic matter distribution. Obtained solutions are found to fulfill all the physical properties for a stable

structure. Furthermore the model checks the stability criteria for viable anisotropic stellar configuration. The obtained model assumes a linear form of equation of state. Considering the surface density $8 \times 10^{14}\ gm/cc$, the model displays the maximum mass to be $3.024\ M_{\odot}$ which follows the Rhoades-Ruffini limit Rhoades and Ruffini (1974). Also the radius corresponding to the maximum mass is found to be $10.31km$.

- I have studied a model for a spherically symmetric anisotropic matter fluid sphere by assuming a specific metric potential $B_0^2(r)$ in Chapter. 3. The field equations are solved assuming a specific form of anisotropy. The obtained solution fulfills the necessary physical and stability criteria. This model is found to maintain linear equation of state. Assuming the surface density of $7.5 \times 10^{14}\ gm/cc$ the maximum mass is found to be $3.113M_{\odot}$ corresponding to the radius $10.49\ km$. Moreover considering slow rotation configuration and using the idea of perturbation the mass-moment of inertia relationship have also been discussed. Interestingly it was found that the maximum mass obtained from the mass-radius plot is approximately 0.22% greater than the mass obtained for the maximum inertia suggesting the stiffness of the EoS.

- Assuming the popular Finch-Skea ansatz (Finch and Skea, 1989), analytic solution of the Einstein field equations have been investigated in Chapter. 4, that describes a relativistic stellar model. A class of exact solutions to the field equations have been examined after considering the corresponding two cases: (i) positive value of anisotropic parameter, and (ii) absence of any anisotropy. One interesting feature possesses by the model is the negative nature of anisotropy. The physical features of the solutions thus obtained have been studied studied graphically as well as numerically for some specific pulsars. The model is also found to be stable under the stability tests.

- Exact solutions describing relativistic stellar configuration have been studied in Chapter. 5 employing the Vaidya and Tikekar (Vaidya and Tikekar, 1982) type of metric potentials. For a spherically symmetric, static and anisotropic stellar configuration, in the Vaidya-Tikekar background spacetime, I have developed new exact class of solutions by assuming a polytropic type equation of state $p_r = \alpha\rho^{1+\frac{1}{n}} - \beta$, where α, β are real constants and n is the polytropic index. Recent data from observed pulsars are taken as input parameters to validate the developed model. Moreover, the impact of the spheroidal curvature parameter of the VT spacetime is observed on the stellar behaviour and on the mass-radius relationship. It is observed that with the increase in the departure from the spherical geometry, values of physical quantities, such as density and pressure, increase.

- In Chapter. 6, two types of spherically symmetric, static, anisotropic stellar models have been discussed. Both the models have been obtained from the Einstein field equations by specific metric potentials and Class I Karmarkar embedding condition. Model I depicts a anisotropic stellar configuration assuming Buchdahl ansatz and this obtained solution describes a stable structure for anisotropic star of maximum mass $4.6\ M_{\odot}$. Model II represents a class of solutions for a spherically symmetric anisotropic matter distribution in Vaidya and Tikekar spheroidal geometry. Thus obtained model is found to be a stable viable stellar model. Additionally, the dependence of the curvature parameter K of the model, which characterizes a departure from homogeneous spherical distribution, is also examined. It is found that the radius of the structure increases with the increase of the parameter K. Hence the star becomes less compact as K increases.

7.2 Future scopes

This thesis emphasizes on obtaining closed form interior solutions of Einstein field equations that describe static, uncharged spherically symmetric structures. Using these solutions one can fine-tune the stellar structure employing the followings:

- To construct more realistic compact stellar objects, one can incorporate charge within the stellar interiors along with the pressure anisotropy. The presence of charge on a spherically symmetric stellar objects prevents the gravitational collapse. Thus the obtained solutions can be employed to find the solutions of Einstein-Maxwell field equations thus obtaining solutions for charged structures.

- When considering the moment of inertia, I have used Bejger-Haensel concept which permits to structure to consider as a slow rotating configuration. However these non-rotating solutions can be used to investigate the rapidly rotating compact stellar structure. Furthermore, these results can be extend to study universality relation. These relations, such as I-Love-Q relation, exist withing the stellar observables, the moment of inertia, I, compactness C (mass to radius ratio), love number associated with the tidal deformability λ, spin induced Q. These relations are applicable to study X-ray, radio and gravitational wave observations. The major benefit of using these universal relations is that these relations do not depend solely on the EoS of the matter distribution. This work can be broaden to study these stellar relations.

- Another approach to study relativistic compact stellar models is to consider the spherical structure as core-envelope configuration where the core of the structure contains the different matter fluid than its surrounding envelope. The present study can be expand considering the structure as core-envelope model.

- The present study is conducted by assuming the interior spacetime as that of the spherically symmetric static star in Schwarzschild coordinates (t, r, θ, ϕ). However, this study can be extend on some other definite 3-space geometry such as spheroidal spacetime, paraboloidal spacetime, pseudo-spheroidal geometry to name a few.

- Observable Universe is mostly consists of dark energy and dark matter. Observation of the dark matter requires the study of the Einstein field equations with the cosmological constant. Also the presence of the dark energy, where matter accelerates in negative way, is found to be the primary cause of the expansion of the Universe. To study the late time expansion of the Universe, that is, to study the Universe in large-scale structure, theory of general relativity needs to be modified. Thus arise the need for the modified theories gravity and this modification can be done either modifying the matter Lagrangian part or by modifying the field of gravitation. To investigate more realistic astrophysical stellar objects, one can make use of this work to study anisotropic compact stellar models assuming modified theory of gravity, such as $f(R)$ gravity, $f(T)$ gravity, $f(R,T)$ gravity, Rastall gravity, Mimetic gravity to name a few.

  Another interesting modified theory of gravity is Teleparallel gravity, where the vanishing curvature is paired with non-vanishing torsion or nonmetricity, or both. Observing these modified theories, namely, metric teleparallel theories (where gravity is described in terms of torsion), symmetric teleparallel theory (torsion free gravity induced to nonmetricity), general teleparallel theory (admitting both torsion and nonmetricity), the present work can be use to examine astrophysical objects on these modified theories, which can describe stellar models more accurately that are compatible to the recent observations by LIGO/ VIRGO/ KAGRA and NICER data.

Farook Rahaman 4/9/23

DR. FAROOK RAHAMAN
Professor
Department of Mathematics
JADAVPUR UNIVERSITY
Kolkata - 700032, W.B., INDIA

Shyam Dey 4/9/23

Associate Professor in Physics
Malda College,
Malda

Lipi Baskey 4/9/23

Bibliography

Abbott et al., R. (2018). $GW170817$: Measurements of neutron star radii and equation of state. *Phys. Rev. Lett.*, 121:161101.

Abreu, H., Hernàndez, H., and Nùñez, L. (2007). Sound speeds, cracking and stability of selfgravitating anisotropic compact objects. *Class. Quan. Grav.*, 24:4631.

Abubekerov, M., Antokhina, E., Cherepashchuk, A., and Shimanskii, V. (2008). The mass of the compact object in the X-Ray binary Her X-1/HZ Her. *Astron. Rep.*, 52:379.

Andrèasson, H. (2009). Sharp bounds on the critical stability radius for relativistic charged spheres. *Commun. Math. Phys.*, 288:715.

Bañados, M., Teitelboim, M., and Zanelli, J. (1992). Black hole in three-dimensional spacetime. *Phys. Rev. Lett.*, 69:1849.

Banerjee, A., Rahaman, F., Jotania, K., Sharma, R., and Karar, I. (2013). Finch-Skea star in $(2+1)$ dimensions. *Gen. Relativ. Gravit.*, 45:717–726.

Barcelo, C. and Visser, M. (2002). Twilight for the energy conditions? *Int. J. Mod. Phys. D*, 11:1553.

Barraco, D. and Hamity, V. (2002). Maximum mass of a spherically symmetric isotropic star. *Phys. Rev. D.*, 65:124028.

Bayin, S. (1982). Anisotropic fluid spheres in general relativity. *Phys. Rev. D*, 26(6):1262.

Bejger, M., Bulik, T., and Haensel, P. (2005). Constraints on the dense matter equation of state from the measurements of PSR J 0737 - 3039, a moment of inertia and PSR J 0751 + 1807 mass. *Mon. Not. R. Astron. Soc.*, 364:635.

Bejger, M. and Haensel, P. (2002). Moments of inertia for neutron and strange stars: limits derived for the crab pulsar. *Astron. Astrophys.*, 396:3.

Bhar, P. (2015a). Strange star admitting Chaplygin equation of state in Finch-Skea space-time. *Astrophys. Space Sci.*, 359:41.

Bhar, P. (2015b). Vaidya–Tikekar type superdense star admitting conformal motion in presence of quintessence field. *Eur. Phys. J. C*, 75:123.

Bhar, P. (2019). Anisotropic compact star model: a brief study via embedding. *Eur. Phys. J. C.*, 79:138.

Bhar, P., Das, S., and Parida, B. (2022). Compact stellar model in Tolman space-time in presence of pressure anisotropy. *Int. J. Geo. Method Mod. Phys*, 19:06.

Bhar, P., Murad, M., and Pant, N. (2015). Relativistic anisotropic stellar model with Tolman VII spacetime. *Astrophys, Space Sci.*, 359:13.

Bhar, P., Rahaman, F., Biswas, R., and Fatima, H. (2014). Exact solution of a $(2 + 1)$-dimensional anisotropic star in Finch and Skea spacetime. *Commun. Theor. Phys.*, 62:221.

Bijalwan, N. and Gupta, Y. (2011). Closed form Vaidya-Tikekar type charged fluid spheres with pressure. *Astrophys. Space Sci.*, 334:293–299.

Bijalwan, N. and Gupta, Y. (2012). Closed form charged fluid with t = constant hypersurfaces as spheroids and hyperboloids. *Astrophys. Sp. Sci.*, 337:455–462.

Bisht, R., Gedela, S., Pant, N., and Tewari, N. (2021). A relativistic model of stellar objects with core-crust-envelope division. *Res. Astron. Astrophys.*, 21(7):162.

Biswas, B. and Bose, S. (2019). Tidal deformability of an anisotropic compact star: Implications of GW170817. *Phys. Rev. D*, 99:104002.

Böhmer, C. and Harko, T. (2006). Bounds on the basic physical parameters for anisotropic compact general relativistic objects. *Class. Quantum Grav.*, 23:6479.

Bombacci, I. (1997). Observational evidence for strange matter in compact objects from the X-ray burster 4U1820-30. *Phys. Rev. C*, 55:1587.

Bondi, H. (1964). The contraction of gravitating spheres. *Proc. R. Soc. Lond. A*, 281(1384):39.

Bondi, H. (1992). Anisotropic spheres in general relativity. *Mon. Not. R. Astron. Soc*, 259:365–368.

Bondi, H. (1999). The gravitational redshift from static spherical bodies. *Mon. Not. R. Astron. Soc.*, 302:337–340.

Boonserm, P., Ngampitipan, T., and Visser, M. (2016). Mimicking static anisotropic fluid spheres in general relativity. *Int. J. Mod. Phys.*, 25(02):1650019.

Breu, C. and Rezzolla, L. (2016). Maximum mass, moment of inertia and compactness of relativistic stars. *Mon. Not. Royal Astro. Soc.*, 459:646–656.

Buchdahl, H. (1959). General relativistic fluid spheres. *Phys. Rev. D*, 116(4):1027.

Buchdahl, H. (1966). General relativistic fluid spheres II: general inequalities for regular spheres. *Astrophys. J.*, 146:275.

Burghardt, R. (2016). *The curvature parameters in gravitational models*. Sep, Austr. Reporton Gravi. ARG-2016-06.

Burrows, A. and Lattimer, J. (1986). The birth of neutron stars. *Astrophys J.*, 307:178.

Canuto, V. (1974). Equation of state at ultrahigh densities. *Ann. Rev. Astron. Astrophys.*, 12:167.

Canuto, V. and Chitre, S. (1973). Solid core in neutron stars. *Nat. Phys. Sci.*, 243(126):63–65.

Cartan, E. (1927). Sur une classe remarquable déspaces de Riemann II. *Bull. Soc. Math.*, 55:114–134.

Carvalho, G., Marinho, R., and Malheiro, M. (2015). Mass-radius diagram for compact stars. *J. Phys. Conf. Ser.*, 630:012058.

Chaisi, M. and Maharaj, S. (2005). Compact anisotropic spheres with prescribed energy density. *Gen. Relativ. Gravit.*, 37:1177–1189.

Chaisi, M. and Maharaj, S. (2006). Anisotropic static solutions in modelling highly compact bodies. *Pramana-J. Phys.*, 66(3):609–614.

Chan, R., Herrera, L., and Santos, N. (1992). Dynamical instability in the collapse of anisotropic matter. *Class. Quantum Gravit.*, 9:133.

Chan, R., Herrera, L., and Santos, N. (1993). Dynamical instability for radiating anisotropic collapse. *Mon. Not. R. Astron. Soc.*, 265(3):533–544.

Chanda, A., Dey, S., and Paul, B. (2019). Anisotropic compact objects in f(T) gravity with Finch–Skea geometry. *Eur. Phys. J C*, 79:502.

Chandrasekhar, S. (1964a). The dynamical instability of gaseous masses approaching the schwarzschild limit in general relativity. *Astrophys. J.*, 140:417.

Chandrasekhar, S. (1964b). A general variational principle governing the radial and nonradial oscillations of gaseous masses. *Astrophys. J.*, 139:664.

Chattopadhyay, P., Deb, R., and Paul, B. (2012). Relativistic solution for a class of static compact charged star in pseudo spheroidal space-time. *Int. J. Mod. Phys.*, 21(08):1250071.

Chattopadhyay, P. and Paul, B. (2010). Relativistic star solutions in higher-dimensional pseudospheroidal space-time. *Pramana J. Phys.*, 74:513.

Chilambwe, B. and Hansraj, S. (2015). n-dimensional isotropic Finch-Skea stars. *Eur. Phys. J. Plus*, 130:19.

Clayton, D. (1983). *Principles of Stellar Evolution and NucleoSynthesis*. University of Chicago Press, Chicago.

Codazzi, D. (1868). Sulle coordinate curvilinee dúna superficie e dello spazio. *Ann. di Mat*, 2:269.

Cosenza, M., Herrera, L., Esculpi, M., and Witten, L. (1981). Some models of anisotropic spheres in general relativity. *J. Math. Phys.*, 22:118.

Darmois, G. (1927). *Les equations de la gravitation einsteinienne*. Mémorial des sciences mathèmatiques XXV, Fasticule XXV, Chap. V.

Das, B., Dey, S., Das, S., and Paul, B. (2022a). Anisotropic compact objects with Finch-Skea geometry in EGB gravity. *Eur. Phys. J. C*, 82:519.

Das, S., Parida, B., Chakraborty, K., and Ray, S. (2022b). Anisotropic compact star with a linear pressure-density relationship. *Int. J of Mod. Phys. D*, 31(7):2250053.

Deb, D., Chowdhury, S., Ray, S., Rahaman, F., and Guha, B. (2017). Relativistic model for anisotropic strange stars. *Ann. Phys.*, 387:239.

Deb, D., Guha, B., Rahaman, F., and Ray, F. (2018). Anisotropic strange stars under simplest minimal matter-geometry coupling in the f(R, T) gravity. *Phys. Rev. D*, 97:084026.

Deb, D., Roy Chowdhury, S., Guha, B., and Ray, S. (2016). *Can strange stars mimic dark energy stars?* arXiv:1611:02253v1.

Delgaty, M. and Lake, K. (1998). Physical acceptability of isolated, static spherically symmetric perfect fluid solutions of Einstein's equations. *Comput. Phys. Commun.*, 115:395–415.

Demorest, P., Pennucci, T., Ransom, S., Roberts, M., and Hessels, J. (2010). A two-solarmass neutron star measured using Shapiro delay. *Nature*, 467:7319.

Dev, K. and Gleiser, M. (2002). Anisotropic stars: exact solutions. *Gen. Relativ. Gravit.*, 34:1793–1818.

Dev, K. and Gleiser, M. (2003). Anisotropic stars II: stability. *Gen. Relativ. Gravit.*, 35:1435–1457.

Dey, M., Bombacci, I., Dey, J., Ray, S., and Samanta, B. (1998). Strange stars with realistic quark vector interaction and phenomenological density-dependent scalar potential. *Phys. Lett. B*, 438:123–128.

d'Inverno, R. (1992). *Introducing Einstein's Relativity*. A Clarendon Press Publication.

Duorah, H. and Ray, R. (1987). An analytical stellar model. *Class. Quantum Grav.*, 4:1691.

Durgapal, M. (1982). A class of new exact solutions in general relativity. *J. Phys. A*, 15:2637.

Durgapal, M. and Bannerji, R. (1983). New analytical stellar model in general relativity. *Phys. Rev. D*, 27:328. erratum Phys. Rev. D (1983) 28:2695.

Durgapal, M. and Fuloria, R. (1985). Analytic relativistic model for a superdense star. *Gen. Relativ. Gravit.*, 17:671–681.

Durgapal, M., Pande, A., and Phuloria, R. (1984). Physically realizable relativistic stellar structures. *Astrophys. Space Sci.*, 102:49–66.

Eddington Kasner, A. (1924). *The Mathematical Theory of Relativity*. Cambridge University Press, Cambridge.

EKSÌ, K. (2016). Neutron stars: Compact objects with relativistic gravity. *Turkish J Phys.*, 40(2):127–138.

Elebert et al, P. (2009). Optical spectroscopy and photometry of SAX J1808.4 - 3658 in outburst. *Mon. Not. Roy. Astron. Soc.*, 395:884.

Errehymy, A., Daoud, M., and Sayouty, E. (2019). A spherically symmetric model of anisotropic fluid for strange quark spheres. *Eur. Phys. J. C*, 79:346.

Esculpi, M., Malaver, M., and Aloma, E. (2007). A comparative analysis of the adiabatic stability of anisotropic spherically symmetric solutions in general relativity. *Gen. Relativ. Gravit.*, 39:633.

Everitt et al., C. (2011). Gravity probe B: Final results of a space experiment to test general relativity. *Physical Review Letters*, 106:221101.

Fatema, S., Murad, M., and Singh, K. (2019). New exact anisotropic static spherically symmetric stellar models satisfying the Eiesland condition. *Ann. Phys.*, 402:1.

Finch, M. (1987). *The Painleve-Gambier Equation and The Relativistic Static Fluid Sphere*. PhD thesis, PhD Thesis, University of Sussex.

Finch, M. and Skea, J. (1989). A realistic stellar model based on an ansatz of Duorah and Ray. *Class. Quantum Grav.*, 6:467.

Freire et al, P. (2011). On the nature and evolution of the unique binary pulsar J1903 +0327. *Mon. Not. Roy. Astron. Soc.*, 412:2763.

Friedman, A. (1965). Isometric embedding of Riemannian manifolds into Euclidean spaces. *Rev. Mod. Phys.*, 37:201.

Frieman, J. and Olinto, A. (1989). Is the sub-millisecond pulsar strange? *Nature*, 341:633–635.

Gangopadhyay, T., Ray, S., Li, X.-D., Dey, J., and Dey, M. (2013). Strange star equation of state fits the refined mass measurement of 12 pulsars and predicts their radii. *Mon. Not. R. Astron. Soc.*, 431:3216.

García, A. and Campuzano, C. (2003). All static circularly symmetric perfect fluid solutions of 2 + 1 gravity. *Phys. Rev. D*, 67:064014.

Gauss, C. (1827). *Disquisitiones Generales circa Supercies Curvas*. The Royal Society.

Gedela, S., Bisht, R., and Pant, N. (2019a). Relativistic modeling of Vela $X-1$ using the Karmarkar condition. *Mod. Phys. Lett. A*, 9:59.

Gedela, S., Bisht, R., and Pant, N. (2020). Relativistic modeling of stellar objects using embedded class one spacetime continuum. *Mod. Phys. Lett. A*, 33(1):2050097.

Gedela, S., Pant, N., Upreti, J., and Pant, R. (2019b). Relativistic core-envelope anisotropic fluid model of super dense stars. *Eur. Phys. J. C.*, 79:566.

Gedela, S., Pant, R., Bisht, R., and Pant, N. (2019c). A new parametric class of exact solutions of EFEs under the Karmarkar condition for anisotropic fluids. *Eur. Phys. Journal A*, 55:95.

Glendenning, N. (1982). The hyperon composition of neutron stars. *Phys. Lett. B*, 114(6):392–396.

Glendenning, N. (1985). Neutron stars are giant hypernuclei ? *Astrophys. J.*, 293:470–493.

Glendenning, N. (1995). Prompt subsidence of a proto-neutron star into a black hole. *Astrophys. J.*, 448:797.

Glendenning, N. (1997). *Compact Stars: Nuclear Physics, Particle Physics, and General Relativity*. Springer New York, NY.

Gokhroo, M. K. and Mehra, A. (1994). Anisotropic spheres with variable energy density in general relativity. *Gen. Relativ. Gravit.*, 26:75.

Gondek-Rosinska, D., Bulik, T., Zdunik, L., Gourgoulhon, E., Ray, S., Dey, J., and Dey, M. (2000). Rapidly rotating compact strange stars. *Astron. Astrophys.*, 363:1005.

Goswami, K., Saha, A., and Chattopadhyay, P. (2022). Anisotropic compact star in modified Vaidya–Tikekar model admitting new solutions and maximum mass. *Pramana J. Phys.*, 96:127.

Govender, M., Maharaj, A., Singh, K., and Pant, N. (2020). Dissipative collapse of a Karmarkar star. *Mod. Phys. Lett. A*, 35(20):2050164.

Gupta, Y. and Goyel, M. (1975). Class two analogues of TY Thomas's theorem and different types of embeddings of static spherically symmetric space-times. *Gen. Relativ. Gravit.*, 6:499.

Gupta, Y. and Jasim, M. (2004). On most general exact solution for Vaidya-Tikekar isentropicsuperdense star. *Astrophys. Space Sci.*, 272:403–415.

Gupta, Y. and Kumar, M. (2005). A superdense star model as charged analogue of Schwarzschild's interior solution. *Gen. Relat. Grav.*, 37(3):575–583.

Güver, T., Özel, F., Cabrera-Lavers, A., and Wroblewski, P. (2010). The distance, mass and radius of the neutron star in 4U 1608 - 52. *Astrophys. J.*, 712:964.

Haensel, P. (2008). *Equation of state of dense matter and maximum mass of neutron stars, Final Stages of Stellar Evolution*. edts. J.M. Hameury, C. Motch EAS Publications Series.

Haensel, P., Potekhin, A., and Yakovlev, D. (2007). Neutron stars I: equation of state and structures.

Haensel, P., Salgado, M., and Bonazzola, S. (1995). Equation of state of dense matter and maximum rotation frequency of neutron stars. *Astron. Astrophys.*, 296:745751.

Haensel, P. and Zdunik, J. (1989). A submillisecond pulsar and the equation of state of dense matter. *Nature*, 340:617.

Hansraj, S. (2017). Generalized spheroidal spacetimes in 5-D Einstein–Maxwell–Gauss–Bonnet gravity. *Eur. Phys. J. C.*, 77:557.

Hansraj, S., Chilambwe, B., and Maharaj, S. (2015). Exact EGB models for spherical static perfect fluids. *Eur. Phys. J. C*, 75:277.

Hansraj, S. and Maharaj, S. (2006). Charged analogue of Finch–Skea stars. *Int. J. Mod. Phys. D*, 15:1311–1327.

Harko, T. and Cheng, K. (2002). Maximum mass and radius for strange stars in the linear approximation of the EOS. *Astron. Astrophys.*, 385:1005.

Harrison, B., Thorne, K., Wakano, M., and Wheeler, J. (1965). *Gravitational theory and gravitational collapse*. University of Chicago Press.

Hawking, S. and Ellis, G. (1973). *The large scale structure of space-time*. Cambridge Monographs on Mathematical Physics, Cambridge University Press.

Heintzmann, H. and Hillebrandt, W. (1975). Neutron stars with an anisotropic equation of state: mass, redshift and stability. *Astrophys. J*, 38:51–55.

Hendi, S., Bordbar, G., Panah, B. E., and Panahiyan, S. (2017). Neutron stars structure in the context of massive gravity. *JCAP*, 07:004.

Hernàndez, H. and Nùñez, L. (2004). Nonlocal equation of state in anisotropic static fluid spheres in general relativity. *Can. J. Phys.*, 82(1):29–51.

Herrera, L. (1992). Cracking of self-gravitating compact objects. *Phys. Lett. A*, 165(3):206.

Herrera, L., Di Prisco, A., Martin, J., Ospino, J., Santos, N., and Troconis, O. (2004). Spherically symmetric dissipative anisotropic fluids: A general study. *Phys. Rev. D*, 69:084026.

Herrera, L., Ospino, J., and Di Prisco, A. (2008). All static spherically symmetric snisotropic solution of Einstein's equations. *Phys. Rev. D*, 77:027502.

Herrera, L. and Ponce de Leon, J. (1985). Isotropic and anisotropic charged spheres admitting a one-parameter group of conformal motions. *J. Math. Phys.*, 26:2302–2307.

Herrera, L. and Santos, N. (1997). Local anisotropy in self-gravitating systems. *Phys. Rep.*, 286:53–130.

Herrera, L. and Santos, N. O. (1995). Jeans mass for anisotropic matter. *Astrophys J*, 438(1):308–313.

Hessels et al., J. (2005). Binary radio pulsars. *PASP Conf. Ser.*, 328:395.

Hewish, A., Bell, S., Pikington, J., Scott, P., and Collins, R. (1968). Observation of a rapidly pulsating radio source. *Nature*, 217:709.

Hilbert, D. (1901). Ueber flächen von constanter Gaussscher kr Ümmung [English translation: On surfaces of constant Gaussian curvature]. *Trans. Amer. Math. Soc.*, 2(1):87–99.

Hillebrandt, W. and Steinmetz, K. (1976). Anisotropic neutron star models: stability against radial and nonradial pulsations. *Astron. Astrophys.*, 53:283–287.

Ipser, J. (1969). Relativistic, spherically symmetric star clusters. III. Stability of compact isotropic models. *Astrophys. J.*, 158:17.

Islam, J. (1969). Some general relativistic inequalities for a star in hydrostatic equilibrium. *Mon. Not. R. Astron. Soc.*, 21:145.

Israel, W. (1966). Singular hypersurfaces and thin shells in general relativity. *Nuo. Cim. B*, 44:1. erratum - ibid. (1967) 48:463.

Ivanov, B. (2002). Maximum bounds on the surface redshifts of anisotropic stars. *Phys. Rev. D.*, 65(10):104011.

Janet, M. (1927). Sur la possibilité de plonger un espace riemannian donné dasn un espace euclidien. *Ann. Soc. Polon. Math.*, 5:38.

Jasim, M., Maurya, S., and Al-Sawaii, A. (2020). A generalised embedding class one static solution describing anisotropic fluid sphere. *Astrophys. and Space Sc.*, 365:9.

Jones, P. (1975). The alignment of the crab pulsar magnetic axis. *Astrophys. Space Sci.*, 33:215–230.

Jotania, K. and Tikekar, R. (2006). Paraboloidal space-time and relativistic models of strange stars. *Int. J. Mod. Phys. D*, 15(08):1175.

Kalam, M., Rahaman, F., Hossein, S., and Ray, S. (2013a). Central density dependent anisotropic compact stars. *Eur. Phys. J. C*, 73:2049.

Kalam, M., Rahaman, F., Molla, S., and Hossein, S. (2014). Anisotropic quintessence stars. *Astrophys. Space Sci.*, 349:865–871.

Kalam, M., Usmani, A., Rahaman, F., Hossein, M., Karar, I., and Sharma, R. (2013b). A relativistic model for strange quark stars. *Int. J. Theor. Phys.*, 52:3319–3328.

Karmarkar, K. (1948). Gravitational metrics of spherically symmetry and class one. *Proc. Ind. Acad. Sci. A*, 27:56.

Karmarkar, S., Mukherjee, S., Sharma, R., and Maharaj, S. (2007). The role of pressure anisotropy on the maximum mass of cold compact stars. *Pramana J. Phys.*, 68:881.

Kasner, E. (1921). Finite representation of the solar gravitational field in flat space of six dimensions. *Am. J. Math.*, 43:130.

Kerr, R. (1963). Gravitational field of a spinning mass as an example of algebraically special metrics. *Phys. Rev. Lett.*, 11:237.

Kippenhahn, R., Weigert, A., and Weiss, A. (2012). *Stellar Structure and Evolution, 2nd Edition*. Astronomy and Astrophysics Library, Springer.

Knutsen, H. (1988). On the stability and physical properties of an exact relativistic model for a superdense star. *Mon. Not. R. astr. Soc*, 232:163–174.

Kohler, M. and Chao, K. (1965). Zentralsymmetrische statische Schwerefelder mit Räumen der Klasse 1. *Z. Naturforsch. A*, 20:1537.

Komathiraj, K. and Maharaj, S. (2007). Tikekar superdense stars in electric fields. *J. Math. Phys.*, 48:042501.

Kovetz, A. (1967). Schwarzschild's criterion for convective instability in general relativity. *Zeitschrift für Astrophysik*, 66:446.

Krori, K., Bargohain, P., and Devi, R. (1984). Some exact anisotropic solutions in general relativity. *Can. J. Phys.*, 62:239.

Kuchowicz, B. (1975). A physically realistic sphere of perfect fluid to serve as a model of neutron stars. *Astro. Space Sci.*, 33:L13–L14.

Kumar, J. and Bharti, P. (2022). Pulsar PSR B0943 + 10 as an isotropic Vaidya–Tikekar-type compact star. *Pramana J. Phys.*, 96:156.

Kumar, J., Maurya, S., Prasad, A., and Banerjee, A. (2019). Relativistic charged spheres: compact stars, compactness and stable configurations. *JCAP*, 11:005.

Kumar, J., Prasad, A., Maurya, S., and Banerjee, A. (2018). Charged Vaidya–Tikekar model for super compact star. *Eur Phys J C*, 78:540.

Lake, K. (2003). All static spherically symmetric perfect-fluid solutions of Einstein's equations. *Phys. Rev. D*, 67:104015.

Lake, K. (2009). Generating static spherically symmetric anisotropic solutions of Einstein's equations from isotropic Newtonian solutions. *Phys. Rev. D*, 80:064039.

Lattimer, J. and Prakash, M. (2001). Neutron star structure and the equation of state. *Astrophys J*, 550:426.

Lattimer, J. and Schutz, B. (2005). Constraining the equation of state with moment of inertia measurements. *Astrophys. J.*, 629:979–984.

Leibovitz, C. (1969). Spherically symmetric static solutions of Einstein's equations. *Phys. Rev. D*, 185:1664.

Li, B., Krastev, P., Hua, D., and Zhang, N. (2019). Towards understanding astrophysical effects of nuclear symmetry energy. *Eur. Phys. J. A*, 55:117.

Li, X.-D., Dai, Z.-G., and Wang, Z.-R. (1995). Is HER X-1 a strange star? *Astron. Astrophys.*, 303:L1.

Li, X.-D., Ray, S., Dey, J., Dey, M., and Bombaci, I. (1999). On the nature of the compact star in 4U1728-34. *Astrophys. J*, 527:L51.

Liebling, S. and Palenzuela, C. (2012). Dynamical boson stars. *Living Rev. Rel.*, 15:6.

Lindblom, L. (1984). Limits on the gravitational redshift form neutron stars. *Astrophys. J*, 278:364–368.

Maharaj, S., D.K., M., and Takisa, P. (2017). A family of Finch and Skea relativistic stars. *Int. J. Mod. Phys. D*, 26:1750014.

Maharaj, S. and Govender, M. (2005). Radiating collapse with vanishing Weyl stresses. *Int. J. Mod. Phys. D*, 14:667.

Maharaj, S. and Leach, P. (1996). Exact solutions for the Tikekar superdense star. *J. Math. Phys.*, 37:430–437.

Maharaj, S. and Maartens, R. (1989). Anisotropic spheres with uniform energy density. *Gen. Relativ. Gravit.*, 21:9.

Maharaj, S., Sunzu, J., and Ray, S. (2014). Some simple models for quark stars. *Eur. Phys. J. Plus*, 129:3.

Mak, M., Dobson jr., P., and Harko, T. (2000). Maximum mass-ratio ratios for compact general relativistic objects in Schwarzschild-de Sitter. *Mod. Phys. Lett. A*, 15:2153–2158.

Mak, M., Dobson jr., P., and Harko, T. (2001). Maximum mass-ratio ratios for charged compact general relativistic objects. *Euro Phys. Lett.*, 55:310–316.

Mak, M. and Harko, T. (2002). An exact anisotropic quark star model. *Chin. J. Astron. Astrophys.*, 2(3):248.

Mak, M. and Harko, T. (2003). Anisotropic stars in general relativity. *Proc. R. Soc. A*, 459(2030):393.

Mak, M. and Harko, T. (2004a). Can the galactic rotation curves be explained in brane world models? *Phys. Rev. D*, 70:024010.

Mak, M. and Harko, T. (2004b). Quark stars admitting a one-parameter group of conformal motions. *Int. J. Mod. Phys. D.*, 13:149–156.

Mansouri, R. and Khaorrami, M. (1966). The equivalence of Darmois-Israel and distributional method for thin shells in general relativity. *J. Math. Phys.*, 37:5672.

Matondo, D., Takisa, P., Maharaj, S., and Ray, S. (2017). Prediction of stellar masses with Finch and Skea geometry. *Astrophys. Space Sci.*, 362:1–8.

Maurya, S., Banerjee, A., and Gupta, Y. (2018a). Exact solution of anisotropic compact stars via mass function. *Astrophys. Space Sci.*, 363:208.

Maurya, S., Banerjee, A., and Hansraj, S. (2018b). Role of pressure anisotropy on relativistic compact stars. *Phys Rev D*, 97:044022.

Maurya, S., Banerjee, A., Jasim, M., Kumar, J., Prasad, A., and Pradhan, A. (2019a). Anisotropic compact stars in the Buchdahl model: A comprehensive study. *Phys. Rev D*, 99:044029.

Maurya, S., Banerjee, A., and Tello-Ortiz, F. (2020a). Buchdahl model in $f(R,T)$ gravity: A comparative study with standard Einstein's gravity. *Phys Dark Uni*, 27:100438.

Maurya, S., Errehymy, A., Singh, K., Tello-Ortiz, F., and Daoud, M. (2020b). Gravitational decoupling minimal geometric deformation model in modified $f(R,T)$ gravity theory. *Phys of Dark Univ.*, 30:100640.

Maurya, S. and Govender, M. (2017). A family of charged compact objects with anisotropic pressure. *Eur. Phys. J. C*, 77:420.

Maurya, S. and Gupta, Y. (2013). Charged fluid to anisotropic fluid distribution in general relativity. *Astrophys Space Sci.*, 344:243–251.

Maurya, S., Gupta, Y., Dayanandan, B., Jasim, M., and Al-Jamel, A. (2017). Relativistic anisotropic models for compact star with equation of state $p = f(\rho)$. *Int J Mod Phys D*, 26(02):1750002.

Maurya, S., Gupta, Y., and Jasim, M. (2015a). Relativistic modelling of stable anisotropic super-dense star. *Reports on Math. Phys.*, 76(1):21–40.

Maurya, S., Gupta, Y., Ray, S., and Chowdhury, S. (2015b). Spherically symmetric charged compact stars. *Eur. Phys. J. C*, 75:389.

Maurya, S., Gupta, Y., Ray, S., and Dayanandan, B. (2015c). Anisotropic models for compact stars. *Eur. Phys. J. C*, 75:225.

Maurya, S., Gupta, Y., Smitha, T. T., and Rahaman, F. (2016). A new exact anisotropic solution of embedding class one. *Eur. Phys. J. A.*, 52:191.

Maurya, S., Maharaj, S., Kumar, J., and Prasad, A. (2019b). Effect of pressure anisotropy on Buchdahl-type relativistic compact stars. *Gen Relativ Gravit*, 51:86.

Maurya, S., Ray, S., Ghosh, S., Manna, S., and Smitha, T. (2018c). A generalized family of anisotropic compact object in general relativity. *Annals of Physics*, 395:152–169.

Maurya, S. and Tello-Ortiz, F. (2019). Generalized relativistic anisotropic compact star models by gravitational decoupling. *Eur. Phys. J. C*, 79:85.

Maurya, S. and Tello-Ortiz, F. (2020). Anisotropic fluid spheres in the framework of $f(R,T)$ gravity theory. *Ann Phys*, 414:168070.

Maurya, S., Tello-Ortiz, F., and Jasim, M. (2020c). An EGD model in the background of embedding class I space–time. *Eur. Phys. J. C*, 80:918.

Maurya et al, S. (2019). Generalized relativistic anisotropic models for compact stars. *Eur. Phys. J C*, 79:85.

Mehra, J. (1998). One month in the history of the discovery of general relativity theory. *Foundations of Physics Letters*, 11(1):41–60.

Meinrenken, E. (2002). *Riemannian Geometry, Lecture Notes*. University of Toronto, Spring.

Miller et al., M. (2019). PSR J0030 + 0451 mass and radius from NICER Data and Implications for the properties of neutron star matter. *ApJL*, 887:L24.

Misner, C. and Sharpe, D. (1964). Relativistic equations for adiabatic, spherically symmetric gravitational collapse. *Phys. Rev. D.*, 136:13571.

Misner, C. and Zapolsky, H. (1964). High-density behavior and dynamical stability of neutron star models. *Phys. Rev. Lett.*, 12:635.

Molina, A., Dadhich, N., and Khugaev, A. (2017). Buchdahl-Vaidya-Tikekar model for stellar interior in pure Lovelock gravity. *Gen. Relativ. Gravit.*, 49:96.

Montgomery, C., Orchiston, W., and Whittingham, I. (2009). Michell, Laplace and the origin of the black hole concept. 12(2):90–96.

Moustakidis, C. (2017). The stability of relativistic stars and the role of the adiabatic index. *Gen. Relativ. Gravit.*, 49:68.

Mukherjee, S., Paul, B., and Dadhich, N. (1997). General solution for a relativistic star. *Class. Quantum Grav.*, 14(12):3475.

Nash, J. (1954). C1-isometric imbeddings. *Ann. of Math.*, 60(2):383–396.

Newman, E. and Janis, A. (1965). Note on the Kerr spinning particle metric. *J. Math. Phys.*, 6:915.

Nordström, G. (1918). On the energy of the gravitational field in Einstein's theory. *Proc. Kon. Ned. Akad. Wet.*, 20:1238.

Ojha, A. and Saxena, H. (2021). A review on Riemannian submanifold Theory. *Int. R. J. of Mod. Engg. Tech. Sci*, 03:12.

Oppenheimer, J. and Volkoff, G. (1939). On massive neutron cores. *Phys. Rev.*, 55:374.

Özel, F. and Freire, P. (2016). Masses, radii, and the equation of state of neutron stars. *Ann. Rev. Astron. Astrophys.*, 54:401.

Özel, F., Güver, T., and Psaltis, D. (2009). The mass and radius of the neutron star in EXO 1745-248. *Astrophys. J.*, 693:1775.

Özel, F., Psaltis, D., Güver, T., Baym, G., Heinske, C., and Guillot, S. (2016). The dense matter equation of state from neutron star radius and mass measurements. *Astrophys J.*, 820(1):28.

Pandey, S. and Sharma, S. (1981). Insufficiency of Karmarkar's condition. *Gen. Relativ. Gravit.*, 14:113.

Pandya, D., Thakore, B., Goti, R., Rank, J., and Shah, S. (2020). Anisotropic compact star model satisfying Karmarkar conditions. *Astrophys. Space Sci.*, 365:1.

Pandya, D. and Thomas, V. (2019). Models of compact stars of embedding class one for anisotropic distributions satisfying Karmarkar condition. *Canadian Journal of Phys.*, 97(3):337–344.

Pandya, D., Thomas, V., and Sharma, R. (2015). Modified Finch and Skea stellar model compatible with observational data. *Astrophys. Space Sci.*, 356:285–292.

Pant, N. (2011). Some new exact solutions with finite central parameters and uniform radial motion of sound. *Astrophys. Space Sci.*, 331:633.

Pant, N., Mehta, R., and Pant, M. (2010). New class of regular and well behaved exact solutions in general relativity. *Astrophys. Space Sci.*, 330:335.

Parui, R. and Sarma, H. (1991). The maximum limit of the density variation parameter λ for a stable neutron star. *Astrophys. Space Sci.*, 186:81.

Parui, R. K. (1995). On the interior of the neutron star (II). *Astrophys. Space Sci.*, 225:1.

Paul, B. (2004). Relativistic star solutions in higher dimensions. *Int. J. Mod. Phys. D*, 13:229.

Paul, B., Das, S., and Sharma, R. (2022). Anisotropic compact objects with colour-flavour locked equation of state in Finch and Skea geometry. *Eur. Phys. J. C*, 137:525.

Poisson, E. (2004). *A Relativist's Toolkit: The Mathematics of Black-Hole Mechanics*. Cambridge University Press.

Ponce de León, J. (1993). Limiting configurations allowed by the energy conditions. *Gen. Relativ. Gravity*, 25:1123.

Pons, J., Walter, F., Lattimer, J., Prakash, M., Neuhäuser, R., and An, P. (2002). Toward a mass and radius determination of the nearby isolated neutron star RX J185635-3754. *Astrophys. J.*, 564:981.

Prakash, M., Baron, E., and Prakash, M. (1990). Rotation of stars containing strange quark matter. *Phys. Lett. B*, 243:175.

Prasad, A., Kumar, J., Maurya, S., and Dayanandan, B. (2019). Relativistic model for anisotropic compact stars using Karmarkar condition. *Astrophys. Space Sci.*, 364:66.

Rahaman, F., Chakraborty, K., Kuhttig, P., Shit, G., and Rahaman, M. (2014). A new deterministic model of strange stars. *Eur. Phys. J. C.*, 74:3126.

Rahaman, F., Ray, S., Jafry, A., and Chakraborty, K. (2010). Singularity free solutions for anisotropic charged fluid with Chaplygin equation of state. *Phys. Rev. D*, 82(10):104055.

Rahaman, F., Sarkar, S., Singh, K., and Pant, N. (2019). Generating functions of worm-holes. *Mod. Phys. Lett. A*, 34:1950010.

Rahaman, M., Singh, K., Errehymy, A., Rahaman, F., and Daoud, M. (2020). Anisotropic Karmarkar stars in $f(R,T)$ gravity. *Eur. Phys. J. C.*, 80:272.

Randall, L. and Sundrum, R. (1999). An alternative to Compactification. *Phys. Rev. Lett.*, 83:3370.

Ratanpal, B., Thomas, V., and Pandya, D. (2016). Anisotropic star on pseudo-spheroidal spacetime. *Astrophys and Space Sci.*, 361:65.

Ravenhall, D. and Pethick, C. (1994). Neutron star moments of inertia. *The Astrophysical Journal*, 424:846–851.

Rawl, M., Orosz, J., McClintock, J., Torres, M., Bayin, C., and Buxton, M. (2011). Refined neutron star mass determinations for six eclipsing X-ray pulsar binaries. *Astrophys. J.*, 730:25.

Reissner, H. (1916). Über die eigengravitation des elektrischen feldes nach der einsteinschen theorie. *Ann. Phys.*, 59:106.

Rhoades, C. and Ruffini, R. (1974). Maximum mass of a neutron star. *Phys. Rev. Lett.*, 32:324–327.

Rothchild, R., Kulkarni, S., and Lingenfelter, R. (1994). Discovery of an X-ray source coincident with the soft γ-ray repeater 0525-66. 368:432–434.

Roupas, Z. and Nashed, G. (2020). Anisotropic neutron stars modelling: constraints in Krori–Barua spacetime. *Eur. Phys. J C*, 80:905.

Rubakov, V. (2014). The null energy condition and its violation. *Phys. Usp.*, 57(2):128.

Ruderman, M. (1972). Pulsars: Structure and dynamics. *Annu. Rev. Astron. Astrophys.*, 10:427.

Samuelsson, L. (2003). *Stellar Models in General Relativity*. Stockholm University.

Sarkar, N., Sarkar, S., Rahaman, F., Singh, K., and Shah, H. (2019a). Anisotropic fluid spheres satisfying the Karmarkar condition. *Mod. Phys. Lett. A*, 34(15):1950113.

Sarkar, N., Singh, K., Sarkar, S., and Rahaman, F. (2019b). Compact star model in class I spacetime. *Eur. Phys. J. C.*, 79:516.

Sasidharan, A. and Sabu, M. (2021). General solution to Vaidya-Tikekar metric. *IJMTT*, 67(8):15.

Sawyer, R. (1972). Condensed π^- phase in neutron-star matter. *Phys. Rev. Lett.*, 29:382. Erratum Phys. Rev. Lett. (1972) 29:823.

Schlaefli, L. (1871). Sugli spazii di curvatura constante. *Ann. di Mat.*, 5:170.

Schwarzschild, K. (1916a). English translation: On the gravitational field of a sphere of incompressible fluid according to Einstein's theory. 24:424.

Schwarzschild, K. (1916b). Úber das gravitationsfeld eines massenpunktes nach der einstein'schen theorie. *Sitz. Deut. Akad. Wiss, Berlin Kl. Math. Phys.*, 1916:189–196. [English translation: On the gravitational field of a point mass, According to Einstein's theory, Gen. Relativ. Gravit. (2003) 35:951-959].

Shamir, M. and Fayyaz, I. (2020). Effect of $f(R)$ gravity modes on compact stars. *Th. Math. Phys.*, 202:112.

Shapiro, S. and Teukolsky, S. (1983). *Black Holes, White Dwarfs, and Neutron Stars: The Physics of Compact Objects*. 2004 WILEY-VCH Verlag GmbH & Co. KGaA.

Sharma, R. and Das, S. (2013). Collapse of a relativistic self-gravitating star with radial heat flux: Impact of anisotropic stresses. *J. Grav.*, 659605:1.

Sharma, R., Das, S., Govender, M., and Pandya, D. (2020). Revisiting Vaidya-Tikekar stellar model in the linear regime. *Ann. Phys.*, 414:168079.

Sharma, R., Das, S., and Thirukannesh, S. (2017). Anisotropic extension of Finch and Skea stellar model. *Astrophys. Space Sci.*, 362:232.

Sharma, R. and Maharaj, S. (2007). A class of relativistic stars with a linear equation of state. *Mon. Not. Roy. Astron. Soc.*, 375:1265.

Sharma, R. and Mukherjee, S. (2001). Her X-1: A quark–diquark star? 16(16):1049.

Sharma, R., Mukherjee, S., Dey, M., and Dey, J. (2002). A general relativistic model for SAX J 1808.4 - 33658. *Mod. Phys. Lett. A*, 17(14):827.

Sharma, R., Mukherjee, S., and Maharaj, S. (2001). General solution for a class of static charged spheres. *Gen. Relativ. Gravit.*, 33:999.

Sharma, R. and Ratanpal, B. (2013). Relativistic stellar model admitting a quadratic equation of state. *Int. J. Mod. Phys. D*, 22:1350074.

Singh, K., Bhar, P., Laishram, M., and Rahaman, F. (2019). A generalised class one static solution. *Heliyon*, 5:8.

Singh, K., Bisht, R., Maurya, S., and Pant, N. (2020a). Static fluid spheres admitting Karmarkar condition. *Chinese Phys. C*, 44(3):035101.

Singh, K., Errehymy, A., Rahaman, F., and Daoud, M. (2020b). Exploring physical properties of compact stars in $f(R)$ gravity: an embedding approach. *Chinese J Phys.*, 44:10.

Singh, K., Maurya, S., Errehymy, A., Rahaman, F., and Daoud, M. (2020c). Physical

properties of class I compact star model for linear and Starobinsky $f(R,T)$ functions. *Phys. of Dark Univ.*, 30:100620.

Singh, K., Pant, N., and Govender, M. (2017). Physical viability of fluid spheres satisfying the Karmarkar condition. *Eur. Phys. J. C.*, 77:100.

Sokolov, A. (1980). Phase transitions in a superfluid neutron liquid. *JETP*, 79:1137–1140.

Stephani, H., Kramer, D., MacCallum, M., Hoenselaers, C., and Herlt, E. (2003). *Exact solutions of Einstein's field equations*. Cambridge University Press, Cambridge.

Sunzu, J. and Mahali, K. (2018). Regular exact models with vanishing anisotropy using Van der Waals equation of state. *Glob. J. Sci. Front. Res.*, 18:19.

Sunzu, J., Maharaj, S., and Ray, S. (2014a). Charged anisotropic models for quark stars. *Astrophys. Space Sci.*, 352:719.

Sunzu, J., Maharaj, S., and Ray, S. (2014b). Quark star model with charged anisotropic matter. *Astrophys. Space Sci.*, 354:517.

Sunzu, J., Mathias, A., and Maharaj, S. (2019). Stellar models with generalized pressure anisotropy. *J. Astrophys. Astron.*, 40:8.

Takisa, P. (2013). *Exact Models Of Compact Stars With Equation of State*. PhD thesis, University of KwaZulu-Natal Durban.

Takisa, P., Maharaj, S., Manjonjo, A., and Moopanar, S. (2017). Spherical conformal models for compact stars. *Eur. Phys. J. C*, 77:713.

Tamta, R. and Fuloria, P. (2020). Analysis of physically realizable stellar models in embedded class one spacetime manifold. *Mod. Phys. Lett. A*, 35(04):2050001.

Tello-Ortiz, F., Malaver, M., Rincòn, À., and Gomez-Leyton, Y. (2020a). Relativistic anisotropic fluid spheres satisfying a non-linear equation of state. *Eur. Phys. J C*, 80:371.

Tello-Ortiz, F., Maurya, S., Errehymy, A., and Singh, K. (2019). Anisotropic relativistic fluid spheres: an embedding class I approach. *Eur. Phys. J. C.*, 79:885.

Tello-Ortiz, F., Maurya, S., and Gomez-Leyton, Y. (2020b). Class I approach as MGD generator. *Eur. Phys. J. C*, 80:324.

Teschl, G. (2012). *Ordinary Differential Equations and Dynamical Systems (Graduate Studies in Mathematics)*.

Thirukkanesh, S. and Maharaj, S. (2008). Charged anisotropic matter with linear equation of state. *Class. Quant. Grav.*, 25:23.

Thirukkanesh, S., Ragel, F., Sharma, R., and Das, S. (2018). Anisotropic generalization of well-known solutions describing relativistic self-gravitating fluid systems: an algorithm. *Eur. Phys. J. C*, 78:31.

Thirukkanesh, S., Sharma, R., and Das, S. (2020). Model of a static spherically symmetric anisotropic fluid distribution in paraboloidal spacetime admitting a polytropic equation of state. *Eur. Phys. J. P*, 135:629.

Thomas, V. and Ratanpal, B. (2007). Non-adiabatic gravitational collapse with anisotropic core. *Int. J. Mod. Phys. D*, 16:1497.

Thomas, V., Ratanpal, B., and Vinodkumar, P. (2005). Core-envelope models of superdense star with anisotropic envelope. *Int. J. Mod. Phys. D*, 14(01):85–96.

Thorne, K. (1971). General relativity and cosmology. In *Proceedings of the International School of Physics "Enrico Fermi", Course 37*.

Tikekar, R. (1990). Exact model for a relativistic star. *J. Math. Phys.*, 31:2454–2458.

Tikekar, R. and Jotania, K. (2005). Relativistic superdense star models of pseudo spheroidal spacetime. *Int. J. Mod. Phys. D*, 14:1037.

Tikekar, R. and Jotania, K. (2007). On relativistic models of strange stars. *Pramana J. Phys.*, 68:397–406.

Tikekar, R. and Thomas, V. (2005). A relativistic core-envelope model on pseudospheroidal space-time. *Pramana*, 64:5–15.

Tolman, R. (1939). Static solutions of Einstein field equations for spheres of fluid. *Phys. Rev.*, 55:364.

Tooper, R. (1965). Adiabatic fluid spheres in general relativity. *Astrophys. J.*, 142:1541.

Urango, D., Ospino, J., Hernàndez, H., and Nùñez, L. (2022). Acceptability conditions and relativistic anisotropic generalized polytropes. *Eur. Phys. J. C*, 82:176.

Vaidya, P. (1951). The gravitational field of a radiating star. *Proc. Indian Acad. Sc. A*, 33:264.

Vaidya, P. and Tikekar, R. (1982). Exact relativistic model for a superdense star. *J. Astrophys. Astron.*, 3:325.

Varela, V., Rahaman, F., Ray, S., Chakraborty, K., and Kalam, M. (2010). Charged anisotropic matter with linear or nonlinear equation of state. *Phys. Rev. D*, 82:044052.

Wald, R. (1984). *General Relativity*. The University of Chicago Press Chicago and London.

Walecka, J. (1974). A theory of highly condensed matter. *Ann. Phys.*, 83:491–529.

Walecka, J. (1975). Equation of state for neutron matter at finite T in a relativistic meanfield theory. *Phys. Lett.*, 59B:109–112.

Whitney, H. (1936). Differentiable Manifolds. *Ann. of Math.*, 37:645–680.

Whitney, H. (1944a). The self-intersection of a smooth n-manifold in $2n$ space. *Ann. of Math.*, 45:220–246.

Whitney, H. (1944b). The singularities of a smooth n-manifold in $(2n-1)$ space. *Amm. of Math.*, 45:246–293.

Will, C. (2006). The confrontation between general relativity and experiment. *Living Reviews in Relativity*, 9:3.

Willmore, T. (1959). *An Introduction to Differential Geometry*. Oxford University Press.

Wolansky, G. (1999). On nonlinear stability of polytropic galaxies. *ANN I H POINCAR-EAN*, 16(1):15–48.

Xu, R., Qiao, G., and Zhang, B. (1999). PSR 0943+10: A bare strange star? *Astrophys. J.*, 522:L109.

Yakovlev, D., Haensel, P., Baym, G., and Pethick, C. (2013). Lev Landau and the concept of neutron stars. *Phys. Usp.*, 56:289–295. Usp. Fiz. Nauk 183 (2013) 307-314.

Zdunik, J. (2000). Strange stars linear approximation of the EoS and maximum QPO frequency. *Astron. Astrophys.*, 359:311.

Zeldovich, Y. (1962). The equation of state at ultra high densities and its relativistic limitations. *Sov. Phys. JETP*, 14:11437.

Zeldovich, Y. (1972). A hypothesis, unifying the structure and the entropy of the universe. *Mon. Not. R. Astron. Soc.*, 160:1.

Zeldovich, Y. and Novikov, I. (1972). *Relativistic astrophysics stars and relativity Vol 1*. University of Chicago Press.